Technische Universität München

Fakultät für Medizin

Combination of drug therapies and radiation against stem cell-enriched glioblastoma-derived spheres

Eno Itunu Essien

Vollständiger Abdruck der von der Fakultät für Medizin der Technischen Universität München zur Erlangung einer

Doktorin der Naturwissenschaften (Dr.rer.nat.)

genehmigten Dissertation.

Vorsitz: Prof. Dr. Wolfgang A. Weber

Prüfer*innen der Dissertation:

1. **Prof. Dr. Michael J. Atkinson**
2. **Prof. Dr. Gabriele Multhoff**

Die Dissertation wurde am 29.09.2022 bei der Technischen Universität München eingereicht und durch die Fakultät für Medizin am 13.12.2022 angenommen.

In Memoriam: PD. Dr. Nataša Anastasov

CONTENTS

ABSTRACT

Glioblastoma remains a difficult cancer to treat successfully despite the multimodal therapeutic strategy of surgery, radiation therapy and chemotherapy with temozolomide (TMZ). One factor that limits effective treatment is the presence of glioblastoma stem-like cells (GSLCs) that are associated with therapeutic resistance and tumor recurrence. The proliferation and survival of GSLCs require the mitogen-activated protein kinase (MAPK) pathway, while Histone deacetylases (HDAC) decrease acetylation to drive the pathogenesis of glioblastoma. From a combined radiation and drug screening platform, we identified potential combinations of HDAC inhibitor (HDACi) and MAPK/ERK kinase inhibitors (MEKi) with ionizing radiation as a novel therapy against glioblastoma.

To mimic the stem-like phenotype of glioblastoma, three established cell lines (LN229, U87 and U251) were enriched for GSLCs by spheroid culture in serum-free medium containing stem cell supplements (hereafter; LN229-sph, U87-sph and U251-sph). The response of these enriched glioblastoma-derived spheres was examined after treatment with the HDACi MS-275 and the MEKi TAK-733 and trametinib as single agents or in combinations following a single dose of 4 Gy irradiation. These were compared to the gold-standard treatment of TMZ and 4 Gy irradiation.

After treatment with TMZ and radiation, there were no significant effects on the GSLC markers and on the dead cell population in any of the three cell lines, confirming that GSLCs are resistant to the standard treatment. In contrast, combining the HDACi and MEKi with radiation significantly reduced sphere formation in the enriched glioblastoma-derived spheres indicating loss of proliferation and self-renewal ability. Also, the individual and co-expression of GSLC markers (Nestin, CD44 and SOX2) were significantly decreased, while the dead cell population was increased upon the combined treatment with radiation.

The differential response of CD44 to the combined treatment among the three glioblastoma-derived spheres suggested the response to combination therapy may be cell-dependent. Interestingly, there was a lack of correlation between the protein and mRNA expression of the GSLC markers after the combined treatment, suggesting an influence of the therapy on translation.

The efficacy of the combined treatment on targeting GSLCs offers an improvement to the standard treatment. Our findings indicate that this combination strategy may potentially improve therapy that could benefit glioblastoma patients.

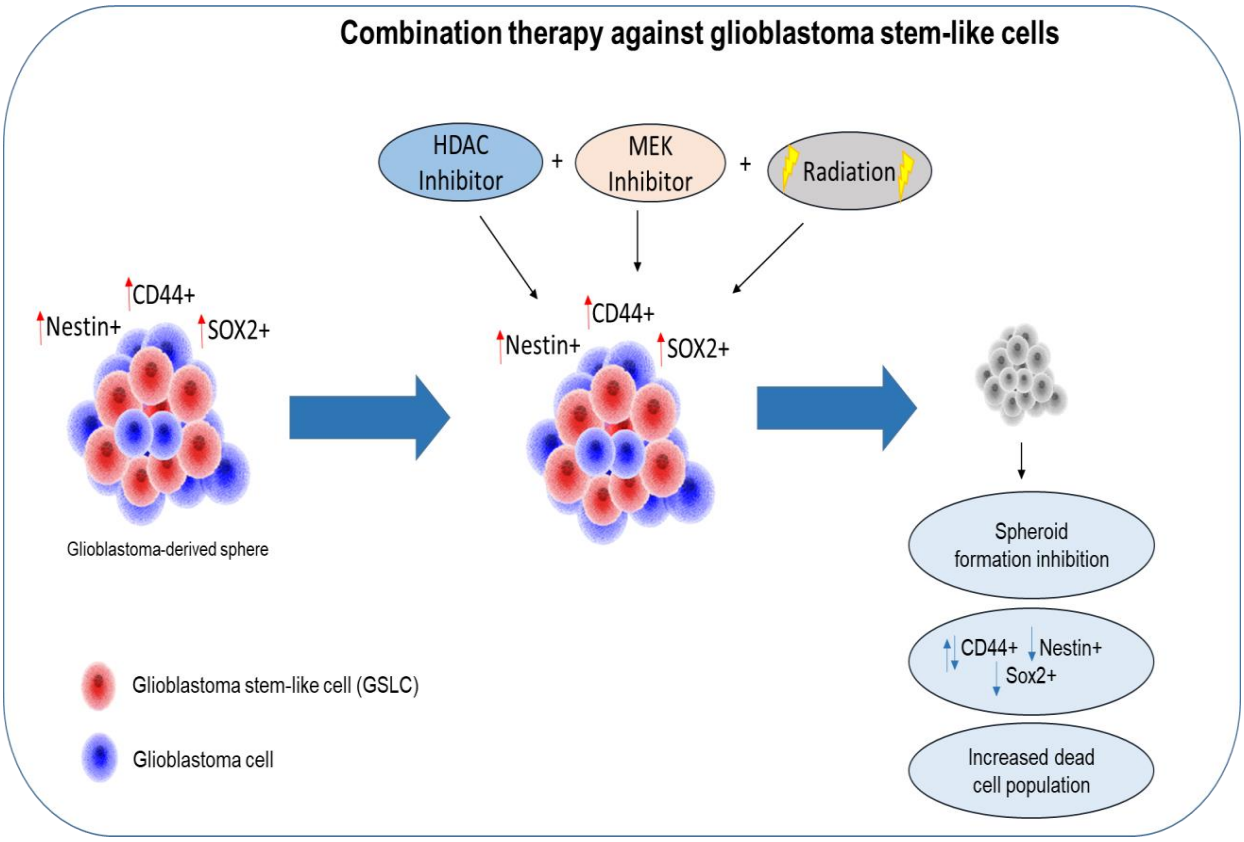

Figure 1: Graphical Abstract summarizing the effect of combining HDACi and MEKi with radiation on glioblastoma-derived spheres. The combined treatment targets the glioblastoma-derived sphere to eradicate glioblastoma by inhibition of sphere formation, reduction of expressed GSLC markers (Nestin, CD44 and SOX2) and increase in the dead cell population.

ZUSAMMENFASSUNG

Das Glioblastom ist trotz der multimodalen Therapiestrategie aus Operation, Strahlentherapie und Chemotherapie mit Temozolomid (TMZ) nach wie vor eine schwer zu behandelnder Krebsart. Der in vielen Fällen unbefriedigende Therapieerfolg ist mit hoher Wahrscheinlichkeit auf das Vorhandensein von Stammzell-ähnlichen Glioblastomzellen (GSLCs) zurückzuführen, welche Therapieresistenz und Tumorrezidive fördern. Die Proliferation und das Überleben von GSLCs wird durch den Mitogen-aktivierten Proteinkinase (MAPK)-Signalweg gesteuert, während Histon-Deacetylasen (HDAC) die Acetylierung verringern, um die Pathogenese des Glioblastoms zu fördern. Auf der Grundlage einer kombinierten Bestrahlungs- und Arzneimittel-Screening-Plattform haben wir potenzielle Kombinationen von HDAC-Inhibitoren (HDACi) und MAPK/ERK-Kinase-Inhibitoren (MEKi) mit ionisierender Strahlung als neuartige Therapie gegen Glioblastom identifiziert.

Um den stammähnlichen Phänotyp des Glioblastoms zu imitieren, wurden drei etablierte Zelllinien (LN229, U87 und U251) durch Sphäroid-Kultur in serumfreiem Medium mit Stammzellzusätzen mit GSLCs angereichert (im Folgenden: LN229-sph, U87-sph und U251-sph). Das Ansprechen dieser angereicherten Glioblastom-Sphären wurde nach einer Behandlung mit dem HDACi MS-275 und den MEKi TAK-733 und Trametinib als Einzel- oder Kombinationspräparat mit einer einmaligen Bestrahlungsdosis von 4 Gy Bestrahlung untersucht. Diese wurden mit der Standard-Behandlung mit TMZ und 4-Gy-Bestrahlung verglichen.

Nach der Behandlung mit TMZ und Bestrahlung gab es bei keiner der drei Zelllinien signifikante Auswirkungen auf die GSLC-Marker und auf die Population der toten Zellen, was bestätigt, dass GSLCs gegen die Standardbehandlung resistent sind. Im Gegensatz dazu führte die Kombination von HDACi und MEKi mit Strahlung zu einer signifikanten Verringerung der Sphärenbildung in den angereicherten Glioblastom-Sphären, was auf einen Verlust der Proliferation und der Fähigkeit zur Selbsterneuerung hindeutet. Auch die individuelle und die Koexpression von GSLC-Markern (Nestin, CD44 und SOX2) waren signifikant verringert, während die Population toter Zellen bei der kombinierten Behandlung mit Strahlung zunahm.

Die unterschiedliche Reaktion von CD44 auf die kombinierte Behandlung in den drei Glioblastom-Sphären deutet darauf hin, dass die Reaktion auf die

Kombinationstherapie zellabhängig sein könnte. Interessanterweise gab es nach der Kombinationsbehandlung keine Korrelation zwischen der Protein- und mRNA-Expression der GSLC-Marker, was auf einen Einfluss der Therapie auf die Translation schließen lässt.

Die Wirksamkeit der kombinierten Behandlung auf die GSLCs stellt eine Verbesserung gegenüber der Standardbehandlung dar. Unsere Ergebnisse deuten darauf hin, dass diese Kombinationsstrategie das Potenzial hat, die Therapie zu verbessern, von der Glioblastom-Patienten profitieren könnten.

ABBREVIATIONS

°C – degree Celsius

µM – micromolar

A_{260} – Absorption at 260nm

A_{280} – Absorption at 280nm

Ab – Antibody

ALDH1 – Aldehyde dehydrogenase 1

BBB – Blood brain barrier

BSA – Bovine Serum Albumin

cDNA – Complementary deoxyribonucleic acid

Ct – Cycle threshold

DMEM – Dulbecco's Modified Eagle's Medium

DMSO – Dimethylsulfoxide

DNA – Deoxyribonucleic acid

ECL – Enhanced chemiluminescence

EGF – Epidermal growth factor

ERK1/2 – Extracellular signal-regulated kinase 1 and 2

FBS – Fetal bovine serum

FGF – Fibroblast growth factor

FMO control – Fluorescence minus one control

GB – Glioblastoma

GEPIA – Gene Expression Profiling Interactive Analysis

GF – Growth factors

GSLCs – Glioblastoma stem-like cells

GTEx – Genotype-Tissue Expression

Gy – Gray

H - Hour

HAT – Histone acetyltransferase

HDAC – Histone deacetylase

HDACi – HDAC inhibitor

kDa – Kilodalton

MAPK – Mitogen activated protein kinase

MEK – MAPK/ERK kinase

MEKi – MEK inhibitor

MGMT – *O*^{6}-methylguanine-DNA methyltransferase

Mins - Minutes

mRNA – Messenger RNA

PBS – Phosphate-buffered saline

PCR – Polymerase chain reaction

PhosSTOP – Phosphatase inhibitor cocktail

pMAPK – Phosphorylated MAPK

RNA – Ribonucleic acid

RT – Room temperature

SOX2 – SRY (sex determining region Y)-box 2

Sph – Spheres

TAK – TAK-733

TCGA – The Cancer Genome Atlas

TMZ – Temozolomide

T-PER – Tissue Protein Extraction Reagent

TRA – Trametinib

µg – microgram

µl – microliter

ULA – Ultra low attachment

1 INTRODUCTION

1.1 Glioblastoma

Glioblastoma is the most common malignant tumor of the Central Nervous System (CNS). It originates from astrocytes and is therefore classified as a WHO grade IV astrocytoma [1]. Glioblastoma accounts for 12% to 15% of all intracranial tumors and 50% to 60 % of astrocytic tumors [2]. The incidence of glioblastoma increases with age and affects men 1.58 times more frequently than women [3]. Due to the recurring nature of glioblastoma, it is characterised by a poor clinical outcome with a median survival of 15 months [4].

Glioblastomas can be distinguished as either primary or secondary glioblastomas. Most glioblastomas are primary glioblastomas (~ 90%) and originate as *de novo* tumors of neural stem cells (NSCs), astrocytes or glial progenitors [1]. Primary glioblastomas develop mostly in elderly patients and are characterised by rapid progression and poor prognosis. Secondary glioblastomas progress from either low-grade (WHO grade II) or anaplastic astrocytoma (WHO grade III) as shown in Figure 2. They occur in younger patients (< 45 years) and have a significantly better prognosis [5].

The understanding of the role of mutations in glioblastoma has evolved over the years. For example, the molecular status of isocitrate dehydrogenases 1 and 2 (*IDH1/2*) is used to distinguish between primary or secondary glioblastoma. The *IDH1/2*-wild-type is linked to primary glioblastomas with tumors located in the supratentorial region of the brain with extensive necrosis and mutations in *p16INK4a*, *TP53*, *PTEN* and *EGFR* [6]. The secondary glioblastomas on the other hand are *IDH*-mutant and are located on the frontal lobe of the brain with limited tumor necrosis and the presence of *p16INK4a*, *TP53* and *ATRX* mutations [6]. A clinical study has confirmed that secondary glioblastomas with IDH-mutations are associated with improved survival [7].

Despite this progress in molecular phenotyping, the overall prognosis and long-term survival of glioblastoma have remained dismal while differential responses to therapies have been observed. Therefore, an understanding of the connection between genetic changes and therapy response could help the development of more personalized therapies and improvement in the clinical outcome. For instance, the methylation

status of O^6-methylguanine-DNA methyltransferase (MGMT) is now widely accepted as a predictive factor for response to the standard therapy [8].

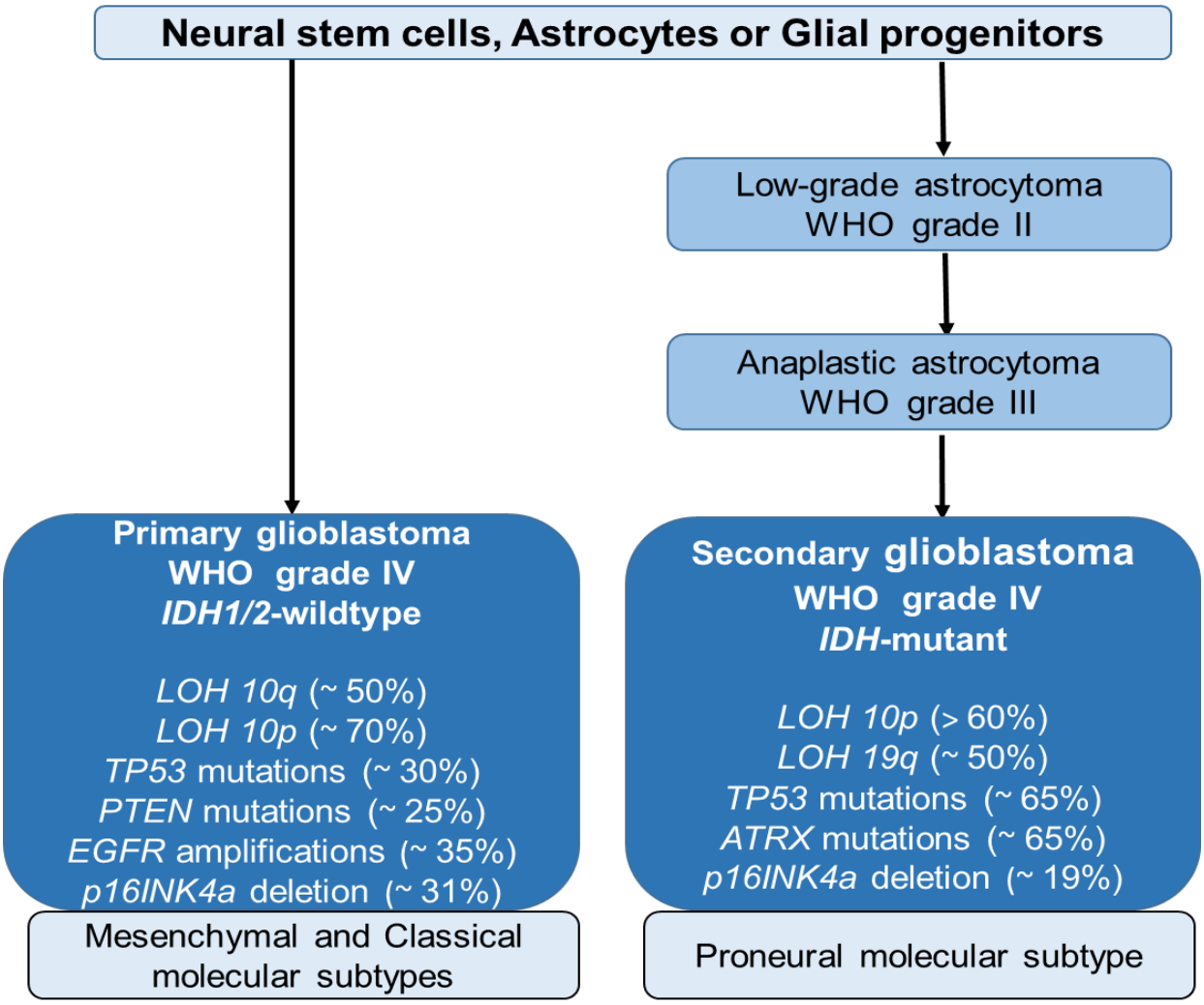

Figure 2: Genetic pathways to primary and secondary glioblastomas. Grade I - II are considered low grade because they are slower growing and less aggressive. Grade III – IV are higher grade as they are more aggressive and grow rapidly. The histological and genetic differences in types of glioblastoma (Grade IV) are shown. (LOH: loss of heterozygosity) (modified from [5])

1.2 Molecular subtype classification of glioblastoma

Intertumoral heterogeneity is one of the characteristics of glioblastoma and includes variations in phenotypic, epigenetic and genetic features between tumors from different patients [8]. In an attempt to gain more knowledge on this, The Cancer Genome Atlas (TCGA) performed a gene expression-based molecular classification of glioblastoma in 2010 [9]. A set of 260 glioblastoma patient samples were compared using a

predictive list of 840 gene mutational events to cluster glioblastoma into four subtypes namely; mesenchymal, classical, proneural and neural [9]. The resultant key genetic markers that were used to classify each glioblastoma subtype are summarised in Table 1.

Table 1: Summary of glioblastoma molecular subtypes and the corresponding key genetic markers [9].

Glioblastoma molecular subtype	Key genetic markers
Mesenchymal	*NF1*, *PTEN*, *CHI3L*, *MET* and NF-kB pathway
Classical	*CDKN2A*, *EGFR*, *NES*, Notch and SHH pathway
Proneural	*PDGFRA*, *IDH1*, *TP53*, *OLIG2* and *SOX* genes
Neural	*NEFL*, *GABRA1*, *SYT1*, *SLC12A5*

In 2017, the TCGA consortium performed a comprehensive gene expression profiling that narrowed down glioblastoma molecular classes into only three subtypes namely; mesenchymal, classical and proneural [10]. This was because the TCGA consortium identified the neural subtype as a normal neural lineage contamination that lacked characteristic gene abnormalities. The three subtypes are discussed more in detail below.

1.2.1 Mesenchymal molecular subtype

The mesenchymal subtype is characterized by a focal hemizygous chromosomal deletion of a region at 17q11.2 containing neurofibromin 1 (*NF1*) resulting in low expression of *NF1* [9]. Out of 20 samples with *NF1* mutations, 14 of them were classified as the mesenchymal subtype [9]. Six out of seven samples with mutations of both *NF1* and *PTEN* involved in the AKT pathway were further classed as mesenchymal subtype [9]. Genes involved in the tumor necrosis factor super family pathway and the NF-kB pathway are associated with the mesenchymal subtype [9]. Some markers highly expressed in this subtype are mesenchymal markers such as *CHI3L1* and *MET* [11] as well as microglial markers such as *CD68*, *PTPRC* and *TNF*.

1.2.2 Classical molecular subtype

The classical subtype is associated with an astroglia gene expression signature and shows a distinct lack of additional aberrations in *TP53*, *NF1*, *PDGFRA* or *IDH1* [9].

100% of the classical glioblastoma subtype were characterised by chromosome 7 amplification and chromosome 10 loss. A high level of *EGFR* amplification in 97% of the classical subtype was observed with 12 samples containing a point or vIII *EGFR* mutation [9]. Focal homozygous deletion of 9p21.3 that targets CDKN2A was significant and co-occurred with *EGFR* amplification in 94% of the classical subtype. This deletion was mutually exclusive with aberrations of the RB pathway genes such as *RB1*, *CDK4* and *CCDN2* [9]. Other highly expressed components of this subtype are the neural precursor and stem cell marker *NES*, Notch and Sonic hedgehog (SHH) signaling pathways.

1.2.3 Proneural molecular subtype

The two major characteristics of the proneural glioblastoma subtype were alterations of *PDGFRA* and point mutations in IDH1 [9]. This subtype was highly enriched with the oligodendrocytic signature and contained several proneural developmental genes such as *SOX* genes along with *DCX*, *DLL3*, *ASCL1* and *TCF4*) [9]. Focal amplifications of the locus at 4q12 containing *PDGFRA* occurred at a much higher rate compared to other subtypes causing high levels in *PDGFRA* gene expression. Four proneural samples further harboured a *PDGFRA* point mutation. Eleven out of twelve mutations in *IDH1* were observed with this subtype with most not having any alterations of *PDGFRA*. *TP53* mutations and loss of heterozygosity was further observed in the samples. Generally, the proneural subtype was associated with younger age, *PDGFRA* overexpression, *IDH1* and *TP53* mutations that have been linked to secondary glioblastoma [12-14].

1.2.4 Recent glioblastoma classification

A more recent study in 2021 has grouped IDH wild-type glioblastoma into four sub-groups using a form of classification based on the biological characteristics of single cells and bulk tumors [15]. The study identified phenotypic patterns of 36 adult glioblastomas from three independent datasets. The four sub-groups of glioblastoma in this study were classified as proliferative/progenitor, neuronal, mitochondrial and glycolytic/plurimetabolic [15]. Of all the four subgroups, the mitochondrial glioblastoma exhibited the most favourable clinical outcome with a marked susceptibility to inhibitors of oxidative phosphorylation. It is expected that this knowledge will help to better design patient therapy, classify clinical and experimental studies as well as develop precise categories for epidemiological studies.

1.3 Standard therapy of Glioblastoma and its limitations

The standard multimodal therapy for glioblastoma is surgical resection followed by adjuvant radiotherapy combined with chemotherapy with temozolomide (TMZ). Recently, Tumor-treating fields are also being applied together with TMZ [4, 16]. These therapeutic strategies and their limitations are discussed more in detail below.

Surgery is currently the initial procedure for the treatment of glioblastoma designed to reduce the tumor mass as well as provide material for histological diagnosis and genotyping of the tumor [17]. It is performed by safe maximal surgical resection of the tumor tissue with the goal of gross-total resection where possible. The benefits of surgical resection are limited due to the aggressive nature of glioblastoma that diffusely infiltrates surrounding tissues in the brain at the time of diagnosis. The acquisition of extensive tumor vascularization [18] that characterises glioblastoma makes complete removal of the tumor more difficult. There have been recent advances such as fluorescence-guided resection with 5-aminolevulinic acid (5-ALA) [19], preoperative imaging using functional MRI [20, 21] and awake brain mapping with intraoperative cortical electrodes [22]. These advances are being developed to optimise the extent of resection and increase safety.

Radiotherapy has remained an important mode of treatment for glioblastoma that is demonstrated to improve survival. It is usually administered 3 to 4 weeks after surgery, delivering a total dose of 60 Gy as 2 Gy fractions over 6 weeks [4]. Typically, concurrent chemotherapy with TMZ is included. For elderly patients with a worse prognosis, hyprofractionated radiotherapy with concurrent and adjuvant TMZ is considered more appropriate due to results of a clinical trial that showed longer survival [23].

A sub-population of cells within the tumor, glioblastoma stem-like cells (GSLCs), are highly resistant to radiation (reviewed by Huang, Z *et al*, 2010 [24]). GSLCs can efficiently repair DNA damage and have a high capacity for repopulation of the tumor, leading to recurrence. Therefore, the therapeutic effects of radiation alone are limited indicating the need for more targeted therapies to overcome radioresistance.

Chemotherapy of glioblastoma is typically by TMZ (75 mg/m^2 daily) during radiotherapy, followed by six cycles of adjuvant TMZ (150-200 mg/m^2 for 5 days every 28-day cycle) as maintenance [4]. TMZ is a DNA-alkylating agent and a second

generation imidazotetrazine with the ability to cross the blood-brain barrier (BBB) [25]. TMZ causes DNA damage by adding methyl groups to nucleotides, typically at the N^7 and O^6 - positions of guanine. However, the DNA repair enzyme MGMT can efficiently repair this DNA damage. Hence, patients with tumors that have acquired epigenetically silencing of MGMT through promoter methylation benefit most from TMZ treatment. This has led to the MGMT status being widely used as a predictive factor for response to the standard therapy [8]. Another challenge to TMZ treatment is the occurrence of severe side effects, which include nausea, thrombocytopenia, neutropenia, myelotoxicity, ulcers and fatigue [26]. TMZ treatment has recently been associated with hyper-mutation and malignant transformation of low-grade glioma into a more aggressive form [27]. All of these limitations with TMZ treatment calls for the development of a more effective therapy.

Due to the almost ubiquitous neo-angiogenesis of glioblastoma, the anti-angiogenic agent Bevacizumab has been tested in two randomized trials in combination with the standard radiochemotherapy. Disappointingly, the progression-free survival was prolonged in both trials, there was increased toxicity and no significant change in overall survival [28, 29].

There are other clinical trials ongoing testing different combination modalities with or without the standard therapy to improve the treatment of glioblastoma [30]. Some of these include testing inhibitors of histone deacetylases and MAPK/ERK kinases which are described in sections 1.6 and 1.7.

Tumor-treating fields (TTF) in combination with the standard chemotherapy TMZ has been approved by the FDA for the treatment of recurrent and newly diagnosed glioblastoma [31]. TTF is an anti-mitotic treatment approach that uses alternating electric fields with low intensity (1-3 V/cm) and intermediate frequency (100-300 kHz) delivered by transducer arrays placed on the scalp of patients [32]. The proposed anti-tumor effect of TTF is suggested to be by inhibition of glioblastoma cell division and organelle assembly, inducing cell death and reducing tumor growth. The approval of TTF was based on results that demonstrated an improved progression-free survival and overall survival when TTF were added as an adjuvant therapy in combination with maintenance TMZ [16, 33]. However, the cost and benefit of TTF remains very controversial and uptake is limited [34].

1.4 Glioblastoma stem-like cells (GSLCs)

Many studies have supported the concept that there is a subpopulation of cells within tumors that possess stem cell properties and have the potential for cancer initiation and repopulation (reviewed by Huang, Z *et al*, 2010 [24]). These cells are called cancer stem cells (CSCs) and are considered to be drivers of tumor growth due to their capacity for self-renewal, proliferation and differentiation (reviewed by Bradshaw *et al*, 2016 [35]). It is suggested that the presence of CSCs result in poor clinical outcome because of their resistance to therapy [36].

CSCs in glioblastoma are termed glioblastoma stem-like cells (GSLCs) because they share some characteristics with non-cancerous neural stem cells and are believed to originate from them [37]. Some of the GSLC characteristics include the ability to self-renew and differentiate into the other cell types (astrocytes, oligodendrocytes and neurons) that form the bulk of the cells within the tumor resulting in intra-tumoral heterogeneity (reviewed by Chen *et al*, 2010 [38]). Glioblastoma cells may convert to GSLCs through a dedifferentiation process induced by epigenetic changes that cause phenotypic plasticity [39]. This interconversion between non-stem and stem state suggests further heterogeneity, making the treatment of glioblastoma tumors much more complex.

In addition to cellular heterogeneities, the molecular signatures used to classify the glioblastoma subtypes (described in section 1.2) are expressed in GSLCs to some extent [40]. Hence, GSLCs have been classified into two distinct sub-groups as proneural or mesenchymal GSLCs [40]. The proneural GSLCs are reportedly similar to fetal neural stem cells while the mesenchymal GSLCs correspond to adult neural stem cells (reviewed by Morokoff *et al*, 2015 [41]). Mesenchymal GSLCs are associated with a worse outcome as they are more resistant to radiation and display an invasive phenotype [42]. They usually occur (*de novo*) in primary glioblastomas while proneural GSLCs are mostly found in Grade III gliomas and secondary glioblastomas (reviewed by Nakano *et al*, 2015 [43].

GSLCs promote therapeutic resistance by their activation of the DNA damage response, which means they are rapidly able to recover from genotoxic stress and thus, contribute to the recurrence of glioblastoma [44-46]. Besides, the chemoresistance of CSCs has been reported in other tumor types and attributed to

increased expressions of ABC (ATP binding cassette) transporters that pump out chemotherapeutic agents [35, 47, 48]. This may suggest that GSLCs are more resistant to chemotherapy than non-stem glioblastoma cells [49].

Apart from conferring therapeutic resistance, GSLCs may also promote tumor angiogenesis owing to their expression of vascular endothelial growth factor (VEGF) [50]. The expression of VEGF is reportedly higher in GSLCs than in non-stem glioblastoma cells indicating a greater angiogenic potential [35]. Further, it was shown that VEGF promoted stem-like phenotypes which eventually enhanced the tumor progression and therapeutic resistance of GSLCs in glioblastomas [51-53].

Therefore, a successful therapy against GSLCs in glioblastoma would aim to secondarily inhibit angiogenesis and lower the DNA damage response as shown in Figure 3.

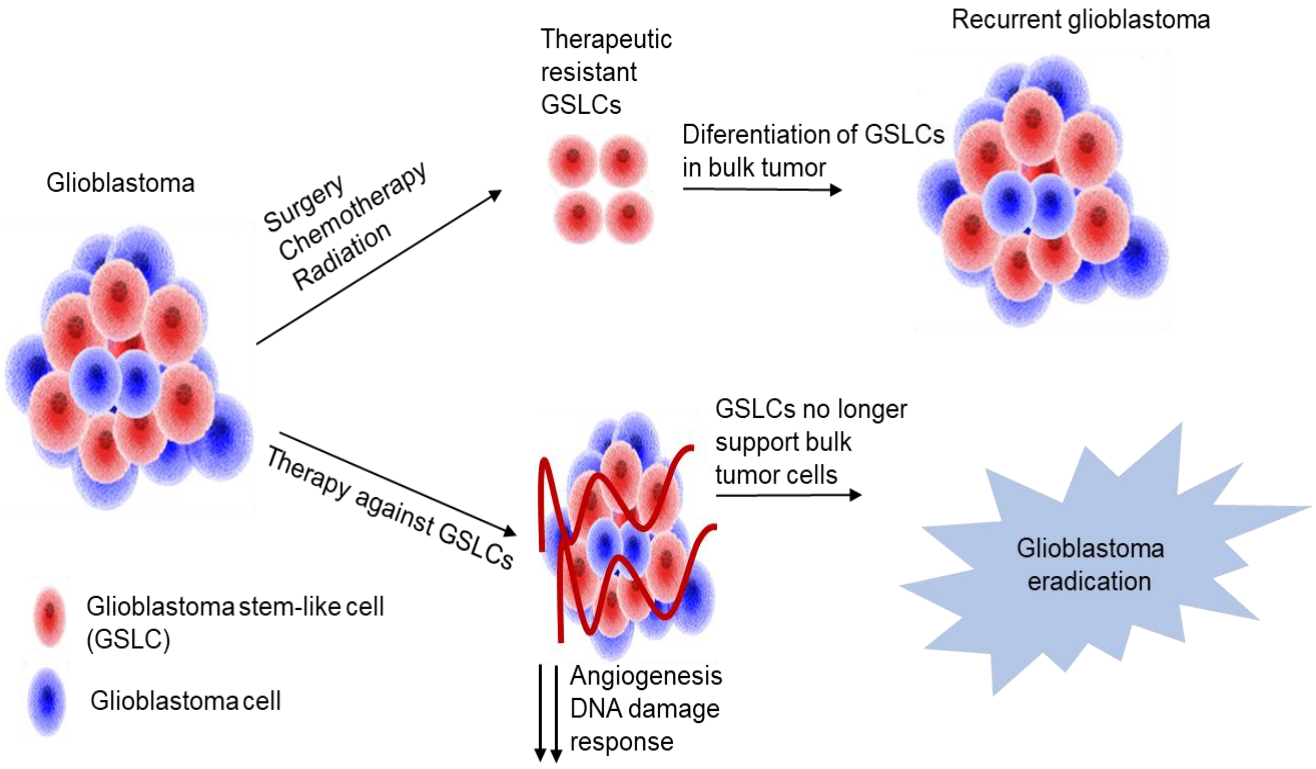

Figure 3: Schematic overview of glioblastoma stem-like cells (GSLCs) in glioblastoma therapy. Residual GSLCs that are resistant to the conventional therapy will lead to recurrence of the tumor while a therapy against GSLCs in glioblastoma will lead to its eradication. Arrows facing down indicate inhibition.

1.5 Molecular markers of GSLCs

GSLCs within glioblastoma can be potentially identified by their expression of molecular markers generally associated with stemness. The first GSLC marker discovered was CD133 (prominin-1 or *PROM-1*), a cell surface glycoprotein marker found on plasma membrane projections [54, 55]. A pioneering study revealed that a few CD133 positive ($CD133^+$) human brain tumor cells were able to initiate a phenocopy of the original tumor when injected into immunodeficient mice, while CD133 negative ($CD133^-$) tumor cells did not [56]. Other studies in glioblastoma have shown that a higher proportion of $CD133^+$ cells correlated with aggressiveness of the tumor, worse prognosis and a poor clinical outcome [57].

Recurrent glioblastomas have been reported to contain a higher percentage of $CD133^+$ cells compared to the primary tumor after radiotherapy and chemotherapy suggesting the expansion of GSLCs [58]. $CD133^+$ glioma cells are further known to accelerate the growth of tumors indicating that it plays a role in tumor recurrence and invasion [59]. All of these studies lead to CD133 been accepted as an ideal GSLC marker. However, it was subsequently demonstrated in nude rats that CD133- cells can initiate glioblastoma tumors that subsequently include CD133+ cells *in vivo* [60]. Others confirmed this finding suggesting that CD133 may not be a perfect marker for early-stage GSLCs [61, 62].

Also, it is possible that no single marker expression will be uniformly informative to identify or target GSLCs due to heterogeneity within the tumor stem cell populations and their resultant expression of different markers (reviewed by Lathia *et al*, 2015 [63]). Several other markers expressed in GSLCs have been identified and categorized based on their cellular location. These include surface markers such as CD15, CD44 and L1CAM; cytoskeletal proteins such as Nestin; transcription factors such as SOX2, OLIG2, OCT4 and NANOG and the cytosolic enzyme ALDH1A1 [35].

1.5.1 CD44

CD44 is a cell surface glycoprotein receptor for the extracellular matrix component glycosaminoglycan hyaluronan (HA) [64]. It has multiple isoforms and is expressed in numerous tissues during development (reviewed by Sneath *et al*, 1998 [65]). CD44 has been associated with pathological activities of cancer cells including cell differentiation, migration, angiogenesis, cellular adhesion and cytokine release [65,

66]. Paradoxically, even though increased expression of CD44 correlates with an increased risk for recurrence of mesenchymal-derived sarcomas [67], high CD44 expression is associated with a better outcome in thyroid cancer [68], ovarian cancer [69], non-small-cell lung cancer [70] and soft tissue sarcomas [67]. This may be due to the studies reporting different variant isoforms or epitopes of CD44, indicating that more research is needed to determine its precise role in the pathology of different cancers.

Nonetheless, it has been shown that glioblastoma cell lines express a higher level of CD44 variants (e.g. CD44s) compared to lower grade astrocytomas suggesting CD44 may be responsible for invasiveness [71, 72]. Further, the inhibition of CD44 by the *in-vivo* treatment with anti-CD44 monoclonal antibody in rats prevented the progression of highly invasive glioblastomas [73]. Thus, CD44 can be considered a GSLC marker as it is co-expressed with other stem cell markers and could be a therapeutic target to minimize tumor progression [74, 75].

1.5.2 Nestin

Nestin is a class VI intermediate filament that was first identified in the cytoplasm of neuroepithelial stem cells [76]. It is not only localized in the cytoplasm, but also present in the nuclei and the cell surface [77, 78]. The expression of Nestin in glioblastoma is associated with the self-renewal capacity of GSLCs, differentiation into progenitor cells, aggressive growth, proliferation, migration, angiogenesis and cytoskeletal organization (reviewed by Tang *et al*, 2021 [79, 80]). These characteristics implicate Nestin as a putative GSLC marker while its co-expression with other GSLC markers may suggest a specific stem-like phenotype [81]. For instance, the increased co-expression of Nestin and CD133 stem cell markers was proposed as an indicator for the aggressiveness and invasiveness of glioblastoma as well as low survival rates of patients [81].

Staberg *et al* reported that colony formation capacity was reduced by downregulating the expression of Nestin through the induction of cellular differentiation (by culture in serum) in glioblastoma neurospheres containing GSLCs [82]. Thus, targeting the GSLC marker Nestin may supress the proliferation of the tumor to improve prognosis and clinical outcome.

1.5.3 SOX2

SOX2 (Sex-determining region Y (SRY)-box 2) is a transcription factor that regulates embryonic development and plays important roles in the maintenance of neural stem cells in adults [83]. SOX2 is also involved in the maintenance of many other cancer stem cell types including GSLCs [35]. Schmitz *et al* first found that SOX2 is overexpressed in glioblastoma at the mRNA and protein level compared to normal brain tissue [83]. This study also reported that the SOX2 expression was restricted to the nuclei of the glioblastoma cells tested. Over the years, subsequent studies have confirmed the overexpression of SOX2 in glioblastoma tumor biopsies and its role in regulating the activity of GSLCs [84, 85].

Along with other transcriptional factors such as OCT-4 and NANOG, high SOX2 expression correlates with the aggressiveness and progression of glioblastoma [86, 87]. Further, SOX2+ glioblastoma cells co-expressing CD133 are more resistant to radiotherapy and standard chemotherapy with TMZ compared to SOX2- glioblastoma cells [45]. These findings implicate SOX2 as a potential target to eliminate GSLCs within glioblastoma. Indeed, experimental downregulation of SOX2 in GSLCs results in the loss of their self-renewal properties, reduced migratory and invasive behaviour, and can lead to cell cycle arrest [88-91].

The transcriptional factors POU3F2, SALL2 and OLIG2 are also essential for the propagation of glioblastoma [92]. All four factors (POU3F2, SALL2, OLIG2 and SOX2) may work together to activate regulatory elements involved in stemness and are able to fully reprogram differentiated glioblastoma cells into induced GSLCs that closely resemble the native GSLCs from humans [92]. Taken together, this evidence shows that SOX2 is required for the maintenance of GSLCs in glioblastoma and could be a suitable therapeutic target against the GSLC population.

1.5.4 ALDH1A1

ALDH (Aldehyde dehydrogenase) is a superfamily of enzymes with various isoforms that are differentially localised in the cytosol, nucleus and mitochondria (reviewed by Ma *et al*, 2011 [93]). The ALDH1 cytosolic isoform has been proposed as a functional universal stem cell marker for the isolation and identification of CSCs in breast cancer [94] with its increased activity associated with poor prognosis and low survival rates [93].

ALDH1 was suggested as a GSLC marker in human glioblastomas [95] while its increased expression has been linked to the pathogenesis of glioblastoma and poor overall survival [96]. It was also demonstrated that 99% of glioblastoma cells from human tumors tested showed ALDH1A1 expression in up to 49% of the tumor cells [97].

Schäfer et al. showed that ALDH1A1 contributes to the resistance of glioblastoma to TMZ [98]. They also showed that the inhibition of ALDH1A1 could sensitize glioblastoma cells to TMZ treatment by increased cytotoxicity, reduced colony formation and induced cell cycle arrest. The same group also showed that ALDH1 expressing glioblastoma cells efficiently form neurospheres, a feature indicating stem cell capacity [95]. As a result, ALDH1A1 is proposed to be a potential target for the treatment of glioblastoma.

1.6 Histone deacetylases in the pathogenesis of glioblastoma

The development of cancers such as glioblastoma is linked to epigenetic changes that include DNA methylation and post-translational histone acetylation. Of particular interest is the modification by histones by acetylation or deacetylation that alters the chromatin structure to regulate the expression of genes (reviewed by Mottamal *et al*, 2015 [99]). This process is controlled by the opposing activities of two groups of enzymes; the Histone acetylases (HATs) and the Histone deacetylases (HDACs) as shown in Figure 4.

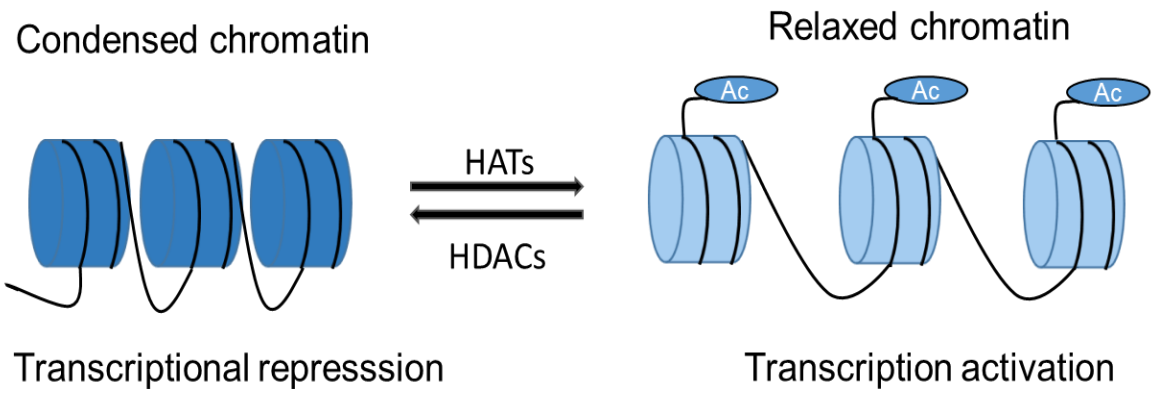

Figure 4: Regulation of histone acetylation by HATs and HDACs. The chromatin structure comprises of nucleosomes formed by DNA (black line) wrapped around histones. Histone acetyltransferase (HATs) add acetyl groups (Ac) onto histone tails to relax the chromatin and

activate gene transcription. Histone deacetylases (HDACs) remove the Ac to condense the chromatin and repress transcription.

HATs add acetyl groups to lysine residues on histones to relax the chromatin structure and activate transcription, while HDACs remove the acetyl group to condense the chromatin structure, repress transcription and silence gene expression (reviewed by Mottamal *et al*, 2015 [99]). An imbalance in the activities of HATs and HDACs contributes to the pathogenesis of cancers including glioblastoma (reviewed by Bezecny *et al*, 2014 [100]).

The increased activity of HDACs in glioblastoma enhances the repression of tumor regulatory genes such as $P21^{WAF1/Cip1}$ [101]. In addition, HDACs not only target histones, but also non-histone proteins such as the transcription factors P53 and NF-kB, the DNA repair enzyme Ku70, hypoxia-inducible factor 1α (HIF-1α), the chaperone Hsp90, α-tubulin, the estrogen and androgen receptors and the signaling mediators (Stat3, Smad7) [99, 102-104]. With HDACs being involved in multiple signaling pathways and overexpressed in glioblastoma, inhibiting their activity can lead to the re-expression of silenced regulatory genes [105]. Hence, HDAC inhibitors have developed as promising therapeutic agents against glioblastomas [100].

1.6.1 HDAC inhibitiors and anti-tumor mechanisms

HDAC inhibitors (HDACis) are small molecule drugs that can inhibit the activity of HDACs by binding the Zn^{2+} pocket that is required for their catalytic action [100]. HDACis have been classified into seven groups based on their targets and chemical structure as; Hydroxamic acid, Benzamides, cyclic peptides, short-chain fatty acids, electrophilic ketones, sirtuin inhibitors and miscellaneous (reviewed by Chen *et al*, 2020 [105]).

HDACis can inactivate various signaling pathways that would in turn inhibit the proliferation of tumor cells through the induction of cell cycle arrest, differentiation, autophagy and either the intrinsic (mitochondrial) or extrinsic (death receptor) apoptotic pathways [106]. These anticancer effects observed with HDACis has led to four of them being approved by the US Food and Drug Administration (FDA) for the treatment of haematological malignancies. The first drug to be approved for the treatment of cutaneous and/or peripheral T-cell lymphoma (CTCL/PTCL) was the hydroxamic acid SAHA (suberanilohydroxamic acid) also known as vorinostat (reviewed by Duvic *et al*,

2007 [107]). This was followed by the approval of the cyclic peptide Romidepsin, and the hydroxamic acids Belinostat and panobinostat [105].

In glioblastoma studies, several HDACis can reportedly cross the BBB to exert anti-tumor effects. For instance, the HDACi trichostatin A (TSA) upregulated the cell cycle inhibitor $p21^{Waf1/Cip1}$ to induce cell cycle arrest in glioblastoma cells [108]. In addition, HDACis such as romidepsin, belinostat and phenylbutyrate increased the levels of proapoptotic genes such as Bad, Bax, Puma and Bim while they decrease the anti-apoptotic genes Bcl-xl and Bcl-2 in glioblastoma cell lines [109]. Additionally, HDACis block angiogenesis by inhibiting VEGF or by impairing vasculogenic mimicry in glioblastoma cells [110, 111]. HDACis can also potentiate damage to the DNA by increasing reactive oxygen species (ROS) through the downregulation of thioredoxin (Trx) that removes ROS, or upregulation of thioredoxin binding protein-2 (TBP-2) that blocks Trx [112].

A more profound anti-tumor effect of HDACis in glioblastoma is their ability to target CSCs in glioblastoma [113]. For example, Chiao *et al* showed that the HDACi SAHA inhibited the growth of GSLCs (*in-vivo*) by inducing autophagy, reducing their proliferation rates and promoting their differentiation [114]. Alvarez *et al* also showed that the HDACis TSA and valproic acid (VPA) were capable of reducing proliferation rates and stem cell marker expression in glioblastoma-derived stem cells [115].

Preclinical studies in glioblastoma have shown that HDACis are promising anti-glioblastoma agents but appear to have a limited efficacy as a single agent [116]. This was evident when clinical trials of glioblastoma revealed that treatment with HDACis did not improve survival [117]. The full therapeutic potential of HDACis in glioblastoma may possibly be achieved when combined with other cytotoxic agents such as ionizing radiation and other chemotherapeutic drugs (reviewed by Suraweera *et al*, 2018 [116]). Therefore, several HDACi combination therapies are ongoing in preclinical studies with some already in clinical trials in recurrent and newly diagnosed glioblastomas [105]. The HDACis in preclinical studies of glioblastoma are MS-275, trichostatin A and FK228 while those that have also entered clinical studies are SAHA, Panobinostat, Valproic acid (VA) and Belinostat [105].

In summary, the various anticancer effects of HDACis in glioblastoma are shown in Figure 5 and illustrates why HDACis were used in this study.

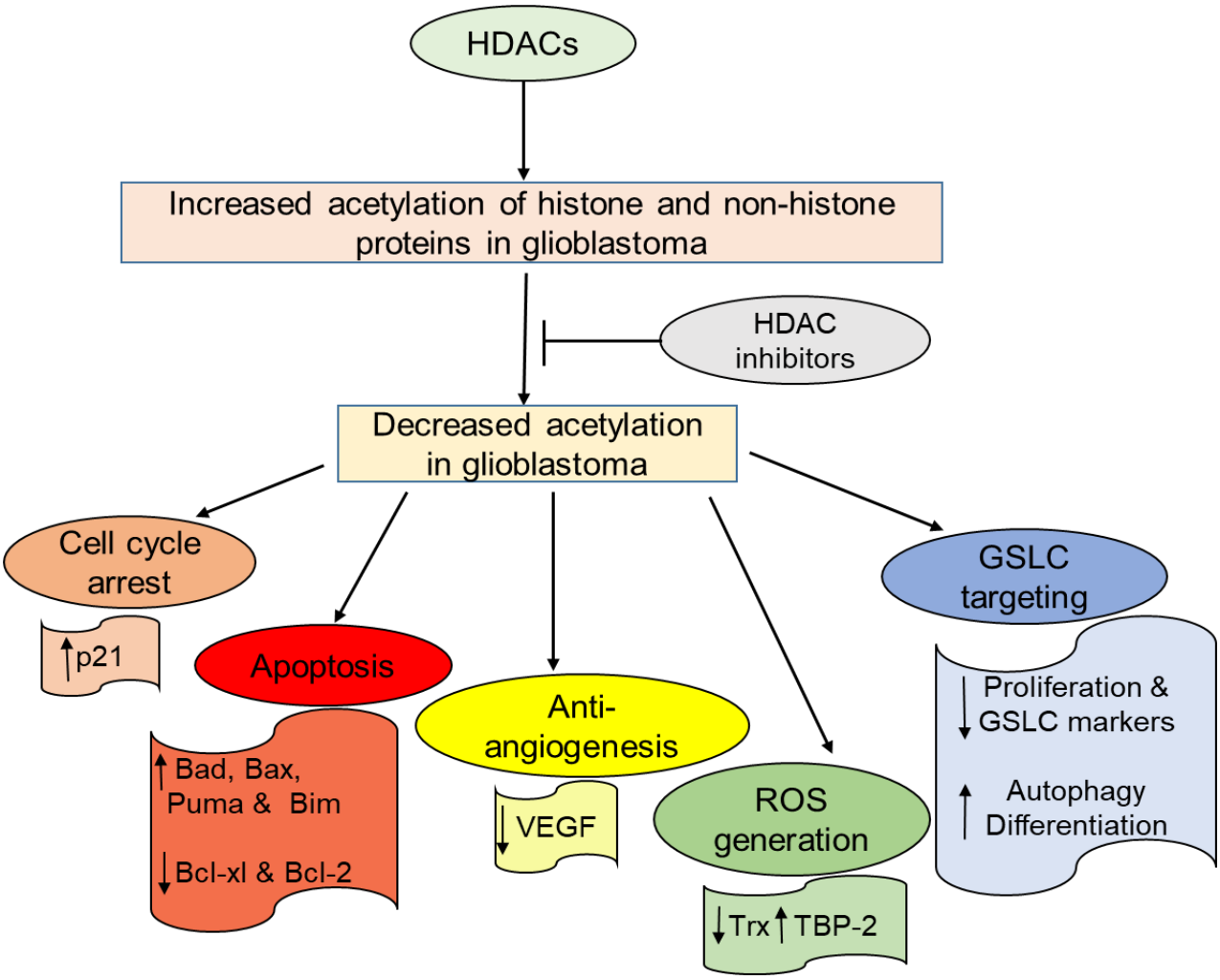

Figure 5: Effects of HDAC inhibitors (HDACis) on glioblastoma cells. The various antitumor pathways induced by HDACis are shown. Arrows pointing upwards represent upregulation while arrows pointing downwards represent downregulation. Modified from [99]**.**

1.6.1.1 The HDAC inhibitor MS-275

MS-275, also known as Entinostat, is a benzamide that selectively inhibits the class I HDACs. Eyupoglu *et al*. identified MS-275 as a promising chemotherapeutic through its ability to induce cell cycle arrest by upregulating $p21^{WAF1/Cip1}$ in glioblastoma cells [118]. The treatment with MS-275 also reduced the growth of glioblastoma cell lines *in vitro* in a concentration dependent manner and induced apoptotic cell death. In addition, the ability of MS-275 to cross the BBB was demonstrated by the increased protein levels of acetylated Histone H3 in brain tissue of syngeneic rats after intratumoral injection. This was confirmed by another study suggesting MS-275 as a potent brain-region selective HDACi [119].

More striking is the ability of MS-275 to reduce the GSLC marker ALDH and inhibit sphere formation in glioblastoma-derived neurospheres [120]. This suggests that MS-275 may have the ability to target GSLCs in glioblastoma.

In combination studies, a phase I clinical study reported that MS-275 was well tolerated either as a single or combined agent with other cytotoxic therapies [121]. MS-275 has been indicated as a potent radiosensitizer of glioblastoma cell lines that was demonstrated by an inhibition of DNA repair after a combined treatment with 5 Gy X-ray irradiation [122]. Further, MS-275 synergizes with other chemotherapies including TMZ, doxorubicin, etoposide and cisplatin to induce apoptosis in glioblastoma cells [123]. The ability of MS-275 to sensitize glioblastoma cells to receptor tyrosine kinase inhibitors (RTKi) has also been reported [124].

1.7 MAPK signaling in glioblastoma

The mitogen-activated protein kinase (MAPK) signaling pathway is one of the dysregulated pathways that plays a role in the initiation and progression of glioblastoma. By highlighting its main regulators, it is also known as the Ras-Raf-MEK-ERK pathway (reviewed by Fremin *et al*, 2010 [125]).

The MAPK signaling can be activated via intrinsic or extrinsic stimulations by growth factors (GFs) and cytokines that act through receptor tyrosine kinases (RTKs), cytokine receptors or G protein-coupled receptors [125]. Once the cells receive these stimuli at the plasma membrane, autophosphorylation of receptor tyrosine residues occurs, which activates Ras through the binding of guanine triphosphate (GTP) [125]. The activated GTP-Ras activates Raf kinases that undergo a series of phosphorylation events. The triggered Raf then functions as MAP Kinase Kinase Kinase (MAPKKK) which activates MAP Kinase Kinase (MAPKK or MEK1/2) to finally activate MAPK (or ERK) [125]. All activation is by phosphorylation, thus MAPK activation phosphorylates nuclear and cytoplasmic substrates to initiate cellular processes that drive the proliferation, growth, differentiation and survival of glioblastoma cells [125]. The Ras-Raf-MEK-ERK pathway also results in the activation of HIF1α to induce VEGF and promote angiogenesis [126]. Overall, the Ras-Raf-MEK-ERK pathway is summarised in Figure 6.

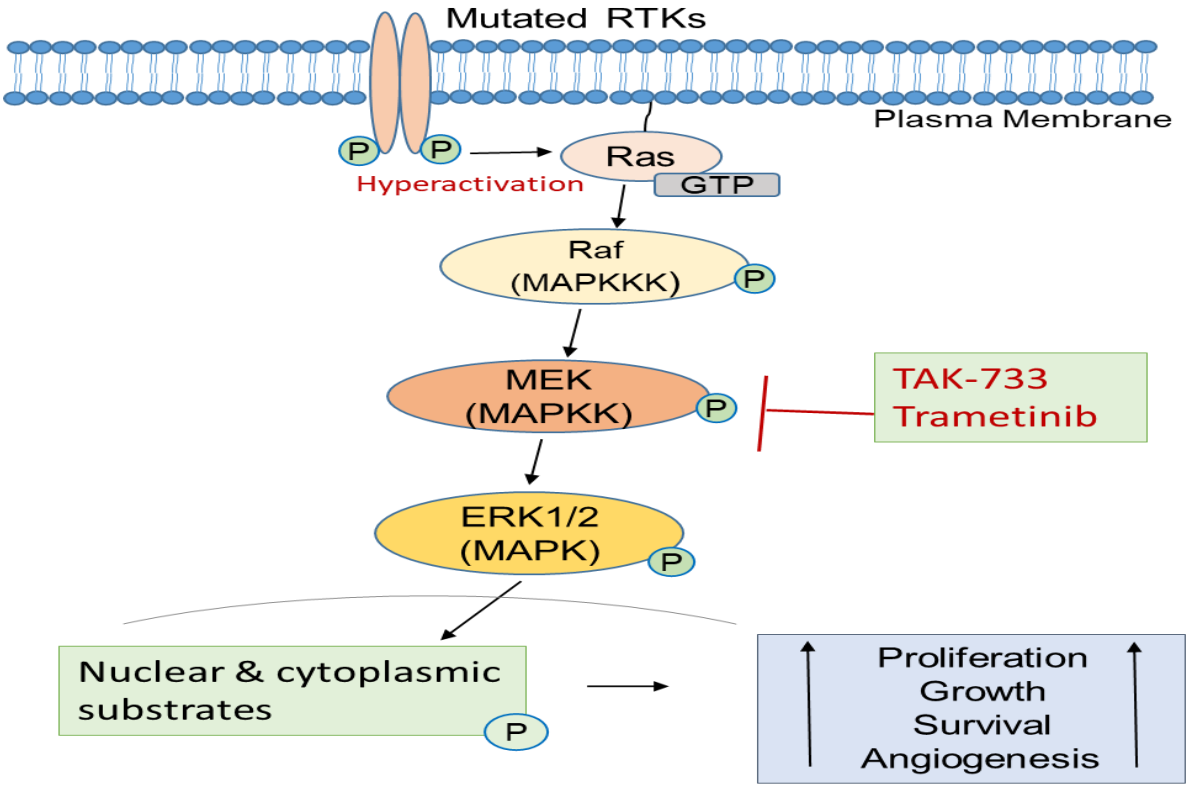

Figure 6: Overview of MAPK signaling. Stimulations of mutated RTKs at the plasma membrane leads to hyperactivation of downstream autophosphorylation events that activates MAPK. Activated MAPK phosphorylates nuclear and cytoplasmic substrates to drive cellular processes that promote survival of GSLCs in glioblastoma. The MEK inhibitors TAK-733 and trametinib stop downstream MAPK activation.

The activating mutation or overexpression of membrane RTKs such as EGFR and PDGFR in glioblastoma leads to the hyperactivation of the MAPK cascade [127]. Hence, most glioblastomas contain high levels of phosphorylated (activated) MAPK (p-MAPK) that has now become a prognostic marker for poor overall survival as well as an indicator of tumors that are resistant to radiotherapy [128]. Mutations of MAPK in glioblastoma are associated with highly invasive and proliferative phenotypes as they regulate proliferation and metastases [129]. Further, MAPK signaling also drives the proliferation and survival of GSLCs (reviewed by Bayin *et al*, 2014 [130]). This suggests that inhibiting MAPK activation could hinder the progression of GSLCs in glioblastoma. One way to do this is by inhibiting MAPKK (MEK), the direct activator of MAPK.

1.7.1 MEK inhibitory drugs

The development of MEK inhibitors (MEKi) to block the MAPK pathway has been researched for the treatment of cancers including glioblastoma with promising results

reported (reviewed by Cheng *et al*, 2017 [131]). Some of the MEK inhibitors that have shown anti-tumor effects include TAK-733, selumetinib, trametinib and cobimetinib [131]. In this study, the MEKi TAK-733 and trametinib were used as illustrated in Figure 6.

1.7.1.1 TAK-733

TAK-733 is a small molecule inhibitor that selectively binds and inhibits the activity of MEK [132]. It is an allosteric inhibitor of MEK that is orally bioavailable and non-ATP-competitive. TAK-733 has not been fully explored in glioblastoma studies but has shown antitumor activities in several cancers, xenograft mouse models and has advanced to phase I clinical trials [133, 134]. Some anticancer effects of TAK-733 include reduced proliferation, induction of cell cycle arrest, apoptotic cell death and reduced tumor growth *in vivo* [135, 136].

TAK-733 demonstrated a safety profile and an efficient MAPK inhibition in the phase I clinical study of patients with uveal melanoma, colon cancer and cutaneous melanoma. However, only limited antitumor activity as a single agent was reported [132]. This suggested TAK-733 could be more potent when combined with other anticancer agents. Recently, it was shown that TAK-733 synergized with radiation to lower the migratory potential of breast cancer cells compared to either alone [133]. Apart from radiation, TAK-733 is also reported to synergize with proteasome and PI3K inhibitors to overcome chemoresistance in multiple myeloma [135]. Therefore, the antitumor effect of TAK-733 may be enhanced when combined with other cytotoxic agents and should be further explored.

1.7.1.2 Trametinib

Trametinib, also known as GSK1120212, is the first MEKi approved by the FDA for the treatment of melanoma [131]. Like TAK-733, it is a non-competitive allosteric inhibitor of MEK. Preclinical studies of trametinib showed its efficacy to inhibit tumor growth *in vivo* in a concentration dependent manner [131]. In clinical studies of melanoma, trametinib as a single agent significantly improved progression free survival and overall survival compared to the standard chemotherapy [137].

The FDA and Europeans Medicine Agency (EMA) have approved the combination of trametinib and the BRAF inhibitor debrafenib for the treatment of BRAF-mutant

unresectable or metastatic melanoma. This was based on results from a phase III trial that showed an improved overall survival compared to dabrafenib alone [138]. Recently, the combination of trametinib and dabrafenib was further investigated in a phase II trial of patients with BRAF-mutant non-small cell lung cancer (NSCLC) [139]. The results showed that there was an improved overall response rate and a prolonged progression free survival compared to the dabrafenib group only.

More recently in brain tumor studies, trametinib is being investigated in a phase II trial of patients with pediatric low-grade gliomas (PLGG) or plexiform neurofibroma (PN) [140]. Other institutional investigations have suggested trametinib as an effective treatment for patients with recurrent or progressive PLGG [141, 142].

Generally, trametinib has shown good safety profile as both monotherapy and combination therapy, thus its efficacy in other treatment combinations for aggressive tumors such as glioblastoma should be explored.

1.8 Combination treatment of tumors with HDACi and MEKi

Combination therapy using HDAC and MEK inhibitors has emerged as a chemotherapeutic strategy for the treatment of many cancers with favourable results reported. This was because of an *in vitro* study that showed that MEKi sensitized human colon, lung and prostate cancer cells to HDACi-induced cell death [143]. This study combined the MEKi PD184352 and the HDACi HC-toxin and reported that the cancer cell death was enhanced compared to either compound alone. Since then, other groups have confirmed this enhanced cell killing effect by testing the combination of other types of HDAC and MEK inhibitors on pancreatic cancer cells, prostate cancer cells and human tumor xenograft models [144-146].

The HDACi MS-275 has been tested in combination with several MEK inhibitors as a combination treatment of cancer. For instance, the MEK inhibitors PD184352 and AZD6244 enhanced the efficacy of MS-275 to supress tumor growth in human colon and lung tumor xenograft models [146]. Also, the combination of MS-275 with the MAPK pathway inhibitor sorafenib has entered a phase I trial of patients with solid tumors or acute myeloid leukemia (AML) [147].

In brain tumor studies, combination of the HDACi sodium butyrate (NaB) and MEKi U0126 impaired the survival of Medulloblastoma cells more efficiently than either inhibitor alone [148]. A phase II study of patients with recurrent high-grade glioma is currently ongoing testing the triple combination of sofranib with the HDACi Valproic acid and sildenafil (NCT01817751). This combination is based on the predicted ability of sorafenib to enhance the activity of valproic acid while the addition of sildenafil is based on its ability to block ABC drug efflux pumps to increase the drug concentrations in the brain.

1.9 Hypothesis

Overall, the evidence provided from preclinical and clinical studies suggest that combining HDAC and MEK inhibitors offers a new therapeutic approach to treat aggressive cancers such as glioblastoma. However, the effect of this combination together with radiation has not been explored in glioblastoma. Moreover, it is not known if this combination of HDAC and MEK inhibition plus radiation is effective against the resistant GSLC population. In this study, we used MS-275 as the HDACi and TAK-733 or trametinib as the MEKi because of their activities against HDACs and MEK.

Therefore, the main hypothesis of this study proposes that the combination of a HDACi (MS-275) and a MEKi (TAK-733 or trametinib) together with radiation treatment will be more effective than the current standard therapy by targeting highly resistant GSLCs in glioblastoma.

To test this hypothesis, we have:

I. Identified the GSLC markers expressed in the glioblastoma cell lines and determined the effect of radiation on their expression.

II. Experimentally enriched the GSLC population by glioblastoma cell line culture as spheres in serum free medium.

III. Analysed the sphere forming ability of the GSLCs-enriched spheres after combined radiochemotherapy.

IV. Analysed the expression of GSLC markers at the protein and RNA level after the combined radiochemotherapy.

2 MATERIALS

2.1 Antibodies

2.1.1 Primary antibodies for immunoblotting

Target Protein	Target Molecular weight (kDa)	Antibody	Catalog number	Dilution used	Company
Actin	42	Mouse	A5441	1:20000	Sigma Aldrich, Steinheim, Germany
ALDH1A1	55	Rabbit	PA5-32127	1:500	Thermo Fisher Scientific, Rockford, USA
CD133	97	Rabbit	Ab16518	1:500	Abcam, Cambridge, UK
CD44	80	Mouse	3570s	1:1000	Cell Signaling Technology, Danvers, MA, USA
Nestin	250	Mouse	MA1-110	1:500	Thermo Fisher Scientific, Rockford, USA
SOX2	35	Rabbit	3579s	1:500	Cell Signaling Technology, Danvers, MA, USA
MAPK	42/44	Rabbit	9101	1:1000	Cell Signaling Technology, Danvers, MA, USA
pMAPK	42/44	Rabbit	9102	1:1000	Cell Signaling Technology, Danvers, MA, USA
Histone-H3	17	Rabbit	9677	1:500	Cell Signaling Technology, Danvers, MA, USA
Acetyl-H3	17	Rabbit	4499	1:500	Cell Signaling Technology, Danvers, MA, USA

2.1.2 Secondary antibodies for immunoblotting

Secondary antibodies	Origin	Catalog number	Dilution used	Company
Goat anti-mouse	Goat	A16066	1:20000	Invitrogen, MD, USA
Goat anti-rabbit	Goat	A16096	1:20000	Invitrogen, MD, USA

2.1.3 Primary antibodies for immunoflourescent staining

Target Protein	Antibody	Catalog number	Dilution used	Company
ALDH1A1	Rabbit	36671	1:100	Cell Signaling Technology, Danvers, MA, USA
CD44	Mouse	3570s	1:400	Cell Signaling Technology, Danvers, MA, USA
CD133	Rabbit	Ab16518	1:100	Abcam, Cambridge, UK
Nestin	Mouse	MA1-110	1:100	Thermo Fisher Scientific, Rockford, USA
SOX2	Rabbit	3579s	1:300	Cell Signaling Technology, Danvers, MA, USA

2.1.4 Secondary antibodies for immunoflourescent staining

Secondary antibodies	Colour	Catalog number	Dilution used	Company
Alexa flour 488 (Goat-anti-mouse)	Green	A11029	1:200	Life Technologies, OR, USA
Cy3 (Goat anti-rabbit)	Red	A10520	1:300	Life Technologies, OR, USA

2.1.5 Antibodies for flow cytometry

Target Protein / Controls	Flourophores	Catalog number	Company
ALDH1A1	FITC	LS-C251174-200	LifeSpan Biosciences, USA
Nestin	APC	MA5-23650	Thermo Fisher scientific, Darmstadt, Germany
SOX2	PerCP-cy 5.5	561506	BD Biosciences, USA
Isotype control	PerCP-cy 5.5	550795	BD Biosciences, USA
CD44	BV 785	103041	Biolegend, CA, USA
Live/dead staining	Zombie aqua	423102	Biolegend, CA, USA

2.2 Buffers and solutions

0.2% Triton X (permeabilization buffer)

Triton X 100	2 ml
PBS	to 998 ml

Antibody Blocking solution (immunofluorescence staining)

1% BSA	10 g
0.15% Glycin	1.5 g
PBS	to 1 L

4% Paraformaldehyde (PFA) fixative

PFA	4 g
PBS	200 ml

1M Tris pH 8.8/6.8

Tris base	121.1 g
Distilled water	to 1 L
HCL	volume to adjust pH

10% Sodium dodecyl sulfate (SDS; for gel preparation)

SDS	10 g
Distilled water	add to 100 ml

10% Ammonium persulfate (APS; for gel preparation)

APS	10 g
Distilled water	add to 100 ml

FACS Buffer (wash buffer for flow cytometry)

0.5% BSA	2.5 g
PBS	add to 500 ml

Towbin Buffer (for transfer of separated proteins)

Tris base	3.03 g
Glycine	14.4 g
Distilled water	700 ml
Methanol	200 ml
Distilled water	up to 1 L

10X TBS-T (Tris-buffered saline, 0.1% Tween 20; 1X as washing buffer)

Tris	4.24 g
Tris-HCL	26 g
NaCl	80 g
Distilled water	to 1 L
Tween 20	10 ml

10X Running Buffer (1X for electrophoresis run)

Tris base	121.1 g
Glycine	576 g
Distilled water	to 4 L
20% SDS	200 ml

Ponceau-S-Red Solution (for protein band visualization)

Ponceau-S-Red	0.2% w/v
Acetic acid	0.5% v/v
Distilled water	to 500 ml

2.3 Chemicals and Drugs

Chemicals	Company
APS (Ammonium persulfate)	EMD Millipore, Darmstadt, Germany
Bovine serum albumin (BSA)	Sigma-Aldrich, Steinheim, Germany
Compensation beads	BD Biosciences, San Diego, USA
DMSO (Dimethyl sulfoxide)	Sigma-Aldrich, Steinheim, Germany
FBS (Fetal bovine serum)	Bio&Sell, Neuherberg, Germany
Glycine	EMD Millipore, Darmstadt, Germany
Milk powder	Roth, Karlsruhe, Germany
Paraformaldehyde (PFA)	Sigma-Aldrich, Steinheim, Germany
Phosphatase inhibitor cocktail (PhosSTOP)	Roche, Mannheim, Germany
Phosphate Buffered Saline (PBS)	Merck, Darmstadt, Germany
Protease inhibitor cocktail	Roche, Mannheim, Germany
SDS (Sodium dodecyl sulfate)	Serva, Heidelberg, Germany
ServaGel (4-12%)	Serva, Heidelberg, Germany
TEMED (Tetramethylethylenediamine)	Roth, Karlsruhe, Germany
Tissue Protein Extract Reagent (T-PER^{TM})	Thermo Fisher Scientific, Rockford, USA
Tris-base	EMD Millipore, Darmstadt, Germany
Triton X	AppliChem Biochemica, Darmstadt,
Trypsin-EDTA 0.05%	Life Technologies, Darmstadt, Germany
Vectashield mounting medium + DAPI	Biozol, Eching, Germany

Drugs	Catalog number	Company
MS-275	S1053	Selleck Chemicals, Houston, TX, USA
TAK-733	S2617	Selleck Chemicals, Houston, TX, USA
Temozolomide	SC-203292	Santa Cruz Biotechnology, Dallas, TX, USA
Trametinib	S2673	Selleck Chemicals, Houston, TX, USA

2.4 Commercial kits

Commercial Kit	Company
ECL™ Select Western Blotting Detection	GE Healthcare, Little Chalfont, UK
Pierce™ BCA protein assay kit	Thermo scientific, Rockford, USA
Precision Plus ProteinTM Standard	Bio-Rad Laboratories, Munich, Germany
CellTiter-Glo® Luminescent Cell Viability Assay	Promega, Madison, WI, USA
Foxp3/transcription factor staining Buffer set	Thermo Fisher Scientific, Darmstadt, Germany
PowerUp™ SYBR™ Green Master Mix	Thermo Fisher Scientific, Vilnius, Lithuania
RT² First Strand kit (50)	Qiagen, Maryland, USA
RT² SYBR Green ROX qPCR	Qiagen, Hilden, Germany
Custom RT2 PCR Array - 96 well	Qiagen, Hilden, Germany
QuantiTect® Reverse Transcription Kit	Qiagen, Hilden, Germany
Maxwell® 16 miRNA Tissue Kit	Promega, Madison, WI, USA
MycoAlert Detection Kit	Lonza Group Ltd., Basel, Switzerland

2.5 Consumables

Consumables	Company
12-well, 96-well ultra-low attachment plates	Corning, NY, USA
25 cm^2, 75 cm^2 ultra-low attachment flasks	Corning, NY, USA
1.5 ml, 2.0 ml Reaction tubes	Eppendorf, Hamburg, Germany
0.2 ml PCR single cap tubes	Biozym, Hessisch Oldendorf, Germany
96-well plates	Applied Biosciences, Woolston, UK
96-well White opaque Tissue Culture Plate	Corning Incorporated, Wiesbaden, Germany
T75, T175 Culture flasks	Greiner Bio-one GmbH, Frickenhausen, Germany
15 ml, 50 ml Reaction tubes	Greiner Bio-one GmbH, Frickenhausen, Germany
Pipettes glass 1, 5, 10, 25, 50 ml	Sigma-Aldrich, Taufkirchen, Germany
Eppendorf tubes	Greiner Bio-one GmbH, Frickenhausen, Germany
Cell scraper 25 cm	Sarstedt. Inc., Nuembrecht, Germany
Cryotube™ vials (1 ml)	Kisker Biotech GmbH, Steinfurt, Germany
FACS tubes with cell strainer caps	Corning, NY, USA
Filter papers	Bio-rad, Carlifonia, USA
Nitrocellulose blotting membrane, AmershamTM ProtranTM 0.2 µm	GE Healthcare, Munich, Germany
PCR 96-well TW-MT-Plates	Biozym, Hessisch Oldendorf, Germany
Adhesive clear qPCR seal	Biozym, Hessisch Oldendorf, Germany
Glass cover slips	VWR, Darmstadt, Germany
Microscope slides	Thermo scientific, Rockford, USA
Nunclon™ Delta surface (96-well plates)	Thermo scientific, Rockford, USA
Slide chamber	Sarstedt, Nümbrecht, Germany

2.6 Equipment

Equipment	Company
X-Strahl RS225 radiation device	X-Strahl LTD, UK
Bead bath	Memmert, Schwalbach, Germany
Centrifuge Rotina 420R	Andreas Hettich, Tuttlingen, Germany
Centrifuge Eppendorf 5424R	Eppendorf, Hamburg, Germany
Centrifuge Biofuge pico	Heraeus Instruments, Osterode, Germany
Cytoflex LX	Beckman coulter, IN, USA
Dual Gel caster	Hoefer, Holliston, USA
Gel electrophoresis chamber	Hoefer, Holliston, USA
Keyence BZ 9000 Microscope	Keyence, Fankfurt, Germany
Microbiological safety cabinet (MSC)	Heraeus, Hanau, Germany
Microscope Axiovert	Zeiss, Jena, Germany
Trans-blot cell	Bio-Rad, Carlifonia, USA
Maxwell® 16 MDx instrument	Promega, Madison, WI, USA
Nanodrop spectrophotometer	PeqLab Biotechnology, Germany
Operetta Imaging System	PerkinElmer Waltham, MA, USA
Pipettes	Eppendorf, Hamburg, Germany
Rectangular glass plates	Hoefer, Holliston, USA
StepOnePlus™ Real-Time PCR System	Applied Biosystems, Darmstadt, Germany
Thermomixer	Eppendorf, Hamburg, Germany
UV-Transilluminator and gel documentation system	Alpha Innotech, Kasendorf, Germany
UV-spectrophotometer infinite M200	TECAN, Crailsheim, Germany
Z1 Coulter Particle Counter	Beckman Coulter, Krefeld, Germany

2.7 Software

Name	Company
Alpha View v. 1.2.1.0	Alpha Innotech, San Leandro, CA, USA
AxioVision AC v. 4.2	Carl Zeiss, Oberkochen, Germany
BZ-II-Analyzer v.1.0	Keyence Cooperation, Osaka, Japan
CytExpert v.2.4.0.28	Beckman coulter, IN, USA
Flowing Software v. 2.5.0	www.flowingsoftware.com
i-control v.1.10	Tecan Group, Männedorf, Switzerland
ImageJ v. 1.50i	https://imagej.net
Columbus v. 2.9.1	PerkinElmer Watham, MA, USA
StepOne™ Software v2.3	Applied Biosystems, Darmstadt, Germany
GraphPad Prism 5	www.graphpad.com/scientific-software/prism/

2.8 Cell lines

2.8.1 Human Glioblastoma cell line (A172)

The A172 human glioblastoma cell line was originally established from the glioblastoma of a 53-year-old male [149]. The Catalogue of Somatic Mutations In Cancer (COSMIC) lists 3,131 mutations of A172 cells [150] and is characterised by *PTEN* mutation and $P14^{ARF}$/*P16* deletion [151]. The cell line was supplied by Sirion Biotech, Martinsried, Germany from stock ATCC® CRL-1620™.

2.8.2 Human Glioblastoma cell line (LN229)

The LN229 glioblastoma cell line was originally established from a 60-year-old white female with right frontal parieto-occipital glioblastoma [PubMed. 10416987]. The COSMIC database lists 3,897 mutation of LN229 [150] including *TP53* mutation and $P14^{ARF}$/*P16* deletion [151]. The LN229 cells were obtained as a kind gift from the Institute of Radiation Medicine, Munich Germany from stock ATCC® CRL-2611™.

2.8.3 Human Glioblastoma cell line (U251)

The U251 glioblastoma cell line cell line was originally established from a 75-year-old male with grade III-IV astrocytoma [152]. 2,059 mutations of U251 were listed in the

COSMIC database [150] including mutations of *TP53* and *PTEN* with *P14^{ARF}/P16* deletion [151]. The cell line was donated by Sirion Biotech, Martinsried, Germany from stock ATCC® HTB-17™.

2.8.4 Human Glioblastoma cell line (U87)

The U87 glioblastoma cell line was formerly named U87-MG and is believed to be originally established from a 44-year old Caucasian female with grade IV glioma [153]. 2,008 mutations of U87-MG were listed in COSMIC database [150] while *PTEN* mutation and *P14^{ARF}/P16* deletion have been reported [151]. The cell line was provided by Sirion Biotech, Martinsried, Germany from stock ATCC® HTB-14™.

The stocks of each cell line obtained were defined as passage N + 1. The used stocks for all experiments were up to passage N + 8.

2.8.5 Glioblastoma-derived spheres

The four human glioblastoma cell lines (A172, LN229, U87 and U251) were each grown as spheres to enrich the stem-like population (hereafter named A172-sph, LN229-sph, U87-sph and U251-sph). The spheres were cultured and used after a minimum of eight passages.

2.9 Culture medium and Supplements

2.9.1 Cell lines and culture medium

Glioblastoma cells	Culture medium	Company
U87, U251, A172	Dulbecco's Modified Eagles Medium (DMEM) 1X (+ GlutaMAX + 4.5 g/l D-Glucose + Pyruvate) + 10% FBS	Gibco Life Technologies, Darmstadt, Germany
LN229	DMEM/F12 1X (+ GlutaMAX + 4.5 g/l D-Glucose + Pyruvate) + 20% FBS	Gibco Life Technologies, Darmstadt, Germany

Glioblastoma spheres	Culture medium	Company
A172-sph, LN229-sph, U87-sph, U251-sph	DMEM/F12 1X (+ GlutaMAX + 4.5 g/l D-Glucose + Pyruvate) + Penicillin-Streptomycin solution (1X) + stem cell medium supplements	Gibco Life Technologies, Darmstadt, Germany

2.9.2 Stem cell medium supplements

Name	Company
B-27 supplement (50X)	Gibco Life Technologies, Darmstadt, Germany
N-2 supplement (100X)	Gibco Life Technologies, Darmstadt, Germany
GlutaMAX supplement (100X)	Gibco Life Technologies, Darmstadt, Germany
D – (+) – Glucose solution 45% in H20 (1X)	Sigma-Aldrich, Steinheim, Germany
Fibroblast Growth factor (FGF) – Basic Human + (25 µg stock; 20 ng/mL in final medium)	Sigma-Aldrich, Steinheim, Germany
Epidermal Growth Factor, (EGF) Human + (0.5 MG stock; 20 ng/mL in final medium)	Sigma-Aldrich, Steinheim, Germany

3 METHODS

3.1 Cell culture

3.1.1 Maintenance of human glioblastoma cell lines in monolayer culture

All human glioblastoma cell lines were passaged as monolayers in tissue-culture T175 flasks. The growth medium (2.9.1) was DMEM supplemented with 4.5 g/l glucose and 10% FBS (for A172, U251, U87) or DMEM/F12 supplemented with 4.5 g/l glucose and 20% FBS (for LN229). The glioblastoma cell lines were maintained under standard cell culture conditions at 37 °C and a humidified atmosphere with 5% carbon dioxide (CO_2). The cells were monitored under a microscope and passaged once 80 - 90% confluence was reached.

To passage the cells, the spent medium was removed and the cells were rinsed with 1X PBS to remove medium. From 0.05% trypsin-EDTA solution, 2 ml was added in a dropwise manner and incubated for 5 mins to detach adherent cells. The trypsin-EDTA reaction was stopped by the addition of 8.5 ml medium. From the suspension, 0.5 ml aliquot was removed to count cells using a Z1 Coulter counter. The remaining cells were centrifuged at 300 x g for 5 mins and the supernatant discarded. The pellet was resuspended in fresh media containing serum to give a split ratio of 1:3 per 25 ml in the culture flasks.

3.1.2 Cell line authentication

To verify the identity of the glioblastoma cell lines used, a genetic profiling service performed by Eurofins, Ebersberg Germany was employed. For this, approximately 10^6 cells were pelleted and stored at -20 °C before they were sent to the company. Eurofins isolated the DNA from the samples and performed short tandem repeat (STR) profiling using the Promega PowerPlex® 21 system. This used 21 independent loci (20 STR markers and Amelogenin sex determination) from the DNA samples. The cell line profiles were then compared by Eurofins to the DSMZ STR profile database. The result showed that all the glioblastoma cell lines identified correctly.

The cell lines were also checked once for mycoplasma contamination using a MycoAlert Detection Kit according to the manufacturer's instructions.

3.1.3 Glioblastoma-derived spheres.

The human glioblastoma cell lines A172, LN229, U87 and U251 were each cultured in T75 Ultra-low attachment (ULA) culture flasks to enable sphere formation and thereby enrich the stem cell population. The stem cell medium was prepared as shown in 2.9.1 and 2.9.2. Since the biological activity of the growth factors reduces with time, they were always added immediately before use. Spent medium was changed every 2-3 days or when the medium began to change colour. The glioblastoma-derived spheres were maintained under standard cell culture conditions without disturbance at 37 °C and 5% CO_2.

The glioblastoma-derived spheres (hereafter labelled; A172-sph, LN229-sph, U87-sph and U251-sph) were passaged every 7 days or when the spheres were more than 200 µm in diameter. To do this, the medium containing the spheres was collected into 50 ml falcon tubes and centrifuged at 300 x g for 5 mins. Afterwards the supernatant was discarded and the spheres resuspended in 5 ml PBS. To discard the PBS, the spheres were centrifuged again at 300 x g for 5 mins and the supernatant discarded.

In order to dissociate the spheres into single cells for counting, 2 ml accutase (or 1 ml depending on the pellet size) was added to the spheres and incubated for 20 - 25 mins. After 10 and 20 mins of incubation, the spheres were gently pipetted up and down to ensure an even distribution of accutase and aid the break-up of the spheres. Once a single cell suspension was achieved, the accutase was neutralised by adding 8.5 ml medium followed by centrifugation at 300 x g for 5 mins. Fresh stem cell medium was added to the single cells from which 0.5 ml was used for counting. Afterwards, 2 x 10^6 was calculated and diluted to give a total volume of 20 ml stem cell medium in the culture flasks for formation of new spheres. The spheres were passaged in this manner for at least eight times before they were used for further experiments.

3.1.4 Cryopreservation and thawing of glioblastoma cells and spheres

After the passaging of either the cells or spheres, about 4 x 10^6 cells per tube were cryopreserved using labelled 1 ml cryo-tubes. To do this, 10% DMSO (100 µl) was added to the tubes as a cryoprotectant. This was followed by the addition of 4 x 10^6 in a volume of 900 µl medium so that total volume in the cryo-tube was 1 ml. Working quickly, the cryo-tubes containing the cell suspension were transferred into a Nalgene

Cryo Freezing container and placed in a -80 °C freezer for at least 24 h. Afterwards, the cells are transferred to liquid nitrogen at -196 °C for long term storage.

To cryopreserve the stem cell enriched sphere-forming cells after eight passages, single cell suspensions were first made before proceeding with the above steps.

The thawing process was carried out as quickly as possible since the cryoprotectant (DMSO) is harmful to the thawed cells. First, the cryo-tubes were taken out of the liquid nitrogen tank and placed on ice for 5 mins to slow down the thawing process. The cryo-tubes were then placed at room temperature (~ 1 min) until the cell suspension was melted. Quickly the cell suspension was transferred into 15 ml falcon tubes containing 5 ml medium and centrifuged at 300 x g for 5 mins. The supernatant containing DMSO was discarded and the cell pellets resuspended in 5 ml medium containing serum. This was transferred to a T175 flask containing 20 ml medium to give a total volume of 25 ml. The same thawing process was performed for glioblastoma-derived spheres, except for the use of T75 ULA flasks containing a total volume of 20 ml single cell suspension of sphere-forming cells. Then the culture flasks containing the cells were stored in an incubator at 37 °C and 5% CO_2.

3.2 Bioinformatic analysis of glioblastoma stem cell marker expression

The GEPIA web server (http://gepia.cancer-pku.cn) was used to provide the glioblastoma stem cell marker expression (accessed on 19th January 2021) in non-cancerous and glioblastoma samples [154]. Since the expressions of CD44, Nestin, SOX2 and ALDH1A1 could be detected in the glioblastoma cell lines (4.2), we decided to compare their levels of expression between non-cancerous and glioblastoma samples. To do this, box plots were generated and downloaded comparing CD44, Nestin, SOX2 and ALDH1A1 between 207 non-cancerous brain tissue and 163 glioblastoma tumor samples from the TCGA and Genotype tissue expression (GTEx) databases. This comparison was done to validate the concept that the glioblastoma stem cell marker expression is higher in glioblastoma compared to non-cancerous brain tissues.

3.3 Treatment of glioblastoma cells and spheres

3.3.1 Treatment with drugs

The drugs used were a HDAC inhibitor (MS-275), MEK inhibitor (TAK-733, and/or Trametinib) and Temozolomide (TMZ). The drugs were purchased as powder and dissolved in DMSO to produce stock concentrations of 10 mM stored at -20 °C (or -80 °C in the case of TAK-733). For treatment, the volume of all drugs diluted in DMSO was prepared such that it only contributed 1% of the total culture volume. The control cultures were treated with 1% DMSO to exclude the effect of DMSO on the cells. The working dilutions of the drugs were prepared in DMSO from 10 mM stock solutions to achieve a 100-fold final concentration range. The treatment of adherent cells was performed 24 h after cell seeding while the treatment of glioblastoma-derived spheres was performed 3 days after seeding to allow enough time for sphere formation.

3.3.2 Irradiation

The irradiation of cells or spheres was performed 24 h after drug treatment of cells or glioblastoma-derived spheres using the RS225 X-ray source. The irradiation rate at 195 kv and 10 mA was 0.826 Gy/min using a 3 mm aluminium filter and placing the plate holding the culture flasks at a distance of 60 cm. A sheet of paper with the diameter dimensions was always used to ensure the even radiation field in the closed chamber unit. The flasks containing the cells or glioblastoma-derived spheres were irradiated at room temperature using an exposure of 4 Gy. The sham-irradiated controls were handled under the same conditions but were not exposed to radiation.

3.4 Immunocytochemistry

Immunocytochemistry was performed to determine and compare the expression of the GSLC markers ALDH1A1, CD44, CD133, Nestin and SOX2 between the glioblastoma cells and the enriched glioblastoma-derived spheres. This was done by immunofluorescence staining using the corresponding antibodies against the GSLC markers and comparing fluorescent signal intensities.

Cell seeding, fixing and blocking: After counting, 3 x 10^5 cells in 1 ml medium were seeded onto 76 mm microscopic slides placed in a 4-well chamber. The cells were left for 30 mins to allow cell attachment. This was followed by the addition of medium to a total volume of 4 ml per well and incubation under standard conditions for 24 h. After this, the cells were fixed with 50 ml of 4% paraformaldehyde in a staining jar for 15

mins at RT and washed three times with PBS. After washing, the cells were placed in 0.2% Triton X-100 for 5 mins to permeabilize the cell membranes and allow antibody binding inside the cells. This step was skipped for the staining of CD133 and CD44 since they are localized on the cell surface. After permeabilization, the cells were washed twice in PBS for 5 mins and then placed in a blocking solution containing 1% BSA and 0.15% Glycine dissolved in PBS. This was done for 1 h at RT to block non-specific antibody binding in the cells.

Application of primary antibody: The primary antibodies were applied in pairs using antibodies from different species (see 2.1.3) to allow double staining (see Table 2). The antibody cocktails were diluted in the blocking solution from which 75 µl was added as 3 drops onto the slides to ensure even distribution. This was done in a cold room and incubated in the dark overnight at 4 °C in a wet slide chamber.

Application of secondary antibody: The following day, the slides were washed in PBS three times for 5 mins to remove the primary antibody. The relevant pair of secondary antibodies was prepared and diluted 1:300 for Goat Anti-rabbit (red; cy3) and 1:200 for Goat Anti-mouse (Green; Alexa flour® 488) in blocking solution (see Table 2). The pairs were selected to match the source of primary antibody so as to enable the simultaneous visualization of two GSLC markers.

Table 2: Double-stained immunoflourescence antibodies for GSLC marker expression

Primary antibodies and dilutions	Secondary antibodies and dilutions
Anti-CD44 (Mouse; 1:400) + Anti-CD133 (Rabbit; 1:100)	Goat Anti-mouse (Green; Alexa flour® 488; 1:200) + Goat Anti-rabbit (red; cy3; 1:300)
Anti-ALDH1A1 (Rabbit; 1:100) + Anti-Nestin (Mouse; 1:100)	
Anti-Sox2 (Rabbit; 1:300) + Anti-Nestin (Mouse; 1:100)	

A volume of 75 µl from the antibody cocktail was added to each slide and incubated for 2 h at RT in the dark. A negative control in which cells were stained with only secondary antibody was included to detect non-specific binding of secondary antibody.

Application of DAPI (4′,6-diamidino-2-phenylindole): In order to stain the nuclei of the cells with DAPI after immunofluorescence staining, the cells were first washed three times in PBS for 5 mins to remove all secondary antibody residues. Afterwards, vectashield mounting medium containing DAPI was applied as a drop onto the cells on the slides. Then the slides were covered with glass cover slips and left to incubate for an hour before viewing under the microscope.

Visualization and image acquisition: To visualize the immunofluorescence staining, a Keyence BZ 9000 fluorescence microscope was used. Images of each slide were acquired using a 20x or 40x magnification. The negative control slides were viewed first to check for any background fluorescence from the experiment. The BZ-II-Analyzer software was used to visualize and acquire overlapping images of the cells showing the double immunofluorescence staining. Up to 50 cells of each cell line were visualized and acquired, while three independent biological replicates were performed.

3.5 CellTiter-Glo® Luminescent Cell Viability Assay

This assay was done to determine how cell viability of the stem cell-enriched sphere-forming cells was affected by the various treatments. The assay was performed using CellTiter-Glo® Luminescent Cell Viability Assays according to the manufacturer's instructions. The CellTiter-Glo® assay is based on the quantitation of ATP in the cells as a luminescent signal representing metabolic activity of viable cells.

To perform the experiment the enriched glioblastoma-derived spheres were dissociated into cells and seeded at 3 x 10^5 cells per well in 12-well ULA plates. The spheres were allowed to form for 72 h followed by treatment with increasing concentrations (1 µM, 10 µM and 50 µM) of MS-275, TAK-733, trametinib and TMZ. The following day the spheres were either sham-irradiated or irradiated at 4 Gy and incubated for 72 h. After this period, the spheres were dissociated with accutase for counting, re-seeded at 1 x 10^4 per well in 96-well white opaque plates and left for 72 h under cell culture conditions. Afterwards, the cell CellTiter-Glo® Reagent was added to the cells and incubated for 10 mins at RT on an orbital shaker gently to avoid dissociating the spheres. The luminescent signal was recorded using a UV-spectrophotometer infinite M200 plate reader and measurements performed in quadruplicate for three independent biological replicates.

3.6 Sphere formation assay

The sphere formation assay was initially developed to isolate and culture neural stem cells [155]. It is now commonly used as an *in vitro* method to assess the cancer stem cell population and their properties [156, 157]. This assay was done to investigate the sphere forming ability of the enriched glioblastoma-derived spheres after treatment with drugs, radiation or both.

The experiment was carried out by first dissociating the enriched spheres into cells. This followed by seeding 1 x 10^6 cells in T25 ULA flasks and incubation at 37 °C and 5% CO_2 for three days to allow sphere formation. After this time, the spheres were treated with single or combined treatments of MS-275, TAK-733 and trametinib (see 3.3.1) and the standard TMZ. The following day the spheres were sham irradiated or irradiated at 4 Gy and harvested 72 h later. To do this the spheres were dissociated with accutase into a single cell suspension for cell counting. After counting, 200 cells per well were seeded in 96-well ULA plates with a total volume of 100 µl stem cell medium in each well. The cells were incubated for 21 days to allow enough time for sphere formation. After this period, images of each well were taken using the operetta high content imaging system. The number of spheres formed were counted in each image by eye. The sphere formation assay consisted of three technical replicates per experiment and three biological replicates. The sphere formation rate was determined by the equation below.

Equation 1: $Sphere\ formation\ rate\ (\%) = \frac{No.\ of\ sphere\ forming\ cells}{Total\ no.\ of\ starting\ cells} \quad X \quad 100$

3.7 Western Blot analysis

The western blot technique of protein immunoblotting was used to quantify proteins in cells or tissues. It is based on the binding of antibodies to the protein of interest that can be quantitatively detected and visualized on a membrane under a chemiluminescent imaging system. This experiment was done to determine how the protein expression of GSLC markers in glioblastoma cells and spheres were influenced by treatment with drugs, radiation or both. The steps in carrying out the western blotting procedure are described below.

3.7.1 Cell seeding, lysis and protein extraction

The glioblastoma cells grown as monolayer were plated in duplicate at a concentration of 4 x 10^5 cells in 6-well coated plates and cultured for 24 h prior to compound treatment. The following day, the cells were sham-irradiated or irradiated at 4 Gy and incubated for 72 h before harvesting. To harvest the cells the medium was removed and the cells washed with PBS followed by manual detachment using a cell scraper. A volume of 1 ml medium was used to collect the cells in falcon tubes and centrifuge them at 300 x g for 5 mins. The supernatant was discarded and the pellets stored at -20 °C.

In the case of the enriched glioblastoma-derived spheres, they were dissociated into single cells and seeded in T25 ULA flasks at a concentration of 3 x 10^6 cells and cultured for 72 h prior to treatment as described above. To harvest the spheres, the medium containing the spheres were collected in corresponding falcon tubes and centrifuged at 300 x g for 5 mins. The spheres were then dissociated by resuspending in 1 ml accutase and stopping the reaction with 5 ml medium once a single cell suspension was achieved. The cells were centrifuged at 300 x g for 5 mins and the supernatant discarded to resuspend the cells in PBS for washing. After this, the cells were centrifuged, supernatant discarded and cell pellets stored at -20 °C.

The pellets (from cells or spheres) were lysed in 40 - 60 µl (depending on size) T-PER (Tissue Protein Extraction Reagent) lysis buffer supplemented with a Protease Inhibitor Cocktail and PhosSTOP (Phosphatase Inhibitor Cocktail). This was followed by incubation on ice for 1 h and centrifugation at 4 °C and 10,000 x g for 10 mins. The supernatant was collected into fresh eppendorf tubes and stored at -20 °C.

3.7.2 Measurement of protein concentration and sample preparation

To measure the protein concentration, the samples were diluted 1:25 in water. Using the Pierce BCA protein assay kit. Albumin protein standards supplied with the kit were prepared at different concentrations namely; 1000 mg/ml, 850 mg/ml, 700 mg/ml, 550 mg/ml, 450 mg/ml, 350 mg/ml, 275 mg/ml, 200 mg/ml, 150 mg/ml, 100 mg/ml, 50 mg/ml and water as control. 10 µl of the protein sample or standard were pipetted in duplicates into wells of a Nunclon 96-well-plate. Next, 200 µl of the working reagent (reagent A and reagent B) supplied with the kit were added per well and the plate incubated for 30 mins at 37 °C.

Afterwards, the absorbance was measured at 562 nm using an Infinite 200 microplate reader. A standard curve of the absorbance as a function of the standard's protein concentration was plotted. With the linear regression equation of the curve (y = mx + c), the protein concentration of the samples was calculated and corrected for the dilution factor. Sample amount for 20 µg of protein was calculated and mixed with 3 µl 4X Laemmli buffer and varying volumes of water so that all samples were of equal volume. The protein samples were denatured at 95 °C for 5 mins, immediately cooled on ice for a few minutes and briefly spun down. The samples were either stored at -20 °C until use or loaded immediately for gel electrophoresis.

3.7.3 Immunoblotting

Preparation of separating and stacking gel: A 12% SDS poly-acrylamide gel was prepared for electrophoretic separation of proteins according to their molecular weight. The components for preparing the separating gel were mixed in the order shown in Table 3.

Table 3: Components of a 12% SDS poly-acrylamide gel

Materials	**Volume for 12% gel (ml)**
Acrylamide 20% / Bis AA 1%	2
H_2O	1.05
1M Tris pH 8,8	1.9
10% SDS	0.05
Mixed	
10% APS	0.05
TEMED	0.005

The mixture was pipetted between glass and aluminum plates separated by spacers, followed by an overlay of 1 ml isopropanol to smooth the gel surface. The gel was left to polymerize at RT for about 30 mins and the isopropanol removed.

The components for the stacking gel were prepared in the order shown in Table 4. The stacking gel mixture was pipetted on top of the separating gel, after which gel combs were inserted. The gel was left to polymerize at RT for about 45 mins or until solid.

Table 4: Stacking gel preparation

Materials	Volume (ml)
Acrylamide 20% / Bis acrylamide 1%	0.3
H_2O	1.4
1M Tris pH 6,8	0.25
10% SDS	0.02
Mixed	
10% APS	0.02
TEMED	0.002

Separation of proteins by SDS-PAGE: The gel combs and clippers were removed and the gels fitted into an electrophoresis chamber already filled with 1X running buffer. On the first well of each gel, 10 µl of a protein molecular weight marker (Precision plus Protein™ Standard Marker Dual Color) was applied followed by the loading of samples. Electrophoresis was run at 160V for about 2 h at RT.

Transfer of proteins: After the gel electrophoresis was completed, the gels were removed from the plates and rinsed in 1X Towbin buffer for about 10 mins on a shaker to achieve equilibrium. The wet electroblotting method was used to transfer the separated proteins from the gel to a nitrocellulose membrane. To do this, first filter papers, sponges and nitrocellulose membrane were pre-equilibrated in 1X Towbin buffer. Afterwards a sandwich was prepared on the transparent side of a gel holder cassette in the following order; sponge - filter paper - membrane - gel - filter paper - sponge. Bubbles were removed with a spatula before closing the cassette and the gel sandwich placed in a trans-blot cell filled with cold 1X Towbin buffer. A cool pack was added to keep the temperature low and a magnetic stirrer used to maintain homogeneous conditions. To further prevent overheating, the trans-blot cell was

placed in a box containing ice on a magnetic stirrer plate and the transfer run at 100V for 90 mins. After transfer the membrane was incubated in Ponceau-S-red to check the efficiency of the transfer. When the protein bands became visible, the Ponceau-S-red solution was decanted and the membrane washed with distilled water to remove excess staining. The position of the bands of the marker proteins were marked with a pen and a copy of the blot scanned. After this, the membranes were cut to the area with the protein of interest using the protein molecular weight marker as a guide.

Incubation with primary and secondary antibodies: The wet membranes were blocked in 1X blocking solution for at least 1 h at RT. In order to be able to detect proteins, the membranes were incubated with the appropriate primary GSLC markers antibodies diluted as shown in 2.1.1. Incubation was done in a 50 ml falcon tube placed on a roller mixer overnight at 4 °C. The following day, the membranes were washed three times for 10 mins in 1X TBST to remove antibody residues. Next, the membranes were incubated with the appropriate HRP-conjugated secondary antibody diluted in 8% milk for 1 h at RT. Afterwards the membrane was washed four times for 10 mins in 1X TBST to remove residues of secondary antibody.

Detection of immunoblot signals by chemiluminescence: The ECL™ Select Western Blotting Detection Reagent was used to detect and quantify the antibody labelling. The reagent consisted of a peroxide and luminol solution which were mixed in equal volumes. The membranes were incubated in this mixture for about 1 min and afterwards the luminescent signal detected and captured using the Alpha Innotech Chemi Imager system.

Stripping and re-probing: To re-probe the membranes the adherent antibodies were stripped with Restore™ PLUS western blot stripping buffer. The membranes were incubated in the stripping buffer for at least 20 mins at RT and washed once in 1X TBST. Afterwards, the blocking and incubation with different primary and secondary antibodies were performed as described above.

Quantification of protein bands: The images of the detected proteins were quantified using the Image-J image analysis software. The band signals were evaluated by normalizing the protein values to that of the endogenous control ß-Actin. The ß-Actin protein was a loading control to ensure the correct interpretation of results across the three biological replicates performed.

3.8 Flow cytometry analysis

Flow cytometry is a technology that uses immunostaining with labelled antibodies to measure the fluorescence intensity of cells and identify surface molecules or cytosolic proteins in a population of cells [158]. This principle was used to analyse the expression of GSLC markers in single cell suspensions obtained after the treatment of the enriched glioblastoma-derived spheres with drugs, radiation or both. A multi-colour antibody panel approach was applied using fluorescently conjugated antibodies with distinct fluorophores against GSLC markers (see 2.1.5). Since a multi-colour approach was used, compensation was done on the flow cytometer to correct for spectral overlap across the channels of the fluorophores. This was done using compensation beads (anti-mouse) stained with the same antibodies used in the flow cytometry experiment.

Given the complexity of the multicolour approach applied, the GSLC marker antibodies for the flow cytometry analysis were first titrated to optimise their detection and dilution before use.

In Figure 7, it is shown that all of the GSLC markers available except ALDH1A1, could be detected in LN229-sph. An increased fluorescence intensity of LN229-sph cells stained with Nestin, CD44 and SOX2 at dilutions of 1:50, 1:100 and 1:200 compared to the unstained cells was observed in the flow cytometric histograms. For ALDH1A1 antibody, there was no difference between the unstained cells and the stained cells at any dilutions implying ALDH1A1 might not be present in the cells (Figure 7).

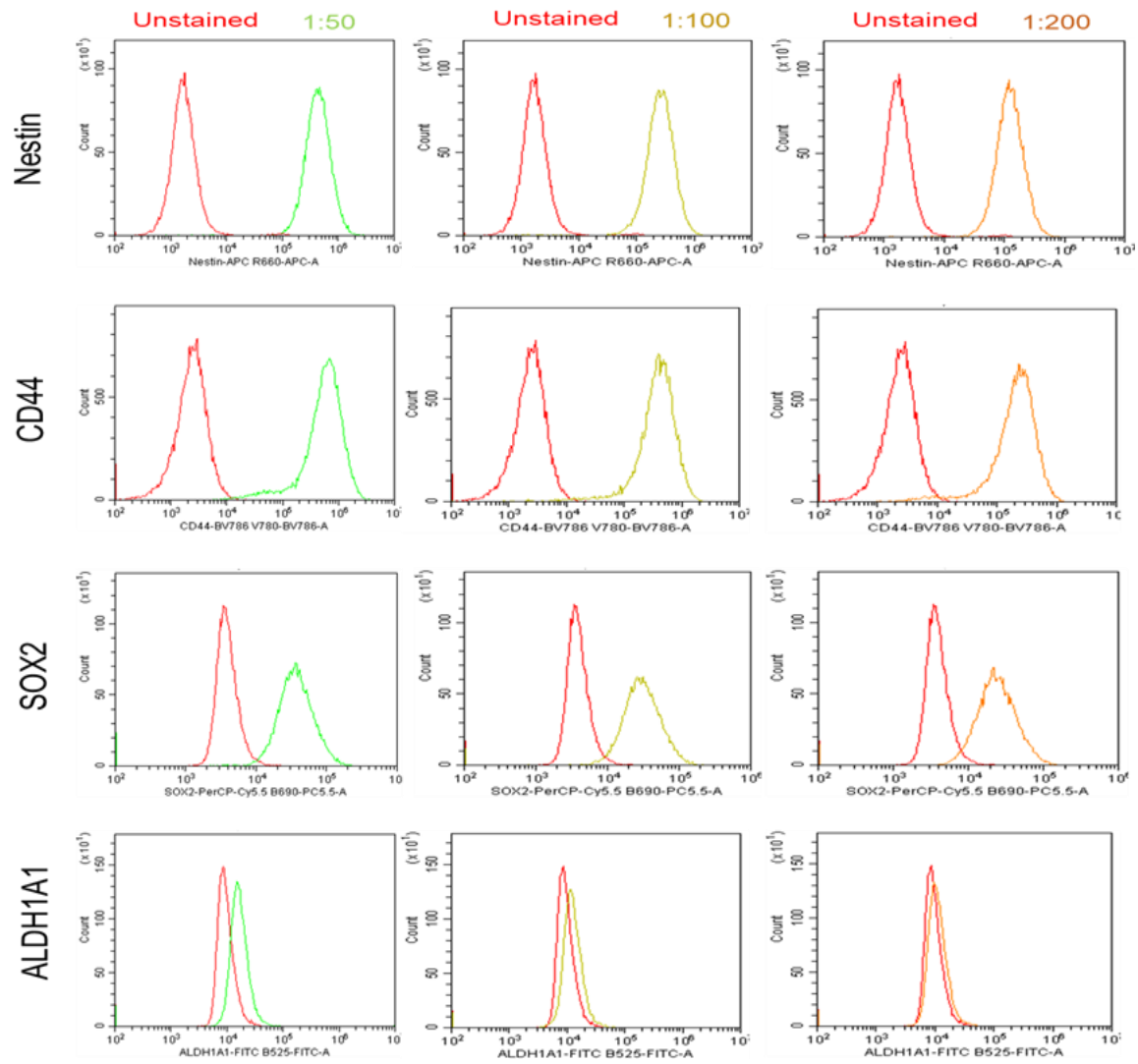

Figure 7: **Antibody detection of GSLC markers in LN229-sph for flow cytometry experiments.** The fluorescently conjugated antibodies for Nestin, CD44, SOX2 and ALDH1A1 were titrated at 1:50, I: 100 and 1:200 to determine their optimal dilutions. The differences between the unstained cells (red) and the antibody-stained cells are shown.

The results were similar in the U87-sph cells where there were increased fluorescent intensities for Nestin and CD44 stained cells at all dilutions compared to the unstained cells (Figure 8).

For SOX2 and ALDH1A1 detection in U87-sph cells, higher dilutions at 1:10, 1:20 and 1:50 were applied due to low levels of the markers. While the fluorescent intensity increased with increasing dilutions for SOX2 staining, no difference was detected with ALDH1A1 staining compared to unstained cells at any dilutions in U87-sph (Figure 8).

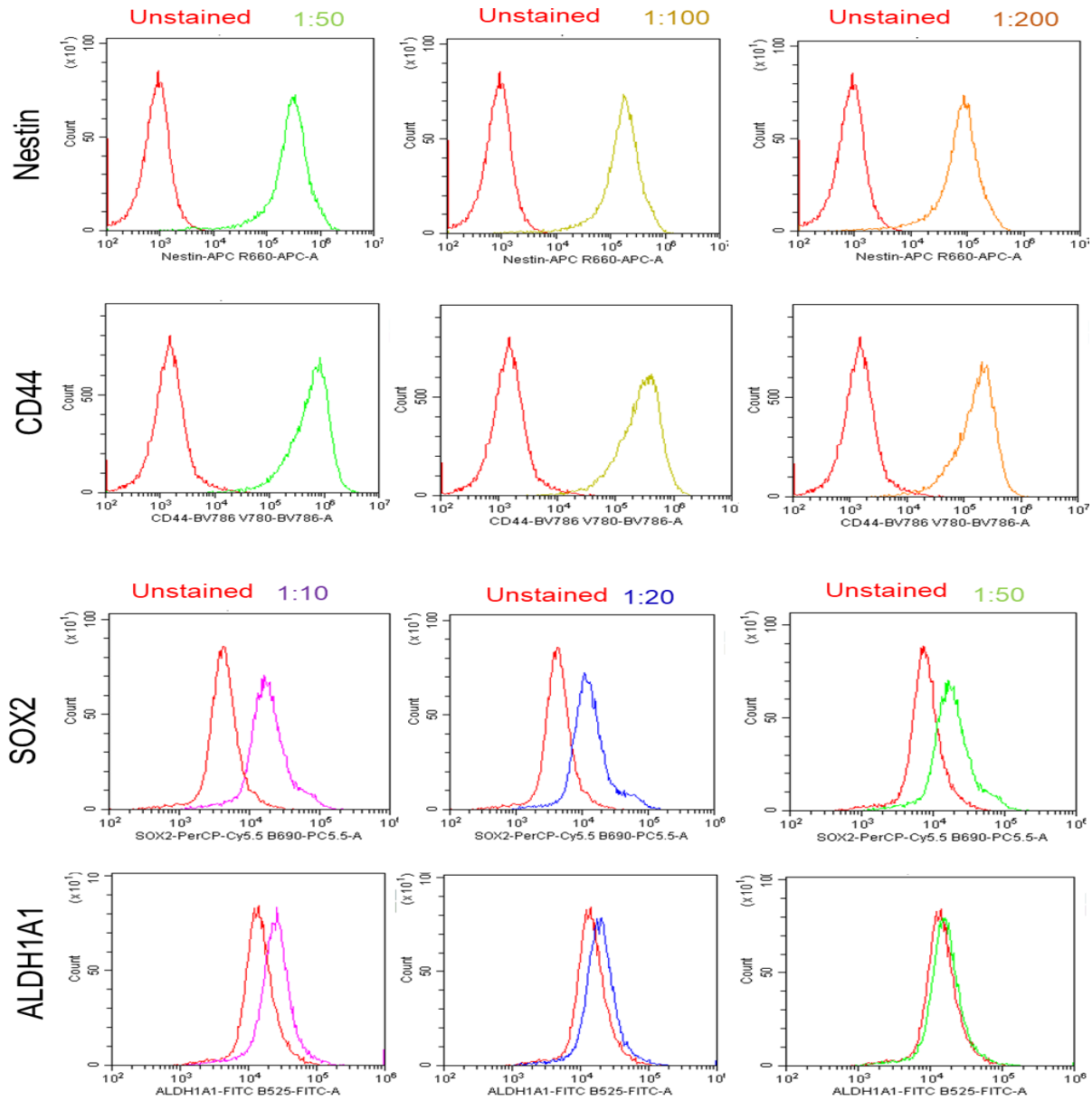

Figure 8: **Antibody detection of GSLC markers in U87-sph for flow cytometry experiments.** The fluorescently conjugated antibodies for Nestin and CD44 were titrated at 1:50, 1:100 and 1:200 (upper two rows) and for SOX2 and ALDH1A1 at 1:10, 1:20 and 1:50 (lower two rows) to determine their optimal dilutions. The differences between the unstained cells (red) and the antibody-stained cells are shown.

Since ALDH1A1 was undetected in LN229-sph and U87-sph, only Nestin, CD44 and SOX2 antibodies were tested in the U251-sph cell line at 1:50, 1:100 and 1:200 (Figure 9). All the three GSLC markers could be detected in U251-sph cells which is evident from the increased fluorescence intensities in comparison to the unstained cells as shown in Figure 9.

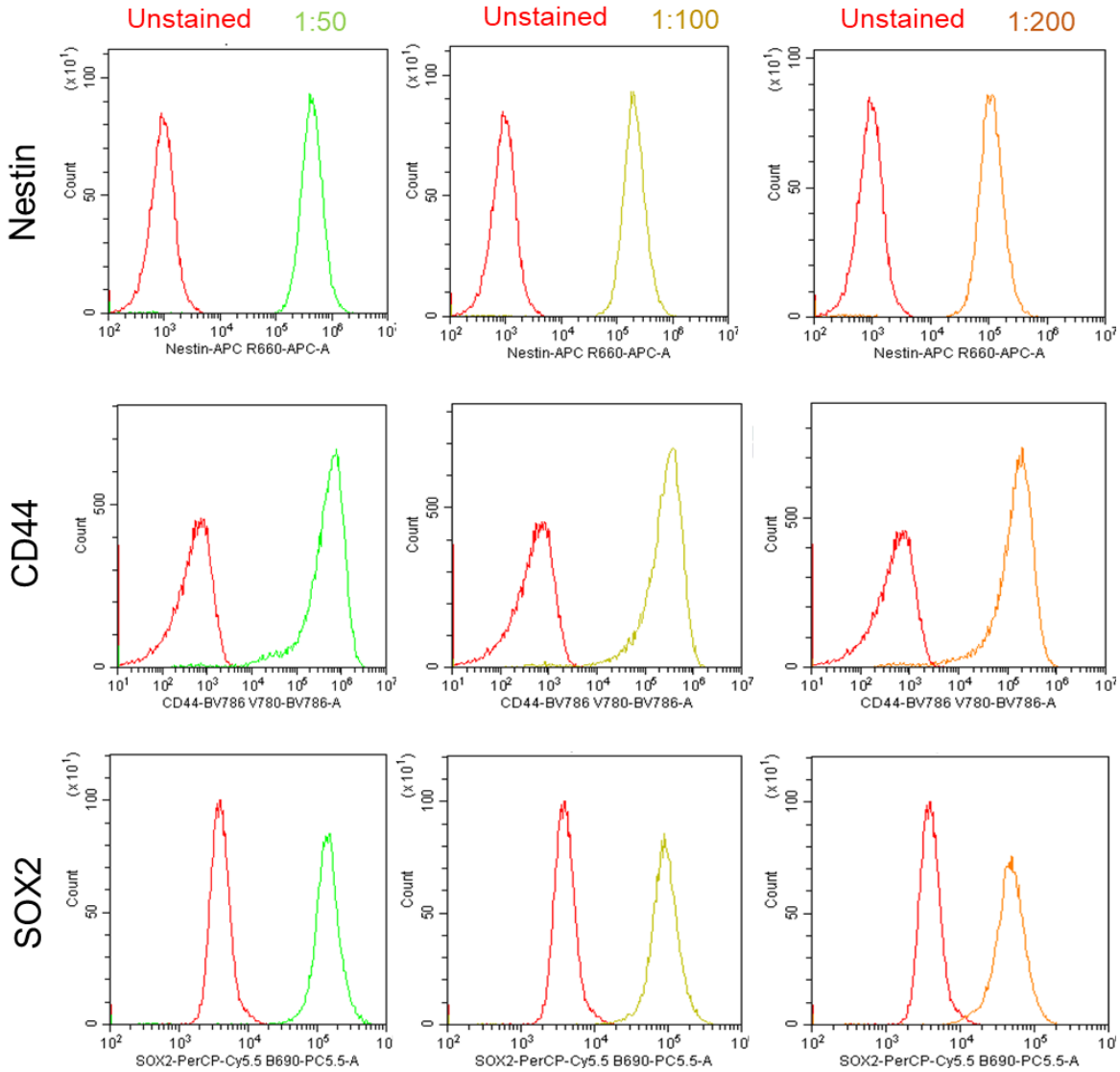

Figure 9: **Antibody detection of GSLC markers in U251-sph for flow cytometry experiments.** The fluorescently conjugated antibodies for Nestin, CD44 and SOX2 were titrated at 1:50, I: 100 and 1:200 to determine their optimal dilutions. The differences between the unstained cells (red) and the antibody-stained cells are shown.

Generally, Nestin, CD44 and SOX2 were well detected in all enriched glioblastoma-derived spheres and analyzed further at 1:100 dilutions except for SOX2 used at 1:20 in U87-sph due to low levels. ALDH1A1 was excluded from further flow cytometry analysis.

Table 5 shows the dilutions used for all subsequent GSLC marker studies using flow cytometry.

Table 5: Optimal antibody dilutions after titration

Antibodies	Fluorophore	Dilution
Nestin	APC	1:100
CD44	BV 785	1:100
SOX2	PerCP-Cy5.5	1:00 (1:20 for U87-sph)
Isotype control	PerCP-Cy5.5	1:100
Live/dead staining	Zombie aqua	1:100

3.8.1 Cell seeding and treatment (for flow cytometry analysis)

To perform the experiment with treatment, 2 x 10^6 cells of the enriched glioblastoma-derived sphere forming cells, were seeded in T25 ULA flasks and sham-irradiated or irradiated at 4 Gy 24 h after drug treatment (see 3.3). After a period of 72 h, the glioblastoma-derived spheres were harvested by dissociation into single cells with accutase and washing with 500 µl PBS before proceeding with the cell surface staining.

3.8.2 Cell surface staining (for flow cytometry analysis of CD44)

The staining of the GSLC marker CD44 found on the surface of cells was done before intracellular staining of proteins. To do this, the cell pellets were first resuspended in 40 µl Fc-block diluted 1:10 in PBS for 10 mins at 4 °C. This was done to block protein epitopes on the cell surface and prevent unspecific binding of the antibodies. After this, the cells were washed once with FACS buffer (PBS + 0.5% BSA) and centrifuged at 1000 x g for 5 mins. The supernatant was discarded and the cells resuspended in 50 µl Zombie aqua dye (1:100 in PBS) to stain dead cells resulting from the various treatments. The live-dead staining was done for 30 mins at RT followed by addition of 1 ml FACs buffer. Centrifugation was done at 1000 x g for 5 mins to discard the supernatant. The antibody master mix containing anti-CD44 was prepared in FACS buffer. From this, 50 µl was added to the cells and incubated at 4 °C for 20 mins. Afterwards the cells were washed with 500 ml FACs buffer and centrifuged at 1000 x g for 5 mins to discard the supernatant.

3.8.3 Intracellular staining (for flow cytometry analysis of SOX2 and Nestin)

Before proceeding with intracellular staining, the cell pellets were fixed and permeabilized to allow the binding of antibodies to intracellular proteins. This was done

using the eBioscience ™ Foxp3 / Transcription Factor Staining Buffer Set. The fixation buffer was prepared according to the manufacturer instructions. The cells were resuspended in 200 µl fixation buffer and incubated for 1 h at RT. After fixation, the cells were washed with 1X permeabilization buffer prepared 1:10 in PBS and centrifuged at 1000 x g for 5 mins to discard the supernatant. The cell pellets were incubated over night at 4 °C to continue the intracellular staining the following day.

Before intracellular staining, the cells were washed once again with 1X permeabilization buffer to allow the antibodies into the cells for binding. After spinning down and discarding the supernatant, the antibody master mix containing anti-Nestin, and anti-SOX2 was prepared in permeabilization buffer. From this, 50 µl was used to resuspend the cells and incubate for 1 h at RT in the dark. After incubation, the cell pellets were washed once with 1 ml permeabilization buffer and centrifuged at 1000 x g for 5 mins to discard the supernatant. This was followed by another washing step but this time with PBS and then centrifugation to discard the supernatant. As a final step, the cells were resuspended in 200 µl PBS and transferred into the corresponding FACS tubes through 40 µm cell strainer caps. This was done to ensure single cell suspensions in the FACS tubes prior to acquisition.

3.8.4 Acquisition and analysis of results

The cells were analyzed by flow cytometry using a CytoFLEX LX flow cytometer and CytExpert software. The gating strategy to set a cut-off for negative and positive population was done using two gating controls. First, unstained cells were used to set negative gates. In addition, fluorescence minus one (FMO) controls that involve all the antibodies except one of each was used to address any spillover-induced background (Figure A18) [159]. Additionally, an isotype control for only SOX2 was included for all samples to set gates against non-specific antibody binding. The gating region on the controls were set to contain less than 1% of the cells for both single and double positive populations. The cytometer was set to acquire 2 x 10^4 cells per treatment for all three biological replicates performed.

3.9 qRT-PCR analysis

Quantitative real-time polymerase chain reaction (qRT-PCR) is a biological technique commonly used for the quantification of gene expressions in cells or tissue samples. This method was used to analyse and quantify the gene expression of GSLC markers

in each cell line after the treatment of drugs, radiation or both. A SYBR Green based qRT-PCR was used for both the RT^2 Profiler PCR Array and for analysis of individual GSLC markers.

3.9.1 RNA isolation

To extract RNA from the samples, the cell pellets were harvested 72 hours after combined drug and radiation treatment and kept on ice or stored at -20 °C overnight. The Maxwell® 16 miRNA Tissue Kit was used for RNA isolation according to the manufacturer's instructions. While the cell pellets were placed on ice, 200 µl of 1-Thioglycerol / Homogenization solution supplied with the kit was added to each sample and left for 15 – 30 secs to homogenize. 200 µl Lysis Buffer and 15 µl Proteinase K was added to the homogenized sample and mixed by vortexing for 20 secs. Incubation was done for 10 mins while the Maxwell RSC cartridges supplied with the kit were prepared for each sample. After incubation, all the lysate was transferred to well 1 and 10 µl of Blue DNase I solution added to well 4 of the cartridges. The cartridges were placed in the cartridge rack and the LEV plungers placed in well 8 of each cartridge. Next, 60 µl nuclease free water was pipetted into 0.5 ml elution tubes and placed in front of the cartridge rack. The cartridge with the samples was then placed in the Maxwell® 16 MDx instrument to start the automated purification run. After 2 h, the run was completed and the eluted RNA samples removed from the instrument and stored at -20 °C.

3.9.2 Quantification of RNA

The concentration of RNA was measured using 1 µl of each sample on a Nanodrop spectrophotometer device. The absorbance was read at 260 nm and 280 nm to determine the concentration and quality of the samples. A good RNA quality has a A260/280 ratio of 1.8 – 2.0. Only samples within this range were used.

3.9.3 RT^2 Profiler PCR Array – GSLC markers

RT^2 Profiler PCR Arrays are designed for the analysis of multiple genes involved in a specific biological pathway. Therefore, this PCR array was used to analyze the level of mRNA expression of eleven GSLC markers in the monolayer glioblastoma cell lines after combined treatment of the drugs and radiation. Following this, specific genes were chosen for validation by individual RT-PCR analysis. The PCR array was in 96-well format and custom designed to contain eleven GSLC marker genes namely; *STAT3*, *NES*, *NANOG*, *ALDH1A1*, *PROM1*, *SOX2*, *OLIG2*, *POU5F1*, *CD44*, *PLAUR*

and *PLAU*. These were selected as potential GSLC markers expressed in glioblastoma. The two housekeeping genes used as controls were *GAPDH* and *TBP*. Three other controls were included in the array. These were a genomic DNA control (GDC) to detect non-transcribed DNA contamination, a reverse-transcription control (RTC) to test the efficiency of the reverse-transcription reaction and a positive PCR control (PPC) to test the efficiency of the PCR reaction itself.

The reverse-transcription reaction for cDNA synthesis was performed using the RT^2 First Strand Kit according to the manufacturer's instructions. To do this, 0.5 µg of total RNA was used. First, a genomic DNA elimination step was done according manufacturer instructions in Table 6. The 10 µl mixture was mixed, centrifuged briefly, incubated for 5 mins at 42 °C and placed immediately on ice for at least 1 min. This followed by the addition of 10 µl reverse-transcription mix to each sample prepared according to Table 7 to have a total volume of 20 µl.

Table 6: Genomic DNA elimination mix for 1 reaction (RT^2 First Strand Kit)

Component	Volume
RNA	0.5 µg
Buffer GE	2 µl
RNase-free water	variable
Total volume	**10 µl**

Table 7: Reverse-transcription mix for 1 reaction

Component	Volume (µl)
5XBuffer BC3	4
Control P2	1
RE3 Reverse Transcriptase Mix	2
RNase-free water	3
Total volume	**10**

The total mixture was incubated in a thermocycler at 42 °C for 15 mins and stopped by incubating at 95 °C for 5 mins. Next, 91 µl RNase-free water was added to each

reaction, mixed and placed on ice or stored at -20 °C before proceeding with the real-time PCR reaction. For the real-time PCR reaction, the RT^2 SYBR Green master mix was used with the components mixed according to Table 8. From this mix, 25 µl was added to each well of the custom RT^2 profiler PCR array and sealed with a transparent adhesive film. The plates were then centrifuged for 1 min at 1000 x g to remove any bubbles and then placed on ice or at 4 °C.

Table 8: Real-time PCR components mix

Component	Volume (µl) 1 well	Volume (µl) 17 wells / sample
2X RT^2 SYBR Green master mix	12.5	212.5
cDNA synthesis reaction	1	17
RNase-free water	11.5	195.5
Total volume	**25**	**425**

The PCR reaction was performed with the StepOnePlus™ Real-time PCR system and the cycling conditions done according to Table 9. Each plate contained three technical replicates while the experiment was repeated once for all cell lines due to the expense. The results are presented in the appendix section B as tables (Table A1 -Table A4).

Table 9: Real-Time PCR cycling mode

Steps	Temperature (°C)	Duration	Cycles
Initial denaturation	95	10 mins	Hold
Denaturation	95	15 secs	40
Annealing / Elongation	60	1 min	
Melt curve stage I	95	15 secs	
Melt curve stage II	60	1 min	
Melt curve stage III	95	15 secs	

3.9.4 RT-PCR for single target

Because the GSLC markers Nestin, CD44, SOX2 and ALDH1A1 were well detected by protein analysis, they were analysed for RT-PCR after the various treatments. The synthesis of cDNA for the single analysis of genes of interest was done using the QuantiTect® Reverse Transcription Kit according to the manufacturer's instructions. From the isolated RNA, 1 µg was used for this reaction. This was calculated and diluted with RNase-free water so that the total volume was 12 µl. After this, a genomic DNA (gDNA) elimination step was done by adding 2 µl gDNA wipeout buffer and incubating for 2 mins at 42 °C in a thermocycler (Table 10).

Table 10: Genomic DNA elimination reaction components

Component	Volume (µl)
gDNA Wipeout Buffer, 7X	2
Template RNA (1 µg)	Variable
RNase-free water	variable
Total volume	**14**

Afterwards the reverse-transcription master mix was prepared according to Table 11 and added to the template RNA (14 µl) to achieve a total volume of 20 µl.

Table 11: Reverse-transcription reaction components

Component	Volume (µl)
Quantiscript Reverse Transcriptase	1
Quantiscript RT Buffer, 5X	4
RT Primer Mix	1
Template RNA	
gDNA elimination reaction	14
Total volume	**20**

The reaction mixture was incubated for 30 mins at 42 °C and then for 3 mins at 95 °C to inactivate the Quantiscript reverse transcriptase. The newly synthesized cDNA samples were placed on ice briefly and stored at -20 °C.

The real-time PCR reaction was performed using the PowerUp™ SYBR™ Green master mix and the StepOnePlus™ Real-time PCR System. All the primers used were designed using the website https://www.genscript.com/tools/pcr-primers-designer/advanced with the annealing temperatures set at 60 °C. The primers were delivered in a stock of 100 pmol/µl primer and pairs were diluted together using RNase-free water to have working concentrations of 5 pmol/µl. Table 12 shows the forward and reverse primers that were used.

Table 12: GSLC marker primers

Gene	Forward Primer	Reverse Primer
CD44	TACTGTACACCCCATCCCAG	TCCATGAGTGGTATGGGACC
NES	GCACCTCAAGATGTCCCTCA	GGGAGTTCTCAGCCTCCAG
SOX2	ATCGACGAGGCTAAGCG	TCATGAGCGTCTTGGTTTTC
ALDH1A1	TCTCGACAAAGCCCTGAAGT	TATTCGGCCAAAGCGTATTC
GAPDH	TGGTATCGTGGAAGGACTCA	CCATCCACAGTCTTCTGGGT
TBP	GCCCGAAACGCCGAATAT	CCGTGGTTCGTGGCTCTCT

While thawing the cDNA on ice, the PCR reaction was prepared according to Table 13. The components were mixed thoroughly and centrifuged briefly to remove air bubbles. Next, 9 µl of the master mix was pipetted into each well of 96-well PCR plates in three technical triplicates. This was followed by addition of 1 µl of the cDNA template so that the total volume in each well was 10 µl. As a negative control, 1 µl of nuclease free water was used as a template.

Table 13: Real-time PCR Master Mix

Component	Volume (µl)
PowerUp™ SYBR™ Green Master Mix (2X)	5
Forward and Reverse primers	1
Nuclease-free water	3
Total volume	**9**

The PCR reaction plate was sealed with a transparent foil to avoid evaporation and spun down at 300 x g for 2 mins to remove any air bubbles. After this, the reaction plate was placed in the instrument and the real-time PCR reaction run according to the program in Table 9 for all primers. After the run was completed, the data was analyzed using the StepOne software v2.3.

Data analysis of real-time PCR amplifications: The signal intensity of the SYBR Green fluorescent dye detected during the PCR amplifications was used to quantify the levels of the specific RNA in the samples. First the raw data and amplification plots were viewed using the StepOne software v2.3. Then the baseline and threshold cycles (C_T) for the amplification curves were calculated using the software. The baseline was set by the initial cycle of PCR where there was very little change in the fluorescent signal. The C_T threshold was automatically set by the StepOne software at a point in the exponential phase of the amplification curve while the C_T value was the number at which the fluorescent signal crossed the threshold as shown in Figure 10.

Since there were three technical replicates per sample, the mean of the C_T value was calculated. To check for non-specificity of the Real-time PCR reaction, the melt curves following the cycling program was checked. A single peak for each amplified product of the target gene is required to rule out non-specific amplifications.

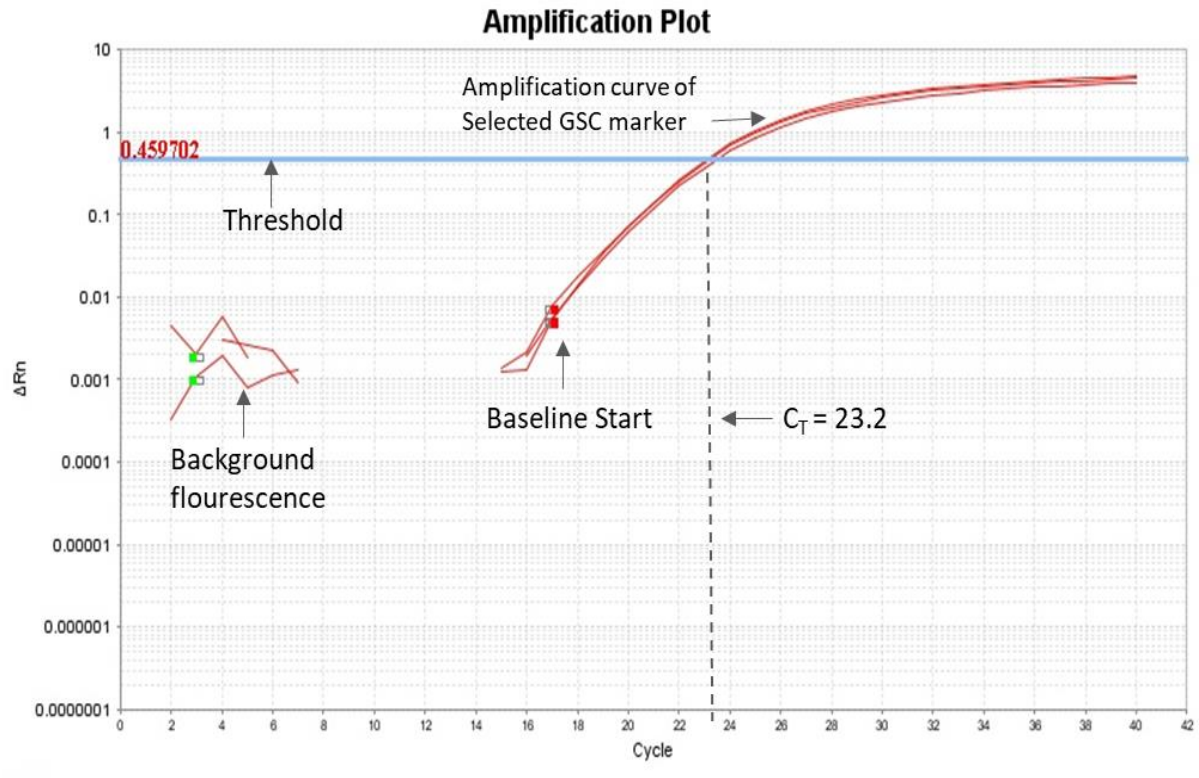

Figure 10: Real-Time PCR amplification plot. A plot showing the amplification curve in technical triplicates of a selected GSLC marker. The plot displays the calculated threshold, start of baseline and the C_T value.

The fold changes of the target genes were calculated using the $2^{-\Delta\Delta Ct}$ method [160] as described in the following steps;

a) The C_T values of the target gene for each sample was normalized to the C_T values of the endogenous gene (*TBP*) and presented as ΔCT;

ΔCT = C_T (target gene) - C_T (endogenous gene)

b) Next the difference in the expression levels of the target genes was calculated by normalizing to the control samples

ΔΔCT = ΔC_T (treated samples) - ΔC_T (control samples)

c) The fold change of the target gene expression was finally calculated as;

$$2^{-\Delta\Delta CT} = 2^{-(\Delta CT\ (\text{treated samples}) - \Delta CT\ (\text{control samples}))}$$

3.10 Statistical analysis

All experiments were performed with a minimum of three biological replicates and with technical replicates as specified. All data presented represent the mean ± standard error of mean (SEM) of the biological replicates. The statistical evaluation of the data was performed comparing the control and treated groups using unpaired two-tailed student's t-test. Statistical significance was assumed if the *p*-value was ≤ 0.05. The *p*-value was denoted as follows *$p \leq 0.05$, **$p \leq 0.01$ and ***$p \leq 0.001$ (versus 0 Gy) or $^{\#}p \leq 0.05$, $^{\#\#}p \leq 0.01$ and $^{\#\#\#}p \leq 0.001$ (versus 4 Gy). A two-way ANOVA analysis was additionally done for cell viability assay, sphere formation assay, western blots, flow cytometry analysis and RT-PCR to confirm the general significant effects of drug treatment and irradiation.

4 RESULTS

4.1 Bioinformatic analysis of stem cell marker gene expression in glioblastoma

To validate the concept that GSLC marker expressions are higher in glioblastoma than in normal brain tissue, we compared their levels of gene expression using publicly available databases from the TCGA and GTEx projects. This was done using the Genetic Expression Profiling Interactive Analysis (GEPIA) web server [154]. The gene expressions of CD44, Nestin, SOX2 and ALDH1A1 were examined in 163 glioblastoma samples and 207 non-cancerous brain tissues within the TCGA and GTEx data. We chose to analyse these GSLC markers genes because their protein expressions were detected in the glioblastoma cell lines as shown in 4.2. The gene expressions of CD44, Nestin and SOX2 were all significantly higher in the glioblastoma samples than in the non-cancerous tissues (Figure 11). In contrast, ALDH1A1 gene expression was higher in non-cancerous brain tissues than in the glioblastoma samples.

4.2 Effect of radiation on the expression of GSLC marker proteins in monolayer glioblastoma cells lines.

All glioblastoma cell lines (A172, LN229, U87 and U251) were analysed by western blotting to detect if the GSLC marker proteins (Nestin, CD44, SOX2 and ALDH1A1) were expressed. The glioblastoma cell lines were further irradiated to determine the effect of 4 Gy radiation on their expression after 24, 48 and 72 hours. The representative results of 24 and 48 hours after irradiation are presented in the appendix section A (Figure A1) showing differential responses of the GSLC markers to radiation. The results after 72 hours are shown in Figure 12.

The quantified data in Figure 12 shows that Nestin expression was increased 72 hours after 4 Gy radiation in A172 but remained unchanged in LN229, U87 and U251. Radiation of 4 Gy increased the expression of CD44 in A172 but again had no significant changes in the other glioblastoma cell lines. The expression of ALDH1A1 and SOX2 (not detected in U87) were also not significantly affected 72 hours after 4 Gy radiation.

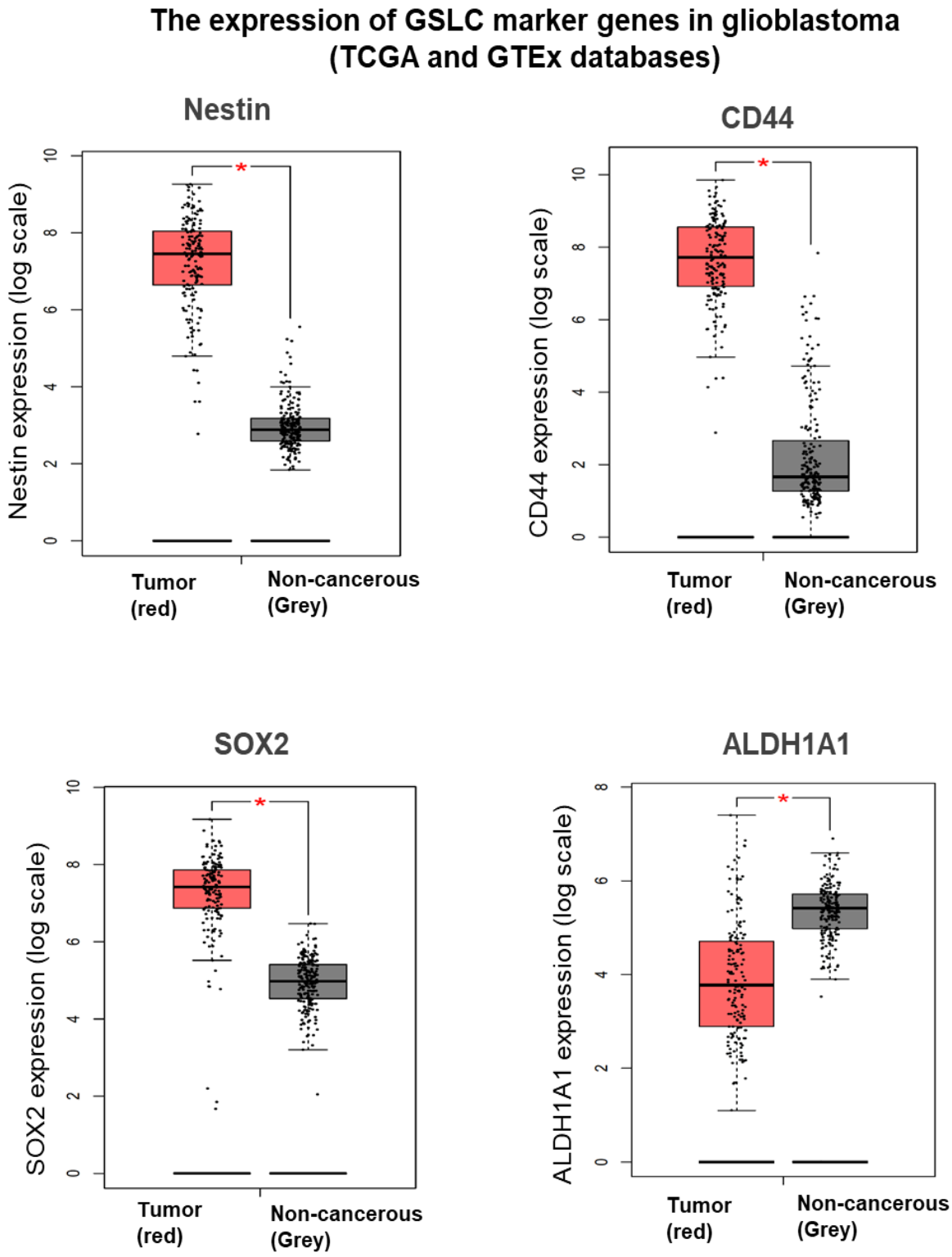

Figure 11: GSLC marker expression in glioblastoma. TCGA and GTEx database comparison of GSLCs marker (CD44, Nestin, SOX2 and ALDH1A1) expression between Tumor (red; 163 samples) and non-cancerous brain tissue (gray; 207 samples). Box plots derived from TCGA normal and GTEx data downloaded via the GEPIA web server (ANOVA: *p-value < 0.05).

Generally, 4 Gy radiation alone after 72 hours had no significant effect on the protein expression of the GSLC markers in all the glioblastoma cell lines tested confirming radioresistance (Figure 12). Because of this, further experiments with HDACi or MEKi treatments were analyzed after 72 hours of radiation for comparison.

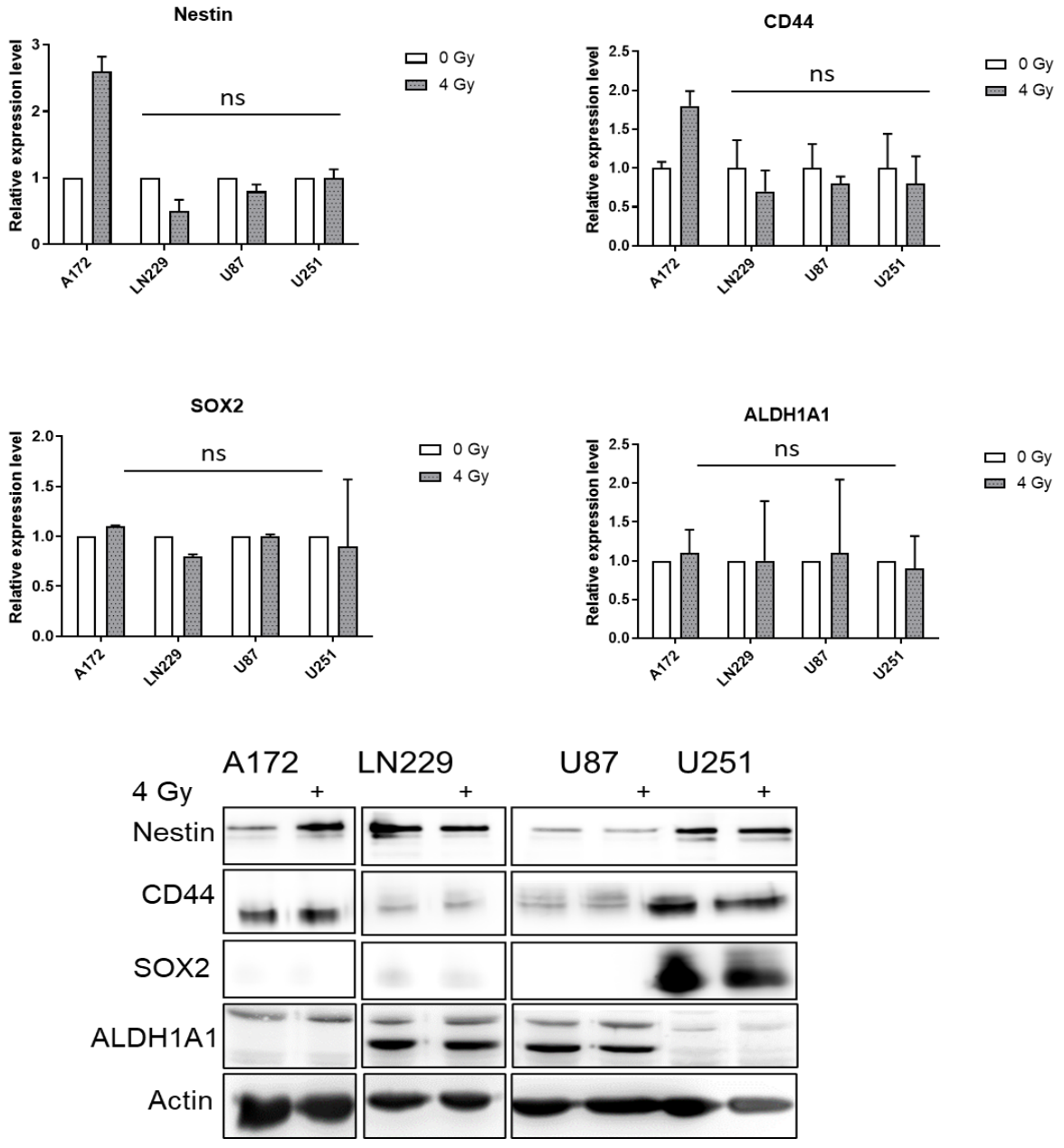

Figure 12: Western blot analysis of GSLC markers after 72 hours of 4 Gy radiation in glioblastoma cell lines. Quantification for Nestin, CD44, SOX2 and ALDH1A1 72 hours after irradiation of A172, LN229, U87 and U251 cell lines. Relative GSLC marker expressions first normalised to Actin and then to sham irradiated control cells (0 Gy) set to 1. Graphs represent mean values (n=3, ns=nonsignificant, T-test) and standard error of mean (SEM). Representative blots of quantified data are shown.

4.3 Responses of GSLC marker proteins to combined treatment of HDACi and MEKi with radiation (Monolayer).

Since 4 Gy radiation alone did not have a significant effect on GSLC marker protein expression after 72 hours, we investigated the efficacy of combining radiation with the HDACi (MS-275) or the MEKi (TAK-733 or trametinib) including the combination of both (MS-275 and TAK-733 or MS-275 and trametinib) with 4 Gy radiation. The treatment concentrations were chosen based on the Genomics of Drug Sensitivity in Cancer (GDSC) databases that revealed the potent concentrations of the HDACi and MEKi in glioblastoma treatment range between 0.9 - 55.5 µM [161]. Therefore, we chose the approximately lowest potent concentration of 1 µM. Additionally, the standard treatment of glioblastoma with TMZ and radiation was applied to control cultures for comparison. TMZ was used at a concentration of 50 µM based on previous testing on glioblastoma cells [75]. The treatment conditions for these experiments together with 4 Gy radiation are listed below;

- 1 µM HDACi MS-275
- 1 µM MEKi TAK-733 (TAK)
- 1 µM Trametinib (TRA)
- 1 µM MS-275 + 1 µM TAK-733
- 1 µM MS-275 + 1 µM Trametinib
- 50 µM TMZ

All results were analysed 72 hours after 4 Gy radiation. The quantified data are presented below while the representative western blots are presented in the appendix section B (Figure A2 - Figure A5)

A172 Monolayer: In A172 cells, TMZ treatment alone and with radiation only showed a potential to reduce SOX2 expression with no other significant effect (Figure 13). MS-275 alone could significantly reduce SOX2 expression with a trend towards a further decrease when combined with 4 Gy radiation. Treatment with TAK-733 alone significantly reduced SOX2 expression as well as CD44 when combined with radiation. Trametinib alone significantly reduced all markers (Nestin, CD44, SOX2 and ALDH1A1) and when combined with radiation, Nestin and CD44 remained significantly lowered. Upon the combined treatment with the HDACi and MEKi (MS-275 and TAK-

733 or MS-275 and trametinib), the expression of Nestin, CD44 and SOX2 were reduced and remained so when combined with 4 Gy radiation (Figure 13). ALDH1A1 expression was not significantly changed by the combined treatments.

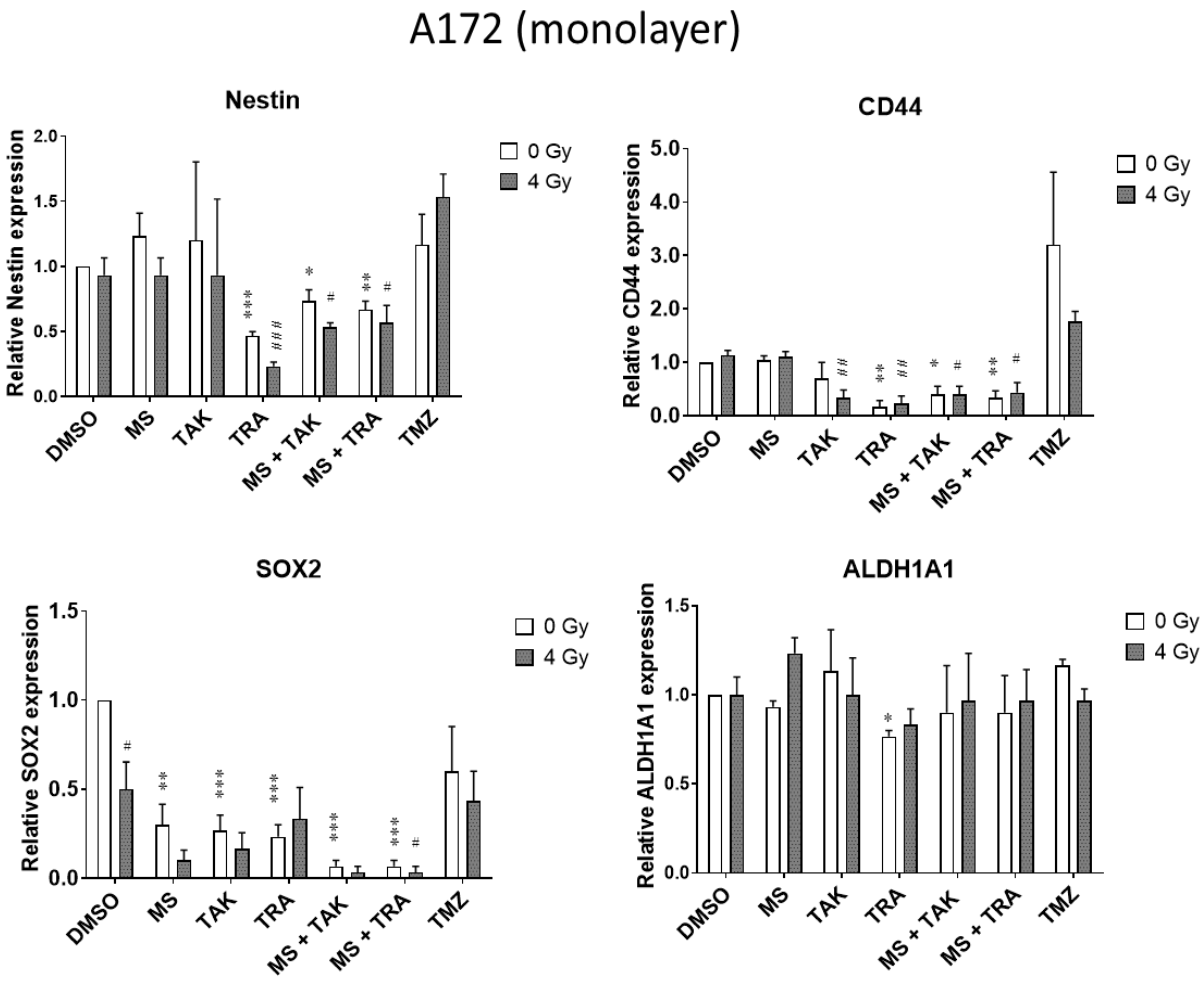

Figure 13: Western blot analysis of GSLC markers 72 hours after combined treatment of drugs and 4 Gy radiation in A172 cells. Quantification data for Nestin, CD44, SOX2 and ALDH1A1 after treatment are shown. (Drugs; 1 µM MS-275 = MS, 1 µM TAK-733 = TAK, 1 µM trametinib = TRA, 50 µM TMZ = TMZ). Relative GSLC marker expressions first normalised to Actin and then to *s*ham irradiated control cells treated with DMSO. [*n* = 3; ± SEM; *Student's *t*-test; **p* ≤ 0.05, ***p* ≤ 0.01, ****p* ≤ 0.001 (versus DMSO 0 Gy); #Student's *t*-test; #*p* ≤ 0.05, ##*p* ≤ 0.01, ###*p* ≤ 0.001 (versus DMSO 4 Gy)].

LN229 Monolayer: In LN229 cells, TMZ treatment alone and with radiation showed no significant effect on all GSLC markers as well as MS-275 treatment alone and with radiation (Figure 14). Treatment with TAK-733 alone significantly reduced Nestin, SOX2 and ALDH1A1 with Nestin and ALDH1A1 remaining significantly decreased

upon radiation exposure. Trametinib treatment with radiation as well as the combination of HDACi and MEKi with radiation could reduce the ALDH1A1 expression while CD44 and SOX2 were not significantly changed. However, the combination of MS-275 and trametinib alone and with radiation could significantly reduce Nestin expression (Figure 14).

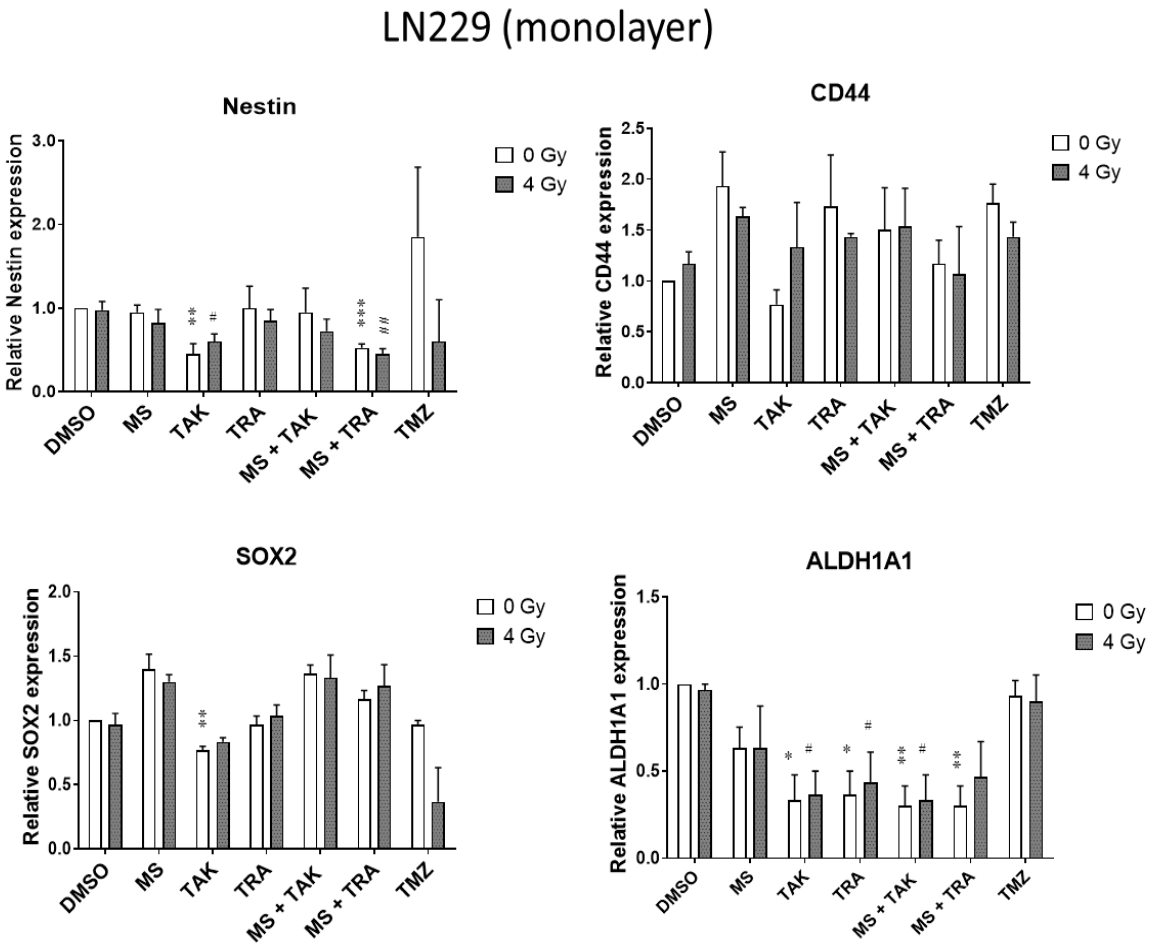

Figure 14: Western blot analysis of GSLC markers after 72 hours combined treatment of drugs and 4 Gy radiation in LN229 cells. Quantification data for Nestin, CD44, SOX2 and ALDH1A1 after treatment are shown. (Drugs; 1 µM MS-275 = MS, 1 µM TAK-733 = TAK, 1 µM trametinib = TRA, 50 µM TMZ = TMZ). Relative GSLC marker expressions first normalized to Actin and then to sham irradiated control cells treated with DMSO. Representative blots of quantified data are shown (down) [*n* = 3; ± SEM; *Student's *t*-test; *$p \leq 0.05$, **$p \leq 0.01$, ***$p \leq 0.001$ (versus DMSO 0 Gy), #Student's *t*-test; #$p \leq 0.05$, ##$p \leq 0.01$ (versus DMSO 4 Gy)].

U87 Monolayer: In U87 cells, TMZ treatment alone displayed no significant effect on all GSLC markers but showed a trend to increase Nestin when combined with radiation (Figure 15). The expression of SOX2 remained undetected by all treatment conditions

except for TMZ and radiation treatment that led to extremely increased SOX2 levels. MS-275 treatment alone significantly reduced ALDH1A1 but did not change Nestin and CD44 while no significant effect of radiation was detected. Treatment with TAK-733 alone and with radiation displayed no significant effect. Similar results were observed with trametinib treatment except for the significant reduction of ALDH1A1, however, no additional effect of radiation was detected. MS-275 and TAK-733 alone significantly reduced ALDH1A1 while MS-275 and trametinib alone and with radiation significantly reduced both CD44 and ALDH1A1 (Figure 15).

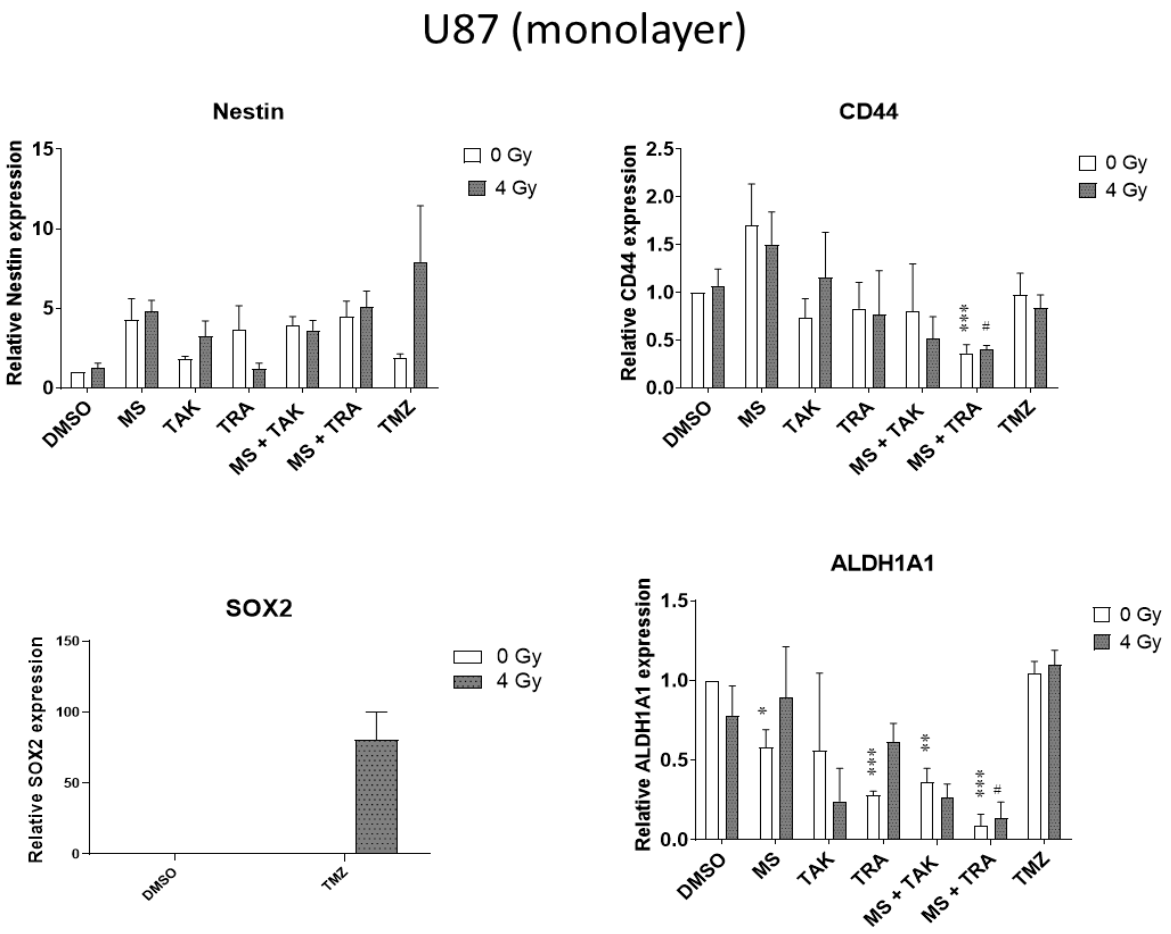

Figure 15: Western blot analysis of GSLC markers after 72 hours combined treatment of drugs and 4 Gy radiation in U87 cells. Quantification data for Nestin, CD44, SOX2 and ALDH1A1 after treatment are shown. (Drugs; 1 µM MS-275 = MS, 1 µM TAK-733 = TAK, 1 µM trametinib = TRA, 50 µM TMZ = TMZ). Relative GSLC marker expressions first normalized to Actin and then to sham irradiated control cells treated with DMSO. Representative blots of quantified data are shown (down) [n = 3; ± SEM; *Student's t-test; *$p \leq 0.05$, **$p \leq 0.01$, ***$p \leq 0.001$ (versus DMSO 0 Gy), #Student's t-test; #$p \leq 0.05$ (versus DMSO 4 Gy)].

U251 Monolayer: in U251 cells, TMZ alone and with radiation showed no significant effect on all GSLC markers. Likewise, all treatments with MS-275, TAK-733 and trametinib alone or with radiation displayed no significant effect. (Figure 16). Upon the combination of HDACi and MEKi, only the combination of MS-275 and TAK-733 plus radiation or MS-275 and trametinib alone significantly reduced Nestin in U251 (Figure 16).

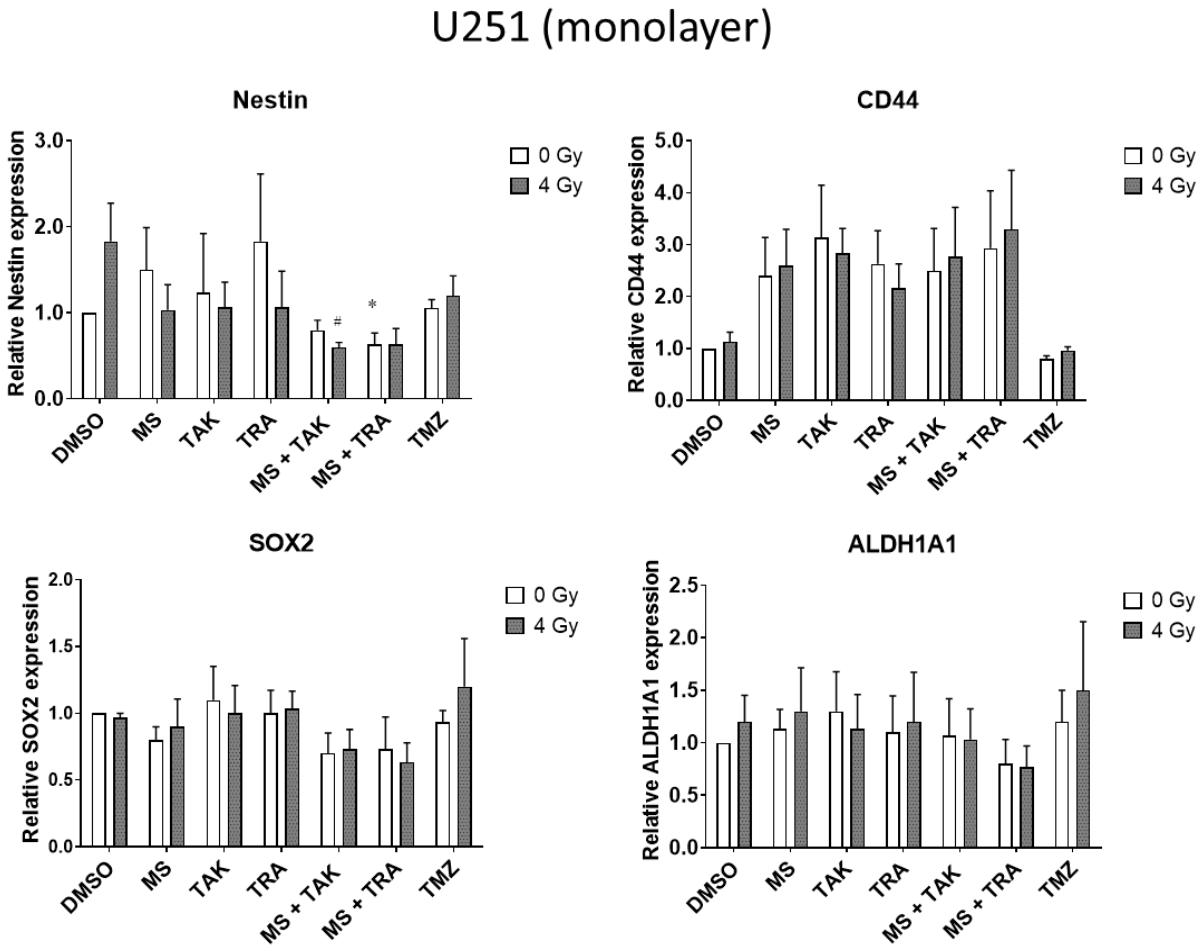

Figure 16: Western blot analysis of GSLC markers after 72 hours combined treatment of drugs and 4 Gy radiation in U251 cells. Quantification data for Nestin, CD44, SOX2 and ALDH1A1 after treatment are shown. (Drugs; 1 µM MS-275 = MS, 1 µM TAK-733 = TAK, 1 µM trametinib = TRA, 50 µM TMZ = TMZ). Relative GSLC marker expressions first normalized to Actin and then to sham irradiated control cells treated with DMSO. Representative blots of quantified data are shown (down) [n = 3; ± SEM; *Student's t-test; *$p \leq 0.05$ (versus DMSO 0 Gy), #Student's t-test; #$p \leq 0.05$ (versus DMSO 4 Gy)].

Taken together, the western blot analysis results revealed differential responses of A172, LN229, U87 and U251 cells to the combined treatment of the HDACi and MEKi

as single or combined drugs with radiation. Since the cell lines tested were differentiated monolayer glioblastoma cell lines, it was difficult to be conclusive on the effectiveness of the combined treatment with radiation against the GSLC population.

4.4 Enrichment of GSLC population by sphere culture

In the order to enrich the stem-like glioblastoma target population based on the established *in vitro* method [162], the glioblastoma cell lines were each cultured in stem cell medium as glioblastoma-derived spheres.

4.4.1 Morphology of glioblastoma cells and stem cell-enriched glioblastoma-derived spheres

The glioblastoma parental cell lines A172, LN229, U87 and U251 were cultured as adherent monolayer cells grown in medium containing serum. Their enriched counterparts were cultured as glioblastoma-derived spheres (A172-sph, LN229-sph, U87-sph and U251-sph) grown in serum-free medium containing stem cell supplements (see 2.9.2).

In Figure 17, the morphology of the adherent glioblastoma cells and their glioblastoma-derived spheres are shown. During adherent culture, it was observed that LN229, U87 and U251 grew faster than A172 cells, however, they all formed monolayers cells exhibiting a mixture of cells with some flat polygonal and some with fibroblast-like morphology with cytoplasmic extensions.

All the glioblastoma cell lines tested successfully formed spheres after the first passage in stem cell medium cultured in ULA flasks. The isolated cells initially floated and aggregated into clusters forming round or ovoid sphere-like structures in the flasks (Figure 17). The spheres formed continued to grow up to a size of about 200 µm in diameter. The ability to form spheres was maintained for eight passages in LN229-sph, U87-sph and U251-sph before they were used for further experiments. In contrast, A172-sph stopped growing after the third passage and could therefore not be used for further analysis.

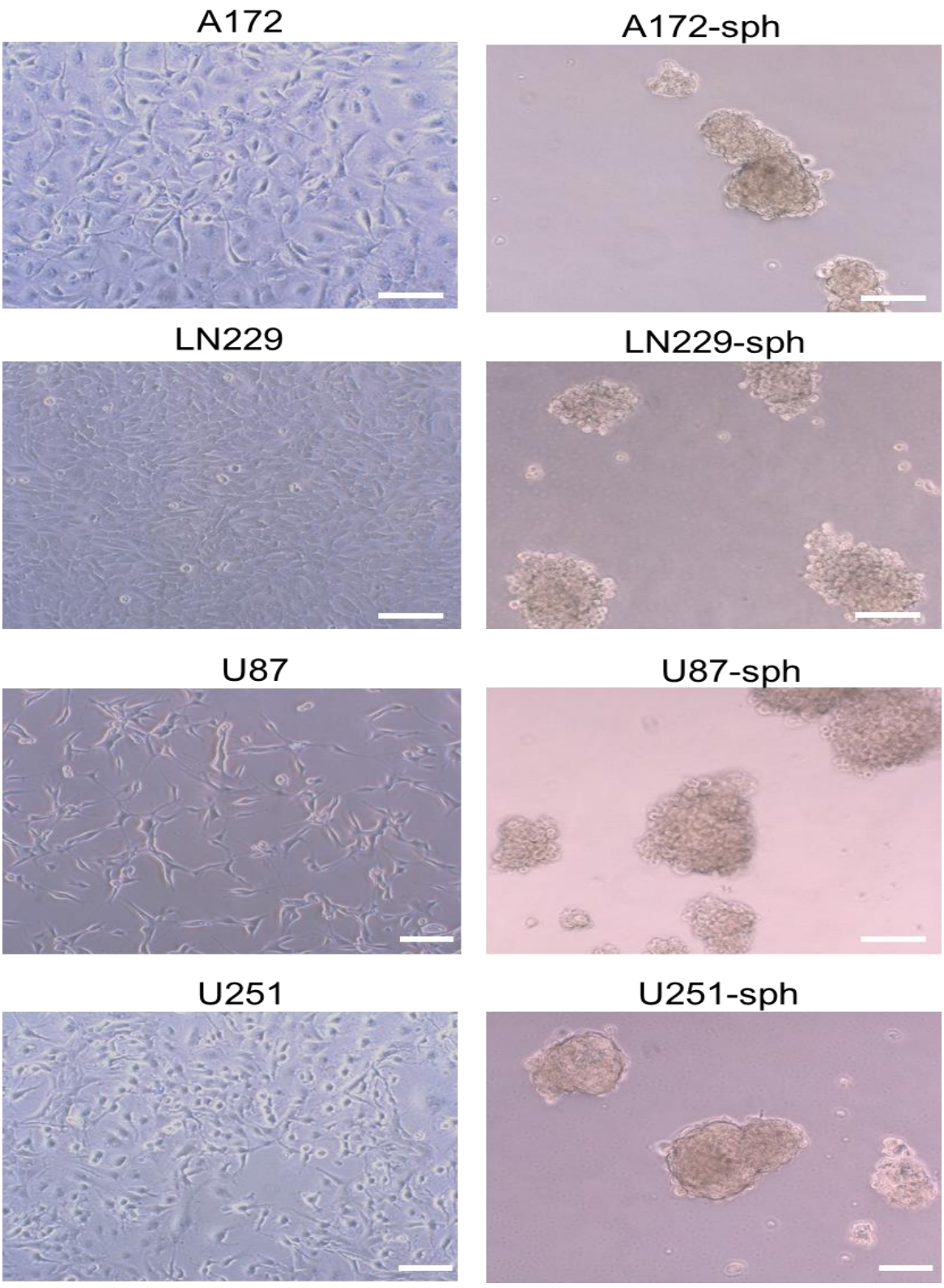

Figure 17: Morphology of glioblastoma cell lines and their glioblastoma-derived spheres. The representative images of the morphology of A172, LN229, U87 and U251 (cultured in medium containing serum as adherent cells) and their glioblastoma-derived spheres A172-sph, LN229-sph, U87-sph and U251-sph (cultured in serum-free medium with stem cell supplements). Scale bar = 100 µm.

4.4.2 Increased expression of GSLC markers after enrichment of glioblastoma cell lines by sphere culture in stem cell medium

In order to determine whether the glioblastoma-derived spheres were enriched for GSLCs at the eighth passage, double-labelling by co-immunoflourescence staining of the stem cell markers was performed. The glioblastoma-derived spheres and their parental cell lines were both immunostained to compare the GSLC marker levels under the two culture conditions. As noted in 4.4.1, the A172 cell line was not studied as spheres were not able to grow after three passages.

Figure 18 shows the increased number of double-labelled cells of CD133 and CD44 in LN229-sph cells compared to their parental LN229 cells. This was also the same for the double-labelling of ALDH1A1 and Nestin and for SOX2 and Nestin in LN229-sph.

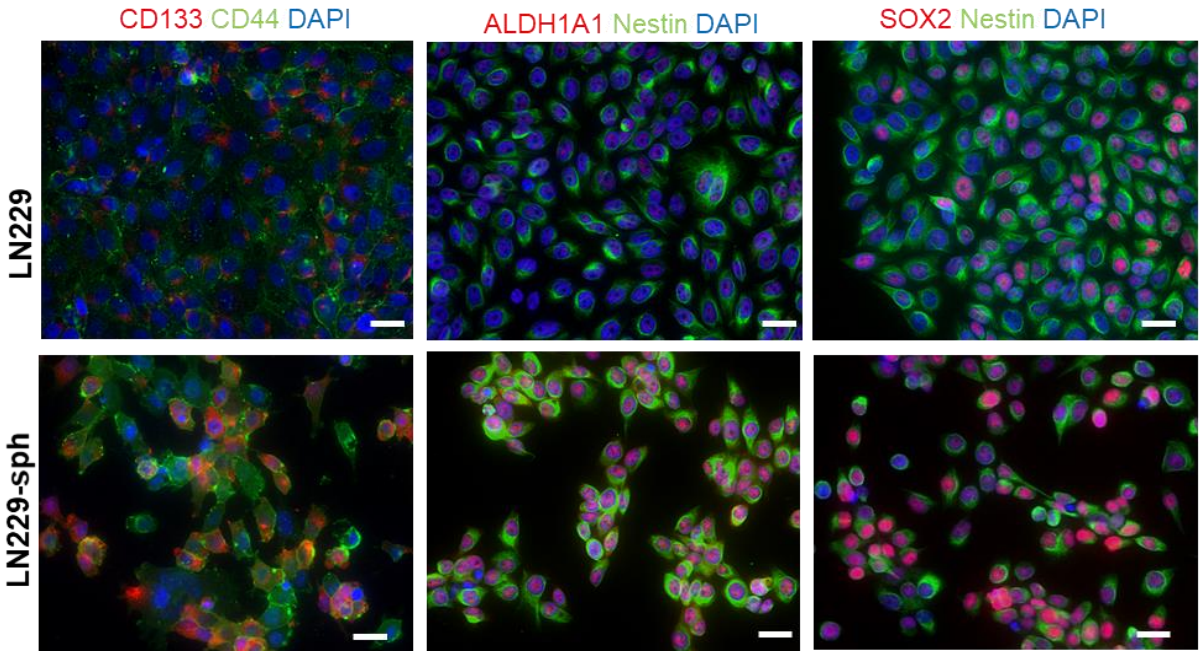

Figure 18: Representative images of co-immunofluorescence staining of LN229 and LN229-sph. The LN229-sph cells showed an increased dual expression of the GSLC markers CD133 (red), CD44 (green), ALDH1A1 (red), Nestin (green) and SOX2 (red) compared to the LN229 parental cells. Scale bar = 100 µm.

A similar result could be observed in the U87 cells as shown in Figure 19. Only a few numbers of U87 monolayer cells were double-labelled for CD133 and CD44, ALDH1A1 and Nestin or SOX2 and Nestin. However, an increased number of double-labelled GSLC markers could be clearly seen in the representative pictures of U87-sph cells.

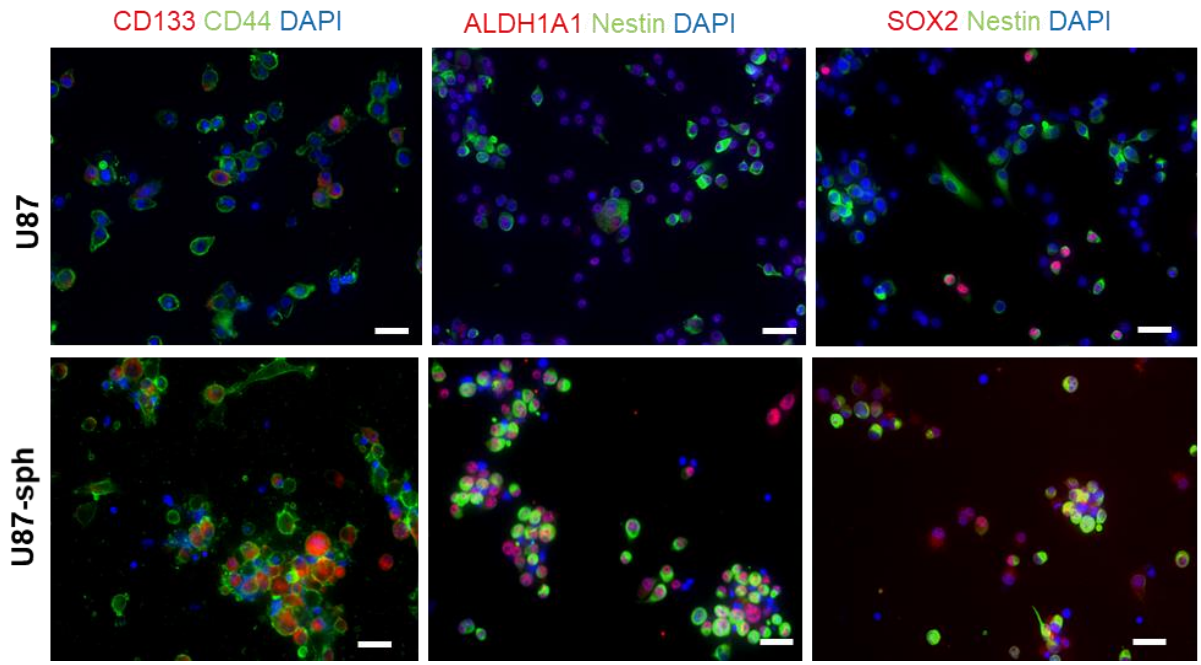

Figure 19: Representative images of co-immunofluorescence staining of U87 and U87-sph. The U87-sph cells showed an increased dual expression of the GSLC markers CD133 (red), CD44 (green), ALDH1A1 (red), Nestin (green) and SOX2 (red) compared to the U87 parental cells. Scale bar = 100 µm.

The representative images for the double-labelling of GSLC markers in U251 and U251-sph are shown in Figure 20. Again, an increased number of double-labelled cells for CD133 and CD44 or SOX2 and Nestin was observed in U251-sph compared to U251. However, ALDH1A1 remained undetected in both U251 and U251-sph.

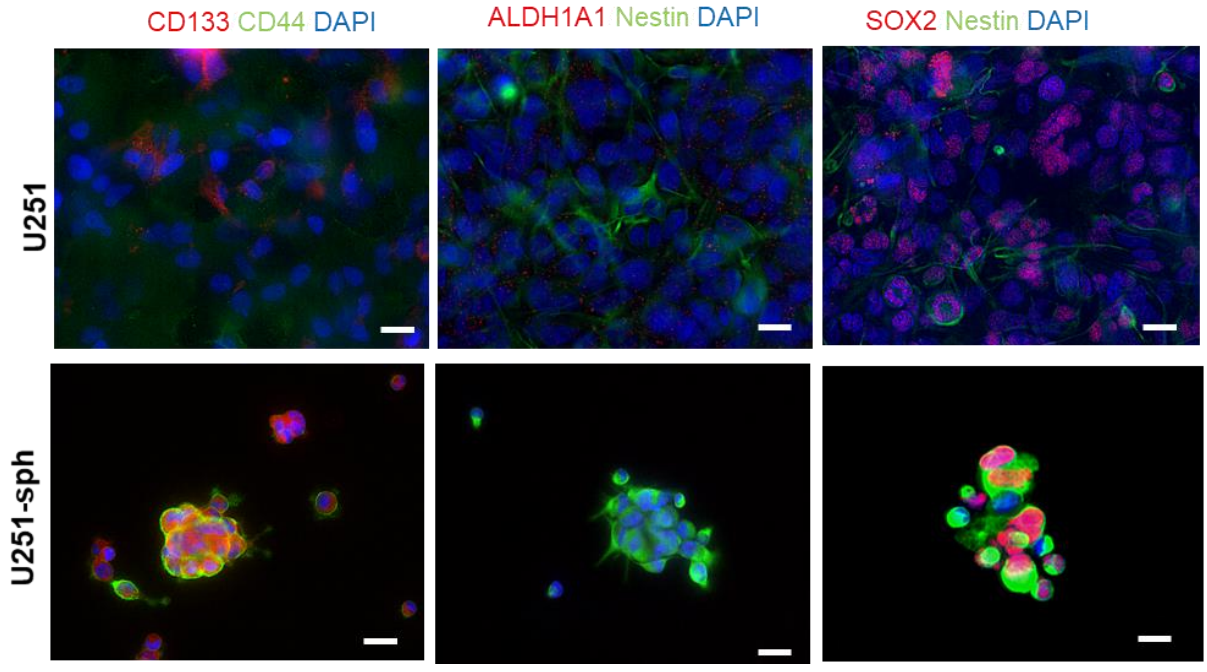

Figure 20: Representative images of co-immunofluorescence staining of U251 and U251-sph. U251-sph cells showed an increased dual expression of the GSLC markers CD133 (red), CD44 (green), Nestin (green) and SOX2 (red) compared to the U251 parental cells. Scale bar = 100 µm.

Overall, the co-immunoflourescence staining images of the cells showed that there was an increased number of double-labelled GSLC markers in the stem cell-enriched glioblastoma-derived spheres compared to their parental cell lines. This suggests that most of the glioblastoma cells acquired more stem cell features under stem cell culture conditions leading to the increased detection of GSLC markers.

Table 14 summarizes the stem cell markers detected in the enriched spheres with the plus sign indicating detection and minus sign no detection.

Table 14: Summary of co-immunofluorescence staining results

Enriched spheres	CD133 CD44	ALDH1A1 Nestin	SOX2 Nestin
LN229-sph	+ +	+ +	+ +
U87-sph	+ +	+ +	+ +
U251-sph	+ +	- +	+ +

*Plus sign indicates detection while minus sign indicates no detection of GSLC markers

4.5 Validation of the inhibitory actions of the HDACi and MEKi on acetylation and MAPK phosphorylation.

The inhibitory actions of MS-275 on protein deacetylation to increase acetylation and of TAK-733 and trametinib on MAPK phosphorylation were confirmed using U87-sph and U251-sph cell models.

Figure 21 shows that acetylated Histone H3 (Acetyl-H3) was increased in U87-sph and U251-sph compared to the 0 Gy DMSO control samples after 48 hours of treatment with 1 µM MS-275. A further increase was observed at 10 µM with a fold change value of up to 26 in both U87-sph and U251-sph. This increase in acetylation was maintained in both with and without 4 Gy radiation confirming the activity of the drug.

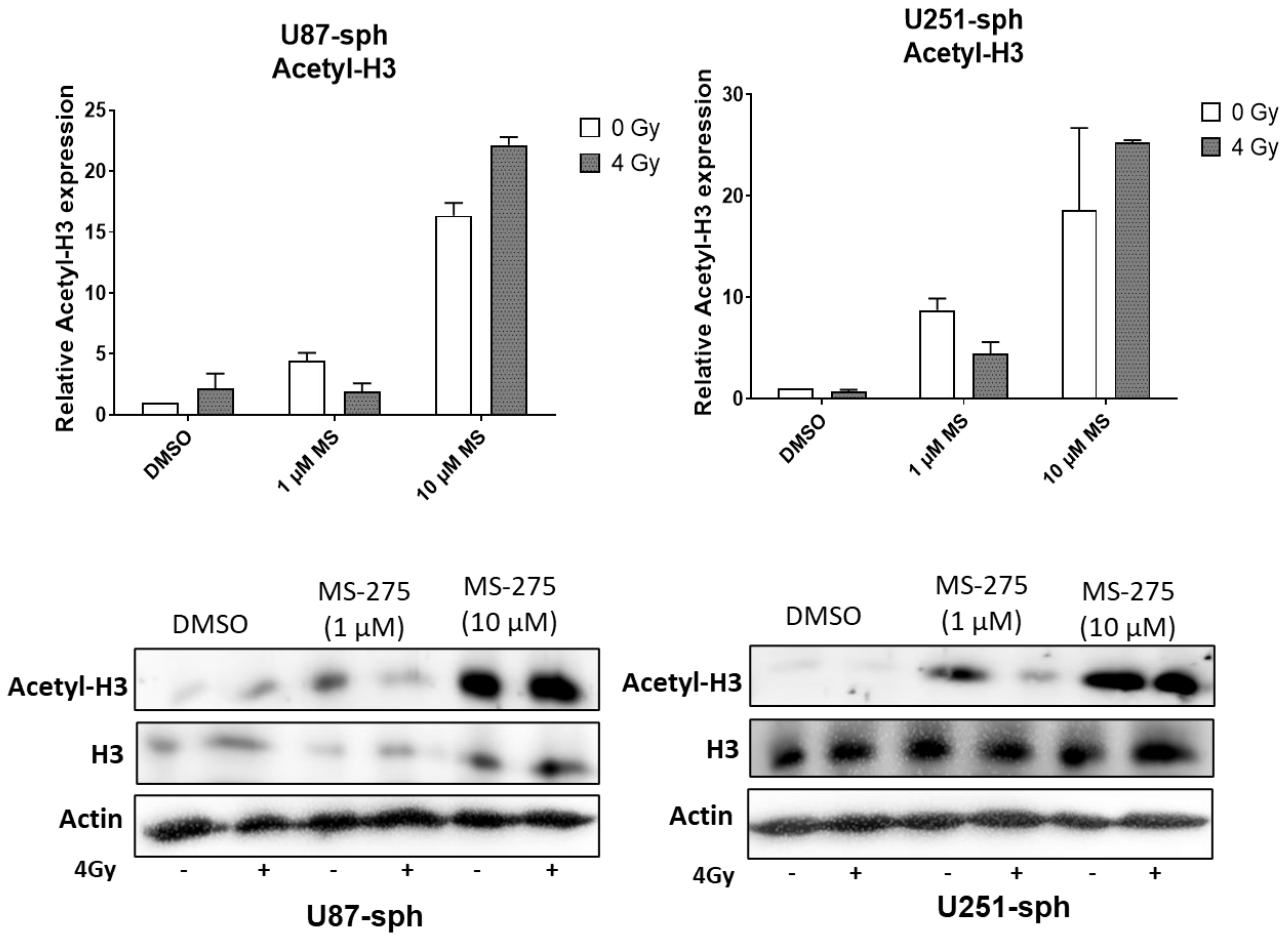

Figure 21: Action of the HDACi MS-275 (MS) in the enriched glioblastoma-derived spheres. Quantification data for Acetyl-H3 (17 kDa) in U87-sph and U251-sph 48 hours after HDACi treatment and 4 Gy irradiation. Relative Acetyl-H3 expression was first normalized to actin and then to the respective 0 Gy DMSO sample (n = 2). Actin (45 kDa) was used as the baseline control for comparison.

The MEK inhibitors TAK-733 and tramentinib were tested by their ability to inhibit the activation of phosphorylated MAPK (pMAPK). In U87-sph, Figure 22 showed that 1 µM TAK-733 reduced pMAPK expression while at 10 µM pMAPK was completely eradicated. Likewise, pMAPK expression was not detected upon treatment with trametinib at both 1 and 10 µM.

In the case of U251-sph, pMAPK levels were only slightly reduced upon treatment with 1 µM TAK-733, however, at 10 µM pMAPK was eradicated. Similar to U87-sph, treatment of U251-sph with trametinib at 1 and 10 µM completely eradicated pMAPK. As seen on the representative blots, neither MEK inhibitor affected the basal levels of MAPK (Figure 22).

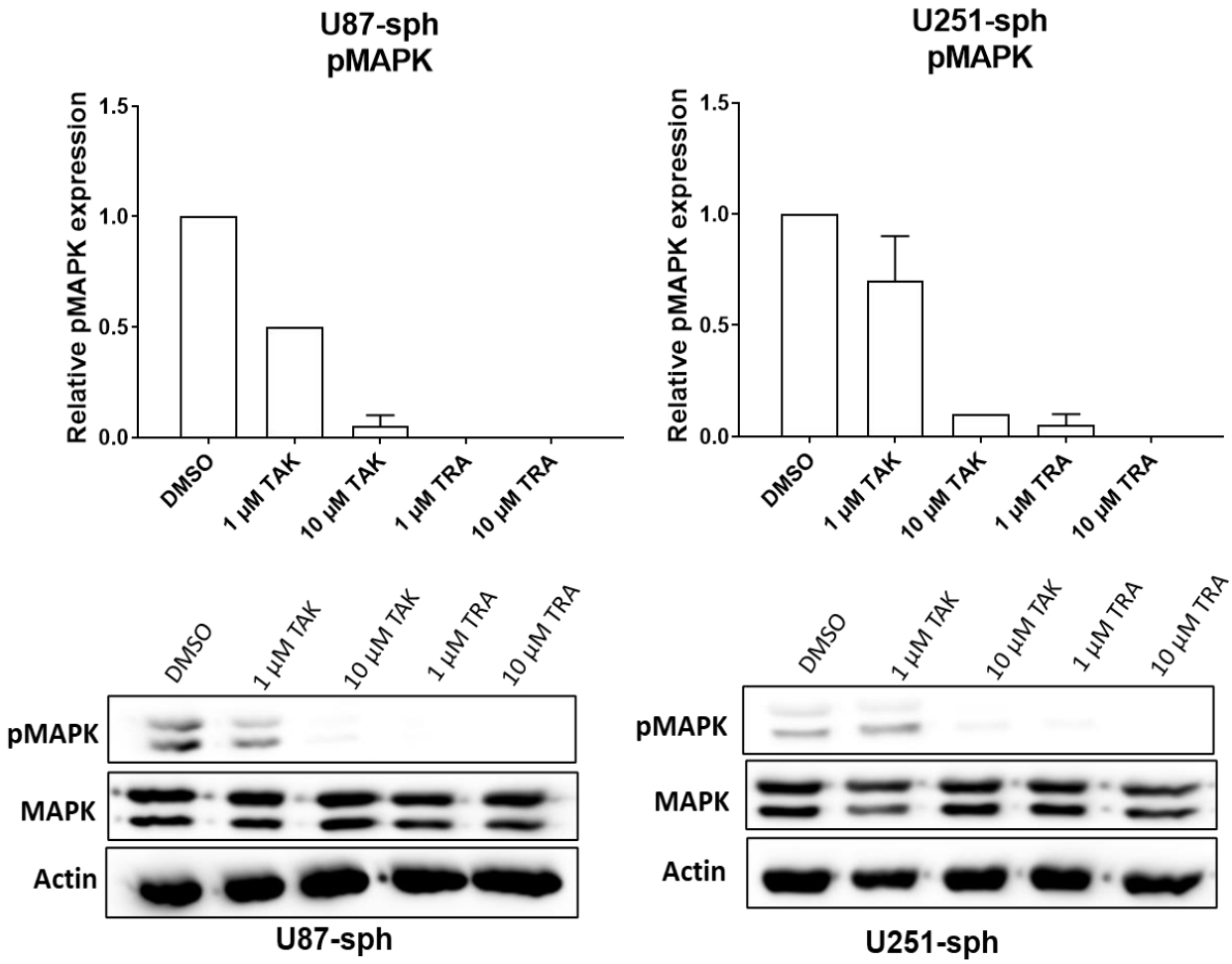

Figure 22: Action of the MEKi TAK-733 (TAK) or trametinib (TRA) in the enriched glioblastoma-derived spheres. Quantification data for pMAPK (42/44 kDa) in U87-sph and U251-sph 48 hours after MEKi treatment. Relative pMAPK expression was first normalized to actin and then to the respective DMSO sample (n = 2). Actin (45 kDa) was used as the baseline control for comparison.

4.6 Cell viability decreased with increasing concentrations of HDACi or MEKi with radiation

In order to identify the doses of drugs where effects on cell viability are observed in combination with 4 Gy radiation, the enriched glioblastoma-derived spheres were treated with increasing concentrations of 1, 10 and 50 µM of each compound. The cell viability was determined 72 hours after radiation exposure.

LN229-sph: Figure 23 shows that in LN229-sph cells, the effect of TMZ to reduce cell viability was lesser compared to the HDACi or MEKi at all concentrations with and without radiation. It can also be seen that the viability was significantly decreased by a

single treatment with the HDACi (MS-275) or MEKi (TAK-733 and trametinib) at 1 µM alone or with radiation compared to treatment with radiation alone. The decrease in cell viability was maintained at 10 and 50 µM concentrations where the cell viability became either extremely low or undetected by single treatment with the HDACi or MEKi or in combination with radiation (Figure 23).

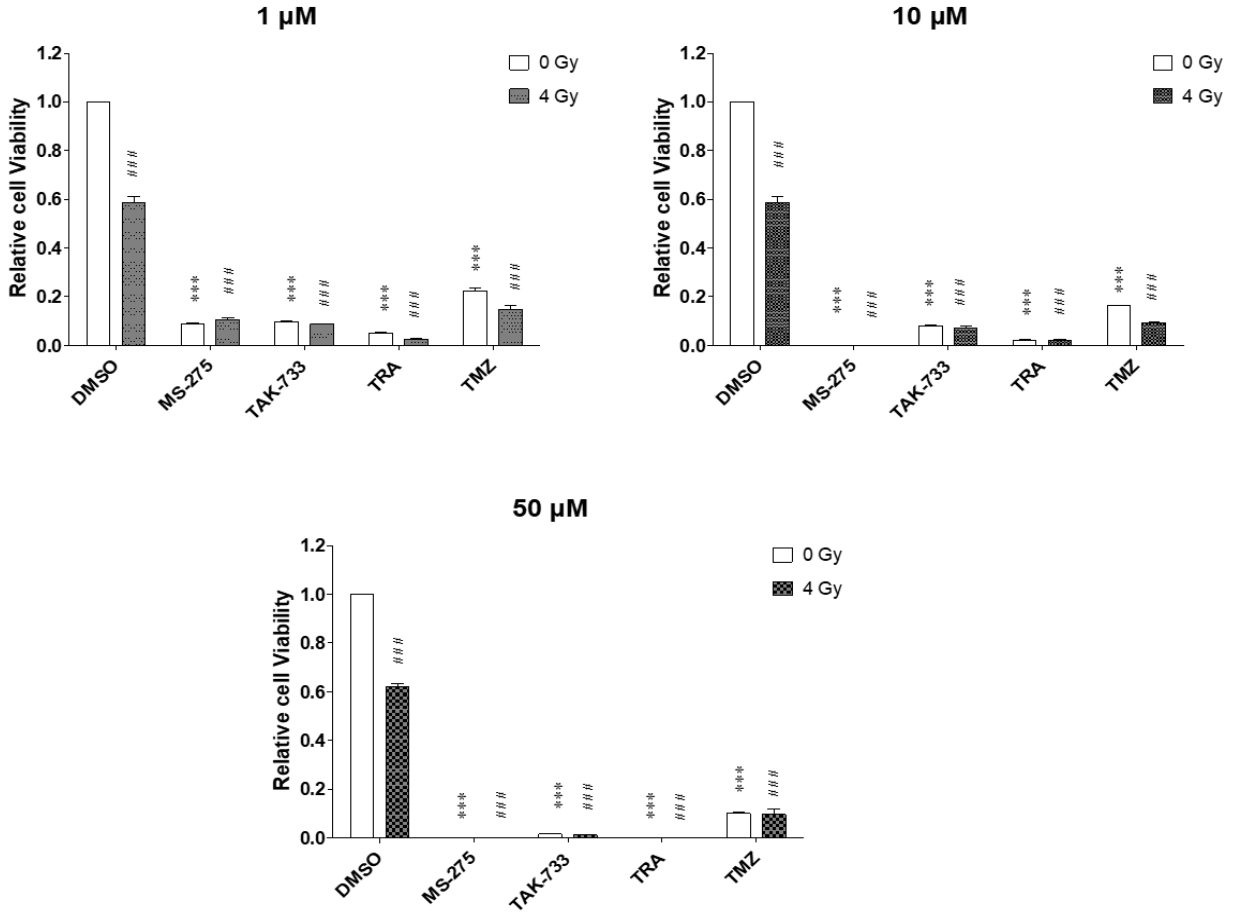

Figure 23: CellTiter-Glo® viability assay of LN229-sph. The cell viability of LN229-sph cells decreased with increasing concentration of drugs. Viability of cells was measured by quantification of luminescence 72 hours after treatment with 1, 10 and 50 µM of drugs and 4 Gy radiation. Data represents mean values ± SEM (n = 3). Bars not visible represent mean values less than or equal to 0. [Student's *t*-test; ***$p \leq 0.001$ (versus DMSO 0 Gy), $^{\#\#\#}p \leq 0.001$ (versus DMSO 4 Gy). 2-way ANOVA; *p*-value <0.0001].

U87-sph: As observed in LN229-sph, viability was always higher in U87-sph cells treated with TMZ and radiation at 1, 10 and 50 µM compared to the HDACi or MEKi treatment with radiation (Figure 23 and Figure 24).

Similar results could also be detected in the U87-sph cells where at 1 µM, the HDACi or MEKi alone or combined treatment with radiation significantly reduced cell viability compared to treatment with radiation alone. As the concentration of the drugs increased to 10 and 50 µM, a greater decrease in viable cells was detected compared to 4 Gy treatment only (Figure 24).

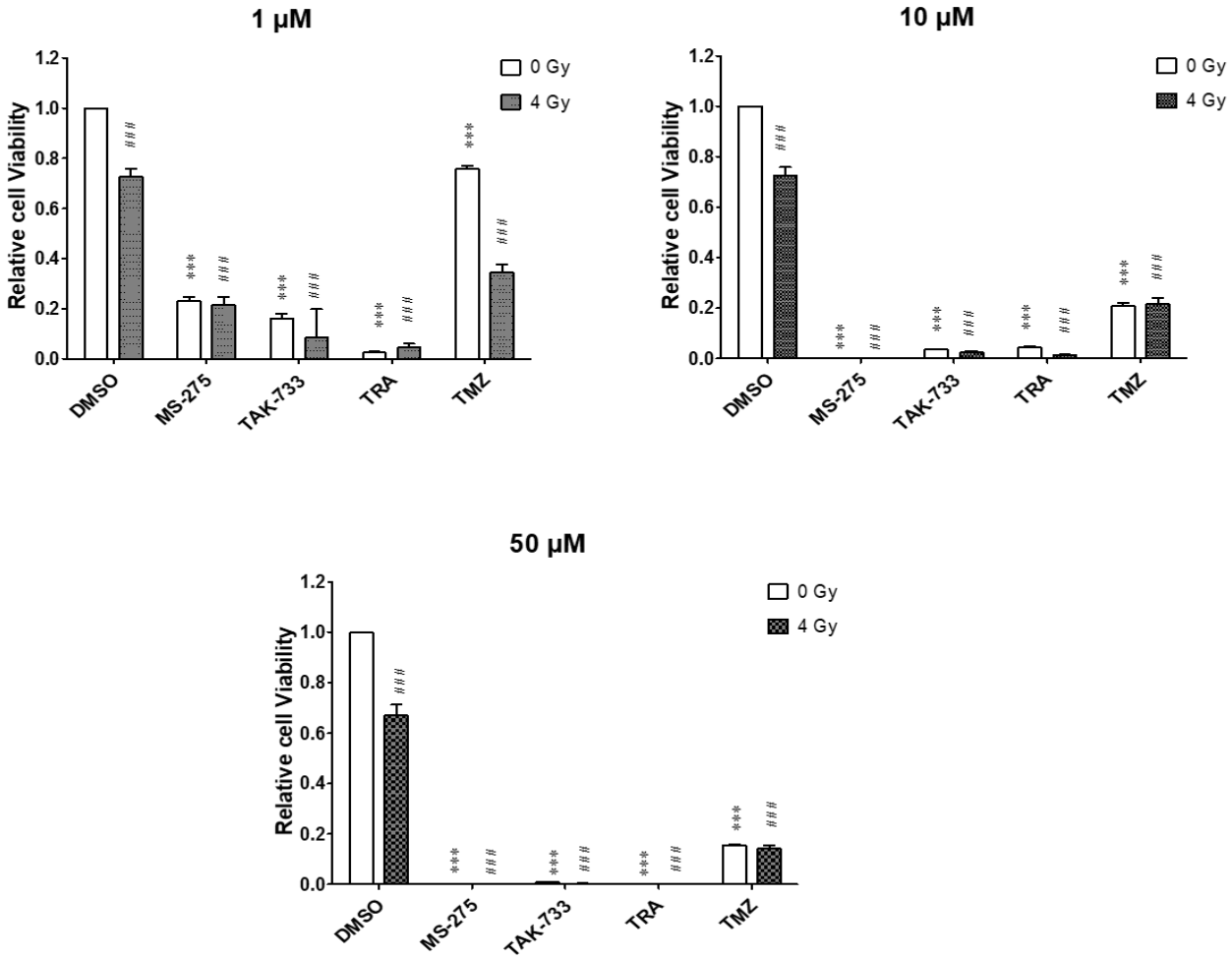

Figure 24: CellTiter-Glo® viability assay of U87-sph. The cell viability of U87-sph cells decreased with increasing concentration of drugs. Viability of cells was measured by quantification of luminescence 72 hours after treatment with 1, 10 and 50 µM of drugs and 4 Gy radiation. Data represents mean values ± SEM (n = 3). Bars not visible represent mean values less than or equal to 0. [Student's *t*-test; ***$p \leq 0.001$ (versus DMSO 0 Gy), $^{\#\#\#}p \leq 0.001$ (versus DMSO 4 Gy). 2-way ANOVA; *p*-value <0.0001].

U251-sph: Interestingly, the viability of the U251-sph cells was significantly increased by a single treatment with the standard compound TMZ at 1, 10 and 50 µM. When combined with radiation, the increase due to TMZ was nullified (Figure 25). The

reduction of U251-sph cell viability after single treatment with the HDACi or MEKi alone or combined with radiation was also detected compared to radiation only. This reduction was maintained at 1, 10 and 50 µM concentrations of the drugs with no remaining viable U251-sph cells detected after treatment with MS-275 at 10 and 50 µM (Figure 25).

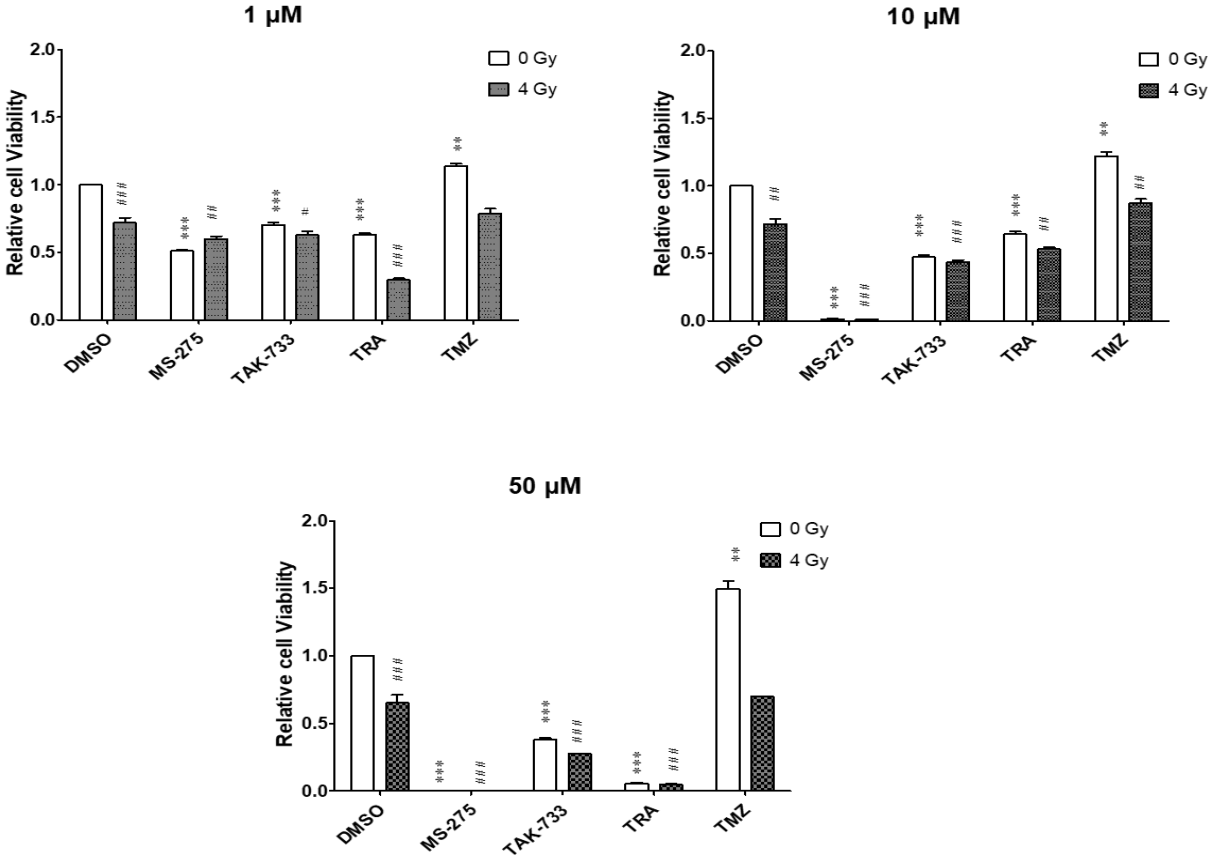

Figure 25: CellTiter-Glo® viability assay of U251-sph. The cell viability of U251-sph cells decreased with increasing concentration of drugs. Viability of cells was measured by quantification of luminescence 72 hours after treatment with 1, 10 and 50 µM of drugs and 4 Gy radiation. Data represents mean values ± SEM (n = 3). Bars not visible represent mean values less than or equal to 0. [Student's *t*-test; ***$p \leq 0.001$ (versus DMSO 0 Gy), $^{###}p \leq 0.001$ (versus DMSO 4 Gy). 2-way ANOVA; *p*-value <0.0001].

Taken together, the results imply that the HDACi and MEKi requires a lower concentration of 1 µM to reduce cell viability as opposed to the standard compound TMZ. For further analysis, the HDAC and MEKi were used at 1 µM because of the cell viability results indicating 10 and 50 µM concentrations were too high. TMZ was used at 50 µM since viability could still be detected at this high concentration.

4.7 Sphere forming ability of cells from GSLC-enriched glioblastoma spheres is inhibited by the combined treatment of HDACi and MEKi with radiation

To further investigate the effect of combining the HDACi and MEKi with radiation compared to either treatment alone, the sphere forming ability of the GSLCs were tested after treatment. The sphere formation rate was defined as the number of spheres divided by the total number of starting cells.

LN229-sph: Figure 26 shows that in LN229-sph, radiation exposure alone at 4 Gy significantly reduced sphere formation capacity. The treatment with TMZ alone or with radiation was a very effective treatment since there were almost no spheres formed.

Also, in the LN229-sph (Figure 26), treatment with the HDACi MS-275 alone or combined with radiation showed no significant effect. Treatment with the MEKi (TAK-733 or trametinib) alone significantly reduced sphere formation compared to the untreated cells (DMSO) with an enhanced reduction observed when combined with 4 Gy radiation.

The combination of HDACi and MEKi reduced the number of spheres formed significantly (***$p \leq 0.001$) compared to the control cells. The addition of radiation to the combined MS-275 and trametinib treatment significantly enhanced the reduction of sphere formation ($^{###}p \leq 0.001$) as no spheres were formed (Figure 26).

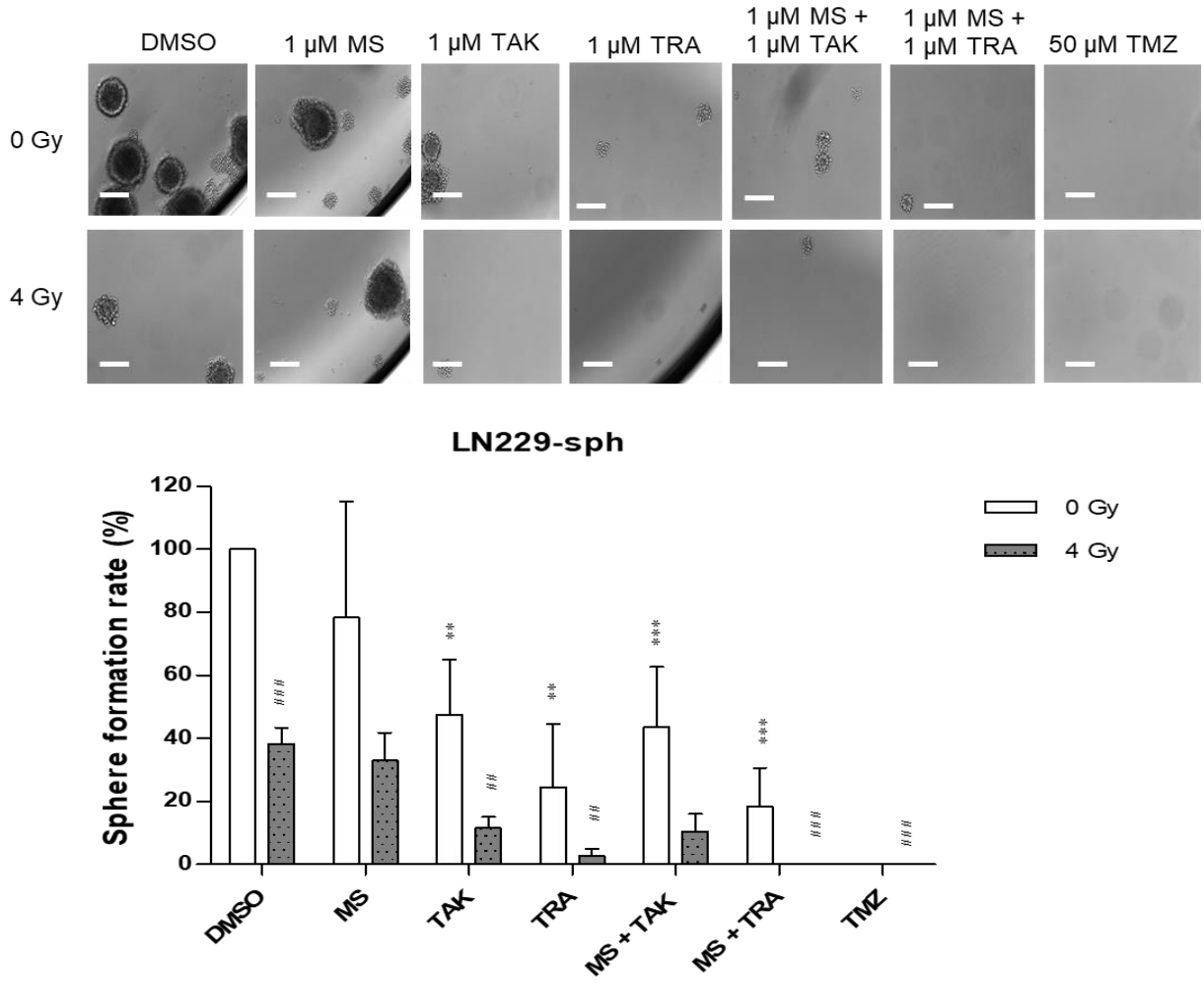

Figure 26: Treatment of HDACi and MEKi with radiation inhibited sphere formation of LN229-sph. Representative images of spheres formed 14 days after treatment of drugs and radiation in LN229-sph cells are shown (up; scale bar = 100 µm). Quantified data represents sphere formation rate (%) normalized to the DMSO treated cells as control set to 100%. Data represents mean values ± SEM (n = 3). [*Student's *t*-test; ** $p \leq 0.01$, *** $p \leq 0.001$ (versus DMSO 0 Gy), ## $p \leq 0.01$ ### $p \leq 0.001$ (versus DMSO 4 Gy). 2-way ANOVA; *p*-value <0.0001]

U87-sph: Comparable results were detected in U87-sph cells as shown in Figure 27. Radiation alone significantly reduced sphere formation while no spheres were formed with TMZ alone. By adding radiation to TMZ, a significant reduction of spheres could be seen compared to the untreated cells.

Also in U87-sph, Figure 27 showed that treatment with MS-275 alone or combined with radiation significantly reduced sphere formation. With the treatment of TAK-733 or trametinib alone, sphere formation was significantly reduced with an enhanced reduction observed when combined with 4 Gy radiation. Significantly fewer spheres

were formed upon the combined treatment of the HDACi and MEKi alone. Like in LN229-sph, the addition of radiation to the combined treatment of HDACi and MEKi significantly led to a greater reduction in sphere formation ($^{\#\#}p \leq 0.01$) compared to the single treatment in U87-sph (Figure 27).

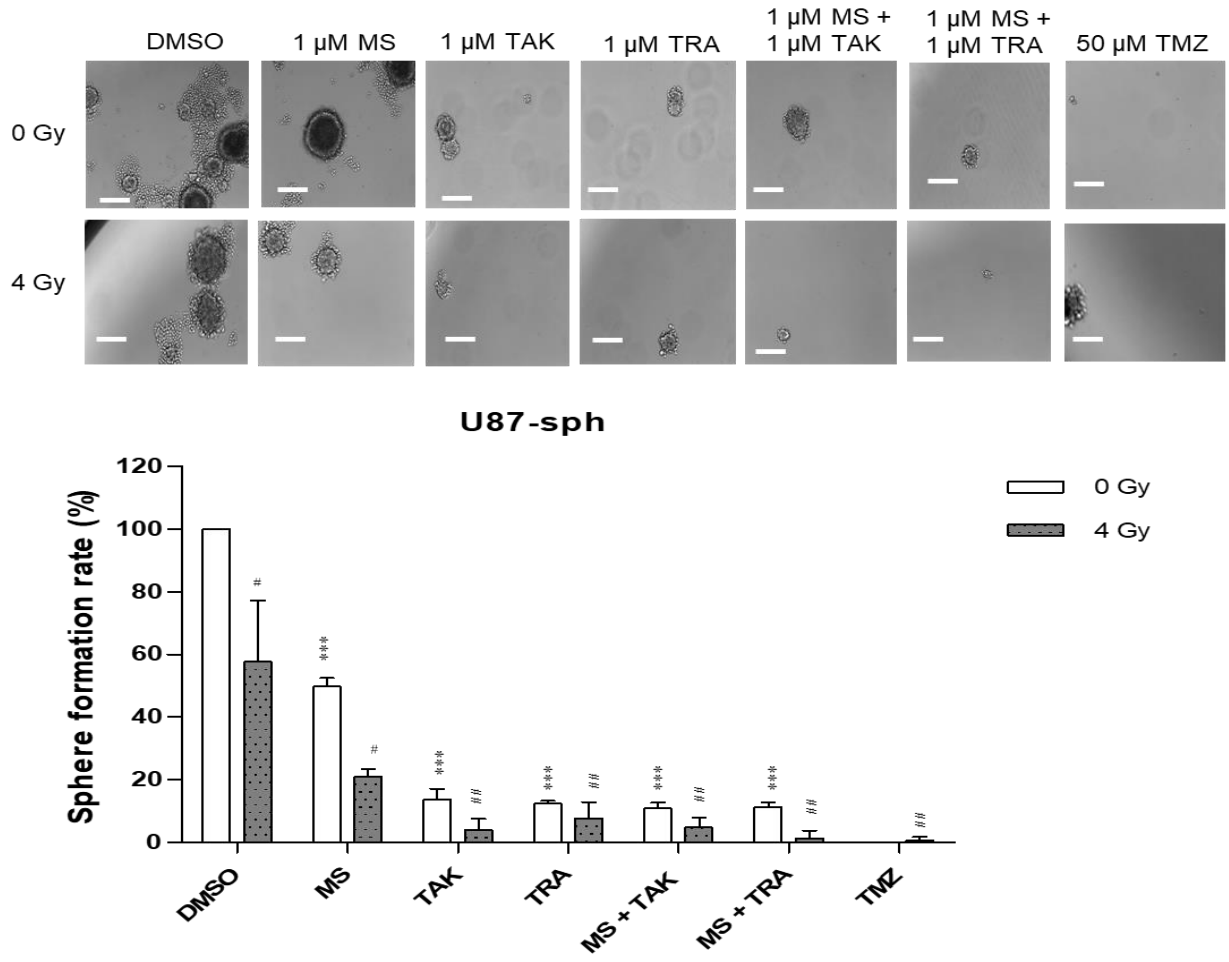

Figure 27: Treatment of HDACi and MEKi with radiation inhibited sphere formation of U87-sph GSLCs. Representative images of spheres formed 14 days after treatment of drugs and radiation in U87-sph cells are shown (up; scale bar = 100 µm). Quantified data represents sphere formation rate (%) normalized to the DMSO treated cells as control set to 100%. Data represents mean values ± SEM (n = 3). [*Student's *t*-test; ***$p \leq 0.001$ (versus DMSO 0 Gy), $^{\#}p \leq 0.05$ $^{\#\#}p \leq 0.01$ (versus DMSO 4 Gy). 2-way ANOVA; *p*-value <0.0001].

U251-sph: In U251-sph, Figure 28 shows that radiation alone did not have a significant effect on sphere formation. TMZ treatment alone significantly reduced sphere formation compared to the untreated cells, however, no additional effect was detected when combined with radiation.

While there was a tendency for MS-725 alone to reduce sphere formation in U251-sph, no significant effect was detected when combined with radiation (Figure 28). Single treatments with TAK-733 or trametinib significantly reduced the number of spheres formed compared to the untreated cells with no additional effect of radiation detected. Upon the combination of the HDACi and MEKi, sphere formation remained inhibited with a greater effect observed by combining MS-275 and trametinib (***$p \leq 0.001$). By adding radiation to the combined treatment, sphere formation remained significantly ($^{\#}p \leq 0.05$) low (Figure 28).

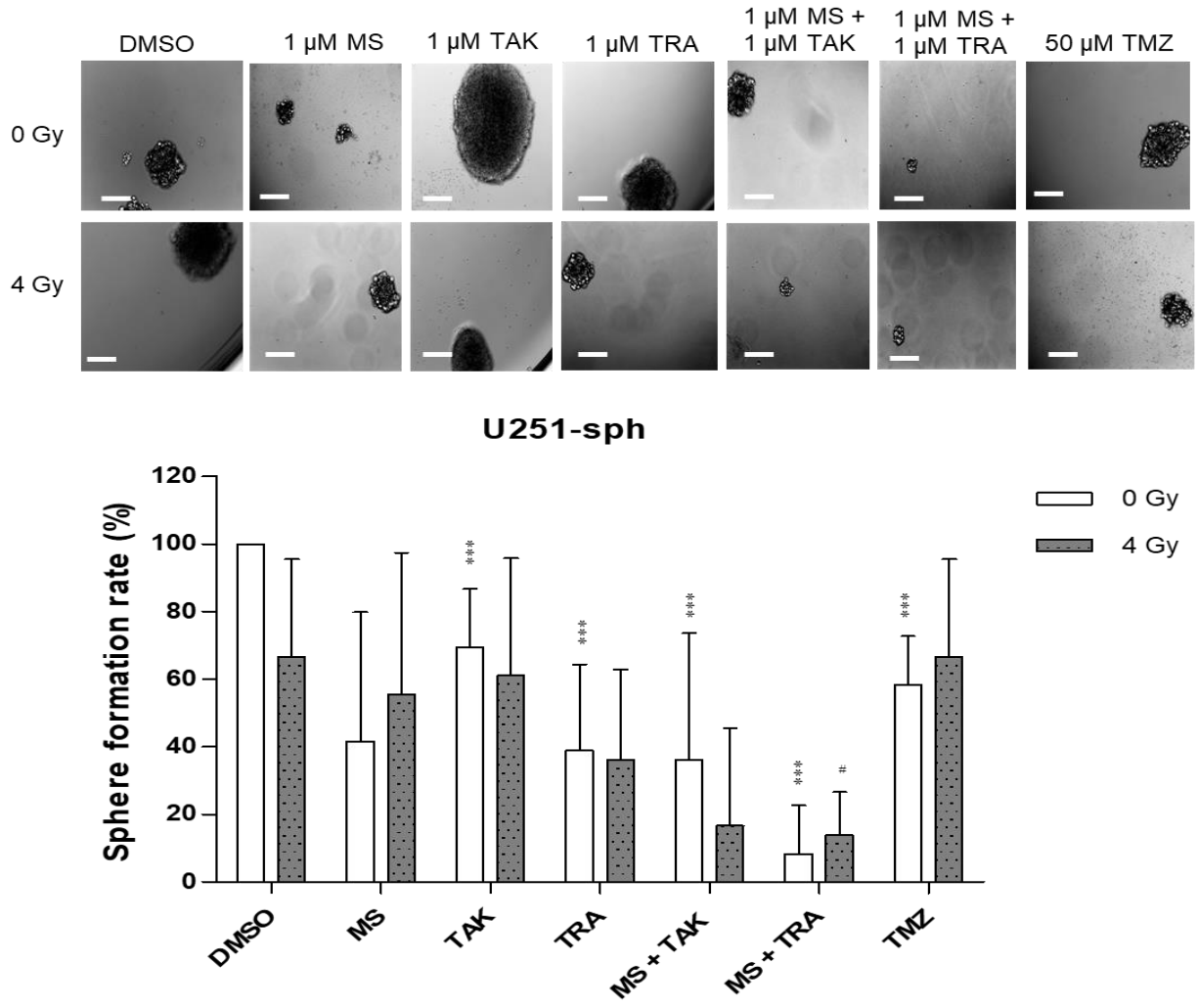

Figure 28: Treatment of HDACi and MEKi with radiation inhibited sphere formation of U251-sph GSLCs. Representative images of spheres formed 14 days after treatment of drugs and radiation in U251-sph cells are shown (up; scale barb=b100 µm). Quantified data represents sphere formation rate (%) normalized to the DMSO treated cells as control set to 100%. Data represents mean values ± SEM (n = 3). [*Student's *t*-test; ***$p \leq 0.001$ (versus DMSO 0 Gy), $^{\#}p \leq 0.05$ (versus DMSO 4 Gy). 2-way ANOVA; *p*-value <0.01].

Generally, treatment with the standard compound TMZ at 50 µM alone or with radiation was more effective in reducing the sphere formation of LN229-sph and U87-sph cells compared to the U251-sph cells (Figure 26 - Figure 28).

Given that sphere formation measures self-renewal of stem cells [163, 164] the results showed that the combined treatment of the HDACi and MEKi with radiation could significantly decrease the self-renewal ability of the GSLCs in some cell lines. This suggests that the combined treatment with radiation has a potential to change the number of GSLCs present. To test this, we investigated the effect of the combined treatment on GSLC markers as presented in 4.8.

4.8 Response of GSLC marker proteins in enriched glioblastoma-derived spheres to combined treatment of HDACi and MEKi with radiation

Next, we determined whether the combination of the HDACi and MEKi with radiation was effective against the protein expressions of the GSLC markers Nestin, CD44, SOX2 and ALDH1A1 in LN229-sph, U87-sph and U251-sph. This was done by western blot quantification performed 72 hours after 4 Gy radiation and combined treatment of the inhibitors.

LN229-sph: The results in Figure 29 show that 4 Gy radiation alone did not have any effect on any GSLC marker in LN229-sph. Treatment with TMZ alone and combined with radiation showed no effect on Nestin, CD44 and SOX2 but significantly reduced ALDH1A1. Similarly, MS-275 treatment alone or combined with radiation significantly reduced ALDH1A1. Treatments with the MEKi TAK-733 or trametinib alone showed no significant effect on Nestin but significantly reduced SOX2 and ALDH1A1. By adding radiation to TAK-733, Nestin, SOX2 and ALDH1A1 were significantly reduced while trametinib with 4 Gy radiation significantly reduced SOX2 and ALDH1A1 (Figure 29).

By combining the HDACi and MEKi in LN229-sph (Figure 29), only MS-275 combined with trametinib alone and with 4 Gy radiation significantly reduced the expression of Nestin compared to treatment with radiation alone ($^{**}p \leq 0.01$, $^{\#\#}p \leq 0.01$). However, both combinations of HDACi and MEKi (MS + TAK and MS + TRA) alone and combined with radiation significantly reduced SOX2 and ALDH1A1. It was observed that all the single and combined treatment conditions showed no significant effect on

CD44 but surprisingly showed a trend to increase its expression in LN229-sph (Figure 29).

To summarize the results in LN229-sph, it was demonstrated that the combination of HDACi and MEKi with radiation could significantly reduce Nestin, SOX2 and ALDH1A1 protein expression with a trend to increase CD44 (Figure 29).

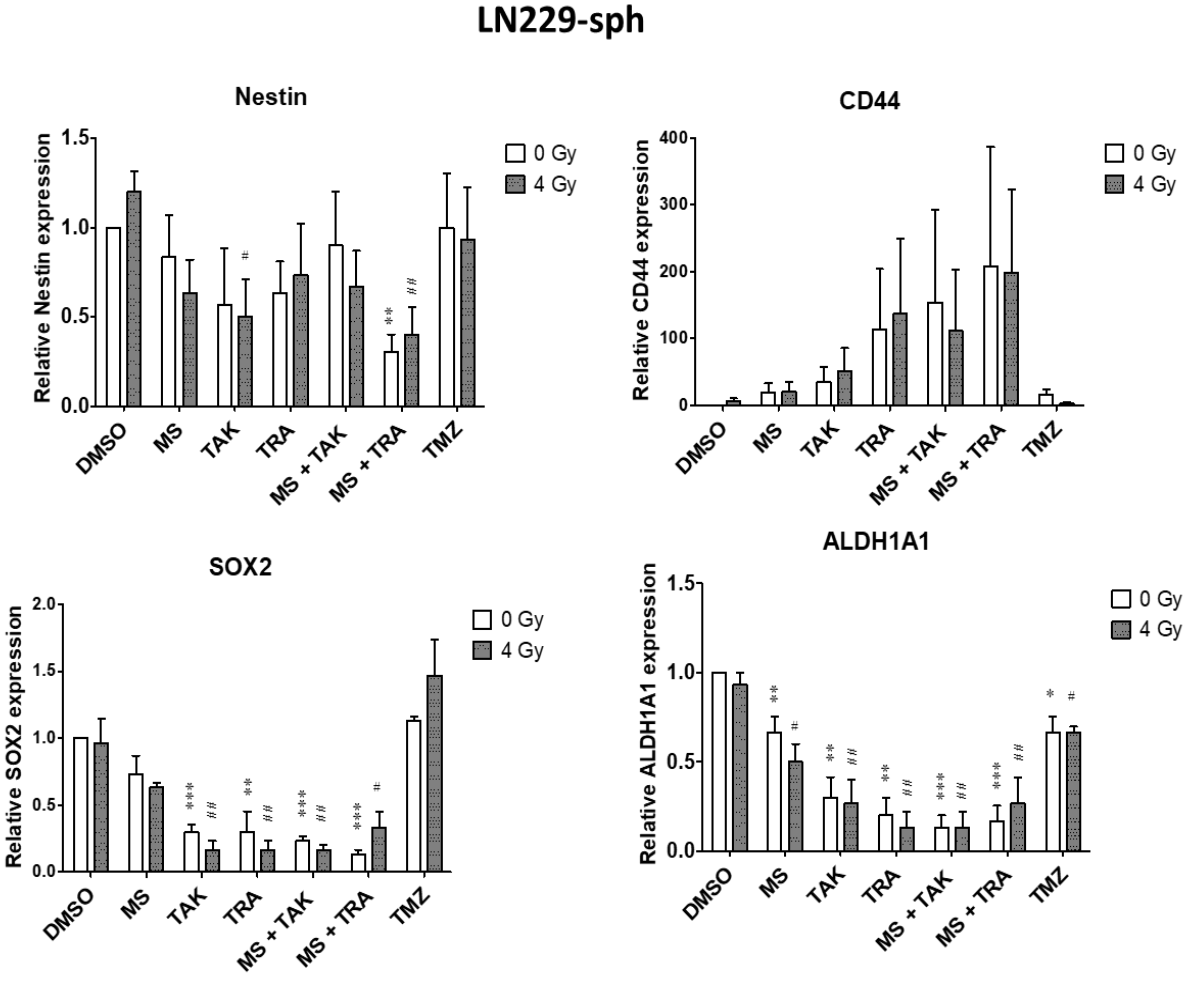

Figure 29: Western blot analysis of GSLC markers after 72 hours combined treatment of drugs and 4 Gy radiation in LN229-sph cells. Quantification data for Nestin, CD44, SOX2 and ALDH1A1 after treatment are shown. (Drugs; 1 µM MS-275 = MS, 1 µM TAK-733 = TAK, 1 µM trametinib = TRA, 50 µM TMZ = TMZ). Relative GSLC marker expressions first normalized to Actin and then to sham irradiated control cells treated with DMSO. [*n* = 3; ± SEM; *Student's *t*-test; **p* ≤ 0.05, ***p* ≤ 0.01, ****p* ≤ 0.001 (versus DMSO 0 Gy), #Student's *t*-test; #*p* ≤ 0.05, ##*p* ≤ 0.01 (versus DMSO 4 Gy). 2-way ANOVA; *p*-value <0.0001 (SOX2, ALDH1A1)]

U87-sph: In U87-sph, Figure 30 shows that radiation alone had no significant effect on the GSLC marker proteins. TMZ treatment alone also did not affect Nestin and CD44

but reduced SOX2 and ALDH1A1. By adding radiation to TMZ, only SOX2 was significantly reduced. A similar result could be seen with MS-275 treatment alone and combined with radiation. Treatment with MEKi TAK-733 or trametinib as single or combined agents with radiation, significantly reduced Nestin, SOX2 and ALDH1A1 with a trend to increase CD44.

By combining the HDACi and MEKi in U87-sph, the expression of Nestin, SOX2 and ALDH1A1 were significantly reduced, with SOX2 completely erradicated by MS-275 and trametinib treatment. Also, the extent of the reduction using combined HDACi and MEKi was further enhanced by the addition of 4 Gy radiation exposure ($^{\#\#}p \leq 0.01$ $^{\#\#\#}p \leq 0.001$). As also seen with LN229-sph, all the treatment conditions showed a tendency to increase CD44 in U87-sph (Figure 30).

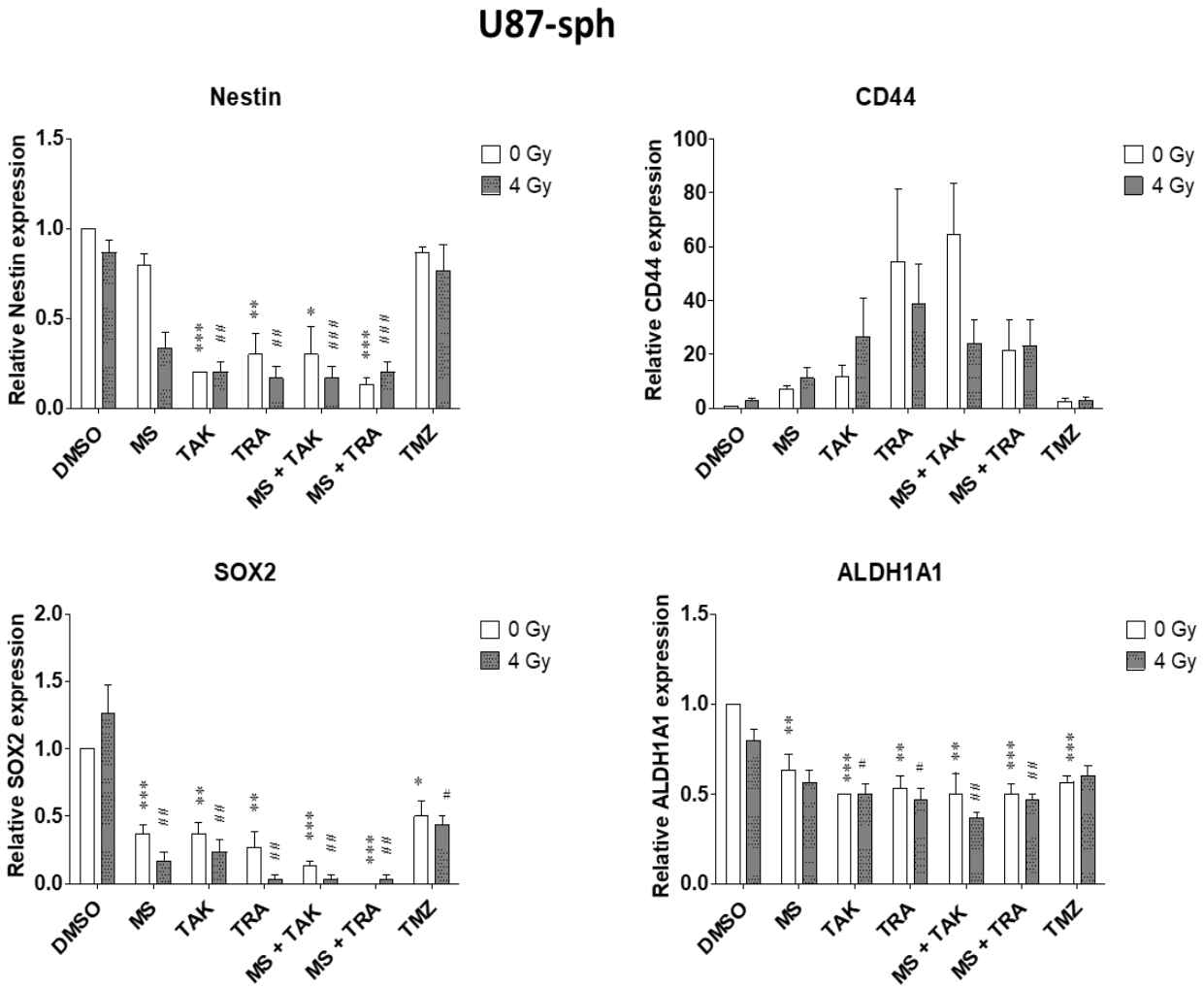

Figure 30: Western blot analysis of GSLC markers after 72 hours combined treatment of drugs and 4 Gy radiation in U87-sph cells. Quantification data for Nestin, CD44, SOX2

and ALDH1A1 after treatment are shown. (Drugs; 1 µM MS-275 = MS, 1 µM TAK-733 = TAK, 1 µM trametinib = TRA, 50 µM TMZ = TMZ). Relative GSLC marker expressions first normalized to Actin and then to sham irradiated control cells treated with DMSO. [*n* = 3; ± SEM; *Student's *t*-test; **p* ≤ 0.05, ***p* ≤ 0.01, ****p* ≤ 0.001 (versus DMSO 0 Gy), #Student's *t*-test; #*p* ≤ 0.05, ##*p* ≤ 0.01 ###*p* ≤ 0.001 (versus DMSO 4 Gy). 2-way ANOVA; *p*-value <0.01 (CD44), *p*-value <0.0001 (Nestin, SOX2, ALDH1A1)]

Generally, the results in U87-sph show that the combination of HDACi and MEKi with radiation could significantly reduce Nestin, SOX2 and ALDH1A1 protein expression with a trend to increase CD44 (Figure 30).

U251-sph: In Figure 31, radiation treatment alone in U251-sph showed no significant effect on any GSLC marker as was also seen with LN229-sph and U87-sph. Likewise, TMZ alone or combined with radiation did not significantly affect their expressions. Treatments with MS-275 alone significantly reduced Nestin and SOX2, but in combination with radiation only reduced Nestin significantly. Similarly, treatments with TAK-733 or trametinib as single or combined agents with radiation could only significantly reduce Nestin while showing no effect on the other GSLC markers.

By combining the HDACi and MEKi alone or together with radiation, Nestin ($^{\#\#\#}p \leq 0.001$) and SOX2 ($^{\#}p \leq 0.01$) expression was significantly eradicated (Figure 31). Additionally, the expression of ALDH1A1 was only significantly reduced by treatment with MS-275 and trametinib combined with 4 Gy radiation ($^{\#\#}p \leq 0.01$). In contrast to LN229-sph and U87-sph, only the combined treatment of the HDACi and MEKi with radiation significantly reduced CD44 expression in U251-sph (Figure 31)

Taken together, the results in U251-sph showed that the combined treatment of HDACi and MEKi with radiation could significantly reduce all GSLC markers (Nestin, CD44, SOX2 and ALDH1A1).

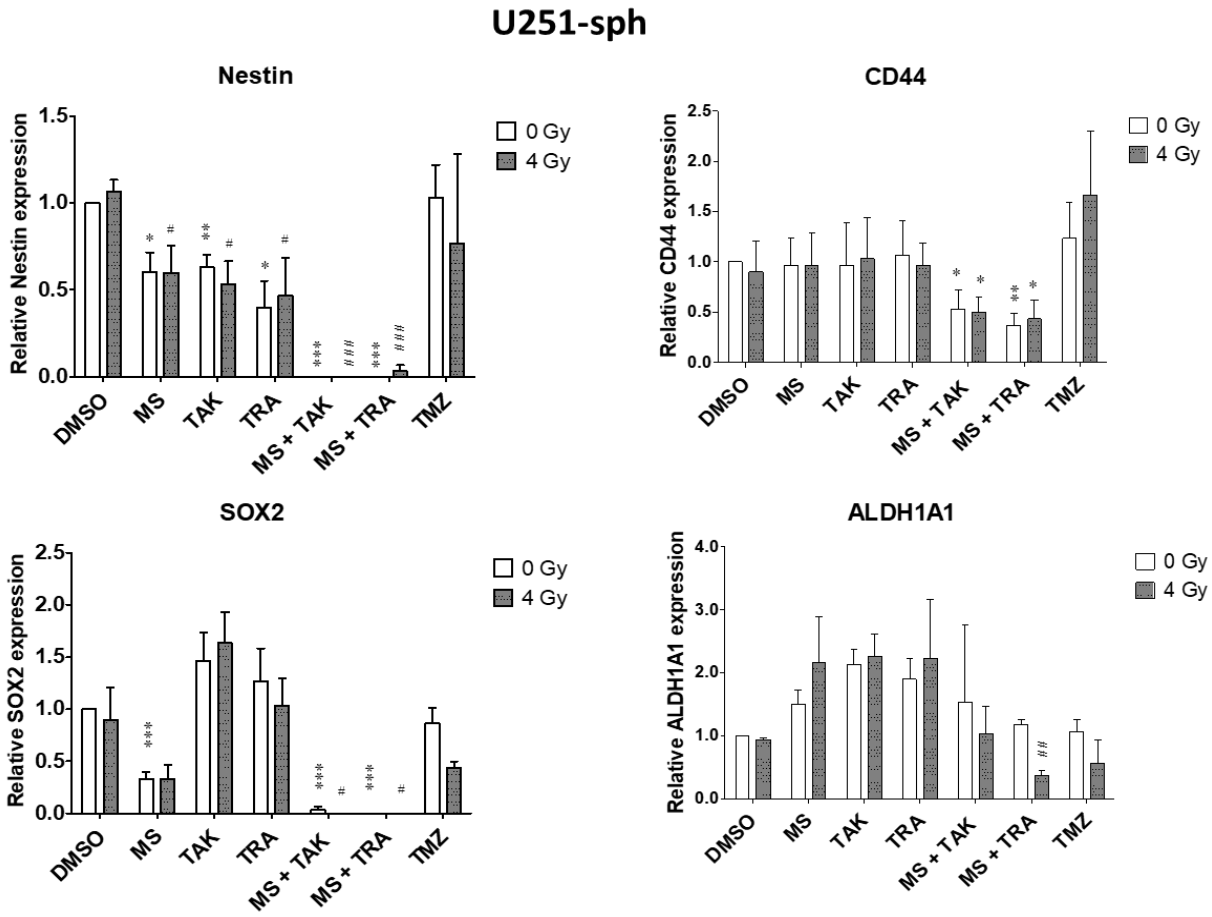

Figure 31: Western blot analysis of GSLC markers after 72 hours combined treatment of drugs and 4 Gy radiation in U251-sph cells. Quantification data for Nestin, CD44, SOX2 and ALDH1A1 after treatment are shown. (Drugs; 1 µM MS-275 = MS, 1 µM TAK-733 = TAK, 1 µM trametinib = TRA, 50 µM TMZ = TMZ). Relative GSLC marker expressions first normalised to Actin and then to sham irradiated control cells treated with DMSO. [n = 3; ± SEM; *Student's t-test; *p ≤ 0.05, **p ≤ 0.01, ***p ≤ 0.001 (versus DMSO 0 Gy), #Student's t-test; #p ≤ 0.05, ##p ≤ 0.01 (versus DMSO 4 Gy). 2-way ANOVA; p-value = 0.03 (ALDH1A1), p-value <0.0001 (Nestin, SOX2)]

In summary, the western blot results demonstrated that TMZ alone or with radiation showed only a little effect on the GSLC markers. The combination of HDACi and MEKi with radiation was the most effective treatment in reducing Nestin, SOX2 and ALDH1A1. Interestingly, cell line dependent differences in the effect on CD44 was observed. This may mean that CD44 functions are different in each cell line resulting in differential responses to the combined with radiation.

In Table 15, a summary of the effect of combining HDACi and MEKi with radiation on the GSLC markers is presented. The representative western blots for all cell lines are presented in the appendix section D (Figure A6 - Figure A8)

Table 15: Summary of the effects of combining HDACi and MEKi with radiation on GSLC markers in LN229-sph, U87-sph and U251-sph.

	LN229-sph		U87-sph		U251-sph	
HDACi + MEKi + 4 Gy	**MS + TAK + 4Gy**	**MS + TRA + 4Gy**	**MS + TAK + 4 Gy**	**MS + TRA + 4 Gy**	**MS + TAK + 4 Gy**	**MS + TRA + 4 Gy**
Nestin	↔	↓	↓	↓	↓	↓
CD44	↑	↑	↑	↑	↓	↓
SOX2	↓	↓	↓	↓	↓	↓
ALDH1A1	↓	↓	↓	↓	↓	↓

*Arrows facing down indicate significant decrease; arrows facing up indicate significant increase while arrow facing both sides indicates no change.

4.9 Flow cytometry analysis of GSLC markers after combined treatment of HDACi and MEKi with radiation in enriched glioblastoma-derived spheres.

In order to confirm the western blot results and confirm our suspicion that the GSLC population was reduced by the combined radiochemotherapy, flow cytometry analysis of the GSLC markers (Nestin+, CD44+ and SOX2+) was performed in LN229-sph, U87-sph and U251-sph. The single and double expression of the GSLCs markers were analyzed 72 hours after compound treatment and 4 Gy radiation as done with the western blot analysis. ALDH1A1 was not detected during flow cytometry analysis and could not be analyzed further.

4.9.1 Expression of single GSLC markers was reduced by the combination of HDACi and MEKi with radiation

LN229-sph: The quantified data for LN229-sph are presented in Figure 32 while representative flow cytometric plots are presented in the appendix section E (Figure A9 - Figure A11). Similar to the western blot analysis result, treatment with radiation alone or TMZ alone or TMZ combined with radiation did not change the Nestin+,

CD44+ and SOX2+ populations in LN229-sph. Likewise, treatment with the HDACi MS-275 alone or combined with radiation showed no significant effect on GSLC marker positive populations. On the other hand, treatment with the MEKi TAK-733 or trametinib as single or combined agents with radiation significantly reduced Nestin+ and SOX2+ populations compared to the untreated cells (Figure 32). However, the CD44+ population was not changed.

The combination of MS-275 and TAK-733 or MS-275 and trametinib alone or together with radiation produced a significant decrease in Nestin+ (MS + TAK = 12 ± 8%, MS + TRA = 10 ± 7%) and SOX2+ (MS + TAK = 15 ± 8%, MS + TRA = 12 ± 7%) population (Figure 32).

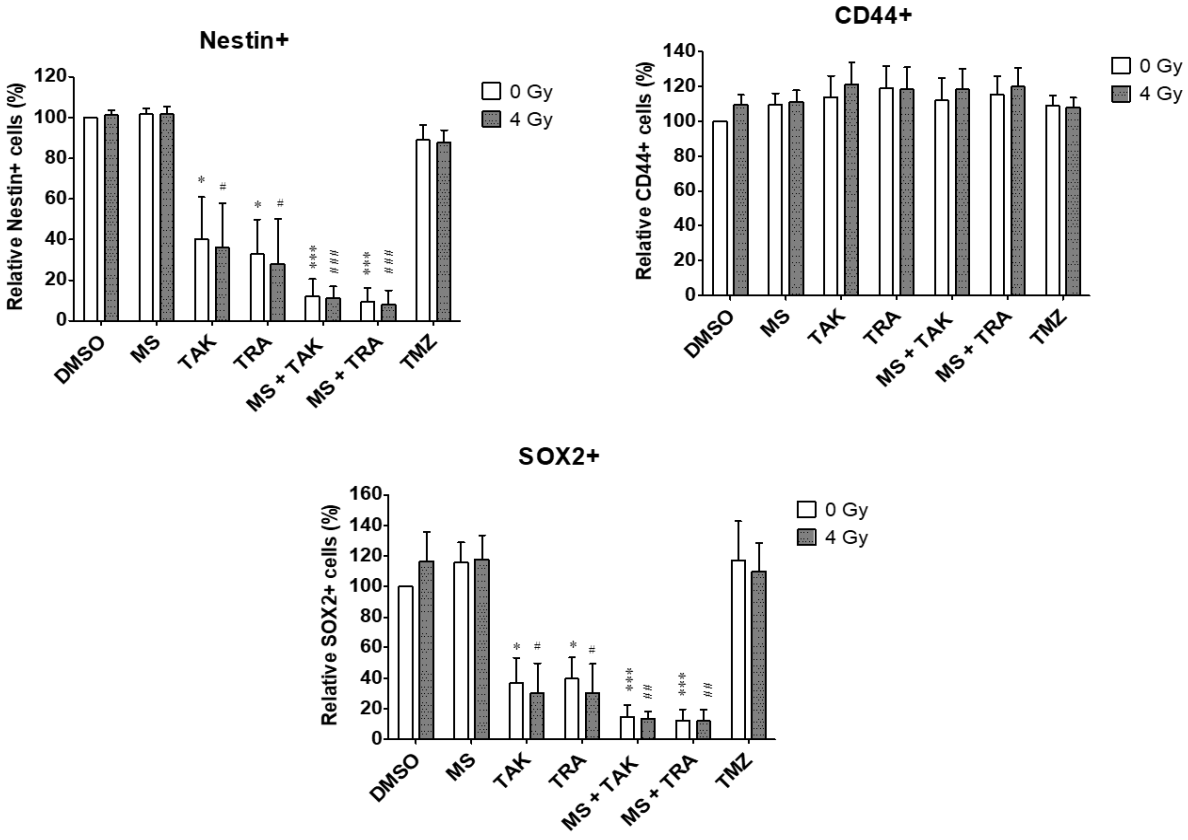

Figure 32: **Flow cytometry analysis of GSLC markers in LN229-sph after treatment of HDACi or MEKi as single or combined drugs with radiation.** Quantification data of Nestin+, CD44+ and SOX2+ relative to sham irradiated control cells (DMSO) set to 100%. Data represents mean values ± SEM (n = 3). [*Student's *t*-test; *$p \leq 0.05$, ***$p \leq 0.001$ (versus DMSO 0 Gy), #Student's *t*-test; $^{\#}p \leq 0.05$, $^{\#\#}p \leq 0.01$ $^{\#\#\#}p \leq 0.001$ (versus DMSO 4 Gy). 2-way ANOVA; *p*-value <0.0001 (Nestin, SOX2)].

Similar to the western blot analysis, it was observed that all the single and combined treatment conditions did not reduce the CD44+ populations in LN229-sph. However, it was demonstrated that the Nestin+ and SOX2+ populations were lowest by the combination of the HDACi and MEKi with radiation.

U87-sph: The same flow cytometric analysis was performed for U87-sph with the representative flow cytometric plots presented in the appendix (Figure A12 - Figure A14) and the quantified data presented in Figure 33. The figure shows that treatment with radiation alone, TMZ alone and TMZ with radiation did not change the Nestin+, CD44+ and SOX2+ populations. Similarly, treatment with MS-275 alone or combined with radiation had no effect on GSLC marker positive populations. As seen with LN229-sph, the treatment with TAK-733 and trametinib significantly reduced the Nestin+ and SOX2+ populations compared to the untreated cells, but did not affect CD44+ populations in U87-sph (Figure 33).

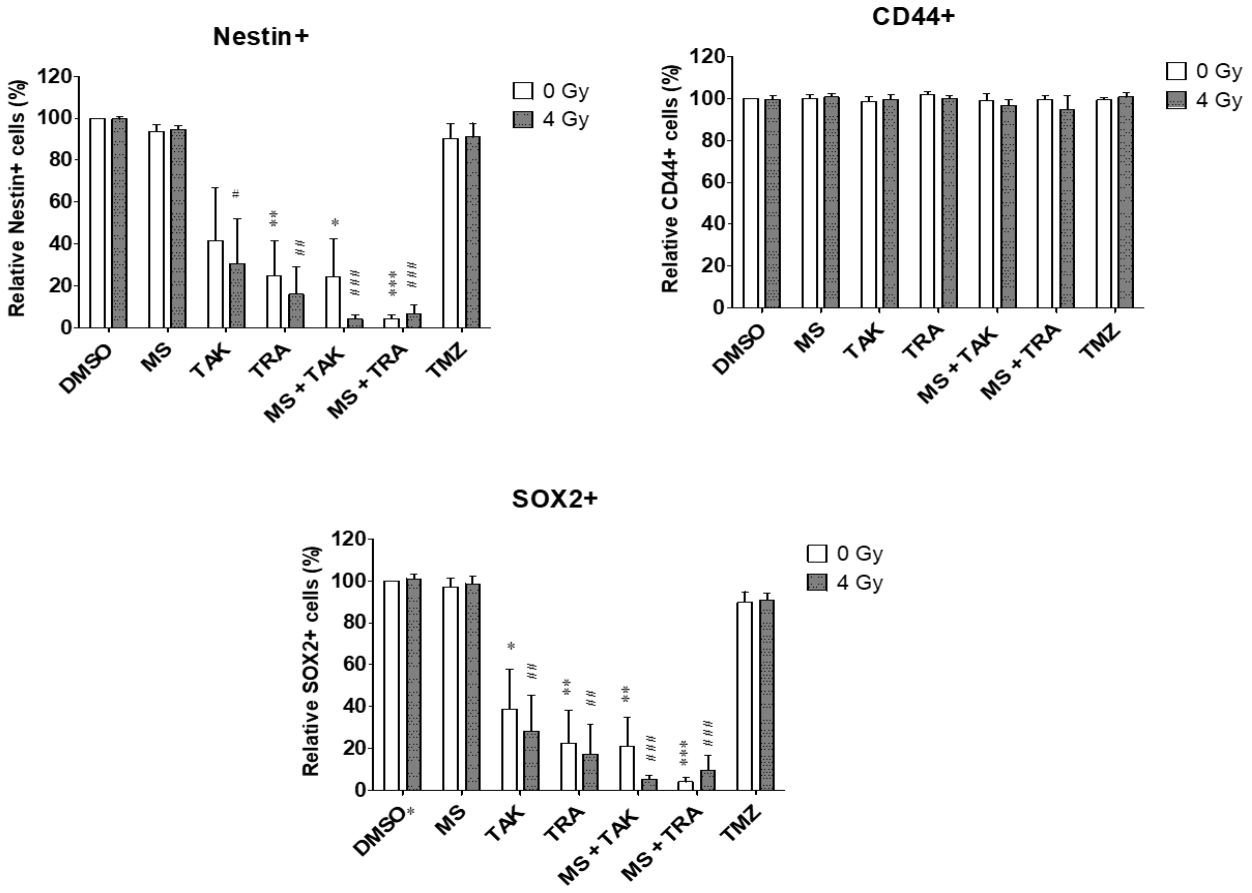

Figure 33: **Flow cytometry analysis of GSLC markers in U87-sph after treatment of HDACi or MEKi as single or combined drugs with radiation.** Quantification data of Nestin+,

CD44+ and SOX2+ relative to sham irradiated control cells (DMSO) set to 100%. Data represents mean values ± SEM (n = 3). [*Student's *t*-test; *$p \leq 0.05$, **$p \leq 0.01$, ***$p \leq 0.001$ (versus DMSO 0 Gy), #Student's *t*-test; $^{\#}p \leq 0.05$, $^{\#\#}p \leq 0.01$ $^{\#\#\#}p \leq 0.001$ (versus DMSO 4 Gy). 2-way ANOVA; *p*-value <0.0001 (Nestin, SOX2)].

By combining MS-275 and TAK-733, Nestin+ (24 ± 19%) and SOX2+ (21 ± 14%) populations were significantly decreased compared to the untreated cells. An enhanced reduction effect when combined with radiation (Nestin+ = 4 ± 2%, SOX2+ = 5 ± 2%) could be further detected. Also, in U87-sph, combining MS-275 and trametinib greatly reduced Nestin+ (4 ± 2%) and SOX2+ (4 ± 2%) alone and by adding radiation (Nestin+ = 7 ± 4%) and SOX2+ = 10 ± 7%). Like in LN229-sph, all single and combined treatments did not affect the CD44+ populations in U87-sph (Figure 33).

Overall, the results confirmed that the combination of HDACi and MEKi with radiation was more effective against the Nestin+ and SOX2+ GSLC population compared to either treatment alone.

U251-sph: Like in LN229-sph and U87-sph, the single expression of the GSLC markers in U251-sph after the various treatments was performed. The representative flow cytometric plots can be found in the appendix (Figure A15 - Figure A17) while the quantified data are presented in Figure 34. The figure shows that radiation, TMZ alone and TMZ with radiation did not change the Nestin+, CD44+ and SOX2+ populations in U251-sph. Likewise, the HDACi (MS-275) or MEKi (TAK-733 or trametinib) as single or combined treatments with radiation did not change Nestin+, CD44+ and SOX2+ populations compared to the untreated cells (Figure 34).

Only the combination of HDACi and MEKi alone and with radiation could significantly reduce the single expressions of all the GSLC markers in U251-sph. Treatment with MS-275 and TAK-733 greatly reduced Nestin+ (42 ± 16%), CD44+ (41 ± 17%) and SOX2+ (44 ± 17%) populations. By adding radiation to the combination, a further reduction of Nestin+ (12 ±1%), CD44+ (10 ± 1%) and SOX2+ (12 ±1%) was detected compared to the untreated cells. Similarly, by treatment with MS-275 and trametinib, Nestin+ (22 ± 7%), CD44+ (20 ± 6%) and SOX2+ (23 ± 7%) populations were significantly reduced. The addition of radiation also enhanced the reduction effect of Nestin+ (9 ± 1%), CD44+ (8 ± 1%) and SOX2+ (9 ± 1%) populations in U251-sph (Figure 34).

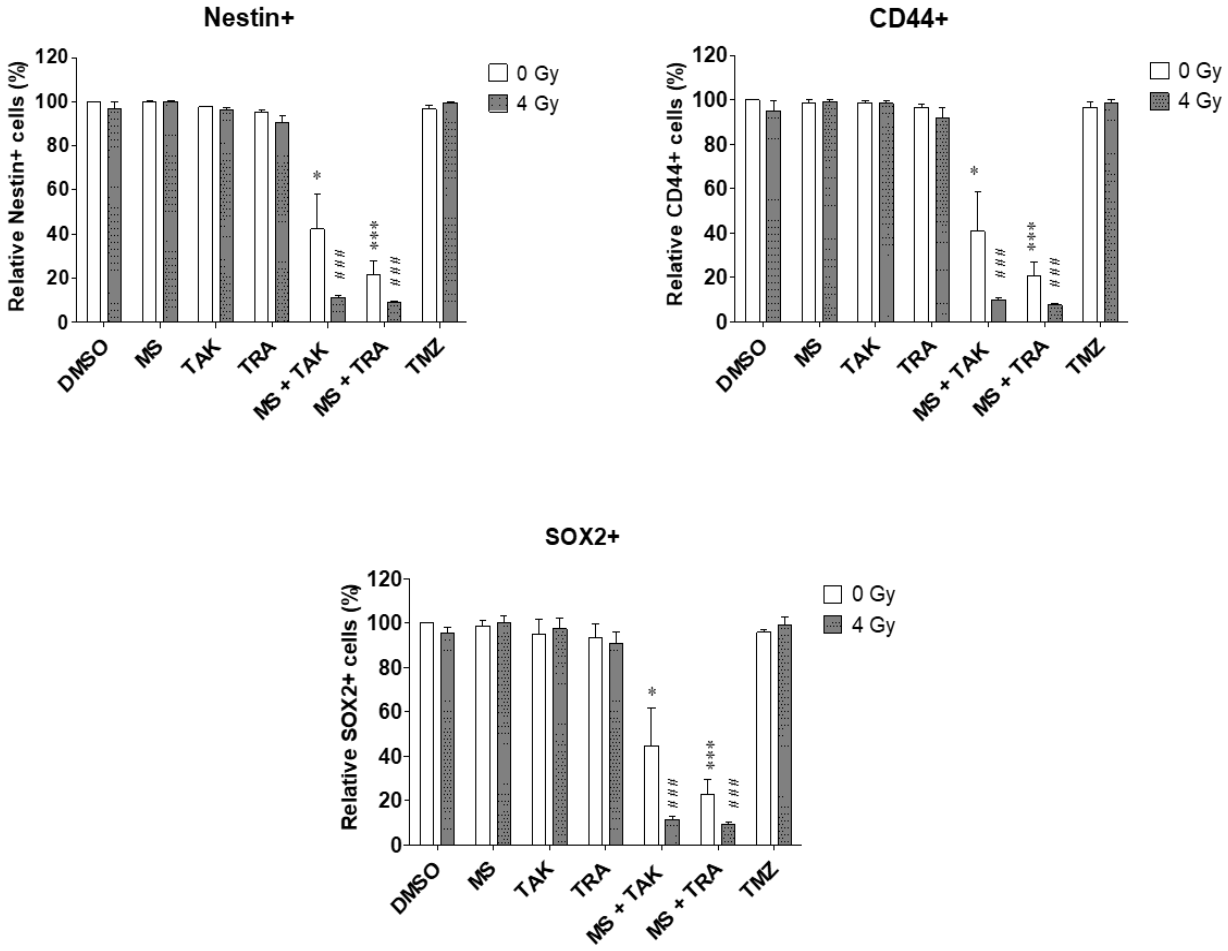

Figure 34: **Flow cytometry analysis of GSLC markers in U251-sph after treatment of HDACi or MEKi as single or combined drugs with radiation.** Quantification data of Nestin+, CD44+ and SOX2+ relative to sham irradiated control cells (DMSO) set to 100%. Data represents mean values ± SEM (n = 3). [*Student's *t*-test; *$p \leq 0.05$, ***$p \leq 0.001$ (versus DMSO 0 Gy), #Student's *t*-test; $^{###}p \leq 0.001$ (versus DMSO 4 Gy). 2-way ANOVA; *p*-value <0.0001 (CD44, Nestin, SOX2)].

The results were similar to that of western blot analysis of U251-sph cells where it was shown that the combination of HDACi and MEKi with radiation was the most effective in reducing the Nestin, CD44 and SOX2 GSLC markers. Table 16 summarizes the comparison of protein analysis results with flow cytometry results in all three glioblastoma-derived spheres. Taken together, the results of the flow cytometry analysis in LN229-sph, U87-sph and U251-sph showed that combining HDACi and MEKi with radiation could significantly reduce the single expression of the GSLC markers compared to either alone. However, only CD44 expression remained unchanged by all treatment conditions in LN229-sph and U87-sph.

Table 16: Comparison of protein analysis and flow cytometry results after the combined treatment of HDACi and MEKi in LN229-sph, U87-sph and U251-sph.

	LN229-sph		U87-sph		U251-sph	
HDACi + MEKi + 4 Gy	**MS + TAK + 4Gy**	**MS + TRA + 4Gy**	**MS + TAK + 4 Gy**	**MS + TRA + 4 Gy**	**MS + TAK + 4 Gy**	**MS + TRA + 4 Gy**
Nestin						
CD44						
SOX2						

* Blue arrows represent western blot analysis while green arrows represent flow cytometry analysis. Arrows facing upward indicate significant increase, arrows facing downwards indicate significant decrease and arrows facing both sides indicate no change.

4.9.2 Double expression of GSLC markers reduced by the combination of HDACi and MEKi with radiation

Even though the western blot and flow cytometry analysis revealed the individual changes in GSLC markers, it is still not clear if the GSLC markers in the same cell are responding to the combined treatment with radiation. Since a multicolor flow cytometry approach was used, we were able analyze the double expression of pairs of the GSLC markers (CD44+Nestin+, Nestin+SOX2+ and CD44+SOX2+) after the combined treatment with radiation.

LN229-sph: The representative flow cytometric plots for CD44+Nestin+, Nestin+SOX2+ and CD44+SOX2+ after the different treatment conditions in LN229-sph are presented in the appendix section F (Figure A19 - Figure A21) and the quantitative data for LN229-sph in Figure 35. The figure shows that all the double expression of the GSLC markers were not changed by treatments with radiation alone, TMZ alone, TMZ with radiation, MS-275 alone and MS-275 with radiation. However, TAK-733 or trametinib as single or combined treatments with radiation significantly reduced the Nestin+SOX2+ population when compared to the untreated cells (Figure 35).

Upon combination of the HDACi and MEKi with radiation in LN229-sph, all three double positive populations were significantly reduced compared to the single treatments. By

the combined treatment of MS-275 and TAK7-33 with radiation, the CD44+Nestin+ (16 ± 10%), Nestin+SOX2+ (12 ± 5%) and CD44+SOX2+ (17 ± 9%) populations were greatly reduced. Similarly, compared to radiation alone, treatment with MS-275 and trametinib with radiation significantly reduced CD44+Nestin+ (13 ± 11%), Nestin+SOX2+ (9 ± 7%) and CD44+SOX2+ (16 ± 11%) populations (Figure 35).

To conclude the results for LN229-sph, combining the HDACi and MEKi with radiation was the most effective treatment in reducing all the three CD44+Nestin+, Nestin+SOX2+ and CD44+SOX2+ double positive populations.

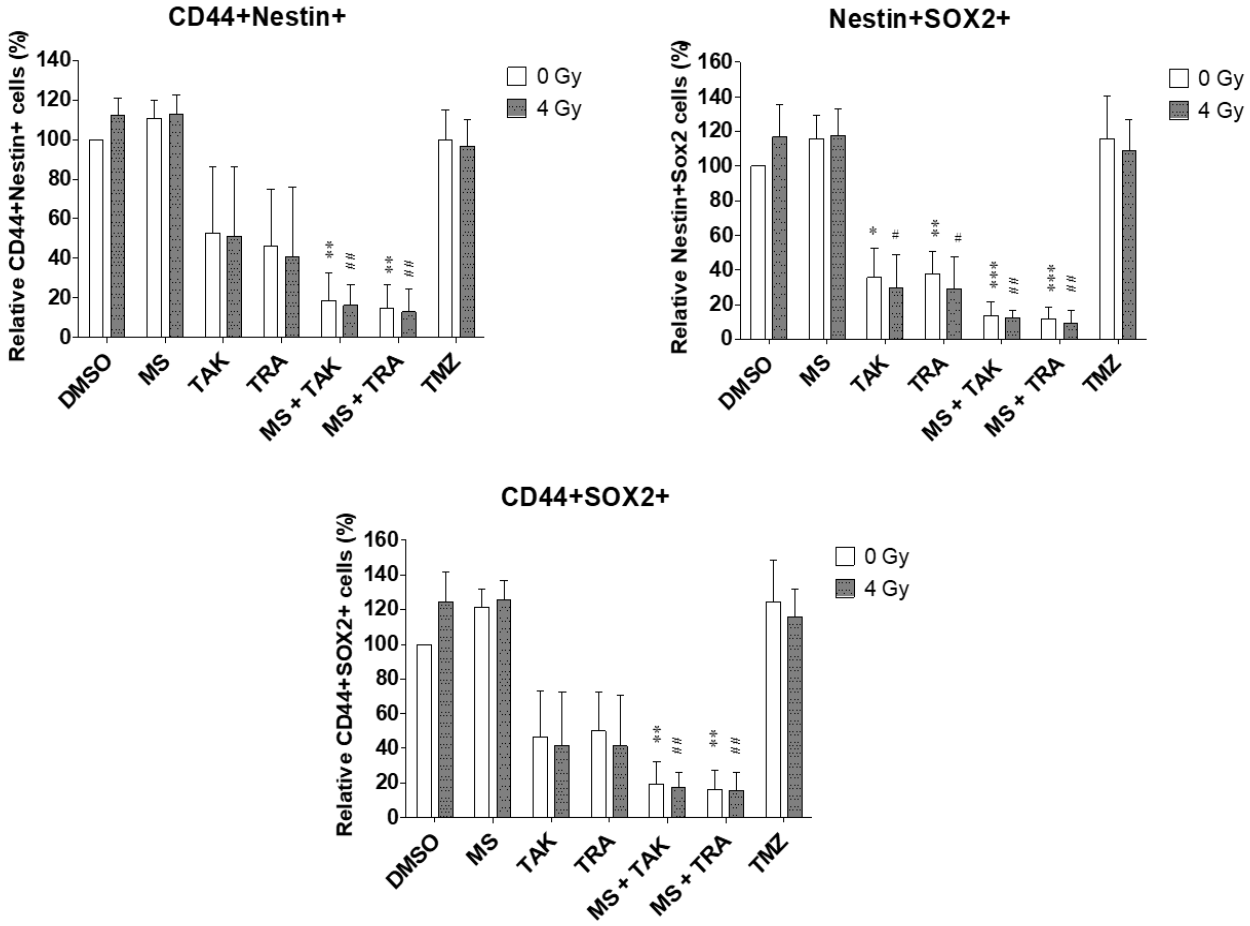

Figure 35: **Flow cytometry analysis of double positive GSLC markers in LN229-sph after treatment of HDACi or MEKi as single or combined drugs with radiation.** Quantification data of CD44+Nestin+, Nestin+SOX2+ and CD44+SOX2+ relative to sham irradiated control cells (DMSO) set to 100%. Data represents mean values ± SEM (n = 3). [*Student's *t*-test; *$p \leq 0.05$, **$p \leq 0.01$, ***$p \leq 0.001$ (versus DMSO 0 Gy), #Student's *t*-test; $^{\#}p \leq 0.05$, $^{\#\#}p \leq 0.01$ (versus DMSO 4 Gy). 2-way ANOVA; *p*-value <0.0001 (CD44+Nestin+, Nestin+SOX2+, CD44+SOX2+)].

U87-sph: The effect of the combined inhibitor treatment was further analyzed in the U87-sph cells. The representative flow cytometric plots for CD44+Nestin+, Nestin+SOX2+ and CD44+SOX2+ in U87-sph are presented in the appendix (Figure A22 - Figure A24) while quantified data are shown in Figure 36.

Like in LN229-sph, radiation alone, TMZ alone, TMZ with radiation, MS-275 alone and MS-275 with radiation did not affect the CD44+Nestin+, Nestin+SOX2+ and CD44+SOX2+ populations in U87-sph. Treatment with TAK-733 significantly reduced Nestin+SOX2+ population while trametinib significantly reduced Nestin+SOX2+ and CD44+SOX2+. An enhanced reduction effect was observed when combining TAK-733 or trametinib with radiation (Figure 36).

By combining the HDACi and MEKi with radiation, all three double positive populations were significantly reduced compared to the single treatments. The combination of MS-275 and TAK-733 with radiation significantly decreased CD44+Nestin+ (6 ± 2%), Nestin+SOX2+ (4 ± 2%) and CD44+SOX2+ (4 ± 2%). By combining MS-275 and trametinib with radiation, a significant reduction of CD44+Nestin+ (9 ± 4%), Nestin+SOX2+ (7 ± 4%) and CD44+SOX2+ (9 ± 6%) was also observed (Figure 36).

Overall, the results for U87-sph show that combining the HDACi and MEKi with radiation was the most effective treatment to reduce the CD44+Nestin+, Nestin+SOX2+ and CD44+SOX2+ double positive populations.

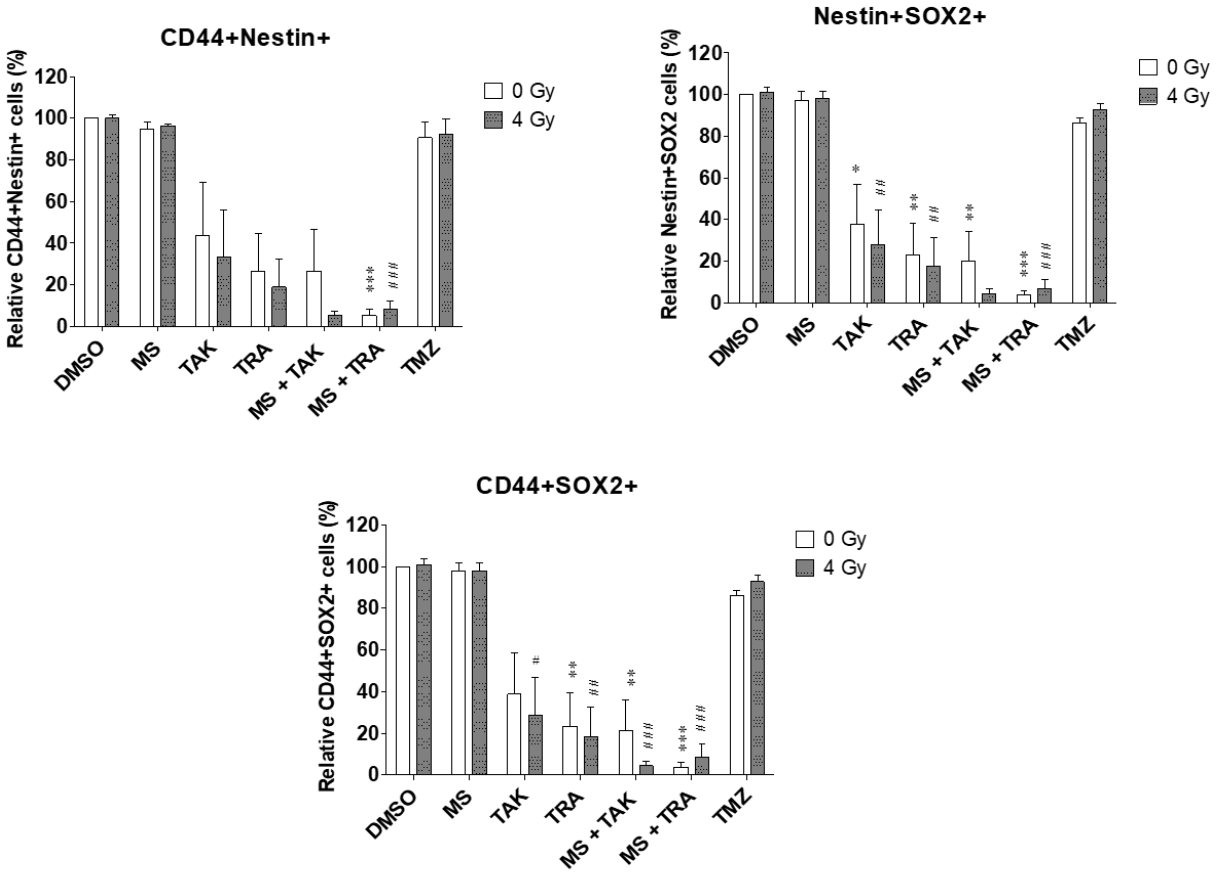

Figure 36: **Flow cytometry analysis of double positive GSLC markers in U87-sph after treatment of HDACi or MEKi as single or combined drugs with radiation.** Quantification data of CD44+Nestin+, Nestin+SOX2+ and CD44+SOX2+ relative to sham irradiated control cells (DMSO) set to 100%. Data represents mean values ± SEM (n = 3). [*Student's *t*-test; *$p \leq 0.05$, **$p \leq 0.01$, ***$p \leq 0.001$ (versus DMSO 0 Gy), #Student's *t*-test; $^{\#}p \leq 0.05$, $^{\#\#}p \leq 0.01$, $^{\#\#\#}p \leq 0.001$ (versus DMSO 4 Gy). 2-way ANOVA; *p*-value <0.0001 (CD44+Nestin+, Nestin+SOX2+, CD44+SOX2+)].

U251-sph: Flow cytometry analysis were repeated for U251-sph after the various treatment. The representative flow cytometric plots for CD44+Nestin+, Nestin+SOX2+ and CD44+SOX2+ in U251-sph are presented in the appendix (Figure A25 - Figure A27) while quantified data are shown in Figure 37. The figure shows that all the treatments with radiation, TMZ, MS-275, TAK-733 and trametinib as single or combined treatments with radiation did not affect the double positive populations.

Upon the combination of HDACi and MEKi, all three double positive populations were significantly decreased. In addition, the decrease in the CD44+Nestin+, Nestin+SOX2+

and CD44+SOX2+ populations were significantly more pronounced when combined with radiation (Figure 37).

The CD44+Nestin+ population decreased from 96 ± 3% with radiation alone to 43 ± 16% with MS-275 and TAK-733 and a further decrease to 12 ± 1% by adding radiation to the combination. With the same combination, the Nestin+SOX2+ and CD44+SOX2+ populations were decreased with comparably low percentage values and an enhanced reduction effect by adding radiation to the combination. Similarly, compared to radiation alone, treatment with MS-275 and trametinib significantly decreased CD44+Nestin+ population to 22 ± 7% and a further decrease to 9 ± 1% with radiation. Comparably low percentage values were also detected for Nestin+SOX2+ and CD44+SOX2+ including an additional effect of radiation (Figure 37).

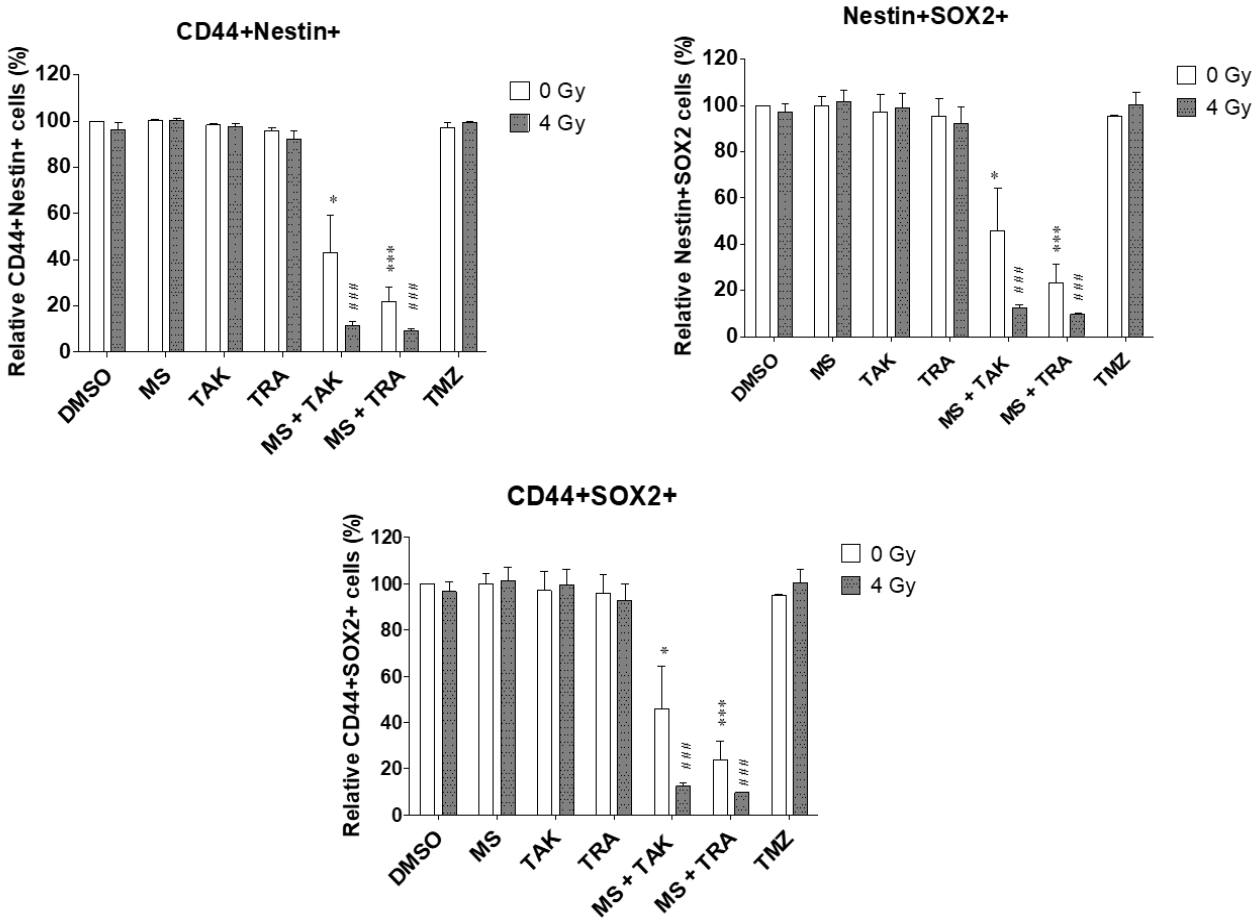

Figure 37: **Flow cytometry analysis of double positive GSLC markers in U251-sph after treatment of HDACi or MEKi as single or combined drugs with radiation.** Quantification data of CD44+Nestin+, Nestin+SOX2+ and CD44+SOX2+ relative to sham irradiated control cells (DMSO) set to 100%. Data represents mean values ± SEM (n = 3). [*Student's *t*-test; **p*

≤ 0.05, ***p ≤ 0.001 (versus DMSO 0 Gy), #Student's t-test; ###p ≤ 0.001 (versus DMSO 4 Gy). 2-way ANOVA; p-value <0.0001 (CD44+Nestin+, Nestin+SOX2+, CD44+SOX2+)].

Taken together, given that the GSLC populations were at the lowest when treated with the HDACi and MEKi with radiation, the results demonstrated that the combined treatment was more effective against the GSLC population compared to the standard treatment of TMZ and radiation or the drugs individually.

4.9.3 Population of dead cells increased by the combined treatment of HDACi and MEKi with radiation

During antibody labelling, a live-dead staining was also included using a Zombie Aqua dye that is permeant for cells with compromised membranes (i.e dead cells) and non-permeant to live cells. Therefore, it was possible to access the live versus dead status of the cells after the different treatment conditions.

The percentage values of the dead cell population after treatment of LN229-sph, U87-sph and U251-sph are shown in Figure 38. The figure showed that radiation alone, and the standard TMZ alone or combined with radiation did not significantly influence the dead cell population when compared to the untreated cells in LN229-sph, U87-sph and U251-sph.

LN229-sph: In LN229-sph (Figure 38), the dead cell population with 4 Gy irradiation alone (14 ± 8%) remained unchanged by treatment with the HDACi MS-275 alone and with radiation. A trend for the MEKi alone to increase the dead cell population was observed with only trametinib plus radiation significantly increasing the percentage of dead cells (73 ± 20%). A further significant increase in the dead cell population was detected by combining MS-275 and TAK-733 alone (84 ± 8%) or with radiation (85 ± 6%) and similarly by combining MS-275 and trametinib alone (88 ± 7%) or with radiation (89 ± 8%).

U87-sph: Comparable results were detected in the U87-sph where the dead cell populations after 4 Gy radiation alone (5 ± 1%) was not significantly changed by MS-275 alone or with radiation (Figure 38). However, the dead cell population was significantly increased by TAK-733 plus radiation (59 ± 23%) and trametinib alone (76 ± 16%) or with radiation (82 ± 12%). A further increase in dead cells was detected upon

combining MS-275 and TAK-733 alone (73 ± 17%) and with radiation (92 ± 3%) or MS-275 and trametinib alone (94 ± 2%) and with radiation (86 ± 9%).

U251-sph: The results were slightly different in U251-sph in that the low percentage of dead cells by treatment with only 4 Gy radiation were not significantly affected by single treatment with the HDACi or MEKi alone and with radiation. Only the combination of HDACi and MEKi alone or together with radiation could significantly increase the population of dead cells. The percentage of dead cells was increased from 8 ± 5% with only 4 Gy radiation to 58 ± 16% with MS-275 and TAK-733 alone and further to 88 ± 1% with radiation and similarly to 78 ± 6% with MS-275 and trametinib alone and further to 90 ± 1% with radiation (Figure 38).

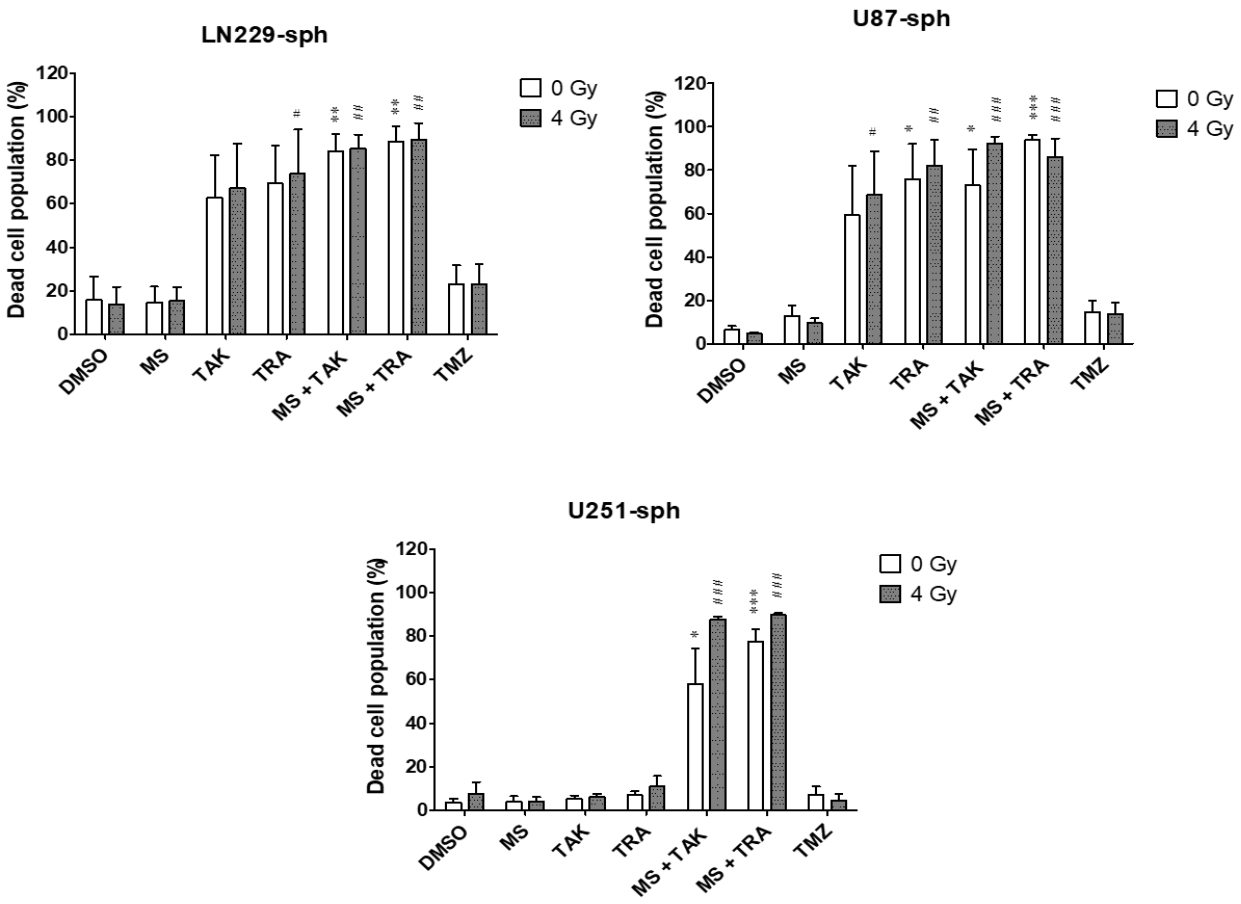

Figure 38: **High population of dead cells after treatment of HDACi or MEKi as single or combined drugs with radiation.** Quantification data showing the percentage of dead cells in LN229-sph, U87-sph and U251-sph after the different treatment conditions. Data represents mean values ± SEM (n = 3). [*Student's *t*-test; *$p \leq 0.05$, **$p \leq 0.01$, ***$p \leq 0.001$ (versus DMSO 0 Gy), #Student's *t*-test; $^{\#}p \leq 0.05$, $^{\#\#}p \leq 0.01$, $^{\#\#\#}p \leq 0.001$ (versus DMSO 4 Gy). 2-way ANOVA; *p*-value <0.0001 (LN229-sph, U87-sph, U251-sph)].

Taken together, the data presented show that the dead cell population was at the highest percentage when treated with the combination of HDACi and MEKi with radiation, while the standard treatment displayed no significant effect.

4.10 Expression of GSLC marker genes upregulated after the combined treatment of HDACi and MEKi with radiation

To establish if the observed changes in protein expression are associated with changes in gene transcriptional status of the GSLC markers in the enriched glioblastoma-derived spheres, quantitative real time PCR was performed. As before, the same treatments were applied to the enriched glioblastoma-derived spheres (LN229-sph, U87-sph and U251-sph). *TBP* served as the endogenous control to derive the relative mRNA expressions of the GSLC marker genes (*NES*, *SOX2*, *CD44*).

LN229-sph: In LN229-sph cells (Figure 39), treatment with radiation alone reduced *NES* and *SOX2* but did not change *CD44* expression. The treatment with TMZ alone or combined with radiation did not affect any of the GSLC marker mRNA expressions. Likewise, MS-275 alone did not affect the GSLC marker mRNA expression, but when combined with radiation showed a trend towards reducing *CD44*. Surprisingly, the treatment with TAK-733 alone upregulated *NES* mRNA but when combined with radiation did not have any significant effect on any GSLC marker. Trametinib alone similarly upregulated *NES* and *SOX2* mRNA with only *NES* mRNA remaining upregulated when combined with radiation. A further upregulation of *NES*, *CD44* and *SOX2* mRNA was detected upon the combination of the HDACi and MEKi alone or combined with radiation (Figure 39).

Generally, only the effects of the combined treatment of HDACi and MEKi with radiation on *CD44* were similar to that of protein analysis with both showing an upregulation of CD44 expression. The rest of the results were not comparable to the results of the protein analysis. The results therefore reveal that the changes in protein levels did not equal changes in mRNA expression.

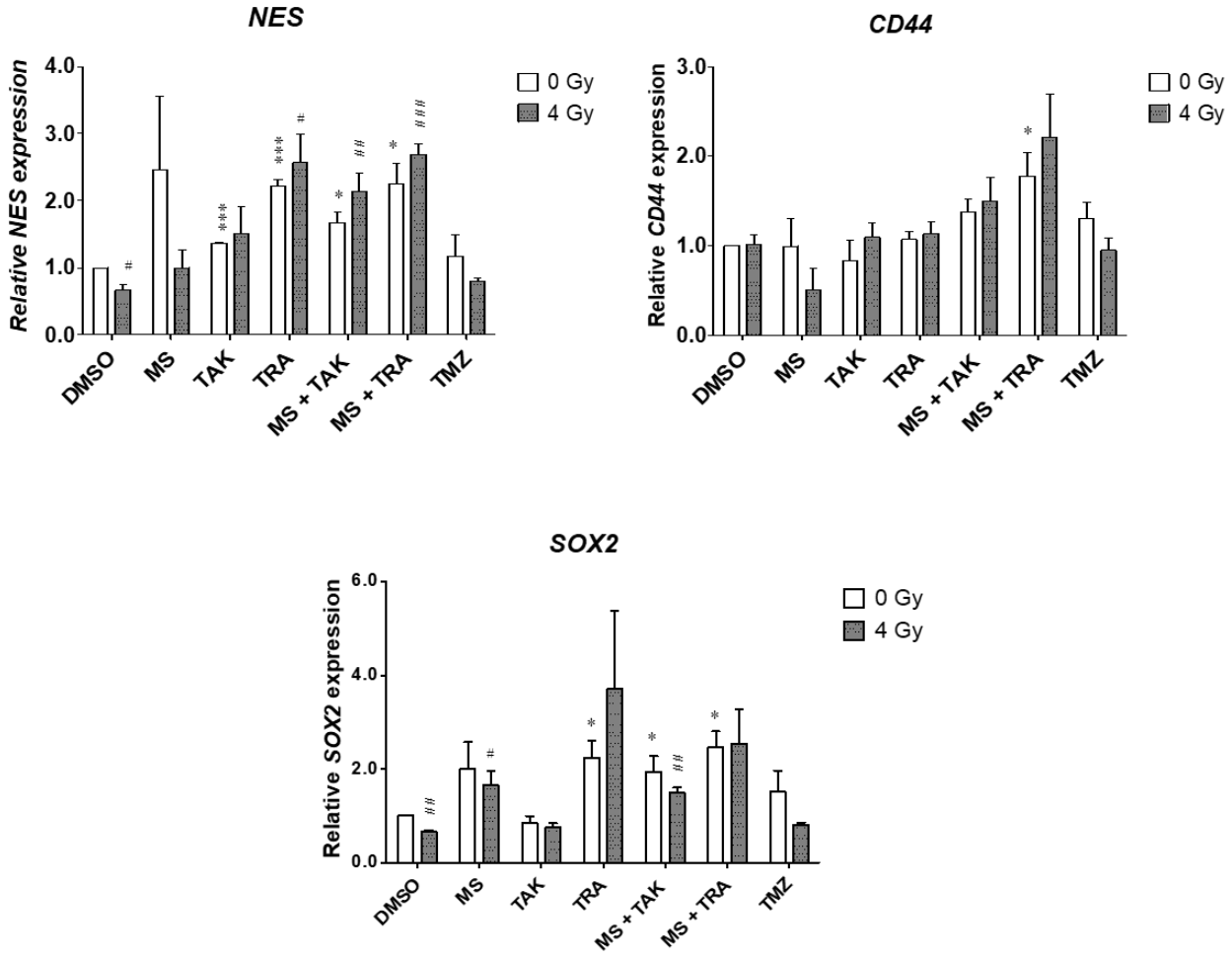

Figure 39: **GSLC marker gene expression in LN229-sph after treatment with HDACi or MEKi as single or combined drugs with radiation.** Fold changes of *NES*, *CD44* and *SOX2* 72 hours after the combined treatment and 4 Gy radiation are shown. The fold changes were calculated compared to sham irradiated control cells (DMSO) set to one. Data represents mean values ± SEM (n = 3). [*Student's *t*-test; *$p \leq 0.05$, ***$p \leq 0.001$ (versus DMSO 0 Gy), #Student's *t*-test; $^{\#}p \leq 0.05$, $^{\#\#}p \leq 0.01$, $^{\#\#\#}p \leq 0.001$ (versus DMSO 4 Gy). 2-way ANOVA; *p*-value <0.001 (*NES*, *CD44*); *p*-value <0.01 (*SOX2*)].

U87-sph: In U87-sph, Figure 40 shows that radiation treatment alone did not change any of the GSLC marker gene expression. However, treatment with TMZ alone upregulated *NES* and downregulated SOX2 but did not affect CD44. By combining TMZ with radiation, no significant effect on the GSLC marker expression was detected. MS-275, TAK-733 and trametinib as single or combined treatments with radiation also did not significantly change *NES*, *CD44* and *SOX2* expressions. Although, a non-significant trend for TAK-733 and trametinib to upregulate *SOX2* expression was observed (Figure 40).

The combination of the HDACi and MEKi alone or together with radiation did not affect *CD44* expression. *NES* expression was upregulated by the combined treatment with no significant additional effect of radiation detected. While there was potential for the combination of MS-275 and TAK with radiation to downregulate *SOX2*, no other significant effect with radiation could be detected (Figure 40).

The results were again not comparable to the effects of the combined treatment with radiation on protein expressions where Nestin and SOX2 were significantly downregulated. Therefore, the results here further confirm that the changes in protein levels was not equal to changes in the mRNA expression of the GSLC markers.

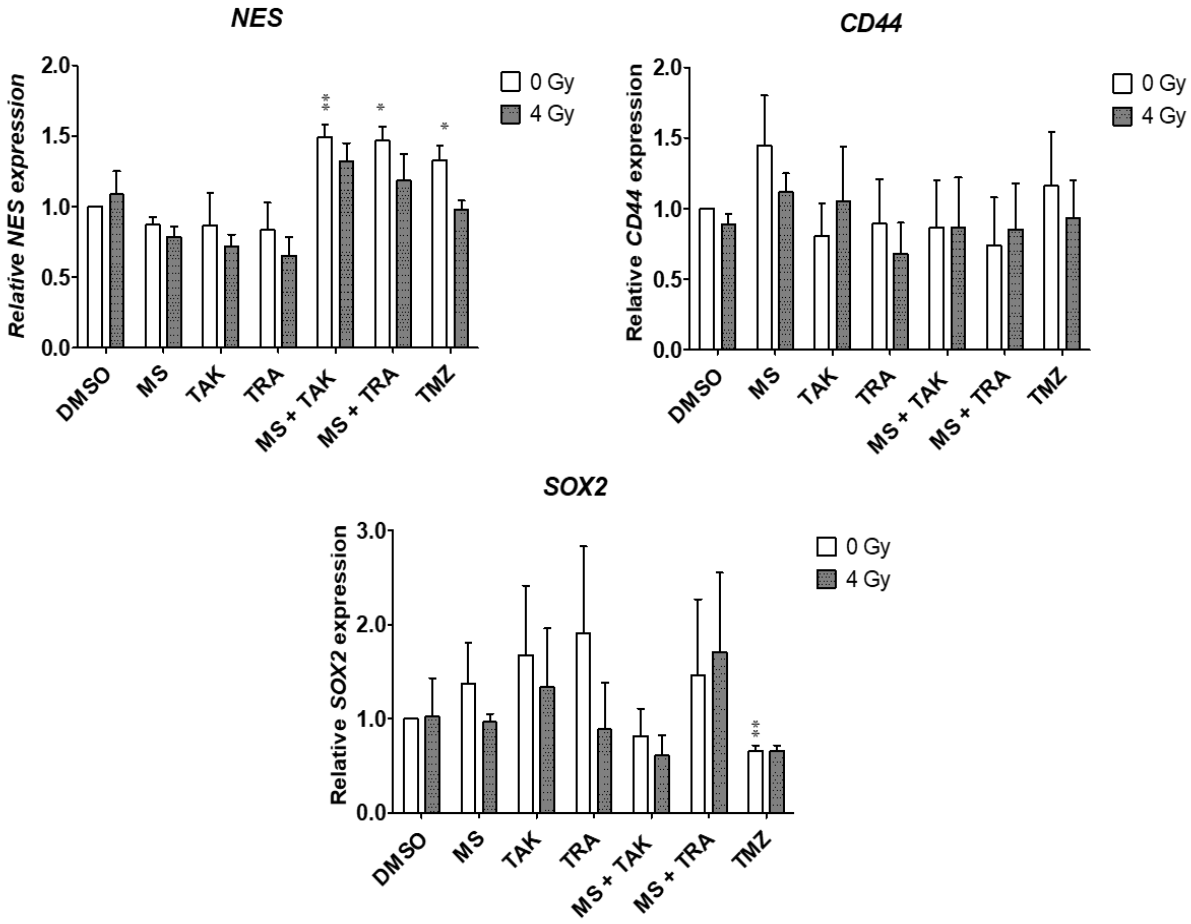

Figure 40: **GSLC marker gene expression in U87-sph after treatment with HDACi or MEKi as single or combined drugs with radiation.** Fold changes of *NES*, *CD44* and *SOX2* 72 hours after the combined treatment and 4 Gy radiation are shown. The fold changes were calculated compared to sham irradiated control cells (DMSO) set to one. Data represents mean values ± SEM (n = 3). [*Student's *t*-test; *$p \leq 0.05$, **$p \leq 0.01$ (versus DMSO 0 Gy). 2-way ANOVA; *p*-value <0.0001 (*NES*)].

U251-sph: Analysis of U251-sph in Figure 41 showed that there was no significant effect of radiation alone on any of the GSLC marker gene expressions. Likewise, TMZ alone or with radiation did not significantly change *NES*, *CD44* or *SOX2*. No change on the GSLC marker expressions was detected with MS-275 alone or combined with radiation. Treatment with TAK-733 alone significantly reduced *NES* expression with no additional effect of radiation detected (Figure 41). No significant effects on *CD44* or *SOX2* expression were detected by single treatments of TAK-733 alone or with radiation. Trametinib treatment alone also showed no significant effect but when combined with radiation, *CD44* was upregulated. Upon combination of the HDACi and MEKi alone or together with radiation, the expressions of *NES*, *CD44* and *SOX2* were not significantly affected. Only the combination of MS-275 and trametinib with radiation significantly upregulated *SOX2* expression (Figure 41).

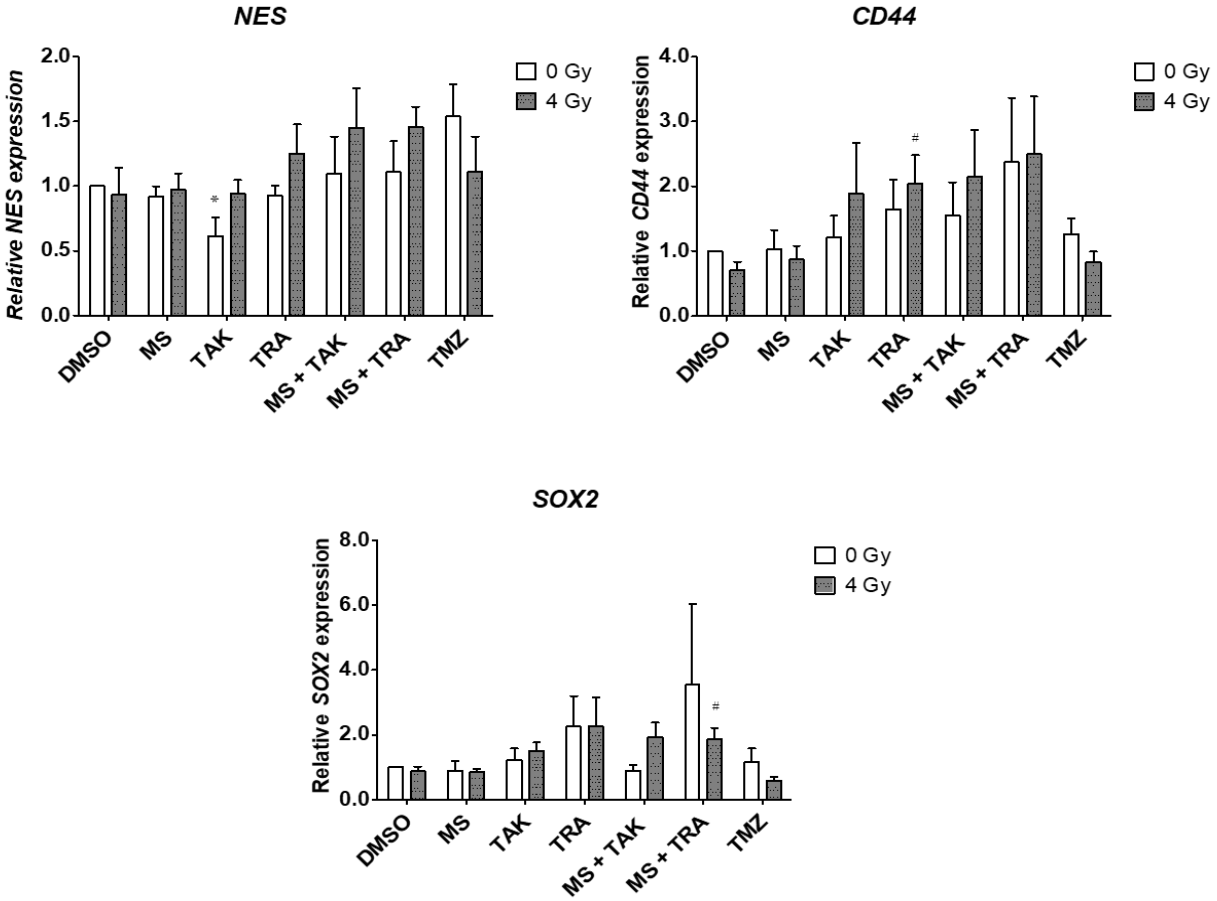

Figure 41: **GSLC marker gene expression in U251-sph after treatment with HDACi or MEKi as single or combined drugs with radiation.** Fold changes of *NES*, *CD44* and *SOX2* 72 hours after the combined treatment and 4 Gy radiation are shown. The fold changes were calculated compared to sham irradiated control cells (DMSO) set to one. Data represents mean

values ± SEM (n = 3). [*Student's *t*-test; **p* ≤ 0.05, (versus DMSO 0 Gy), #Student's *t*-test; #*p* ≤ 0.05 (versus DMSO 4 Gy)].

Generally, the combination of the HDACi and MEKi alone or together with radiation mostly upregulated the gene expressions of the GSLC markers in LN229-sph, U87-sph and U251-sph. In contrast, the results of western blot analysis showed that the combined treatment with radiation significantly reduced protein expressions of Nestin, SOX2 and CD44 (only in U251-sph). This was further validated by flow cytometry analysis that showed the same results. The differential results between the protein and mRNA expression of the GSLC markers after the combined treatment with radiation therefore reveal that the changes in protein levels do not always reflect the mRNA expression. To confirm this, the results were recalculated using *GAPDH* as the endogenous control with the results presented in the appendix section G (Figure A28 - Figure A30). Table 17 summarizes the results of comparing protein and RNA analysis after the combined treatment of HDACi and MEKi with radiation.

Table 17: Comparison of results from protein and RNA analysis after the combined treatment of HDACi and MEKi with radiation

	LN229-sph		U87-sph		U251-sph	
HDACi + MEKi + 4 Gy	**MS + TAK + 4Gy**	**MS + TRA + 4Gy**	**MS + TAK + 4 Gy**	**MS + TRA + 4 Gy**	**MS + TAK + 4 Gy**	**MS + TRA + 4 Gy**
Nestin						
CD44						
SOX2						

* Blue arrows represent protein analysis; green arrows represent flow cytometry analysis; red arrows represent RNA analysis. Arrows facing upward indicate significant increase, arrows facing downwards indicate significant decrease and arrows facing both sides indicates no change.

5 DISCUSSION

To date, glioblastoma remains a difficult cancer to treat despite the use of standardized multimodal therapy that includes surgery, radiation and chemotherapy with the DNA-alkylating agent TMZ [4]. Apart from severe side effects arising from the use of TMZ, glioblastoma tumors rapidly develop resistance to the standard treatment [26, 165]. One limiting factor for the effective treatment of glioblastoma is the presence of GSLCs within the tumor that are highly radioresistant, promote tumor recurrence and enhance tumor cell proliferation, angiogenesis, metastasis and differentiation [24]. Therefore, an efficacious therapy against the radioresistant GSCLs would be expected to improve outcome.

The development of small molecule inhibitors of key enzymatic processes offers hope of novel therapies. Of these are the HDACi and MEKi drugs that have been identified for their anti-tumor activities in glioblastoma [131, 166]. HDACis act by increasing acetylation in cancer cells to facilitate the re-expression of silenced tumor suppressor genes while also activating cellular processes that selectively kill tumor cells [100]. MEKi have the potential to inhibit the MAPK pathway that is upregulated in GSLCs to drive their proliferation and survival [125, 131]. Despite the proven anti-tumor activities of the HDACi and MEKi as single treatments, their full therapeutic potential may be realized when combined with other anti-tumor agents [116].

The combination of HDACi and MEKi as a therapeutic strategy for cancer was first suggested from *in-vitro* studies that showed MEKi sensitized colon, lung and prostate cells to HDACi-induced cell death [143]. This study demonstrated that MEKi not only enhanced the HDACi-induced apoptotic cell death, but also the generation of ROS in the tumor cells. Since then, the efficacy of combining HDACi and MEKi has been investigated in other studies of pancreatic cancer, leukemia and breast cancer with promising results reported [144, 167, 168].

In glioblastoma, the efficacy of combining HDACi and MEKi has neither been fully explored, nor is it known if such a combined treatment is effective against CSCs, or if radiation provides further benefit. Therefore, the goal of this study was to examine the efficacy of combining the HDACi (MS-275) and MEKi (TAK-733 or trametinib) with or without ionizing radiation as a novel therapeutic strategy for glioblastoma. We hypothesize that the combined treatment, by including radiation, will be more effective

against the highly resistant GSLCs compared to either drug alone. To investigate our hypothesis, we used the monolayer cultures of glioblastoma cell lines A172, LN229, U87 and U251 as well as stem cell-enriched glioblastoma-derived spheres (LN229-sph, U87-sph and U251-sph) that mimics a GSLC phenotype.

5.1 GSLC marker expressions are not affected by radiation alone in monolayer glioblastoma cell lines

The expression of the GSLC markers Nestin, CD44, SOX2 and ALDH1A1 that identifies the GSLC population [35, 95] was used to measure the effect of treatment. These GSLC markers are typically highly expressed in glioblastoma and are possibly markers of cells with potential to escape therapy and repopulate a tumor [72, 83, 169]. To establish that there are changes in expression levels of GSLC markers in glioblastoma, we compared GSLC marker gene expression between glioblastoma and normal brain tissue using the GEPIA web database [154]. Indeed, we found that, Nestin, CD44 and SOX2 were highly upregulated in glioblastoma samples compared to non-cancerous tissues while in contrast, ALDH1A1 was downregulated in the glioblastoma samples (Figure 11). This was not expected since the increased expression of ALDH1A1 has been linked to the pathogenesis and poor overall survival of glioblatoma [96]. However, there have been contrasting data showing higher ALDH1A1 expression is associated with a significantly better survival of glioblastoma patients [97]. This suggests that ALDH1A1 may have a distinct role and prognostic value in glioblastoma and may not be a suitable GSLC marker. More studies to define the function of ALDH1A1 expression in glioblastoma and clinical outcome are therefore required.

Because GSLCs are known to be resistant to radiation [24], we looked at what effect 4 Gy radiation alone had on the GSLC markers (Nestin, CD44, SOX2 and ALDH1A1) expressed in the monolayer glioblastoma cell lines after 24, 48 and 72 hours. While the GSLC markers fluctuated slightly at 24 and 48 hours after 4 Gy irradiation, there was no significant influence of radiation after 72 hours (Figure A1 and Figure 12). This finding was consistent with other studies that have demonstrated very little influence of similar radiation dose on GSLCs [170, 171]. Since there was no change in GSLC markers after 72 hours with radiation alone, we chose to analyze the efficacy of combining the HDACi and MEKi treatment 72 hours after 4 Gy radiation exposure for comparison.

5.2 Differing responses among the monolayer glioblastoma cells to the combined treatment of HDACi and MEKi with radiation

Initially, we tested the effect of the HDACi and MEKi as single or combined treatments with 4 Gy radiation on the monolayer glioblastoma cell lines and analysed the changes in the protein expressions of the GSLC markers. We observed that the GSLC markers responded differentially to the combined radiochemotherapy in each cell line compared to radiation alone.

Generally, the standard treatment of TMZ alone or with radiation either increased or did not affect the expressions of the GSLC markers in all the glioblastoma cell lines tested. Interestingly, even though SOX2 could not be detected in the unexposed U87 cell line, treatment with the standard TMZ and radiation induced its expression. This may suggest that the standard treatment is able to induce a stem-like phenotype in glioblastoma as a means of resistance. This finding is related to other studies that have reported the induction of GSLCs in glioblastoma cells following treatment with TMZ [172]

Nestin, CD44 and SOX2 were all significantly reduced by the combined treatment with radiation in the A172 cell line without affecting ALDH1A1 expression. In LN229, the combined treatment with radiation significantly reduced Nestin and ALDH1A1 but in contrast increased CD44 and SOX2 expressions. In the case of U87, the combined treatment with radiation significantly reduced ALDH1A1 expression but upregulated Nestin. Only the combination of MS-275 and trametinib could significantly reduce CD44 with no additional effect of radiation observed. While there was potential for the combined treatment with radiation to reduce Nestin in U251 cell line, no effect could be detected on the expressions of CD44, SOX2 and ALDH1A1 (Figure 13 - Figure 16). These differential responses observed may be due to changes in the intra-tumoral heterogeneity, one of the morphological hallmarks of glioblastoma [173]. Therefore, the different changes of the GSLC markers after the combined treatment may be associated with the different molecular mutations present within each cell line. For example, although both A172 and LN229 contain EGFR mutations according to the cBioportal database of cancer cell lines [174, 175], their responses to the combined treatment with radiation were dissimilar. Apart from the EGFR mutation, the glioblastoma cell lines also contained other distinctive mutations that could further influence their response to the applied radiochemotherapy.

In addition, it is important to point out that the combined treatment with radiation was designed to be effective against the GSLC population but may also affect the non-GSLC components too. However, the monolayer glioblastoma cell lines tested included mostly differentiated cells that have been cultured long term in medium containing serum where this culture method is known to result in the reduction of GSLCs in glioblastoma [176, 177]. This could explain the differential responses observed and why it was difficult to be conclusive on the efficacy of the combined treatment with radiation against the GSLC population using monolayer glioblastoma cells.

5.3 Glioblastoma cell lines were enriched for GSLCs by sphere culture in stem cell medium

Because the target for the proposed radiochemotherapy was the GSLC population in glioblastoma, we proceeded to enrich the glioblastoma cell lines for GSLCs. We did this by culturing glioblastoma cells as spheres in low adherence culture flasks with serum-free medium containing stem cell supplements, an approach that has been used successfully in other published studies of glioblastoma [163, 171, 178, 179].

The LN229-sph, U87-sph and U251-sph glioblastoma-derived spheres (Figure 17) were successfully maintained as spheroid culture for 8 weeks, while the A172-sph stopped growing and forming spheres after the third passage. Immunofluorescence staining of GSLC markers at the eighth passage confirmed the increase in GSLC markers (Figure 18 - Figure 20) in all the three glioblastoma-derived spheres studied compared to their parental counterpart. This result was similarly demonstrated by Liu *et al* [171] where they showed that GSLC markers (CD133, Nestin and SOX2) were increased in U87-sph and U251-sph compared to the parental cell lines. Thus, the method of enrichment was successful and the LN229-sph, U87-sph and U251-sph were hereafter referred to as stem cell-enriched glioblastoma-derived spheres.

5.4 Actions of HDACi and MEKi and their effect on the cell viability of glioblastoma-derived spheres

Before testing the efficacy of combining the HDACi and MEKi with radiation, the specific inhibitory activities of the individual drugs were tested on the enriched glioblastoma-derived spheres.

As expected, treatment with the HDACi MS-275 alone or in combination with radiation increased acetyl-H3 in both U87-sph and U251-sph (Figure 21). This indicated the successful inhibition of HDACs and is in line with other published data on the activity of MS-275 [118, 119, 122]. Treatment with the MEKi TAK-733 and trametinib successfully inhibited pMAPK in both U87-sph and U251-sph (Figure 22). Given that the MAPK pathway is only activated by the phosphorylation of MAPK through MEK activation, the successful inhibition of pMAPK by both TAK-733 and trametinib validates their activities as MEK inhibitors and corresponds to previously published data [180, 181].

Cell viability analysis showed that treatment with the HDACi or MEKi together with 4 Gy radiation resulted in a dose-dependent decrease in viability compared to treatment with TMZ with radiation in LN229-sph, U87-sph and U251-sph. This result indicated a greater treatment sensitivity of the glioblastoma-derived spheres to HDACi or MEKi treatment with radiation than that achieved with the standard treatment of TMZ and radiation. This finding is comparable with a previous study that showed that GSLCs were less sensitive to TMZ treatment through cell viability quantification [75].

5.5 Combined treatment of HDACi and MEKi with radiation reduced sphere formation and protein expressions of GSLC markers

After establishing that the viability of the cells could be reduced at low concentrations (1 µM), we tested the effect of combining the HDACi and MEKi 72 hours after 4 Gy radiation. The sphere formation assay was used to measure the self-renewal of the stem cell-enriched sphere forming cells since sphere formation is a typical feature of CSCs. [156, 163] We found that combining the HDACi and MEKi (both at 1 µM) resulted in very low number of spheres formed compared to the untreated cells (Figure 26 - Figure 28). By adding radiation to the combination, the number of spheres formed were significantly much lower compared to the individual treatments with HDACi or MEKi combined with radiation. Sphere formation means that there is aggregation of undifferentiated cells to form clumps that indicates the ongoing proliferation of stem-like cells [182]. Therefore, the reduced ability to form spheres upon the combination of the HDACi and MEKi with radiation means the self-renewal and proliferation of the enriched glioblastoma-derived spheres was inhibited.

In parallel, we found that the standard TMZ alone or combined with radiation at a concentration of 50 µM could efficiently reduce the number of spheres formed, especially in LN229-sph and U87-sph. In cancer treatment, combination therapies are usually applied to enhance effectiveness, therefore lower doses of the single drugs involved are often desired to reduce the risk of drug toxicity to healthy surrounding cells [183]. Hence, the use of the HDACi and MEKi at 1 µM may suggest less toxicity and better tolerance level for glioblastoma treatment as opposed to TMZ [184]. However, it should be pointed out that this suggestion is based on the effect of the combined therapy on cells (*in-vitro*) that may differ when applied to the tumors *in-vivo*.

Next, we analysed the changes in protein expressions of the GSLC markers in the enriched glioblastoma-derived spheres after the combined treatment with radiation as previously done in the parental cell lines. Generally, no significant effect on GSLC markers was observed with TMZ treatment alone or with radiation. However, the combination of the HDACi and MEKi with radiation significantly reduced the protein expressions of Nestin, SOX2 and ALDH1A1 in LN229-sph and U87-sph compared to treatment with radiation alone. In U251-sph, the combined treatment completely eradicated Nestin and SOX2 while only the combination of the HDACi MS-275 and MEKi trametinib with radiation could significantly reduce ALDH1A1 expression (Figure 29 - Figure 31). The decrease of the GSLC markers by the combined radiochemotherapy suggests the loss of GSLC marker positive cells to hinder tumorigenesis. For example, Gangemi *et al* reported that the loss of SOX2 expression stopped proliferation and resulted in loss of tumorigenicity in GSLCs [88]. Since the GSLC markers identify the GSLC population, it is possible that the reduced GSLC markers indicate a reduction in the resistant GSLC population [82].

While the protein expression of CD44 in U251-sph was significantly reduced by the combined treatment alone and with radiation, CD44 was surprisingly increased by all treatment conditions in LN229-sph and U87-sph. This implies that the sensitivity of CD44 expression to the different treatments may be cell line dependent. Similar to our finding, differential responses of protein expressions in the GSLC lines have been reported [171]. The study showed that via protein analysis, cell-cycle-related proteins in U87-sph and U251-sph responded differently to the same treatment of 8 Gy radiation. Another possible explanation for the differential responses could be the different genetic mutations present in the cell lines. This was supported by a study that

reported unique genetic profiles of GSLCs that may influence their individual responses to the combined radiochemotherapy [185]. Therefore, the same response of different cell lines to the same combined therapy should not be expected.

Generally, the GSLC markers were lowered more by the combined treatment (1 µM) with radiation compared to the standard treatment with TMZ (50 µM) and radiation. Even though 50 µM TMZ alone or with radiation could efficiently inhibit sphere formation, there was very limited effectiveness against the protein expressions of the GSLC markers. One possible reason for this may be due to the different endpoints used. The protein expressions of the GSLC markers were analyzed 72 hours after compound and radiation treatment while in the case of sphere formation assay, the GSLCs were reseeded as single cells and cultured for an additional 14 days before final analysis.

Nonetheless, the results of the protein analysis demonstrated that combining the HDACi and MEKi with radiation at low concentrations was more effective against the GSLC markers than the standard TMZ with radiation.

5.6 HDACi and MEKi with radiation reduced single and double expressions of GSLC markers and increased the dead cell population.

To further validate the efficacy of combining the HDACi and MEKi with radiation, a multicolour flow cytometry approach was used to analyse changes in the GSLC population 72 hours after the combined treatment. The GSLC population could be identified as those cells expressing Nestin, CD44 and SOX2 while ALDH1A1 remained undetected in the flow cytometry experiments (Figure 7 - Figure 9) and was therefore excluded.

First, the single positive populations (Nestin+, CD44+ and SOX2+) were analysed after the various treatments. As observed in protein analysis, the percentage of Nestin+ and SOX2+ GSLC populations were the lowest when treated by the combination of the HDACi and MEKi with radiation (Figure 32 - Figure 34). The CD44+ population was only reduced in U251-sph by the combined treatment with radiation. In general, the flow cytometry results correlated with those of the protein analysis of the GSLC markers after the combined treatment of the HDACi and MEKi with radiation.

There has been a dispute in the literature whether a single GSLC marker can be used to accurately identify the GSLC population [35, 186]. Since we developed a multicolour approach, it was possible to analyse the expression of pairs of GSLC markers after the combined treatment with radiation. All three double positive populations (CD44+Nestin+, Nestin+SOX2+ and CD44+SOX2+) were significantly at their lowest percentage upon treatment with the HDACi and MEKi with radiation in all the enriched glioblastoma-derived spheres (Figure 35 - Figure 37). This finding confirms that the combined treatment with radiation was the most effective against the GSLC population compared to either alone.

Apart from the analysis of the single and double expressions of the GSLC markers after treatment, a live/dead staining revealed the percentage of dead cells after each treatment condition. As expected, the dead cell population in the GSLCs was at the highest percentage when treated with the HDACi and MEKi with radiation compared to either single treatment alone (Figure 38). These data therefore suggests that the significant reduction in GSLC markers by the combined treatment with radiation may be due to the killing of the GSLC population within the enriched glioblastoma-derived spheres. This observation correlates with the previously described induction of apoptosis by the combination of HDACi and MEKi in prostate cancer cells [145]. Although this study did not include radiation or use CSCs, our study suggests that adding radiation to the combined therapy may increase the killing of the CSC population.

We also observed that treatment with TMZ alone or with radiation did not have any effect on the GSLC population. The standard treatment either increased or did not affect the single and double expressions of the GSLC markers in all the enriched glioblastoma-derived spheres. The percentage of dead cells after treatment with TMZ alone or with radiation was also very low compared to the high dead cell fraction observed with the combined treatment with radiation. Our findings are similar to other studies that have shown TMZ chemoresistance of GSLCs and glioblastoma [187-189].

One possible explanation for the chemoresistance to TMZ may be related to the expression of the DNA repair enzyme MGMT [49]. The DNA damage caused by TMZ can efficiently be repaired by MGMT, therefore only glioblastoma cells and GSLCs with an epigenetically silenced expression of MGMT will benefit from TMZ treatment [190]. Although our study did not check the MGMT status of the stem cell-enriched

glioblastoma-derived spheres, published studies have shown that all of the established parental glioblastoma cell lines (LN229, U87 and U251) are MGMT-negative making them sensitive to TMZ [191, 192]. However, it has been revealed that GSLCs induced from parental MGMT-negative U251 cell lines can become MGMT-positive [192]. Therefore, we propose that the stem cell-enriched glioblastoma-derived spheres may have acquired MGMT that influenced the ineffectiveness of TMZ alone or combined with radiation against the GSLC population.

The reported anti-tumour effects of combining HDACi and MEKi in other cancers include enhanced ROS generation and cell death in colon, lung and prostate cancer cells [143, 146], induction of growth arrest and apoptosis in leukaemia cells [167], and killing of pancreatic, liver and kidney tumor cells [193]. More recently, there are *in vivo* studies that also revealed that the combination of HDACi and MEKi can inhibit tumour growth in xenograft models of colorectal cancer [194], pancreatic cancer [144], breast cancer [168] and lung cancer [195]. While these are promising results, there is little information on the effect of this combination on CSCs. In addition to all of the above data, we now show here that the cytotoxic effects of adding radiation to the HDACi and MEKi combination may be more effective against the GSLC population than the drugs alone or the standard TMZ with radiation.

5.7 HDACi and MEKi with radiation upregulated GSLC marker gene mRNA transcripts

Since we observed that the expressions of the GSLC markers were reduced by the combined treatment with radiation, we further looked at the effects on RNA level by analysing the GSLC marker genes (*NES*, *CD44* and *SOX2*) after treatment. Surprisingly we found that the GSLC marker genes were mostly upregulated in all the GSLCs after the combined treatment with radiation (Figure 39 - Figure 41). The lack of correlation between the protein and mRNA expressions of the GSLC markers after treatment suggests that the protein levels did not correspond to their gene transcripts [196].

One possible explanation for this discovery is that the combined treatment with radiation resulted in post-transcriptional modifications that repressed the translation of the GSLC marker genes into proteins [197]. Given the many processes that influence the rate of translation, we speculate that the combined treatment could have influenced

the translation efficiency through functional protein modifications like phosphorylation or proteolysis [198]. Besides, regulatory elements such as microRNAs or RNA-binding proteins may increase when exposed to radiation [199].

Experimental noise or error could also influence the correlation of the GSLC marker genes and protein expressions [197, 200]. For instance, actin was used as reference protein for the protein expressions while *TBP* was the endogenous control for the gene expressions. All of these factors mentioned may explain the observed absence of correlation in GSLC marker gene and protein expressions after the HDACi and MEKi treatment with radiation. Similar to our findings, other studies have reported an inverse correlation of mRNA and proteins which means the amount of proteins cannot always be predicted based on mRNA expression alone [201-203]. Conversely, opposing views exist where significant correlations between protein and mRNA expressions of human carcinomas were reported [204].

Further studies are required to determine how the combination of HDACi and MEKi with radiation regulates GSLC marker expression at the transcriptional, translational and post-translational levels. This knowledge will help to improve our understanding on the efficacy of the proposed radiochemotherapy.

5.8 Conclusion

The existence of GSLCs within the glioblastoma tumor remains a challenge for designing successful treatments of glioblastoma due to their ability to promote resistance. Since monotherapy has proven ineffective in clinical trials, a combination therapy may enhance the efficacy of each single agent involved. One approach is the combination of HDACi and MEKi that has been investigated in other cancers. The goal of our study was to test the efficacy of combining HDACi and MEKi via a new strategy of adding radiation, which itself remains part of the standard therapy. We show here for the first time that the proposed combined radiochemotherapy may be effective against the GSLC population.

The efficacy of combining the HDACi and MEKi with radiation was tested using three stem cell-enriched glioblastoma-derived spheres (LN229-sph, U87-sph, U251-sph) that mimics a GSLC phenotype. Even though the standard TMZ with radiaton inhibited sphere formation, our data showed that the GSLC markers detected (Nestin, CD44 and SOX2) and dead cell population were not affected by the standard treatment. The

significant reduction in sphere forming ability of the glioblastoma-derived spheres by the HDACi and MEKi with radiation compared to radiation alone or single treatments indicated that proliferation and self-renewal ability was inhibited. GSLC markers that were used to identify the GSLC population were also significantly reduced while the dead cell population was at highest after the HDACi and MEKi with radiation. Our findings suggest that the combined treatment with radiation may have a greater potential for the cell killing of GSLCs compared to the single treatments alone.

Although more research is needed, our *in vitro* study suggests that the novelty of combining HDACi and MEKi with radiation may be a promising multimodal glioblastoma therapy against the highly resistant GSLCs (Figure 42).

Since we used established glioblastoma cell lines to enrich for GSLCs, it should be pointed out that the stem cell-enriched glioblastoma-derived spheres may not fully represent the *in vivo* target GSLC population. Based on our *in vitro* data, it will be necessary to use other (preclinical) models that are more representative of *in vivo* tumors to test the efficacy of the proposed combination therapy. This could be via the study of low-passage glioblastoma patient-derived primary GSLCs or tumor cells recovered by fluorescence-activated cell sorting (FACS) to isolate side populations expressing GSLC markers. Moreover, further validations performed *in vivo* will help to improve our understanding on the combined therapy as well as uncover any side effects on non-cancerous neural stem cells.

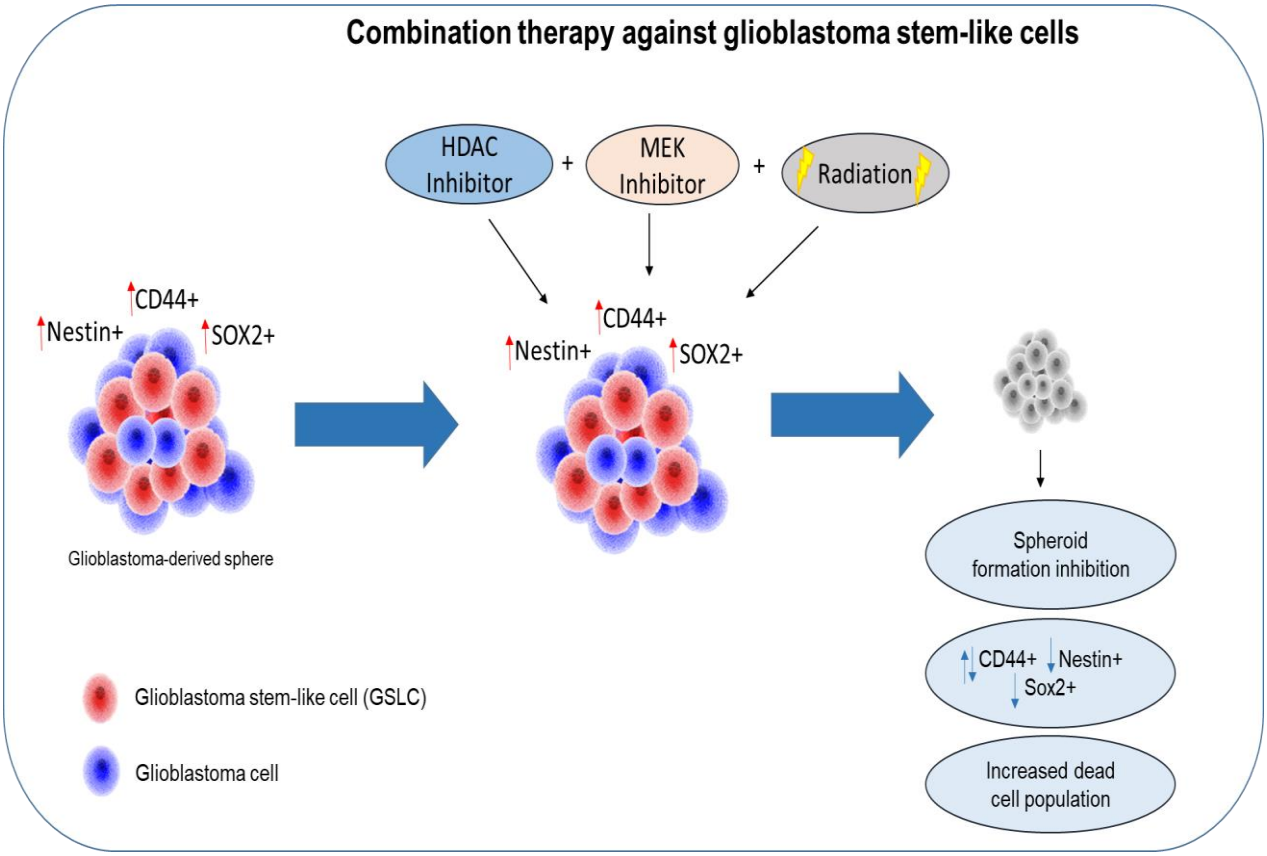

Figure 42: Graphical abstract summarizing the effect of combining HDACi and MEKi with radiation on glioblastoma-derived spheres. The combined treatment targets the glioblastoma-derived spheres to eradicate glioblastoma by inhibition of sphere formation, reduction of expressed GSLC markers (Nestin, CD44 and SOX2) and increase in the dead cell population.

REFERENCES

1. Zong H, Verhaak RGW, Canoll P. The cellular origin for malignant glioma and prospects for clinical advancements. Expert Rev Mol Diagn. 2012;12(4):383-94. doi: 10.1586/erm.12.30. PubMed PMID: 22616703.

2. Veliz I, Loo Y, Castillo O, Karachaliou N, Nigro O, Rosell R. Advances and challenges in the molecular biology and treatment of glioblastoma-is there any hope for the future? Ann Transl Med. 2015;3(1):7-. doi: 10.3978/j.issn.2305-5839.2014.10.06. PubMed PMID: 25705639.

3. Ostrom QT, Gittleman H, Liao P, Vecchione-Koval T, Wolinsky Y, Kruchko C, et al. CBTRUS Statistical Report: Primary brain and other central nervous system tumors diagnosed in the United States in 2010-2014. Neuro-oncology. 2017;19(suppl_5):v1-v88. Epub 2017/11/09. doi: 10.1093/neuonc/nox158. PubMed PMID: 29117289.

4. Stupp R, Mason WP, van den Bent MJ, Weller M, Fisher B, Taphoorn MJ, et al. Radiotherapy plus concomitant and adjuvant temozolomide for glioblastoma. The New England journal of medicine. 2005;352(10):987-96. Epub 2005/03/11. doi: 10.1056/NEJMoa043330. PubMed PMID: 15758009.

5. Ohgaki H, Kleihues P. The definition of primary and secondary glioblastoma. Clinical cancer research : an official journal of the American Association for Cancer Research. 2013;19(4):764-72. Epub 2012/12/05. doi: 10.1158/1078-0432.Ccr-12-3002. PubMed PMID: 23209033.

6. Louis DN, Perry A, Reifenberger G, von Deimling A, Figarella-Branger D, Cavenee WK, et al. The 2016 World Health Organization Classification of Tumors of the Central Nervous System: a summary. Acta Neuropathologica. 2016;131(6):803-20. doi: 10.1007/s00401-016-1545-1.

7. Chen JR, Yao Y, Xu HZ, Qin ZY. Isocitrate Dehydrogenase (IDH)1/2 Mutations as Prognostic Markers in Patients With Glioblastomas. Medicine (Baltimore). 2016;95(9):e2583. doi: 10.1097/md.0000000000002583. PubMed PMID: 26945349; PubMed Central PMCID: PMCPMC4782833.

8. Weller M, Felsberg J, Hartmann C, Berger H, Steinbach JP, Schramm J, et al. Molecular Predictors of Progression-Free and Overall Survival in Patients With Newly Diagnosed Glioblastoma: A Prospective Translational Study of the German Glioma Network. Journal of Clinical Oncology. 2009;27(34):5743-50. doi: 10.1200/JCO.2009.23.0805.

9. Verhaak RGW, Hoadley KA, Purdom E, Wang V, Qi Y, Wilkerson MD, et al. Integrated genomic analysis identifies clinically relevant subtypes of glioblastoma characterized by abnormalities in PDGFRA, IDH1, EGFR, and NF1. Cancer Cell. 2010;17(1):98-110. doi: 10.1016/j.ccr.2009.12.020. PubMed PMID: 20129251.

10. Wang Q, Hu B, Hu X, Kim H, Squatrito M, Scarpace L, deCarvalho AC, Lyu S, Li P, Li Y, Barthel F, Cho HJ, Lin YH, Satani N, Martinez-Ledesma E, Zheng S, Chang E, Sauvé CG, Olar A, Lan ZD, Finocchiaro G, Phillips JJ, Berger MS, Gabrusiewicz KR, Wang G, Eskilsson E, Hu J, Mikkelsen T, DePinho RA, Muller F, Heimberger AB, Sulman EP, Nam DH, Verhaak RGW. Tumor Evolution of Glioma-Intrinsic Gene Expression Subtypes Associates with Immunological Changes in the Microenvironment. Cancer Cell. 2017 Jul 10;32(1):42-56.e6. doi: 10.1016/j.ccell.2017.06.003. Erratum in: Cancer Cell. 2018 Jan 8;33(1):152. PMID: 28697342; PMCID: PMC5599156.

11. Phillips HS, Kharbanda S, Chen R, Forrest WF, Soriano RH, Wu TD, et al. Molecular subclasses of high-grade glioma predict prognosis, delineate a pattern of disease progression, and resemble stages in neurogenesis. Cancer Cell. 2006;9(3):157-73. Epub 2006/03/15. doi: 10.1016/j.ccr.2006.02.019. PubMed PMID: 16530701.

12. Arjona D, Rey JA, Taylor SM. Early genetic changes involved in low-grade astrocytic tumor development. Current molecular medicine. 2006;6(6):645-50. Epub 2006/10/07. doi: 10.2174/156652406778195017. PubMed PMID: 17022734.

13. Furnari FB, Fenton T, Bachoo RM, Mukasa A, Stommel JM, Stegh A, et al. Malignant astrocytic glioma: genetics, biology, and paths to treatment. Genes Dev. 2007;21(21):2683-710. Epub 2007/11/03. doi: 10.1101/gad.1596707. PubMed PMID: 17974913.

14. Kleihues P, Ohgaki H. Primary and secondary glioblastomas: from concept to clinical diagnosis. Neuro-oncology. 1999;1(1):44-51. Epub 2001/09/12. doi: 10.1093/neuonc/1.1.44. PubMed PMID: 11550301; PubMed Central PMCID: PMCPMC1919466.

15. Garofano L, Migliozzi S, Oh YT, D'Angelo F, Najac RD, Ko A, et al. Pathway-based classification of glioblastoma uncovers a mitochondrial subtype with therapeutic vulnerabilities. Nature Cancer. 2021;2(2):141-56. doi: 10.1038/s43018-020-00159-4.

16. Stupp R, Taillibert S, Kanner A, Read W, Steinberg D, Lhermitte B, et al. Effect of Tumor-Treating Fields Plus Maintenance Temozolomide vs Maintenance Temozolomide Alone on Survival in Patients With Glioblastoma: A Randomized Clinical Trial. JAMA. 2017;318(23):2306-16. doi: 10.1001/jama.2017.18718. PubMed PMID: 29260225.

17. Tan AC, Ashley DM, López GY, Malinzak M, Friedman HS, Khasraw M. Management of glioblastoma: State of the art and future directions. CA Cancer J Clin. 2020 Jul;70(4):299-312. doi: 10.3322/caac.21613. Epub 2020 Jun 1. PMID: 32478924..

18. Alifieris C, Trafalis DT. Glioblastoma multiforme: Pathogenesis and treatment. Pharmacology & therapeutics. 2015;152:63-82. Epub 2015/05/07. doi: 10.1016/j.pharmthera.2015.05.005. PubMed PMID: 25944528.

19. Stummer W, Pichlmeier U, Meinel T, Wiestler OD, Zanella F, Reulen HJ. Fluorescence-guided surgery with 5-aminolevulinic acid for resection of malignant glioma: a randomised controlled multicentre phase III trial. The Lancet Oncology. 2006;7(5):392-401. Epub 2006/05/02. doi: 10.1016/s1470-2045(06)70665-9. PubMed PMID: 16648043.

20. Berntsen EM, Gulati S, Solheim O, Kvistad KA, Torp SH, Selbekk T, et al. Functional magnetic resonance imaging and diffusion tensor tractography incorporated into an intraoperative 3-dimensional ultrasound-based neuronavigation system: impact on therapeutic strategies, extent of resection, and clinical outcome. Neurosurgery. 2010;67(2):251-64. Epub 2010/07/21. doi: 10.1227/01.Neu.0000371731.20246.Ac. PubMed PMID: 20644410.

21. Abhinav K, Yeh F-C, Mansouri A, Zadeh G, Fernandez-Miranda JC. High-definition fiber tractography for the evaluation of perilesional white matter tracts in high-grade glioma surgery. Neuro-oncology. 2015;17(9):1199-209. Epub 2015/06/27. doi: 10.1093/neuonc/nov113. PubMed PMID: 26117712.

22. Hervey-Jumper SL, Berger MS. Maximizing safe resection of low- and high-grade glioma. Journal of neuro-oncology. 2016;130(2):269-82. Epub 2016/11/03. doi: 10.1007/s11060-016-2110-4. PubMed PMID: 27174197.

23. Perry JR, Laperriere N, O'Callaghan CJ, Brandes AA, Menten J, Phillips C, et al. Short-Course Radiation plus Temozolomide in Elderly Patients with Glioblastoma. The New England

journal of medicine. 2017;376(11):1027-37. Epub 2017/03/16. doi: 10.1056/NEJMoa1611977. PubMed PMID: 28296618.

24. Huang Z, Cheng L, Guryanova OA, Wu Q, Bao S. Cancer stem cells in glioblastoma--molecular signaling and therapeutic targeting. Protein & cell. 2010;1(7):638-55. Epub 2011/01/05. doi: 10.1007/s13238-010-0078-y. PubMed PMID: 21203936.

25. Weller M, Steinbach JP, Wick W. Temozolomide: a milestone in the pharmacotherapy of brain tumors. Future oncology (London, England). 2005;1(6):747-54. Epub 2006/03/25. doi: 10.2217/14796694.1.6.747. PubMed PMID: 16556052.

26. Trinh VA, Patel SP, Hwu W-J. The safety of temozolomide in the treatment of malignancies. Expert Opinion on Drug Safety. 2009;8(4):493-9. doi: 10.1517/14740330902918281.

27. Choi S, Yu Y, Grimmer MR, Wahl M, Chang SM, Costello JF. Temozolomide-associated hypermutation in gliomas. Neuro-oncology. 2018;20(10):1300-9. doi: 10.1093/neuonc/noy016. PubMed PMID: 29452419.

28. Chinot OL, Wick W, Mason W, Henriksson R, Saran F, Nishikawa R, et al. Bevacizumab plus radiotherapy-temozolomide for newly diagnosed glioblastoma. The New England journal of medicine. 2014;370(8):709-22. Epub 2014/02/21. doi: 10.1056/NEJMoa1308345. PubMed PMID: 24552318.

29. Wirsching HG, Tabatabai G, Roelcke U, Hottinger AF, Jörger F, Schmid A, et al. Bevacizumab plus hypofractionated radiotherapy versus radiotherapy alone in elderly patients with glioblastoma: the randomized, open-label, phase II ARTE trial. Ann Oncol. 2018;29(6):1423-30. Epub 2018/04/13. doi: 10.1093/annonc/mdy120. PubMed PMID: 29648580.

30. Ghosh D, Nandi S, Bhattacharjee S. Combination therapy to checkmate Glioblastoma: clinical challenges and advances. Clin Transl Med. 2018;7(1):33-. doi: 10.1186/s40169-018-0211-8. PubMed PMID: 30327965.

31. Rominiyi O, Vanderlinden A, Clenton SJ, Bridgewater C, Al-Tamimi Y, Collis SJ. Tumour treating fields therapy for glioblastoma: current advances and future directions. British Journal of Cancer. 2021;124(4):697-709. doi: 10.1038/s41416-020-01136-5.

32. Carrieri FA, Smack C, Siddiqui I, Kleinberg LR, Tran PT. Tumor Treating Fields: At the Crossroads Between Physics and Biology for Cancer Treatment. Frontiers in oncology. 2020;10(1991). doi: 10.3389/fonc.2020.575992.

33. Taphoorn MJB, Dirven L, Kanner AA, Lavy-Shahaf G, Weinberg U, Taillibert S, Toms SA, Honnorat J, Chen TC, Sroubek J, David C, Idbaih A, Easaw JC, Kim CY, Bruna J, Hottinger AF, Kew Y, Roth P, Desai R, Villano JL, Kirson ED, Ram Z, Stupp R. Influence of Treatment With Tumor-Treating Fields on Health-Related Quality of Life of Patients With Newly Diagnosed Glioblastoma: A Secondary Analysis of a Randomized Clinical Trial. JAMA Oncol. 2018 Apr 1;4(4):495-504. doi: 10.1001/jamaoncol.2017.5082. PMID: 29392280; PMCID: PMC5885193.

34. Lassman AB, Joanta-Gomez AE, Pan PC, Wick W. Current usage of tumor treating fields for glioblastoma. Neurooncol Adv. 2020;2(1):vdaa069. Epub 20200604. doi: 10.1093/noajnl/vdaa069. PubMed PMID: 32666048; PubMed Central PMCID: PMCPMC7345837.

35. Bradshaw A, Wickremsekera A, Tan ST, Peng L, Davis PF, Itinteang T. Cancer Stem Cell Hierarchy in Glioblastoma Multiforme. Frontiers in surgery. 2016;3:21. Epub 2016/05/06. doi: 10.3389/fsurg.2016.00021. PubMed PMID: 27148537; PubMed Central PMCID: PMCPMC4831983.

36. Desai A, Yan Y, Gerson SL. Concise Reviews: Cancer Stem Cell Targeted Therapies: Toward Clinical Success. Stem Cells Transl Med. 2019;8(1):75-81. Epub 20181017. doi: 10.1002/sctm.18-0123. PubMed PMID: 30328686; PubMed Central PMCID: PMCPMC6312440.

37. Schneider M, Ströbele S, Nonnenmacher L, Siegelin MD, Tepper M, Stroh S, et al. A paired comparison between glioblastoma "stem cells" and differentiated cells. Int J Cancer. 2016;138(7):1709-18. Epub 20151117. doi: 10.1002/ijc.29908. PubMed PMID: 26519239.

38. Chen R, Nishimura MC, Bumbaca SM, Kharbanda S, Forrest WF, Kasman IM, et al. A hierarchy of self-renewing tumor-initiating cell types in glioblastoma. Cancer cell. 2010;17(4):362-75. Epub 2010/04/14. doi: 10.1016/j.ccr.2009.12.049. PubMed PMID: 20385361.

39. Safa AR, Saadatzadeh MR, Cohen-Gadol AA, Pollok KE, Bijangi-Vishehsaraei K. Glioblastoma stem cells (GSCs) epigenetic plasticity and interconversion between differentiated non-GSCs and GSCs. Genes Dis. 2015 Jun;2(2):152-163. doi: 10.1016/j.gendis.2015.02.001. PMID: 26137500; PMCID: PMC4484766.

40. Chandran UR, Luthra S, Santana-Santos L, Mao P, Kim SH, Minata M, et al. Gene expression profiling distinguishes proneural glioma stem cells from mesenchymal glioma stem cells. Genomics data. 2015;5:333-6. Epub 2015/08/08. doi: 10.1016/j.gdata.2015.07.007. PubMed PMID: 26251826; PubMed Central PMCID: PMCPMC4523279.

41. Morokoff A, Ng W, Gogos A, Kaye AH. Molecular subtypes, stem cells and heterogeneity: Implications for personalised therapy in glioma. J Clin Neurosci. 2015 Aug;22(8):1219-26. doi: 10.1016/j.jocn.2015.02.008. Epub 2015 May 6. PMID: 25957782.

42. Mao P, Joshi K, Li J, Kim SH, Li P, Santana-Santos L, et al. Mesenchymal glioma stem cells are maintained by activated glycolytic metabolism involving aldehyde dehydrogenase 1A3. Proc Natl Acad Sci U S A. 2013;110(21):8644-9. Epub 2013/05/08. doi: 10.1073/pnas.1221478110. PubMed PMID: 23650391; PubMed Central PMCID: PMCPMC3666732.

43. Nakano I. Stem cell signature in glioblastoma: therapeutic development for a moving target. Journal of Neurosurgery JNS. 2015;122(2):324-30. doi: 10.3171/2014.9.JNS132253.

44. Bleau A-M, Hambardzumyan D, Ozawa T, Fomchenko EI, Huse JT, Brennan CW, et al. PTEN/PI3K/Akt pathway regulates the side population phenotype and ABCG2 activity in glioma tumor stem-like cells. Cell Stem Cell. 2009;4(3):226-35. doi: 10.1016/j.stem.2009.01.007. PubMed PMID: 19265662.

45. Bao S, Wu Q, McLendon RE, Hao Y, Shi Q, Hjelmeland AB, et al. Glioma stem cells promote radioresistance by preferential activation of the DNA damage response. Nature. 2006;444(7120):756-60. Epub 2006/10/20. doi: 10.1038/nature05236. PubMed PMID: 17051156.

46. Rich JN, Bao S. Chemotherapy and cancer stem cells. Cell Stem Cell. 2007;1(4):353-5. Epub 2008/03/29. doi: 10.1016/j.stem.2007.09.011. PubMed PMID: 18371369.

47. Eramo A, Ricci-Vitiani L, Zeuner A, Pallini R, Lotti F, Sette G, et al. Chemotherapy resistance of glioblastoma stem cells. Cell death and differentiation. 2006;13(7):1238-41. Epub 2006/02/04. doi: 10.1038/sj.cdd.4401872. PubMed PMID: 16456578.

48. Hirschmann-Jax C, Foster AE, Wulf GG, Nuchtern JG, Jax TW, Gobel U, et al. A distinct "side population" of cells with high drug efflux capacity in human tumor cells. Proc Natl Acad Sci U S A. 2004;101(39):14228-33. Epub 2004/09/24. doi: 10.1073/pnas.0400067101. PubMed PMID: 15381773; PubMed Central PMCID: PMCPMC521140.

49. Liu G, Yuan X, Zeng Z, Tunici P, Ng H, Abdulkadir IR, et al. Analysis of gene expression and chemoresistance of CD133+ cancer stem cells in glioblastoma. Mol Cancer. 2006;5:67. Epub 2006/12/05. doi: 10.1186/1476-4598-5-67. PubMed PMID: 17140455; PubMed Central PMCID: PMCPMC1697823.

50. Bao S, Wu Q, Sathornsumetee S, Hao Y, Li Z, Hjelmeland AB, et al. Stem cell-like glioma cells promote tumor angiogenesis through vascular endothelial growth factor. Cancer Res. 2006;66(16):7843-8. Epub 2006/08/17. doi: 10.1158/0008-5472.Can-06-1010. PubMed PMID: 16912155.

51. Heddleston JM, Li Z, Lathia JD, Bao S, Hjelmeland AB, Rich JN. Hypoxia inducible factors in cancer stem cells. Br J Cancer. 2010;102(5):789-95. Epub 2010/01/28. doi: 10.1038/sj.bjc.6605551. PubMed PMID: 20104230; PubMed Central PMCID: PMCPMC2833246.

52. Heddleston JM, Li Z, McLendon RE, Hjelmeland AB, Rich JN. The hypoxic microenvironment maintains glioblastoma stem cells and promotes reprogramming towards a cancer stem cell phenotype. Cell cycle (Georgetown, Tex). 2009;8(20):3274-84. Epub 2009/09/23. doi: 10.4161/cc.8.20.9701. PubMed PMID: 19770585; PubMed Central PMCID: PMCPMC2825672.

53. Li Z, Bao S, Wu Q, Wang H, Eyler C, Sathornsumetee S, et al. Hypoxia-inducible factors regulate tumorigenic capacity of glioma stem cells. Cancer cell. 2009;15(6):501-13. Epub 2009/05/30. doi: 10.1016/j.ccr.2009.03.018. PubMed PMID: 19477429; PubMed Central PMCID: PMCPMC2693960.

54. Fargeas CA, Corbeil D, Huttner WB. AC133 antigen, CD133, prominin-1, prominin-2, etc.: prominin family gene products in need of a rational nomenclature. Stem Cells. 2003;21(4):506-8. Epub 2003/07/02. doi: 10.1634/stemcells.21-4-506. PubMed PMID: 12832703.

55. Singh SK, Clarke ID, Terasaki M, Bonn VE, Hawkins C, Squire J, et al. Identification of a cancer stem cell in human brain tumors. Cancer Res. 2003;63(18):5821-8. Epub 2003/10/03. PubMed PMID: 14522905.

56. Singh SK, Hawkins C, Clarke ID, Squire JA, Bayani J, Hide T, et al. Identification of human brain tumour initiating cells. Nature. 2004;432(7015):396-401. Epub 2004/11/19. doi: 10.1038/nature03128. PubMed PMID: 15549107.

57. Yan X, Ma L, Yi D, Yoon JG, Diercks A, Foltz G, et al. A CD133-related gene expression signature identifies an aggressive glioblastoma subtype with excessive mutations. Proc Natl Acad Sci U S A. 2011;108(4):1591-6. Epub 2011/01/12. doi: 10.1073/pnas.1018696108. PubMed PMID: 21220328; PubMed Central PMCID: PMCPMC3029739.

58. Tamura K, Aoyagi M, Ando N, Ogishima T, Wakimoto H, Yamamoto M, et al. Expansion of CD133-positive glioma cells in recurrent de novo glioblastomas after radiotherapy and

chemotherapy. Journal of neurosurgery. 2013;119(5):1145-55. Epub 2013/09/03. doi: 10.3171/2013.7.Jns122417. PubMed PMID: 23991844.

59. Calabrese C, Poppleton H, Kocak M, Hogg TL, Fuller C, Hamner B, et al. A perivascular niche for brain tumor stem cells. Cancer cell. 2007;11(1):69-82. Epub 2007/01/16. doi: 10.1016/j.ccr.2006.11.020. PubMed PMID: 17222791.

60. Wang J, Sakariassen P, Tsinkalovsky O, Immervoll H, Bøe SO, Svendsen A, et al. CD133 negative glioma cells form tumors in nude rats and give rise to CD133 positive cells. International journal of cancer. 2008;122(4):761-8. Epub 2007/10/24. doi: 10.1002/ijc.23130. PubMed PMID: 17955491.

61. Prestegarden L, Svendsen A, Wang J, Sleire L, Skaftnesmo KO, Bjerkvig R, et al. Glioma cell populations grouped by different cell type markers drive brain tumor growth. Cancer Res. 2010;70(11):4274-9. Epub 2010/05/13. doi: 10.1158/0008-5472.Can-09-3904. PubMed PMID: 20460538.

62. Beier D, Hau P, Proescholdt M, Lohmeier A, Wischhusen J, Oefner PJ, et al. CD133(+) and CD133(-) glioblastoma-derived cancer stem cells show differential growth characteristics and molecular profiles. Cancer Res. 2007;67(9):4010-5. Epub 2007/05/08. doi: 10.1158/0008-5472.Can-06-4180. PubMed PMID: 17483311.

63. Lathia JD, Mack SC, Mulkearns-Hubert EE, Valentim CLL, Rich JN. Cancer stem cells in glioblastoma. Genes & Development. 2015;29(12):1203-17. doi: 10.1101/gad.261982.115. PubMed PMID: PMC4495393.

64. Lesley J, English N, Perschl A, Gregoroff J, Hyman R. Variant cell lines selected for alterations in the function of the hyaluronan receptor CD44 show differences in glycosylation. J Exp Med. 1995 Aug 1;182(2):431-7. doi: 10.1084/jem.182.2.431. PMID: 7543138; PMCID: PMC2192117.

65. Sneath RJ, Mangham DC. The normal structure and function of CD44 and its role in neoplasia. Mol Pathol. 1998 Aug;51(4):191-200. doi: 10.1136/mp.51.4.191. PMID: 9893744; PMCID: PMC395635.

66. Naor D, Nedvetzki S, Golan I, Melnik L, Faitelson Y. CD44 in cancer. Crit Rev Clin Lab Sci. 2002 Nov;39(6):527-79. doi: 10.1080/10408360290795574. PMID: 12484499.

67. Maula S, Huuhtanen RL, Blomqvist CP, Wiklund TA, Laurila P, Ristamäki R. The adhesion molecule CD44v6 is associated with a high risk for local recurrence in adult soft tissue sarcomas. Br J Cancer. 2001 Jan;84(2):244-52. doi: 10.1054/bjoc.2000.1590. PMID: 11161384; PMCID: PMC2363706.

68. Gasbarri A, Martegani MP, Del Prete F, Lucante T, Natali PG, Bartolazzi A. Galectin-3 and CD44v6 isoforms in the preoperative evaluation of thyroid nodules. J Clin Oncol. 1999;17(11):3494-502. Epub 1999/11/05. doi: 10.1200/jco.1999.17.11.3494. PubMed PMID: 10550147.

69. Saegusa M, Machida D, Hashimura M, Okayasu I. CD44 expression in benign, premalignant, and malignant ovarian neoplasms: relation to tumour development and progression. J Pathol. 1999 Nov;189(3):326-37. doi: 10.1002/(SICI)1096-9896(199911)189:3<326::AID-PATH425>3.0.CO;2-6. PMID: 10547593.

70. Pirinen R, Hirvikoski P, Böhm J, Kellokoski J, Moisio K, Virén M, et al. Reduced expression of CD44v3 variant isoform is associated with unfavorable outcome in non-small cell

lung carcinoma. Human pathology. 2000;31(9):1088-95. Epub 2000/10/03. doi: 10.1053/hupa.2000.16277. PubMed PMID: 11014576.

71. Eibl RH, Pietsch T, Moll J, Skroch-Angel P, Heider KH, von Ammon K, Wiestler OD, Ponta H, Kleihues P, Herrlich P. Expression of variant CD44 epitopes in human astrocytic brain tumors. J Neurooncol. 1995 Dec;26(3):165-70. doi: 10.1007/BF01052619. PMID: 8750182.

72. Kaaijk P, Troost D, Morsink F, Keehnen RMJ, Leenstra S, Bosch DA, et al. Expression of CD44 splice variants in human primary brain tumors. Journal of neuro-oncology. 1995;26(3):185-90. doi: 10.1007/BF01052621.

73. Breyer R, Hussein S, Radu DL, Pütz K-M, Gunia S, Hecker H, et al. Disruption of intracerebral progression of rat C6 glioblastoma by in vivo treatment with anti-CD44 monoclonal antibody. Journal of neurosurgery. 2000;92(1):140-9. doi: 10.3171/jns.2000.92.1.0140.

74. Naruse M, Shibasaki K, Yokoyama S, Kurachi M, Ishizaki Y. Dynamic Changes of CD44 Expression from Progenitors to Subpopulations of Astrocytes and Neurons in Developing Cerebellum. PLoS One. 2013;8(1):e53109. doi: 10.1371/journal.pone.0053109.

75. Brown DV, Filiz G, Daniel PM, Hollande F, Dworkin S, Amiridis S, et al. Expression of CD133 and CD44 in glioblastoma stem cells correlates with cell proliferation, phenotype stability and intra-tumor heterogeneity. PLoS One. 2017;12(2):e0172791. doi: 10.1371/journal.pone.0172791.

76. Klein WM, Wu BP, Zhao S, Wu H, Klein-Szanto AJP, Tahan SR. Increased expression of stem cell markers in malignant melanoma. Modern Pathology. 2007;20(1):102-7. doi: 10.1038/modpathol.3800720.

77. Veselska R, Kuglik P, Cejpek P, Svachova H, Neradil J, Loja T, et al. Nestin expression in the cell lines derived from glioblastoma multiforme. BMC Cancer. 2006;6:32. Epub 2006/02/07. doi: 10.1186/1471-2407-6-32. PubMed PMID: 16457706; PubMed Central PMCID: PMCPMC1403792.

78. Jin X, Jin X, Jung JE, Beck S, Kim H. Cell surface Nestin is a biomarker for glioma stem cells. Biochemical and biophysical research communications. 2013;433(4):496-501. Epub 2013/03/26. doi: 10.1016/j.bbrc.2013.03.021. PubMed PMID: 23524267.

79. Tang X, Zuo C, Fang P, Liu G, Qiu Y, Huang Y, et al. Targeting Glioblastoma Stem Cells: A Review on Biomarkers, Signal Pathways and Targeted Therapy. Frontiers in oncology. 2021;11:701291-. doi: 10.3389/fonc.2021.701291. PubMed PMID: 34307170.

80. Matsuda Y, Hagio M, Ishiwata T. Nestin: a novel angiogenesis marker and possible target for tumor angiogenesis. World journal of gastroenterology. 2013;19(1):42-8. Epub 2013/01/18. doi: 10.3748/wjg.v19.i1.42. PubMed PMID: 23326161; PubMed Central PMCID: PMCPMC3545228.

81. Zhang M, Song T, Yang L, Chen R, Wu L, Yang Z, et al. Nestin and CD133: valuable stem cell-specific markers for determining clinical outcome of glioma patients. Journal of Experimental & Clinical Cancer Research. 2008;27(1):85. doi: 10.1186/1756-9966-27-85.

82. Staberg M, Villingshøj M, Stockhausen M, Poulsen H. P01.20: Epigenetic treatment and induction of differentiation in glioblastoma multiforme neurosphere cells leads to downregulation of EGFR, EGFRVIII and Nestin together with reduced colony formation in vitro. Neuro Oncol. 2014 Sep;16(Suppl 2):ii31. doi: 10.1093/neuonc/nou174.113. PMCID: PMC4185454..

83. Schmitz M, Temme A, Senner V, Ebner R, Schwind S, Stevanovic S, et al. Identification of SOX2 as a novel glioma-associated antigen and potential target for T cell-based immunotherapy. Br J Cancer. 2007;96(8):1293-301. Epub 2007/03/22. doi: 10.1038/sj.bjc.6603696. PubMed PMID: 17375044; PubMed Central PMCID: PMCPMC2360145.

84. Garros-Regulez L, Aldaz P, Arrizabalaga O, Moncho-Amor V, Carrasco-Garcia E, Manterola L, et al. mTOR inhibition decreases SOX2-SOX9 mediated glioma stem cell activity and temozolomide resistance. Expert opinion on therapeutic targets. 2016;20(4):393-405. Epub 2016/02/16. doi: 10.1517/14728222.2016.1151002. PubMed PMID: 26878385; PubMed Central PMCID: PMCPMC4898154.

85. Annovazzi L, Mellai M, Caldera V, Valente G, Schiffer D. SOX2 expression and amplification in gliomas and glioma cell lines. Cancer genomics & proteomics. 2011;8(3):139-47. Epub 2011/04/27. PubMed PMID: 21518820.

86. Guo Y, Liu S, Wang P, Zhao S, Wang F, Bing L, Zhang Y, Ling EA, Gao J, Hao A. Expression profile of embryonic stem cell-associated genes Oct4, Sox2 and Nanog in human gliomas. Histopathology. 2011 Oct;59(4):763-75. doi: 10.1111/j.1365-2559.2011.03993.x. PMID: 22014056.

87. Ben-Porath I, Thomson MW, Carey VJ, Ge R, Bell GW, Regev A, et al. An embryonic stem cell-like gene expression signature in poorly differentiated aggressive human tumors. Nature genetics. 2008;40(5):499-507. Epub 2008/04/30. doi: 10.1038/ng.127. PubMed PMID: 18443585; PubMed Central PMCID: PMCPMC2912221.

88. Gangemi RM, Griffero F, Marubbi D, Perera M, Capra MC, Malatesta P, Ravetti GL, Zona GL, Daga A, Corte G. SOX2 silencing in glioblastoma tumor-initiating cells causes stop of proliferation and loss of tumorigenicity. Stem Cells. 2009 Jan;27(1):40-8. doi: 10.1634/stemcells.2008-0493. PMID: 18948646.

89. Hägerstrand D, He X, Bradic Lindh M, Hoefs S, Hesselager G, Ostman A, et al. Identification of a SOX2-dependent subset of tumor- and sphere-forming glioblastoma cells with a distinct tyrosine kinase inhibitor sensitivity profile. Neuro-oncology. 2011;13(11):1178-91. Epub 2011/09/24. doi: 10.1093/neuonc/nor113. PubMed PMID: 21940738; PubMed Central PMCID: PMCPMC3199157.

90. Alonso MM, Diez-Valle R, Manterola L, Rubio A, Liu D, Cortes-Santiago N, et al. Genetic and epigenetic modifications of Sox2 contribute to the invasive phenotype of malignant gliomas. PLoS One. 2011;6(11):e26740. Epub 2011/11/10. doi: 10.1371/journal.pone.0026740. PubMed PMID: 22069467; PubMed Central PMCID: PMCPMC3206066.

91. Oppel F, Müller N, Schackert G, Hendruschk S, Martin D, Geiger KD, et al. SOX2-RNAi attenuates S-phase entry and induces RhoA-dependent switch to protease-independent amoeboid migration in human glioma cells. Mol Cancer. 2011;10:137. Epub 2011/11/11. doi: 10.1186/1476-4598-10-137. PubMed PMID: 22070920; PubMed Central PMCID: PMCPMC3228695.

92. Suvà ML, Rheinbay E, Gillespie SM, Patel AP, Wakimoto H, Rabkin SD, et al. Reconstructing and reprogramming the tumor-propagating potential of glioblastoma stem-like cells. Cell. 2014;157(3):580-94. Epub 2014/04/15. doi: 10.1016/j.cell.2014.02.030. PubMed PMID: 24726434; PubMed Central PMCID: PMCPMC4004670.

93. Ma I, Allan AL. The Role of Human Aldehyde Dehydrogenase in Normal and Cancer Stem Cells. Stem Cell Reviews and Reports. 2011;7(2):292-306. doi: 10.1007/s12015-010-9208-4.

94. Douville J, Beaulieu R, Balicki D. ALDH1 as a functional marker of cancer stem and progenitor cells. Stem cells and development. 2009;18(1):17-25. Epub 2008/06/25. doi: 10.1089/scd.2008.0055. PubMed PMID: 18573038.

95. Rasper M, Schäfer A, Piontek G, Teufel J, Brockhoff G, Ringel F, et al. Aldehyde dehydrogenase 1 positive glioblastoma cells show brain tumor stem cell capacity. Neuro-oncology. 2010;12(10):1024-33. doi: 10.1093/neuonc/noq070.

96. Campos B, Centner FS, Bermejo JL, Ali R, Dorsch K, Wan F, Felsberg J, Ahmadi R, Grabe N, Reifenberger G, Unterberg A, Burhenne J, Herold-Mende C. Aberrant expression of retinoic acid signaling molecules influences patient survival in astrocytic gliomas. Am J Pathol. 2011 May;178(5):1953-64. doi: 10.1016/j.ajpath.2011.01.051. PMID: 21514413; PMCID: PMC3081142.

97. Adam SA, Schnell O, Pöschl J, Eigenbrod S, Kretzschmar HA, Tonn JC, Schüller U. ALDH1A1 is a marker of astrocytic differentiation during brain development and correlates with better survival in glioblastoma patients. Brain Pathol. 2012 Nov;22(6):788-97. doi: 10.1111/j.1750-3639.2012.00592.x. Epub 2012 Apr 19. PMID: 22417385; PMCID: PMC8057636.

98. Schäfer A, Teufel J, Ringel F, Bettstetter M, Hoepner I, Rasper M, et al. Aldehyde dehydrogenase 1A1—a new mediator of resistance to temozolomide in glioblastoma. Neuro-oncology. 2012;14(12):1452-64. doi: 10.1093/neuonc/nos270.

99. Mottamal M, Zheng S, Huang TL, Wang G. Histone Deacetylase Inhibitors in Clinical Studies as Templates for New Anticancer Agents. Molecules (Basel, Switzerland). 2015;20(3):3898-941. doi: 10.3390/molecules20033898. PubMed PMID: PMC4372801.

100. Bezecny P. Histone deacetylase inhibitors in glioblastoma: pre-clinical and clinical experience. Medical Oncology. 2014;31(6):985. doi: 10.1007/s12032-014-0985-5.

101. Mottet D, Pirotte S, Lamour V, Hagedorn M, Javerzat S, Bikfalvi A, et al. HDAC4 represses p21WAF1/Cip1 expression in human cancer cells through a Sp1-dependent, p53-independent mechanism. Oncogene. 2009;28(2):243-56. doi: 10.1038/onc.2008.371.

102. de Ruijter AJ, van Gennip AH, Caron HN, Kemp S, van Kuilenburg AB. Histone deacetylases (HDACs): characterization of the classical HDAC family. The Biochemical journal. 2003;370(Pt 3):737-49. Epub 2002/11/14. doi: 10.1042/bj20021321. PubMed PMID: 12429021; PubMed Central PMCID: PMCPMC1223209.

103. Barneda-Zahonero B, Parra M. Histone deacetylases and cancer. Mol Oncol. 2012;6(6):579-89. Epub 2012/09/12. doi: 10.1016/j.molonc.2012.07.003. PubMed PMID: 22963873; PubMed Central PMCID: PMCPMC5528343.

104. Rajendran R, Garva R, Krstic-Demonacos M, Demonacos C. Sirtuins: molecular traffic lights in the crossroad of oxidative stress, chromatin remodeling, and transcription. Journal of biomedicine & biotechnology. 2011;2011:368276. Epub 2011/09/14. doi: 10.1155/2011/368276. PubMed PMID: 21912480; PubMed Central PMCID: PMCPMC3168296.

105. Chen R, Zhang M, Zhou Y, Guo W, Yi M, Zhang Z, et al. The application of histone deacetylases inhibitors in glioblastoma. J Exp Clin Cancer Res. 2020;39(1):138-. doi: 10.1186/s13046-020-01643-6. PubMed PMID: 32682428.

106. Marks PA, Richon VM, Rifkind RA. Histone deacetylase inhibitors: inducers of differentiation or apoptosis of transformed cells. Journal of the National Cancer Institute. 2000;92(15):1210-6. Epub 2000/08/03. PubMed PMID: 10922406.

107. Duvic M, Vu J. Vorinostat: a new oral histone deacetylase inhibitor approved for cutaneous T-cell lymphoma. Expert Opinion on Investigational Drugs. 2007;16(7):1111-20. doi: 10.1517/13543784.16.7.1111.

108. Bajbouj K, Mawrin C, Hartig R, Schulze-Luehrmann J, Wilisch-Neumann A, Roessner A, et al. P53-dependent antiproliferative and pro-apoptotic effects of trichostatin A (TSA) in glioblastoma cells. Journal of neuro-oncology. 2012;107(3):503-16. Epub 2012/01/25. doi: 10.1007/s11060-011-0791-2. PubMed PMID: 22270849.

109. Sawa H, Murakami H, Ohshima Y, Sugino T, Nakajyo T, Kisanuki T, et al. Histone deacetylase inhibitors such as sodium butyrate and trichostatin A induce apoptosis through an increase of the bcl-2-related protein Bad. Brain Tumor Pathol. 2001;18(2):109-14. doi: 10.1007/bf02479423. PubMed PMID: 11908866.

110. Pastorino O, Gentile MT, Mancini A, Del Gaudio N, Di Costanzo A, Bajetto A, et al. Histone Deacetylase Inhibitors Impair Vasculogenic Mimicry from Glioblastoma Cells. Cancers. 2019;11(6). Epub 2019/05/31. doi: 10.3390/cancers11060747. PubMed PMID: 31146471; PubMed Central PMCID: PMCPMC6627137.

111. Sawa H, Murakami H, Ohshima Y, Murakami M, Yamazaki I, Tamura Y, et al. Histone deacetylase inhibitors such as sodium butyrate and trichostatin A inhibit vascular endothelial growth factor (VEGF) secretion from human glioblastoma cells. Brain Tumor Pathol. 2002;19(2):77-81. Epub 2003/03/08. doi: 10.1007/bf02478931. PubMed PMID: 12622137.

112. Marks PA. Thioredoxin in cancer--role of histone deacetylase inhibitors. Seminars in cancer biology. 2006;16(6):436-43. Epub 2006/09/26. doi: 10.1016/j.semcancer.2006.09.005. PubMed PMID: 17095247.

113. Dvorakova M, Vanek T. Histone deacetylase inhibitors for the treatment of cancer stem cells. MedChemComm. 2016;7(12):2217-31. doi: 10.1039/C6MD00297H.

114. Chiao MT, Cheng WY, Yang YC, Shen CC, Ko JL. Suberoylanilide hydroxamic acid (SAHA) causes tumor growth slowdown and triggers autophagy in glioblastoma stem cells. Autophagy. 2013;9(10):1509-26. Epub 20130815. doi: 10.4161/auto.25664. PubMed PMID: 23962875.

115. Alvarez AA, Field M, Bushnev S, Longo MS, Sugaya K. The effects of histone deacetylase inhibitors on glioblastoma-derived stem cells. J Mol Neurosci. 2015;55(1):7-20. Epub 20140530. doi: 10.1007/s12031-014-0329-0. PubMed PMID: 24874578.

116. Suraweera A, O'Byrne KJ, Richard DJ. Combination Therapy With Histone Deacetylase Inhibitors (HDACi) for the Treatment of Cancer: Achieving the Full Therapeutic Potential of HDACi. Frontiers in oncology. 2018;8:92. Epub 2018/04/14. doi: 10.3389/fonc.2018.00092. PubMed PMID: 29651407; PubMed Central PMCID: PMCPMC5884928.

117. Polivka J Jr, Polivka J, Holubec L, Kubikova T, Priban V, Hes O, Pivovarcikova K, Treskova I. Advances in Experimental Targeted Therapy and Immunotherapy for Patients with

Glioblastoma Multiforme. Anticancer Res. 2017 Jan;37(1):21-33. doi: 10.21873/anticanres.11285. PMID: 28011470.

118. Eyupoglu IY, Hahnen E, Trankle C, Savaskan NE, Siebzehnrubl FA, Buslei R, et al. Experimental therapy of malignant gliomas using the inhibitor of histone deacetylase MS-275. Mol Cancer Ther. 2006;5(5):1248-55. Epub 2006/05/30. doi: 10.1158/1535-7163.mct-05-0533. PubMed PMID: 16731757.

119. Simonini MV, Camargo LM, Dong E, Maloku E, Veldic M, Costa E, et al. The benzamide MS-275 is a potent, long-lasting brain region-selective inhibitor of histone deacetylases. Proc Natl Acad Sci U S A. 2006;103(5):1587-92. Epub 2006/01/25. doi: 10.1073/pnas.0510341103. PubMed PMID: 16432198; PubMed Central PMCID: PMCPMC1360572.

120. Sun P, Xia S, Lal B, Eberhart CG, Quinones-Hinojosa A, Maciaczyk J, et al. DNER, an epigenetically modulated gene, regulates glioblastoma-derived neurosphere cell differentiation and tumor propagation. Stem Cells. 2009;27(7):1473-86. doi: 10.1002/stem.89. PubMed PMID: 19544453.

121. Pili R, Salumbides B, Zhao M, Altiok S, Qian D, Zwiebel J, et al. Phase I study of the histone deacetylase inhibitor entinostat in combination with 13-cis retinoic acid in patients with solid tumours. British journal of cancer. 2012;106(1):77-84. Epub 2011/12/01. doi: 10.1038/bjc.2011.527. PubMed PMID: 22134508.

122. Camphausen K, Burgan W, Cerra M, Oswald KA, Trepel JB, Lee M-J, et al. Enhanced Radiation-Induced Cell Killing and Prolongation of γH2AX Foci Expression by the Histone Deacetylase Inhibitor MS-275. Cancer Research. 2004;64(1):316.

123. Bangert A, Häcker S, Cristofanon S, Debatin K-M, Fulda S. Chemosensitization of glioblastoma cells by the histone deacetylase inhibitor MS275. Anti-cancer drugs. 2011;22(6).

124. Liffers K, Kolbe K, Westphal M, Lamszus K, Schulte A. Histone Deacetylase Inhibitors Resensitize EGFR/EGFRvIII-Overexpressing, Erlotinib-Resistant Glioblastoma Cells to Tyrosine Kinase Inhibition. Targeted Oncology. 2016;11(1):29-40. doi: 10.1007/s11523-015-0372-y.

125. Fremin C, Meloche S. From basic research to clinical development of MEK1/2 inhibitors for cancer therapy. J Hematol Oncol. 2010;3:8. Epub 2010/02/13. doi: 10.1186/1756-8722-3-8. PubMed PMID: 20149254; PubMed Central PMCID: PMCPMC2830959.

126. Pearson JRD, Regad T. Targeting cellular pathways in glioblastoma multiforme. Signal Transduction and Targeted Therapy. 2017;2(1):17040. doi: 10.1038/sigtrans.2017.40.

127. da Rocha AB, Mans DR, Regner A, Schwartsmann G. Targeting protein kinase C: new therapeutic opportunities against high-grade malignant gliomas? The oncologist. 2002;7(1):17-33. Epub 2002/02/21. doi: 10.1634/theoncologist.7-1-17. PubMed PMID: 11854544.

128. Pelloski CE, Lin E, Zhang L, Yung WK, Colman H, Liu JL, et al. Prognostic associations of activated mitogen-activated protein kinase and Akt pathways in glioblastoma. Clin Cancer Res. 2006;12(13):3935-41. Epub 2006/07/05. doi: 10.1158/1078-0432.Ccr-05-2202. PubMed PMID: 16818690.

129. Gao CF, Xie Q, Su YL, Koeman J, Khoo SK, Gustafson M, et al. Proliferation and invasion: plasticity in tumor cells. Proc Natl Acad Sci U S A. 2005;102(30):10528-33. Epub 2005/07/19. doi: 10.1073/pnas.0504367102. PubMed PMID: 16024725; PubMed Central PMCID: PMCPMC1180792.

130. Bayin NS, Modrek AS, Placantonakis DG. Glioblastoma stem cells: Molecular characteristics and therapeutic implications. World journal of stem cells. 2014;6(2):230-8. Epub 2014/04/29. doi: 10.4252/wjsc.v6.i2.230. PubMed PMID: 24772249; PubMed Central PMCID: PMCPMC3999780.

131. Cheng Y, Tian H. Current Development Status of MEK Inhibitors. Molecules. 2017;22(10). Epub 2017/09/29. doi: 10.3390/molecules22101551. PubMed PMID: 28954413; PubMed Central PMCID: PMCPMC6151813.

132. Adjei AA, LoRusso P, Ribas A, Sosman JA, Pavlick A, Dy GK, et al. A phase I dose-escalation study of TAK-733, an investigational oral MEK inhibitor, in patients with advanced solid tumors. Investigational new drugs. 2017;35(1):47-58. Epub 2016/09/21. doi: 10.1007/s10637-016-0391-2. PubMed PMID: 27650277.

133. Anastasov N, Hirmer E, Klenner M, Ott J, Falkenberg N, Bao X, et al. MEK1 Inhibitor Combined with Irradiation Reduces Migration of Breast Cancer Cells Including miR-221 and ZEB1 EMT Marker Expression. Cancers. 2020;12(12). doi: 10.3390/cancers12123760.

134. Dong Q, Dougan DR, Gong X, Halkowycz P, Jin B, Kanouni T, O'Connell SM, Scorah N, Shi L, Wallace MB, Zhou F. Discovery of TAK-733, a potent and selective MEK allosteric site inhibitor for the treatment of cancer. Bioorg Med Chem Lett. 2011 Mar 1;21(5):1315-9. doi: 10.1016/j.bmcl.2011.01.071. Epub 2011 Jan 22. PMID: 21310613.

135. de la Puente P, Muz B, Jin A, Azab F, Luderer M, Salama NN, et al. MEK inhibitor, TAK-733 reduces proliferation, affects cell cycle and apoptosis, and synergizes with other targeted therapies in multiple myeloma. Blood Cancer Journal. 2016;6(2):e399-e. doi: 10.1038/bcj.2016.7.

136. Micel LN, Tentler JJ, Tan A-C, Selby HM, Brunkow KL, Robertson KM, et al. Antitumor Activity of the MEK Inhibitor TAK-733 against Melanoma Cell Lines and Patient-Derived Tumor Explants. Molecular Cancer Therapeutics. 2015;14(2):317-25. doi: 10.1158/1535-7163.Mct-13-1012.

137. Menzies AM, Long GV. Dabrafenib and trametinib, alone and in combination for BRAF-mutant metastatic melanoma. Clin Cancer Res. 2014;20(8):2035-43. Epub 2014/03/04. doi: 10.1158/1078-0432.Ccr-13-2054. PubMed PMID: 24583796.

138. Long GV, Stroyakovskiy D, Gogas H, Levchenko E, de Braud F, Larkin J, Garbe C, Jouary T, Hauschild A, Grob JJ, Chiarion-Sileni V, Lebbe C, Mandalà M, Millward M, Arance A, Bondarenko I, Haanen JB, Hansson J, Utikal J, Ferraresi V, Kovalenko N, Mohr P, Probachai V, Schadendorf D, Nathan P, Robert C, Ribas A, DeMarini DJ, Irani JG, Swann S, Legos JJ, Jin F, Mookerjee B, Flaherty K. Dabrafenib and trametinib versus dabrafenib and placebo for Val600 BRAF-mutant melanoma: a multicentre, double-blind, phase 3 randomised controlled trial. Lancet. 2015 Aug 1;386(9992):444-51. doi: 10.1016/S0140-6736(15)60898-4. Epub 2015 May 31. PMID: 26037941.

139. Planchard D, Besse B, Groen HJM, Hashemi SMS, Mazieres J, Kim TM, et al. Phase 2 Study of Dabrafenib Plus Trametinib in Patients With BRAF V600E-Mutant Metastatic NSCLC: Updated 5-Year Survival Rates and Genomic Analysis. J Thorac Oncol. 2022;17(1):103-15. Epub 20210826. doi: 10.1016/j.jtho.2021.08.011. PubMed PMID: 34455067.

140. Perreault S, Larouche V, Tabori U, Hawkin C, Lippé S, Ellezam B, et al. A phase 2 study of trametinib for patients with pediatric glioma or plexiform neurofibroma with refractory tumor and activation of the MAPK/ERK pathway: TRAM-01. BMC Cancer. 2019;19(1):1250.

Epub 2019/12/29. doi: 10.1186/s12885-019-6442-2. PubMed PMID: 31881853; PubMed Central PMCID: PMCPMC6935133.

141. Manoharan N, Choi J, Chordas C, Zimmerman MA, Scully J, Clymer J, et al. Trametinib for the treatment of recurrent/progressive pediatric low-grade glioma. Journal of neuro-oncology. 2020;149(2):253-62. Epub 2020/08/12. doi: 10.1007/s11060-020-03592-8. PubMed PMID: 32780261.

142. Paul MR, Pehlivan KC, Milburn M, Yeh-Nayre L, Elster J, Crawford JR. Trametinib-based Treatment of Pediatric CNS Tumors: A Single Institutional Experience. Journal of pediatric hematology/oncology. 2020;42(8):e730-e7. Epub 2020/05/14. doi: 10.1097/mph.0000000000001819. PubMed PMID: 32398601.

143. Ozaki K, Minoda A, Kishikawa F, Kohno M. Blockade of the ERK pathway markedly sensitizes tumor cells to HDAC inhibitor-induced cell death. Biochem Biophys Res Commun. 2006 Jan 27;339(4):1171-7. doi: 10.1016/j.bbrc.2005.11.131. Epub 2005 Dec 5. PMID: 16338224.

144. Chao M-W, Chang L-H, Tu H-J, Chang C-D, Lai M-J, Chen Y-Y, et al. Combination treatment strategy for pancreatic cancer involving the novel HDAC inhibitor MPT0E028 with a MEK inhibitor beyond K-Ras status. Clinical Epigenetics. 2019;11(1):85. doi: 10.1186/s13148-019-0681-6.

145. Corno C, Arrighetti N, Ciusani E, Corna E, Carenini N, Zaffaroni N, et al. Synergistic Interaction of Histone Deacetylase 6- and MEK-Inhibitors in Castration-Resistant Prostate Cancer Cells. Frontiers in Cell and Developmental Biology. 2020;8(610). doi: 10.3389/fcell.2020.00610.

146. Toshiaki Sakamoto, Kei-ichi Ozaki, Kohsuke Fujio, Shu-hei Kajikawa, Shin-ichi Uesato, Kazushi Watanabe, Susumu Tanimura, Takehiko Koji, and Michiaki Kohno. "Blockade of the ERK pathway enhances the therapeutic efficacy of the histone deacetylase inhibitor MS-275 in human tumor xenograft models" *Biochemical and Biophysical Research Communications* 433, (2013): 456-462. doi: 10.1016/j.bbrc.2013.03.009.

147. Ngamphaiboon N, Dy G, Ma WW, Zhao Y, Reungwetwattana T, DePaolo D, et al. A phase I study of the histone deacetylase (HDAC) inhibitor entinostat, in combination with sorafenib in patients with advanced solid tumors. Investigational new drugs. 2014;33. doi: 10.1007/s10637-014-0174-6.

148. da Cunha Jaeger M, Ghisleni EC, Cardoso PS, Siniglaglia M, Falcon T, Brunetto AT, et al. HDAC and MAPK/ERK Inhibitors Cooperate To Reduce Viability and Stemness in Medulloblastoma. Journal of Molecular Neuroscience. 2020;70(6):981-92. doi: 10.1007/s12031-020-01505-y.

149. Giard DJ, Aaronson SA, Todaro GJ, Arnstein P, Kersey JH, Dosik H, et al. In vitro cultivation of human tumors: establishment of cell lines derived from a series of solid tumors. Journal of the National Cancer Institute. 1973;51(5):1417-23. Epub 1973/11/01. doi: 10.1093/jnci/51.5.1417. PubMed PMID: 4357758.

150. Tate JG, Bamford S, Jubb HC, Sondka Z, Beare DM, Bindal N, et al. COSMIC: the Catalogue Of Somatic Mutations In Cancer. Nucleic Acids Research. 2018;47(D1):D941-D7. doi: 10.1093/nar/gky1015.

151. Ishii N, Maier D, Merlo A, Tada M, Sawamura Y, Diserens AC, et al. Frequent co-alterations of TP53, p16/CDKN2A, p14ARF, PTEN tumor suppressor genes in human glioma

cell lines. Brain Pathology (Zurich, Switzerland). 1999;9(3):469-79. Epub 1999/07/23. doi: 10.1111/j.1750-3639.1999.tb00536.x. PubMed PMID: 10416987.

152. Bigner DD, Bigner SH, Pontén J, Westermark B, Mahaley MS, Ruoslahti E, et al. Heterogeneity of Genotypic and phenotypic characteristics of fifteen permanent cell lines derived from human gliomas. Journal of Neuropathology and Experimental Neurology. 1981;40(3):201-29. Epub 1981/05/01. doi: 10.1097/00005072-198105000-00001. PubMed PMID: 6260907.

153. Pontén J, Macintyre EH. Long term culture of normal and neoplastic human glia. Acta Pathol Microbiol Scand. 1968;74(4):465-86. doi: 10.1111/j.1699-0463.1968.tb03502.x. PMID: 4313504.154. Tang Z, Li C, Kang B, Gao G, Li C, Zhang Z. GEPIA: a web server for cancer and normal gene expression profiling and interactive analyses. Nucleic Acids Res. 2017;45(W1):W98-w102. Epub 2017/04/14. doi: 10.1093/nar/gkx247. PubMed PMID: 28407145; PubMed Central PMCID: PMCPMC5570223.

155. Reynolds BA, Weiss S. Generation of neurons and astrocytes from isolated cells of the adult mammalian central nervous system. Science. 1992;255(5052):1707. doi: 10.1126/science.1553558.

156. Nicolis SK. Cancer stem cells and "stemness" genes in neuro-oncology. Neurobiol Dis. 2007 Feb;25(2):217-29. doi: 10.1016/j.nbd.2006.08.022. Epub 2006 Dec 1. PMID: 17141509.

157. Pastrana E, Silva-Vargas V, Doetsch F. Eyes wide open: a critical review of sphere-formation as an assay for stem cells. Cell Stem Cell. 2011;8(5):486-98. doi: 10.1016/j.stem.2011.04.007. PubMed PMID: 21549325.

158. McKinnon KM. Flow Cytometry: An Overview. Curr Protoc Immunol. 2018;120:5.1.-5.1.11. doi: 10.1002/cpim.40. PubMed PMID: 29512141.

159. Maecker HT, Trotter J. Flow cytometry controls, instrument setup, and the determination of positivity. Cytometry Part A : the journal of the International Society for Analytical Cytology. 2006;69(9):1037-42. Epub 2006/08/05. doi: 10.1002/cyto.a.20333. PubMed PMID: 16888771.

160. Livak KJ, Schmittgen TD. Analysis of relative gene expression data using real-time quantitative PCR and the 2(-Delta Delta C(T)) Method. Methods (San Diego, Calif). 2001;25(4):402-8. Epub 2002/02/16. doi: 10.1006/meth.2001.1262. PubMed PMID: 11846609.

161. Yang W, Soares J, Greninger P, Edelman EJ, Lightfoot H, Forbes S, Bindal N, Beare D, Smith JA, Thompson IR, Ramaswamy S, Futreal PA, Haber DA, Stratton MR, Benes C, McDermott U, Garnett MJ. Genomics of Drug Sensitivity in Cancer (GDSC): a resource for therapeutic biomarker discovery in cancer cells. Nucleic Acids Res. 2013 Jan;41(Database issue):D955-61. doi: 10.1093/nar/gks1111. Epub 2012 Nov 23. PMID: 23180760; PMCID: PMC3531057.

162. Galli R, Binda E, Orfanelli U, Cipelletti B, Gritti A, De Vitis S, et al. Isolation and Characterization of Tumorigenic, Stem-like Neural Precursors from Human Glioblastoma. Cancer Research. 2004;64(19):7011. doi: 10.1158/0008-5472.CAN-04-1364.

163. Yuan X, Curtin J, Xiong Y, Liu G, Waschsmann-Hogiu S, Farkas DL, et al. Isolation of cancer stem cells from adult glioblastoma multiforme. Oncogene. 2004;23(58):9392-400. Epub 2004/11/24. doi: 10.1038/sj.onc.1208311. PubMed PMID: 15558011.

164. Fukaya R, Ohta S, Yamaguchi M, Fujii H, Kawakami Y, Kawase T, et al. Isolation of cancer stem-like cells from a side population of a human glioblastoma cell line, SK-MG-1. Cancer letters. 2010;291(2):150-7. Epub 2009/11/17. doi: 10.1016/j.canlet.2009.10.010. PubMed PMID: 19913993.

165. Hegi ME, Diserens AC, Gorlia T, Hamou MF, de Tribolet N, Weller M, et al. MGMT gene silencing and benefit from temozolomide in glioblastoma. The New England Journal of Medicine. 2005;352(10):997-1003. Epub 2005/03/11. doi: 10.1056/NEJMoa043331. PubMed PMID: 15758010.

166. Reddy RG, Bhat UA, Chakravarty S, Kumar A. Advances in histone deacetylase inhibitors in targeting glioblastoma stem cells. Cancer Chemother Pharmacol. 2020 Aug;86(2):165-179. doi: 10.1007/s00280-020-04109-w. Epub 2020 Jul 7. PMID: 32638092.

167. Nishioka C, Ikezoe T, Yang J, Koeffler HP, Yokoyama A. Inhibition of MEK/ERK signaling synergistically potentiates histone deacetylase inhibitor-induced growth arrest, apoptosis and acetylation of histone H3 on p21waf1 promoter in acute myelogenous leukemia cell. Leukemia. 2008;22(7):1449-52. doi: 10.1038/sj.leu.2405079.

168. Torres-Adorno AM, Lee J, Kogawa T, Ordentlich P, Tripathy D, Lim B, et al. Histone Deacetylase Inhibitor Enhances the Efficacy of MEK Inhibitor through NOXA-Mediated MCL1 Degradation in Triple-Negative and Inflammatory Breast Cancer. Clinical Cancer Research. 2017;23(16):4780. doi: 10.1158/1078-0432.CCR-16-2622.

169. Zhang M, Song T, Yang L, Chen R, Wu L, Yang Z, et al. Nestin and CD133: valuable stem cell-specific markers for determining clinical outcome of glioma patients. J Exp Clin Cancer Res. 2008;27(1):85. Epub 2008/12/26. doi: 10.1186/1756-9966-27-85. PubMed PMID: 19108713; PubMed Central PMCID: PMCPMC2633002.

170. Bao S, Wu Q, McLendon RE, Hao Y, Shi Q, Hjelmeland AB, et al. Glioma stem cells promote radioresistance by preferential activation of the DNA damage response. Nature. 2006;444(7120):756-60. doi: 10.1038/nature05236.

171. Liu J, Liu Y, Xie T, Luo L, Xu C, Gao Q, et al. Radiation-induced G2/M arrest rarely occurred in glioblastoma stem-like cells. International Journal of Radiation Biology. 2018;94(4):394-402. doi: 10.1080/09553002.2018.1440094.

172. Gao X-Y, Zang J, Zheng M-H, Zhang Y-F, Yue K-Y, Cao X-L, et al. Temozolomide Treatment Induces HMGB1 to Promote the Formation of Glioma Stem Cells via the TLR2/NEAT1/Wnt Pathway in Glioblastoma. Frontiers in Cell and Developmental Biology. 2021;9(76). doi: 10.3389/fcell.2021.620883.

173. Bergmann N, Delbridge C, Gempt J, Feuchtinger A, Walch A, Schirmer L, et al. The Intratumoral Heterogeneity Reflects the Intertumoral Subtypes of Glioblastoma Multiforme: A Regional Immunohistochemistry Analysis. Frontiers in oncology. 2020;10:494-. doi: 10.3389/fonc.2020.00494. PubMed PMID: 32391260.

174. Cerami E, Gao J, Dogrusoz U, Gross BE, Sumer SO, Aksoy BA, et al. The cBio cancer genomics portal: an open platform for exploring multidimensional cancer genomics data. Cancer discovery. 2012;2(5):401-4. Epub 2012/05/17. doi: 10.1158/2159-8290.Cd-12-0095. PubMed PMID: 22588877; PubMed Central PMCID: PMCPMC3956037.

175. Gao J, Aksoy BA, Dogrusoz U, Dresdner G, Gross B, Sumer SO, et al. Integrative analysis of complex cancer genomics and clinical profiles using the cBioPortal. Science signaling. 2013;6(269):pl1. Epub 2013/04/04. doi: 10.1126/scisignal.2004088. PubMed PMID: 23550210; PubMed Central PMCID: PMCPMC4160307.

176. Lee J, Kotliarova S, Kotliarov Y, Li A, Su Q, Donin NM, Pastorino S, Purow BW, Christopher N, Zhang W, Park JK, Fine HA. Tumor stem cells derived from glioblastomas cultured in bFGF and EGF more closely mirror the phenotype and genotype of primary tumors than do serum-cultured cell lines. Cancer Cell. 2006 May;9(5):391-403. doi: 10.1016/j.ccr.2006.03.030. PMID: 16697959.

177. Gómez-Oliva R, Domínguez-García S, Carrascal L, Abalos-Martínez J, Pardillo-Díaz R, Verástegui C, et al. Evolution of Experimental Models in the Study of Glioblastoma: Toward Finding Efficient Treatments. Frontiers in Oncology. 2021;10(3245). doi: 10.3389/fonc.2020.614295.

178. Zhang S, Xie R, Wan F, Ye F, Guo D, Lei T. Identification of U251 glioma stem cells and their heterogeneous stem-like phenotypes. Oncol Lett. 2013;6(6):1649-55. doi: 10.3892/ol.2013.1623.

179. Liu J, Gao Q, Xie T, Liu Y, Luo L, Xu C, et al. Synergistic effect of TRAIL and irradiation in elimination of glioblastoma stem-like cells. Clinical and Experimental Medicine. 2018;18(3):399-411. doi: 10.1007/s10238-018-0504-7.

180. Arnold A, Yuan M, Price A, Harris L, Eberhart CG, Raabe EH. Synergistic activity of mTORC1/2 kinase and MEK inhibitors suppresses pediatric low-grade glioma tumorigenicity and vascularity. Neuro-oncology. 2020;22(4):563-74. Epub 2019/12/17. doi: 10.1093/neuonc/noz230. PubMed PMID: 31841591; PubMed Central PMCID: PMCPMC7158655.

181. Selvasaravanan KD, Wiederspohn N, Hadzalic A, Strobel H, Payer C, Schuster A, et al. The limitations of targeting MEK signalling in Glioblastoma therapy. Sci Rep. 2020;10(1):7401-. doi: 10.1038/s41598-020-64289-6. PubMed PMID: 32366879.

182. Kanabur P, Guo S, Simonds GR, Kelly DF, Gourdie RG, Verbridge SS, et al. Patient-derived glioblastoma stem cells respond differentially to targeted therapies. Oncotarget. 2016;7(52):86406-19. doi: 10.18632/oncotarget.13415. PubMed PMID: 27863440.

183. Bayat Mokhtari R, Homayouni TS, Baluch N, Morgatskaya E, Kumar S, Das B, et al. Combination therapy in combating cancer. Oncotarget. 2017;8(23):38022-43. Epub 2017/04/15. doi: 10.18632/oncotarget.16723. PubMed PMID: 28410237; PubMed Central PMCID: PMCPMC5514969.

184. Chamberlain MC. Temozolomide: therapeutic limitations in the treatment of adult high-grade gliomas. Expert Review of Neurotherapeutics. 2010;10(10):1537-44. doi: 10.1586/ern.10.32.

185. Wallenborn M, Xu L-X, Kirsten H, Rohani L, Rudolf D, Ahnert P, et al. Molecular analyses of glioblastoma stem-like cells and glioblastoma tissue. PLoS One. 2020;15(7):e0234986. doi: 10.1371/journal.pone.0234986.

186. Lee G, Auffinger B, Guo D, Hasan T, Deheeger M, Tobias AL, et al. Dedifferentiation of Glioma Cells to Glioma Stem-like Cells By Therapeutic Stress-induced HIF Signaling in the Recurrent GBM Model. Molecular Cancer Therapeutics. 2016;15(12):3064. doi: 10.1158/1535-7163.MCT-15-0675.

187. Yamada R, Nakano I. Glioma stem cells: their role in chemoresistance. World neurosurgery. 2012;77(2):237-40. Epub 2012/04/17. doi: 10.1016/j.wneu.2012.01.004. PubMed PMID: 22501017.

188. Hombach-Klonisch S, Mehrpour M, Shojaei S, Harlos C, Pitz M, Hamai A, et al. Glioblastoma and chemoresistance to alkylating agents: Involvement of apoptosis, autophagy, and unfolded protein response. Pharmacology & Therapeutics. 2018;184:13-41. Epub 2017/10/31. doi: 10.1016/j.pharmthera.2017.10.017. PubMed PMID: 29080702.

189. Brown DV, Filiz G, Daniel PM, Hollande F, Dworkin S, Amiridis S, et al. Expression of CD133 and CD44 in glioblastoma stem cells correlates with cell proliferation, phenotype stability and intra-tumor heterogeneity. PLoS One. 2017;12(2):e0172791-e. doi: 10.1371/journal.pone.0172791. PubMed PMID: 28241049.

190. Wick W, Weller M, van den Bent M, Sanson M, Weiler M, von Deimling A, Plass C, Hegi M, Platten M, Reifenberger G. MGMT testing--the challenges for biomarker-based glioma treatment. Nat Rev Neurol. 2014 Jul;10(7):372-85. doi: 10.1038/nrneurol.2014.100. Epub 2014 Jun 10. PMID: 24912512.

191. Perazzoli G, Prados J, Ortiz R, Caba O, Cabeza L, Berdasco M, et al. Temozolomide Resistance in Glioblastoma Cell Lines: Implication of MGMT, MMR, P-Glycoprotein and CD133 Expression. PLoS One. 2015;10(10):e0140131. Epub 20151008. doi: 10.1371/journal.pone.0140131. PubMed PMID: 26447477; PubMed Central PMCID: PMCPMC4598115.

192. Qiu ZK, Shen D, Chen YS, Yang QY, Guo CC, Feng BH, et al. Enhanced MGMT expression contributes to temozolomide resistance in glioma stem-like cells. Chin J Cancer. 2014;33(2):115-22. Epub 20130806. doi: 10.5732/cjc.012.10236. PubMed PMID: 23958055; PubMed Central PMCID: PMCPMC3935013.

193. Zhang G, Park MA, Mitchell C, Hamed H, Rahmani M, Martin AP, et al. Vorinostat and Sorafenib Synergistically Kill Tumor Cells via FLIP Suppression and CD95 Activation. Clinical Cancer Research. 2008;14(17):5385. doi: 10.1158/1078-0432.CCR-08-0469.

194. Carson R, Celtikci B, Fenning C, Javadi A, Crawford N, Carbonell LP, et al. HDAC Inhibition Overcomes Acute Resistance to MEK Inhibition in BRAF-Mutant Colorectal Cancer by Downregulation of c-FLIPL. Clinical cancer research : An official journal of the American Association for Cancer Research. 2015;21(14):3230-40. Epub 20150326. doi: 10.1158/1078-0432.Ccr-14-2701. PubMed PMID: 25813020; PubMed Central PMCID: PMCPMC4504978.

195. Yamada T, Amann JM, Tanimoto A, Taniguchi H, Shukuya T, Timmers C, et al. Histone Deacetylase Inhibition Enhances the Antitumor Activity of a MEK Inhibitor in Lung Cancer Cells Harboring RAS Mutations. Mol Cancer Ther. 2018;17(1):17-25. Epub 2017/10/29. doi: 10.1158/1535-7163.Mct-17-0146. PubMed PMID: 29079711.

196. Chen G, Gharib TG, Huang CC, Taylor JM, Misek DE, Kardia SL, et al. Discordant protein and mRNA expression in lung adenocarcinomas. Mol Cell Proteomics. 2002;1(4):304-13. doi: 10.1074/mcp.m200008-mcp200. PubMed PMID: 12096112.

197. Greenbaum D, Colangelo C, Williams K, Gerstein M. Greenbaum D, Colangelo C, Williams K, Gerstein M. Comparing protein abundance and mRNA expression levels on a genomic scale. Genome Biol 4: 117. Genome biology. 2003;4:117. doi: 10.1186/gb-2003-4-9-117.

198. de Sousa Abreu R, Penalva LO, Marcotte EM, Vogel C. Global signatures of protein and mRNA expression levels. Mol Biosyst. 2009;5(12):1512-26. Epub 2009/10/01. doi: 10.1039/b908315d. PubMed PMID: 20023718.

199. Moertl S, Mutschelknaus L, Heider T, Atkinson MJ. MicroRNAs as novel elements in personalized radiotherapy. Translational Cancer Research. 2016:S1262-S9.

200. Maier T, Güell M, Serrano L. Correlation of mRNA and protein in complex biological samples. FEBS Lett. 2009 Dec 17;583(24):3966-73. doi: 10.1016/j.febslet.2009.10.036. PMID: 19850042.

201. Anderson L, Seilhamer J. A comparison of selected mRNA and protein abundances in human liver. Electrophoresis. 1997 Mar-Apr;18(3-4):533-7. doi: 10.1002/elps.1150180333. PMID: 9150937.

202. Gygi SP, Rochon Y, Franza BR, Aebersold R. Correlation between protein and mRNA abundance in yeast. Molecular and cellular biology. 1999;19(3):1720-30.

203. Lichtinghagen R, Musholt PB, Lein M, et al. Different mRNA and protein expression of matrix metalloproteinases 2 and 9 and tissue inhibitor of metalloproteinases 1 in benign and malignant prostate tissue. European Urology. 2002 Oct;42(4):398-406. DOI: 10.1016/s0302-2838(02)00324-x. PMID: 12361907.

204. Ørntoft TF, Thykjaer T, Waldman FM, Wolf H, Celis JE. Genome-wide study of gene copy numbers, transcripts, and protein levels in pairs of non-invasive and invasive human transitional cell carcinomas. Molecular & cellular proteomics : MCP. 2002;1(1):37-45. Epub 2002/07/04. doi: 10.1074/mcp.m100019-mcp200. PubMed PMID: 12096139.

APPENDICES

Appendix A: Representative western Blots after 24 and 48 h of 4 Gy radiation in monolayer glioblastoma cell lines.

After 24 hours of 4 Gy radiation exposure, the expression of Nestin was lost in A172 cells and remained so after 48 hours of irradiation. In LN229 cells, Nestin expression was reduced after 24 hours of irradiation but became increased in LN229 after 48 hours of irradiation compared to their 0 Gy controls. The Nestin expression in U87 cells was increased at both 24 and 48 hours after irradiation while in U251 cells, Nestin could only be detected after 48 hours of irradiation indicating an increase in expression.

The expression of CD44 was reduced after 24 and 48 hours of 4 Gy irradiation in all the cell lines compared to the 0 Gy control.

SOX2 expression after 24 and 48 hours of irradiation was reduced in the U251 cells and remained undetected in the other cell lines.

ALDH1A1 expression was reduced in all cell lines at both 24 and 48 hours after 4 Gy irradiation.

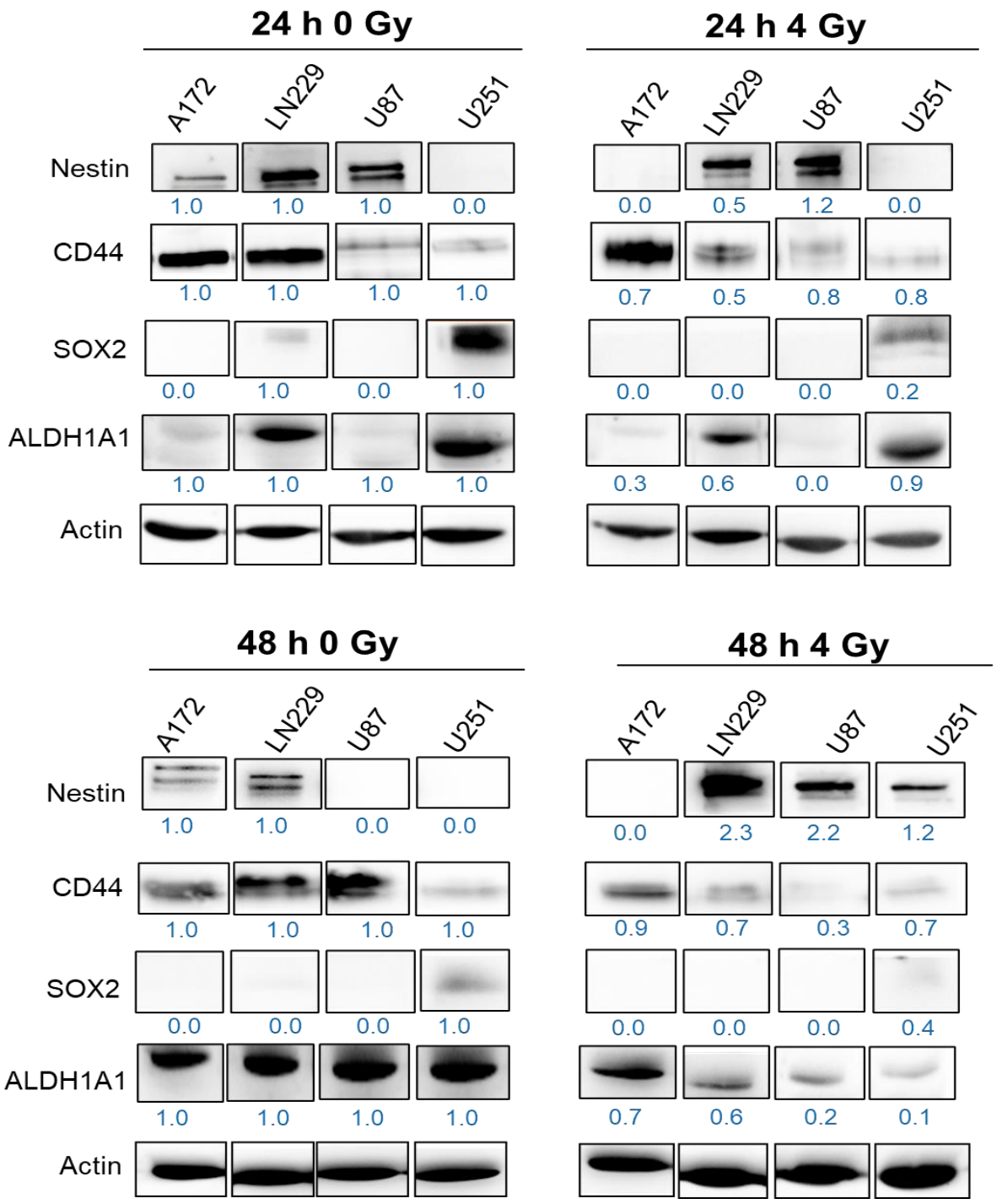

Figure A1: Representative blots of GSLC marker proteins after radiation. Representative blots of Nestin (250 kDa), CD44 (80 kDa), SOX2 (35 kDa) and ALDH1A1 (55 kDa) in A172, LN229, U87 and U251 cell lines at 24 (up) and 48 (down) hours after radiation. The fold change values below each blot were calculated by normalization to the respective 0 Gy sample. Proteins not detected were indicated as 0.0. Actin (42 kDa) was used as the endogenous control.

Appendix B: Analysis of GSLC marker genes in monolayer glioblastoma cell lines after HDACi and MEKi with radiation by RT^2 Profiler arrays

RT^2 Profiler PCR array was performed (as described in 3.9.3) to analyse the gene expression of 11 GSLCs markers after the treatment with HDACi or MEKi as single or combined treatments with radiation. The experiment was performed once and the corresponding fold change (with *GAPDH* as control) versus the untreated cells (DMSO 0 Gy) of each treatment condition in A172, LN229, U87 and U251 are shown in Table A1 - Table A4 respectively. The GSLC marker genes and their description are listed in Table A5.

Table A1: List of RT^2 Profiler genes with their corresponding fold change versus untreated cells (DMSO 0 Gy) in A172 cell line after the indicated treatments.

Treatment	A172	*STAT3*	*SOX2*	*NES*	*OLIG2*	*NANOG*	*POU5F1*	*ALDH1A1*	*CD44*	*PROM1*	*PLAUR*	*PLAU*
	DMSO 0Gy	1	1	1	1	1	1	1	1	1	1	1
	DMSO 4Gy	1.1	0.6	0.7	0.8	1.7	1.6	1.5	1.1	1.0	1.3	1.1
	1 µM MS 0Gy	0.6	0.3	1.0	0.8	0.4	0.9	1.0	0.8	0.4	1.1	0.2
	1 µM MS 4Gy	0.7	0.1	0.7	0.8	0.5	1.6	0.6	0.9	0.3	1.0	0.2
	1 µM TAK 0Gy	2.0	0.4	0.7	0.7	3.6	2.9	1.8	0.3	1.6	0.7	0.5
	1 µM TAK 4Gy	2.0	0.2	0.5	0.7	2.2	5.9	3.9	0.2	1.5	0.7	0.4
	1 µM TRA 0Gy	1.8	0.5	0.6	0.7	3.2	5.3	1.7	0.2	2.5	0.6	0.4
	1 µM TRA 4Gy	2.3	0.3	0.5	0.9	2.2	8.0	1.2	0.2	2.5	0.6	0.3
	1 µM MS + 1 µM TAK 0Gy	1.6	0.3	0.7	0.8	2.8	6.2	8.6	0.3	2.0	0.8	0.3
	1 µM MS + 1 µM TAK 4Gy	1.6	0.1	0.6	0.5	3.9	5.1	1.5	0.3	1.5	0.7	0.2
	1 µM MS + 1 µM TRA 0Gy	1.4	0.2	0.7	0.5	1.1	4.2	1.5	0.2	1.5	0.7	0.2
	1 µM MS + 1 µM TRA 4Gy	1.7	0.1	0.4	0.6	2.7	4.9	6.0	0.2	1.5	0.7	0.1
	1 µM TMZ 0Gy	1.3	0.3	0.6	2.7	16.4	1.5	12.3	2.0	2.2	1.5	1.0
	1 µM TMZ 4Gy	2.0	0.6	0.8	0.9	5.9	2.7	4.0	2.3	1.9	2.8	1.9

Table A2: List of RT² Profiler genes with their corresponding fold change versus untreated cells (DMSO 0 Gy) in LN229 cell line after the indicated treatments.

Treatment	LN229	*STAT3*	*SOX2*	*NES*	*OLIG2*	*NANOG*	*POU5F1*	*ALDH1A1*	*CD44*	*PROM1*	*PLAUR*	*PLAU*
	DMSO 0Gy	1	1	1	1	1	1	1	1	1	1	1
	DMSO 4Gy	1.8	4.3	2.2	1.3	1.1	1.8	26.5	2.2	5.8	9.7	3.4
	1 µM MS 0Gy	1.2	3.4	1.8	1.0	1.2	1.6	22.0	2.0	8.4	5.6	1.6
	1 µM MS 4Gy	1.4	1.5	1.6	1.0	1.0	2.0	1.2	1.4	1.1	2.7	1.0
	1 µM TAK 0Gy	2.4	2.1	2.3	1.4	6.4	3.8	2.0	1.9	5.7	4.1	1.7
	1 µM TAK 4Gy	2.9	3.1	1.6	0.9	4.1	3.9	3.8	1.1	5.6	2.4	3.1
	1 µM TRA 0Gy	3.0	2.2	1.8	1.1	3.7	6.2	1.8	1.0	3.6	1.9	1.7
	1 µM TRA 4Gy	3.4	2.9	2.0	1.2	3.8	5.4	2.5	1.9	4.3	4.3	2.5
	1 µM MS + 1 µM TAK 0Gy	1.9	3.5	1.5	0.9	1.2	2.6	10.9	1.2	10.8	2.5	1.7
	1 µM MS + 1 µM TAK 4Gy	2.0	3.3	2.3	0.5	1.3	2.0	9.0	1.1	13.1	2.3	1.6
	1 µM MS + 1 µM TRA 0Gy	1.5	3.1	2.0	1.0	0.4	1.9	10.4	1.2	10.0	2.3	1.9
	1 µM MS + 1 µM TRA 4Gy	1.7	3.2	1.9	0.9	1.4	2.4	5.3	1.2	11.5	2.4	1.4
	1 µM TMZ 0Gy	1.9	1.7	2.2	1.1	1.8	1.5	1.9	1.8	2.0	5.8	3.8
	1 µM TMZ 4Gy	1.6	1.5	1.9	0.6	1.1	1.1	2.4	1.7	2.2	5.4	3.8

Table A3: List of RT^2 Profiler genes with their corresponding fold change versus untreated cells (DMSO 0 Gy) in U87 cell line after the indicated treatments.

Treatment	U87	*STAT3*	*SOX2*	*NES*	*OLIG2*	*NANOG*	*POU5F1*	*ALDH1A1*	*CD44*	*PROM1*	*PLAUR*	*PLAU*
	DMSO 0Gy	1	1	1	1	1	1	1	1	1	1	1
	DMSO 4Gy	1.3	1.1	1.0	1.0	1.2	1.0	1.4	1.2	1.6	1.2	1.2
	1 µM MS 0Gy	1.1	2.2	4.5	1.1	1.4	1.1	9.2	1.7	4.5	0.8	1.5
	1 µM MS 4Gy	1.2	2.0	4.0	0.9	1.2	0.9	14.2	1.8	6.0	0.8	1.7
	1 µM TAK 0Gy	1.5	0.5	0.9	0.5	1.6	2.2	1.3	0.2	1.2	0.7	0.9
	1 µM TAK 4Gy	1.3	0.6	0.6	0.3	2.1	1.9	2.6	0.2	1.1	0.6	0.8
	1 µM TRA 0Gy	1.2	0.7	0.7	0.7	0.9	1.9	2.5	0.1	0.9	0.5	0.6
	1 µM TRA 4Gy	1.3	0.7	0.7	0.4	0.9	1.7	1.0	0.1	0.8	0.5	0.7
	1 µM MS + 1 µM TAK 0Gy	1.4	2.4	4.2	0.7	0.6	1.4	129.6	0.3	2.4	0.6	0.3
	1 µM MS + 1 µM TAK 4Gy	1.5	2.3	3.7	0.2	0.5	1.3	87.9	0.3	2.8	0.6	0.3
	1 µM MS + 1 µM TRA 0Gy	1.8	4.3	3.9	0.8	0.4	1.7	58.0	0.3	4.6	0.5	0.2
	1 µM MS + 1 µM TRA 4Gy	1.6	1.9	3.7	0.8	0.5	1.4	27.1	0.3	2.7	0.5	0.2
	1 µM TMZ 0Gy	2.1	1.0	1.9	1.8	2.4	1.6	1.7	1.5	3.1	1.5	1.7
	1 µM TMZ 4Gy	2.2	1.1	2.2	1.4	3.4	1.9	3.4	1.5	2.6	1.5	1.7

Table A4: List of RT² Profiler genes with their corresponding fold change versus untreated cells (DMSO 0 Gy) in U251 cell line after the indicated treatments.

Treatment	U251	*STAT3*	*SOX2*	*NES*	*OLIG2*	*NANOG*	*POU5F1*	*ALDH1A1*	*CD44*	*PROM1*	*PLAUR*	*PLAU*
	DMSO 0Gy	1	1	1	1	1	1	1	1	1	1	1
	DMSO 4Gy	1.3	1.3	1.3	1.1	0.7	1.3	1.0	1.3	1.0	1.7	1.2
	1 µM MS 0Gy	0.8	1.3	1.4	1.7	0.6	1.2	1.7	2.0	1.3	2.4	0.9
	1 µM MS 4Gy	0.9	1.3	1.6	2.0	1.1	1.5	2.0	1.9	2.0	3.3	1.1
	1 µM TAK 0Gy	2.1	1.7	0.9	1.4	2.5	1.8	2.1	2.1	2.1	1.2	0.9
	1 µM TAK 4Gy	1.8	1.3	0.9	0.9	3.4	1.8	1.4	1.7	1.4	1.1	0.7
	1 µM TRA 0Gy	1.5	1.3	0.8	0.9	3.3	1.4	1.1	1.8	1.1	1.0	0.7
	1 µM TRA 4Gy	2.0	1.4	1.0	1.5	3.4	1.1	1.8	1.9	1.8	1.2	0.8
	1 µM MS + 1 µM TAK 0Gy	0.8	0.9	0.7	0.9	1.0	0.8	1.1	2.3	1.1	1.8	0.3
	1 µM MS + 1 µM TAK 4Gy	1.4	1.3	0.9	0.9	2.3	1.1	1.6	2.8	1.6	2.0	0.3
	1 µM MS + 1 µM TRA 0Gy	0.9	1.1	0.8	0.2	1.0	1.3	1.9	2.6	1.7	1.8	0.3
	1 µM MS + 1 µM TRA 4Gy	1.0	1.1	0.9	0.8	1.2	1.0	1.7	2.6	1.2	1.9	0.3
	1 µM TMZ 0Gy	1.7	1.0	1.1	2.9	1.4	1.7	0.9	1.2	1.1	1.8	0.7
	1 µM TMZ 4Gy	1.4	0.9	1.2	1.0	0.8	1.3	0.7	1.3	0.9	2.3	0.9

Table A5: List of RT² Profiler PCR array genes and their description

Gene Symbol	Official Full Name
STAT3	signal transducer and activator of transcription 3 (acute-phase response factor)
SOX2	SRY (sex determining region Y)-box 2
NES	Nestin
OLIG2	oligodendrocyte lineage transcription factor 2
NANOG	Nanog homeoboxTP53
POU5F1	POU class 5 homeobox 1
ALDH1A1	aldehyde dehydrogenase 1 family, member A1
CD44	CD44 molecule (Indian blood group)
PROM1	prominin 1
PLAUR	plasminogen activator, urokinase receptor
PLAU	plasminogen activator, urokinase
TBP	TATA box binding protein
GAPDH	glyceraldehyde-3-phosphate dehydrogenase

Appendix C: Representative western Blots after HDACi and MEKi with radiation in monolayer glioblastoma cell lines.

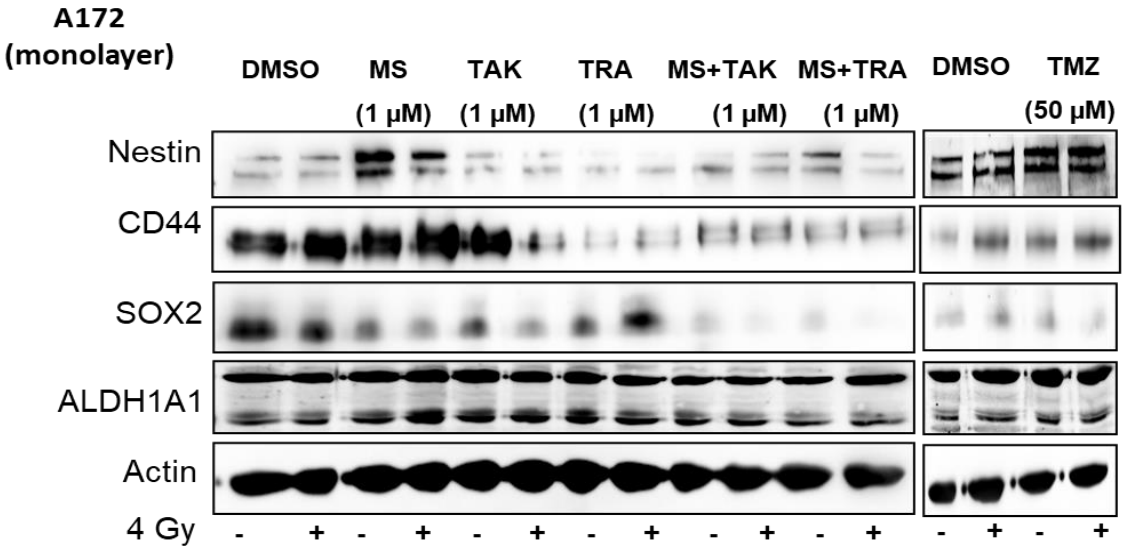

Figure A2: A172 Monolayer representative blots of quantified data from Figure 13 are shown.

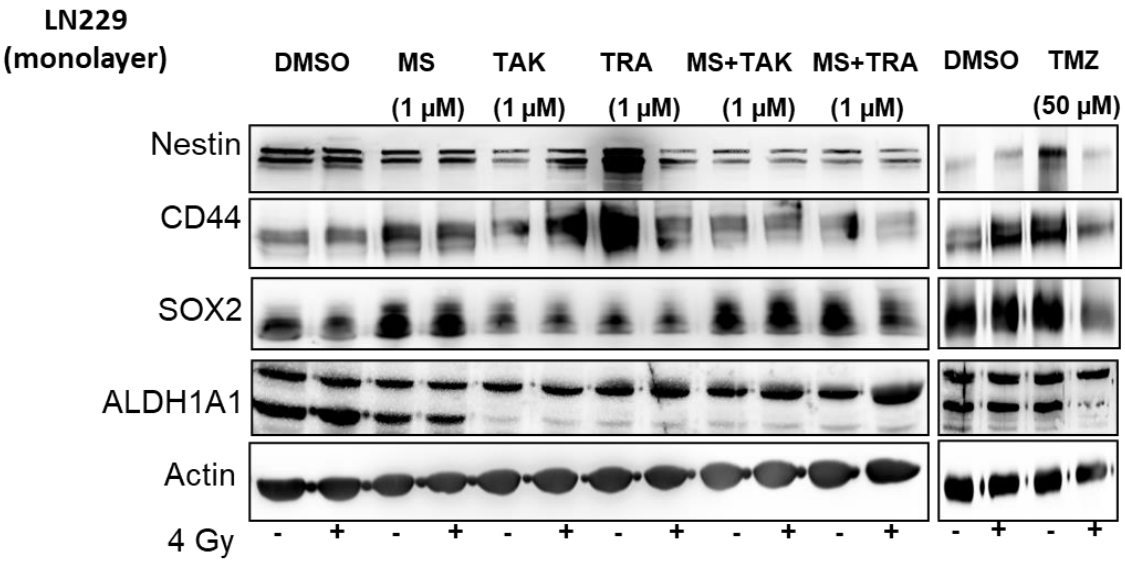

Figure A3: LN229 Monolayer representative blots of quantified data from Figure 14 are shown.

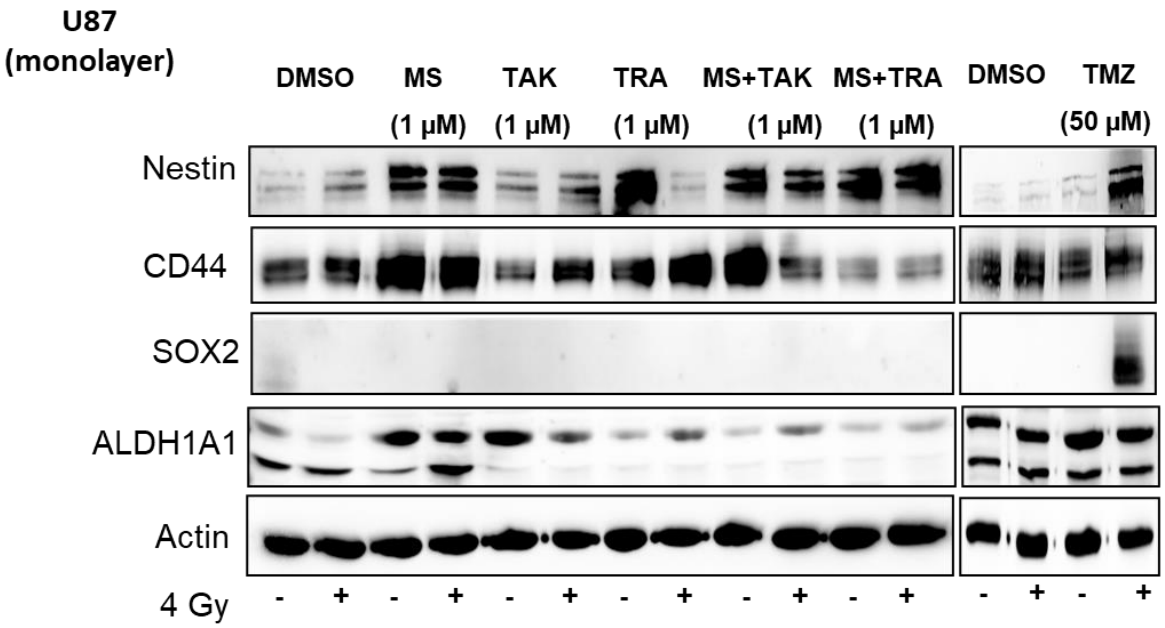

Figure A4: U87 Monolayer representative blots of quantified data from Figure 15 are shown.

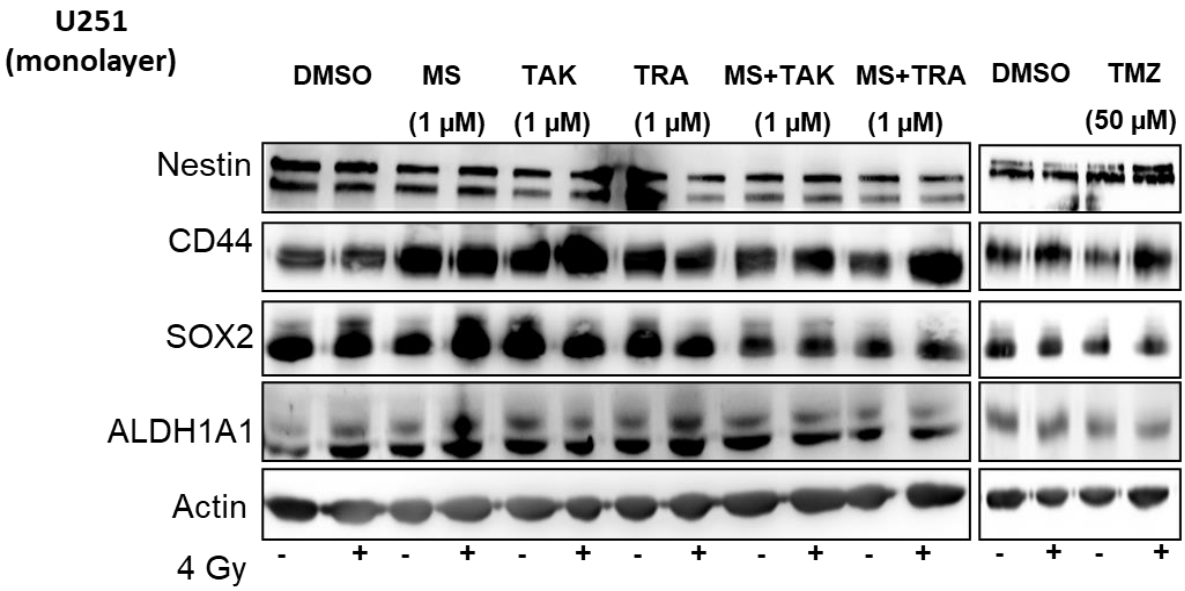

Figure A5: U251 Monolayer representative blots of quantified data from Figure 16 are shown.

Appendix D: Representative western Blots after HDACi and MEKi with radiation in stem-cell enriched glioblastoma-derived spheres.

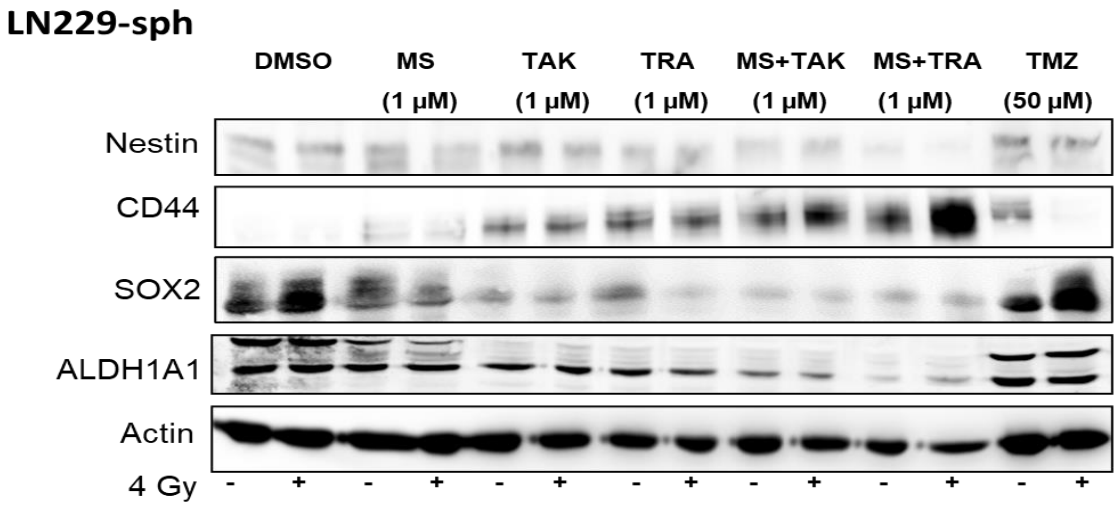

Figure A6: LN229-sph representative blots of quantified data from Figure 29 are shown

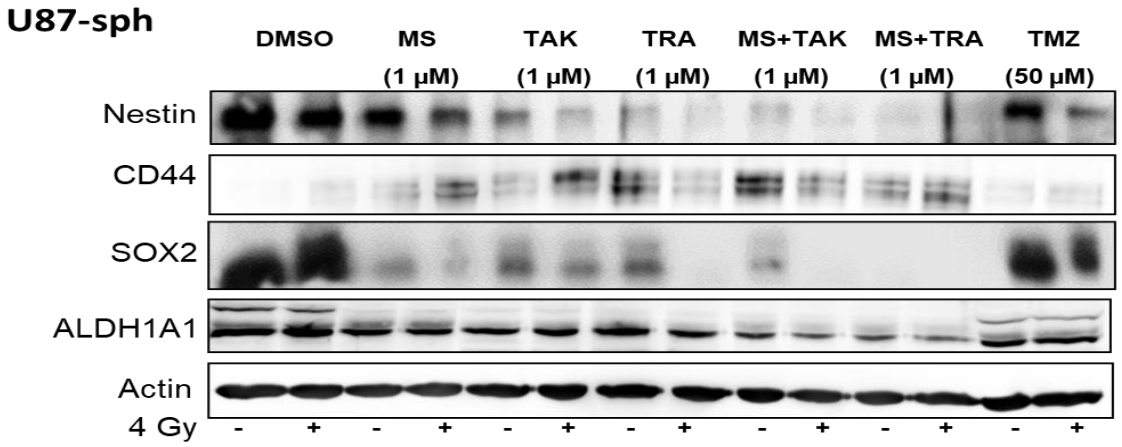

Figure A7: U87-sph representative blots of quantified data from Figure 30 are shown.

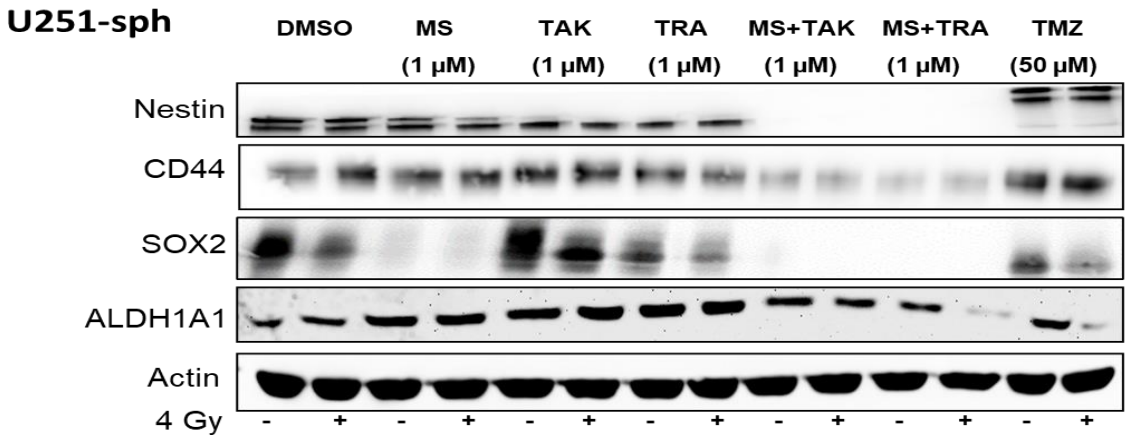

Figure A8: U251-sph representative blots of quantified data from Figure 31 are shown.

Appendix E: Representative pictures of flow cytometric plots of single GSLC markers after combined HDACi and MEKi with radiation.

The cells were analyzed by flow cytometry using a CytoFLEX LX flow cytometer and CytExpert software. The CytoFLEX LX instrument has a capacity for 21 channels of fluorescence detection and is equipped with a 355 nm (UV) laser, 405 nm (Violet) laser, 488 nm (Blue) laser, 561 nm (Yellow Green) laser, 638 nm (Red) laser and 808 nm (Infrared) laser. Fluorescence and side scatter light of the CytoFLEX LX were delivered by fiber optics to Avalanche Photo Diode detector arrays while the emission profiles were collected by reflective optics and single transmission band pass filters. Unstained cells were used to set the voltages while compensation beads were used to compensate and correct for spectral overlap across the fluorescent channels.

In flow cytometry analysis, the gating technique used to set a cut-off for the negative and positive populations was done using two gating controls. First control was with unstained cells to set the region for negative and positive populations while the fluorescence minus one (FMO) control was used to address any spillover induced background (Figure A9 and Figure A10). An additional isotype control was included for SOX2 to avoid non-specific antibody binding since there were lower levels (Figure A11). The gating region on the controls was set to contain less than 1% of the single positive populations.

LN229-sph: The representative pictures for LN229-sph in Figure 32 showing the controls and percentage values for Nestin+, CD44+ and SOX2+ populations after the different treatments are shown in Figure A9, Figure A10, Figure A11 respectively.

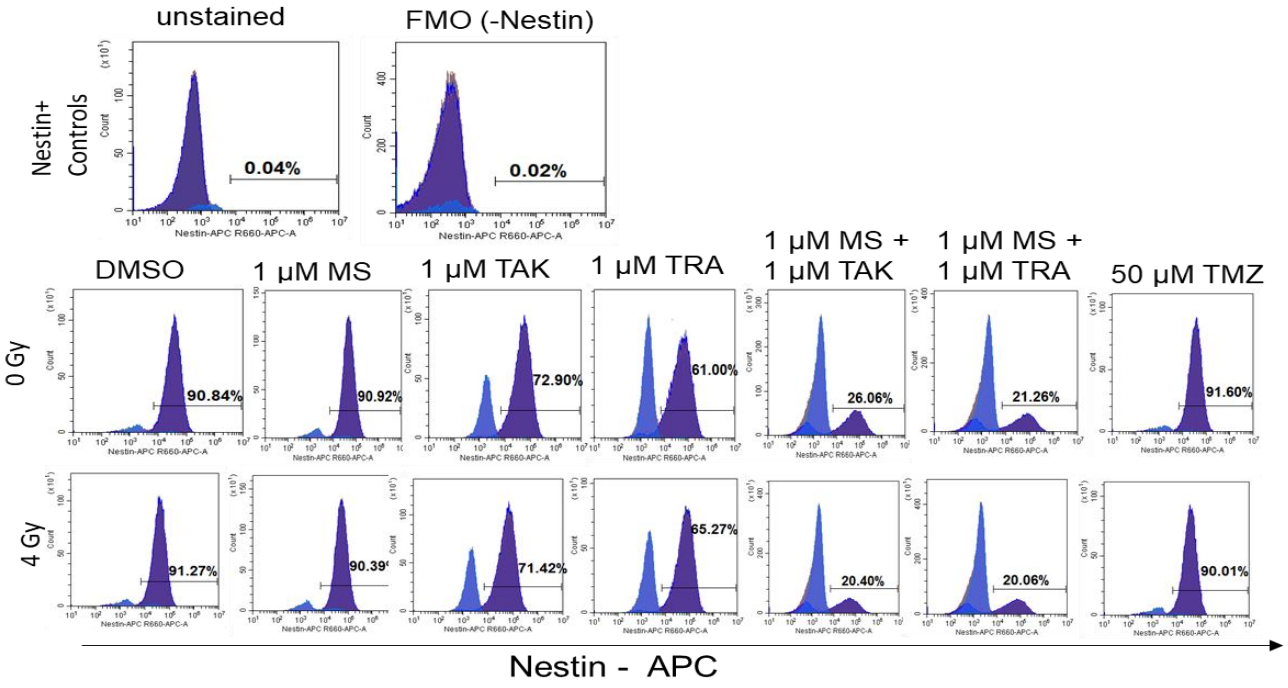

Figure A9: Representative flow cytometric histograms for the single positive populations of Nestin+ in LN229-sph after the indicated treatment conditions. Unstained and FMO controls for gating positive populations are shown (upper rows). Percentage values inside each flow cytometric plot represents percentage of single positive cells from a total of approximately 2 x 10^4 cells acquired.

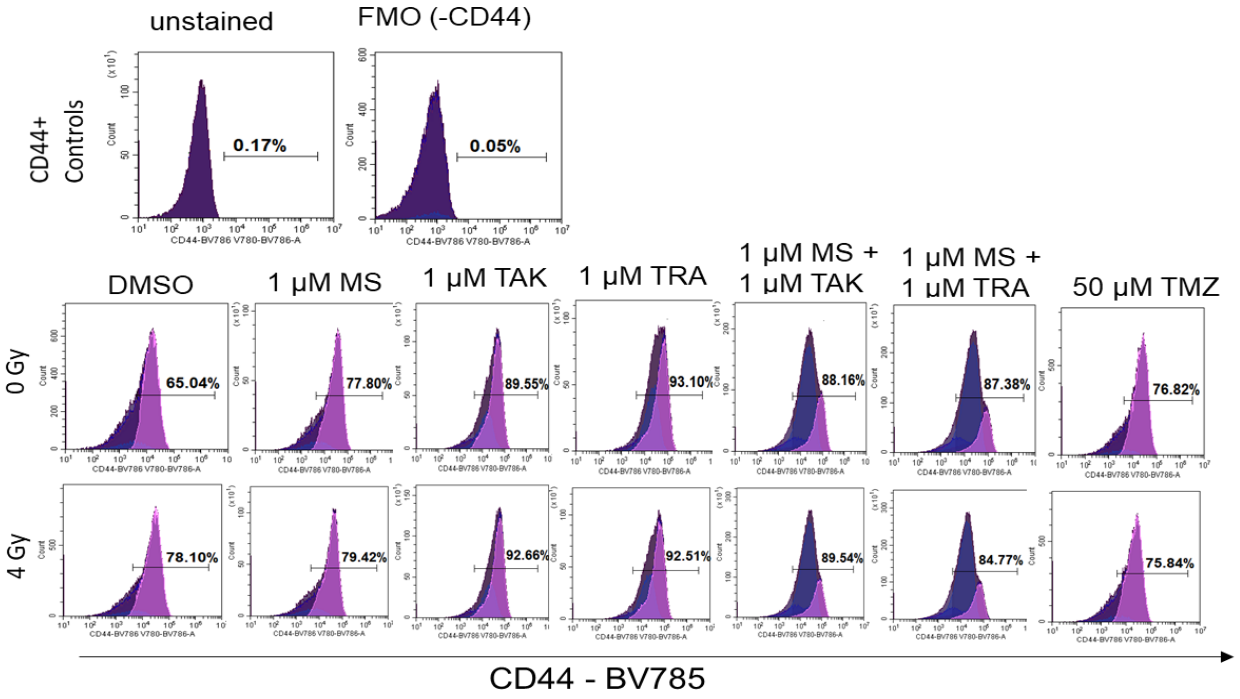

Figure A10: Representative flow cytometric histograms for the single positive populations of CD44+ in LN229-sph after the indicated treatment conditions. Unstained

and FMO controls for gating positive populations are shown (upper rows). Percentage values inside each flow cytometric plot represents percentage of single positive cells from a total of approximately 2 x 10^4 cells acquired.

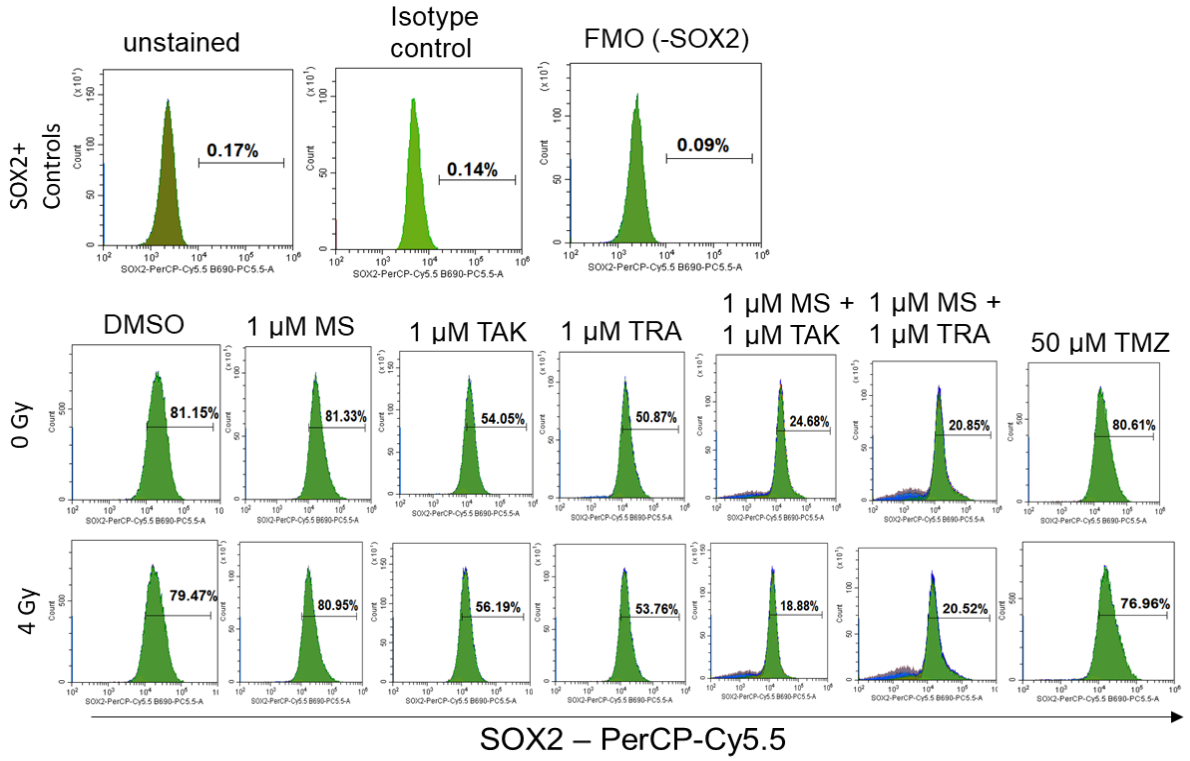

Figure A11: Representative flow cytometric histograms for the single positive populations of SOX2+ in LN229-sph after the indicated treatment conditions. Unstained and FMO controls for gating positive populations are shown (upper rows). Percentage values inside each flow cytometric plot represents percentage of single positive cells from a total of approximately 2 x 10^4 cells acquired.

U87-sph: The representative pictures for U87-sph in Figure 33 showing the controls and percentage values for Nestin+, CD44+ and SOX2+ populations after the different treatments are shown in Figure A12, Figure A13, Figure A14 respectively.

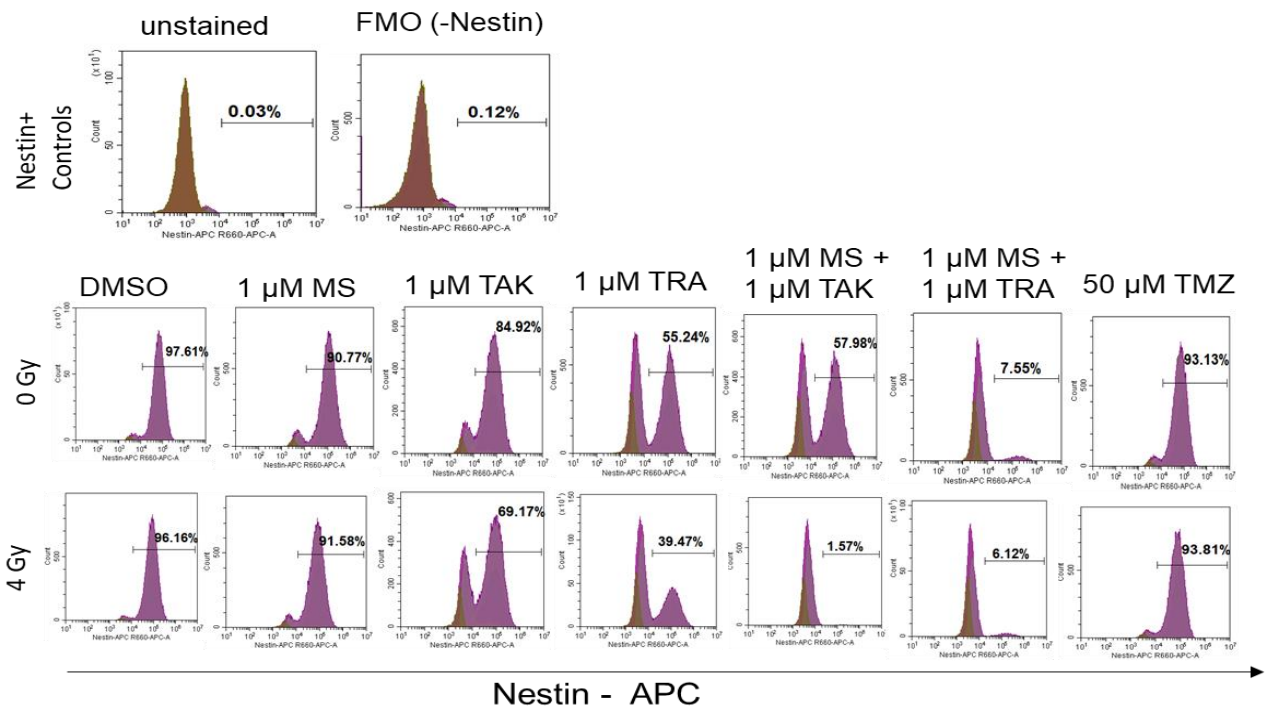

Figure A12: Representative flow cytometric histograms for the single positive populations of Nestin+ in U87-sph after the indicated treatment conditions. Unstained and FMO controls for gating positive populations are shown (upper rows). Percentage values inside each flow cytometric plot represents percentage of single positive cells from a total of approximately 2 x 10^4 cells acquired.

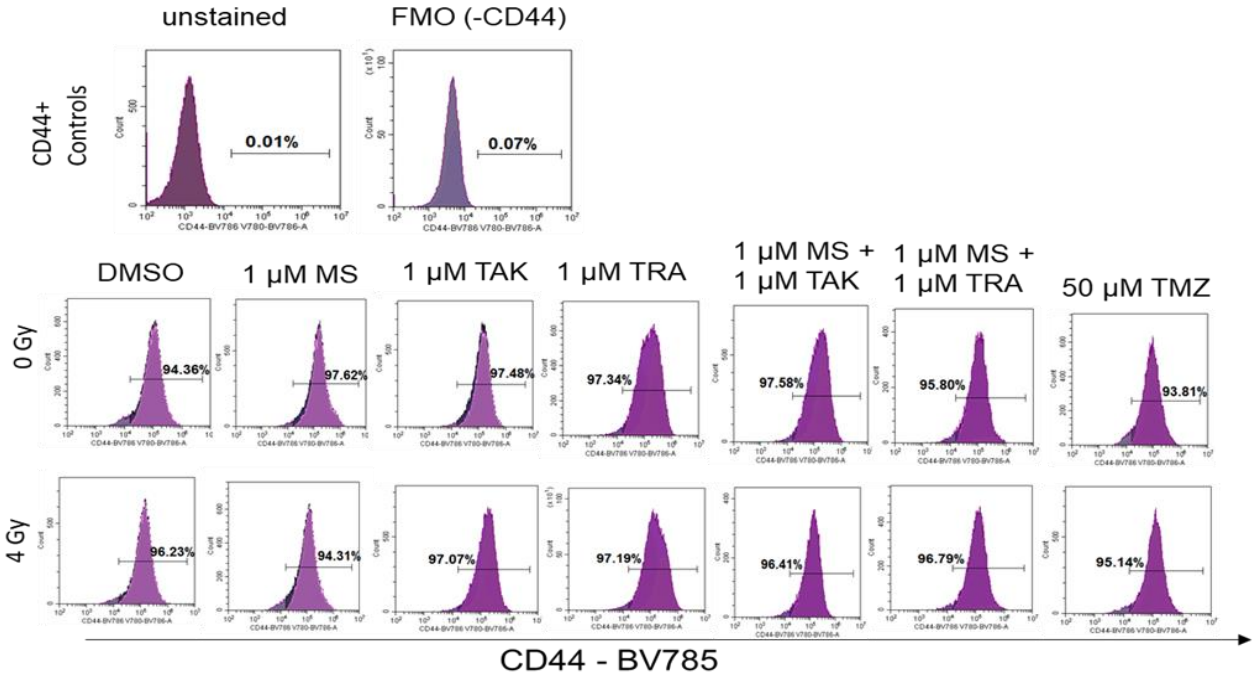

Figure A13: Representative flow cytometric histograms for the single positive populations of CD44+ in U87-sph after the indicated treatment conditions. Unstained and

FMO controls for gating positive populations are shown (upper rows). Percentage values inside each flow cytometric plot represents percentage of single positive cells from a total of approximately 2 x 10^4 cells acquired.

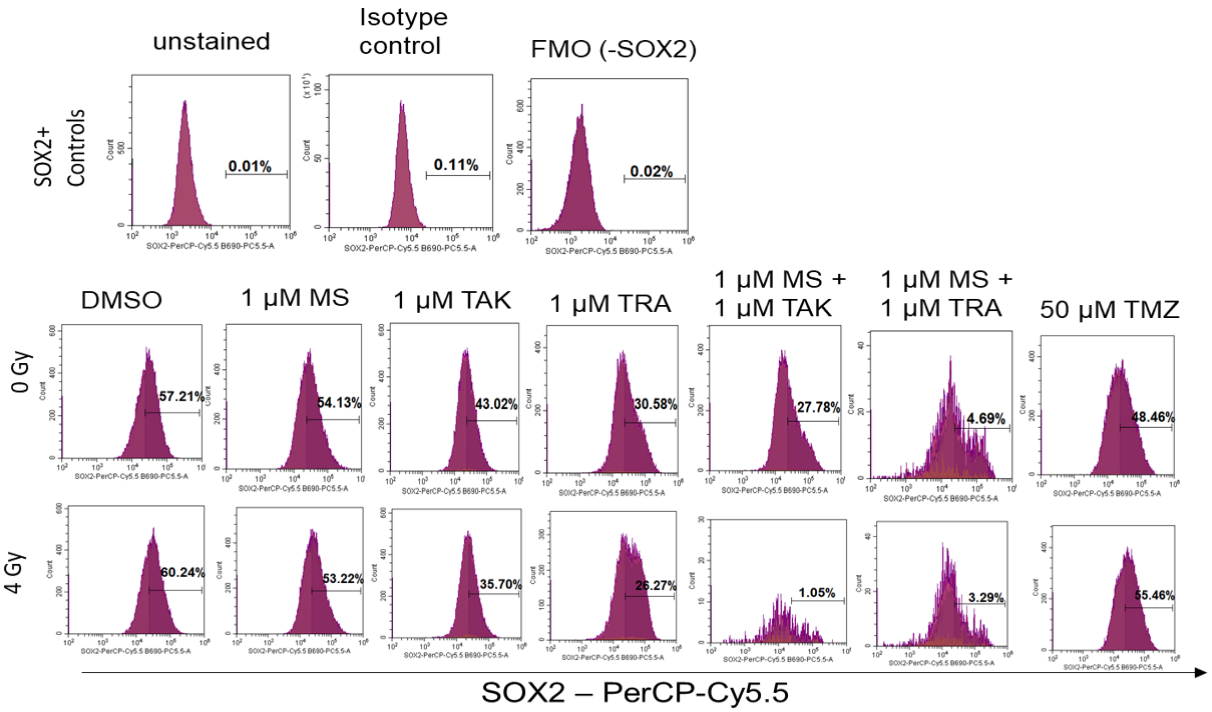

Figure A14: Representative flow cytometric histograms for the single positive populations of SOX2+ in U87-sph after the indicated treatment conditions. Unstained and FMO controls for gating positive populations are shown (upper rows). Percentage values inside each flow cytometric plot represents percentage of single positive cells from a total of approximately 2 x 10^4 cells acquired.

U251-sph: The representative pictures for U251-sph in Figure 34 showing the controls and percentage values for Nestin+, CD44+ and SOX2+ populations after the different treatments are shown in Figure A15, Figure A16, Figure A17 respectively.

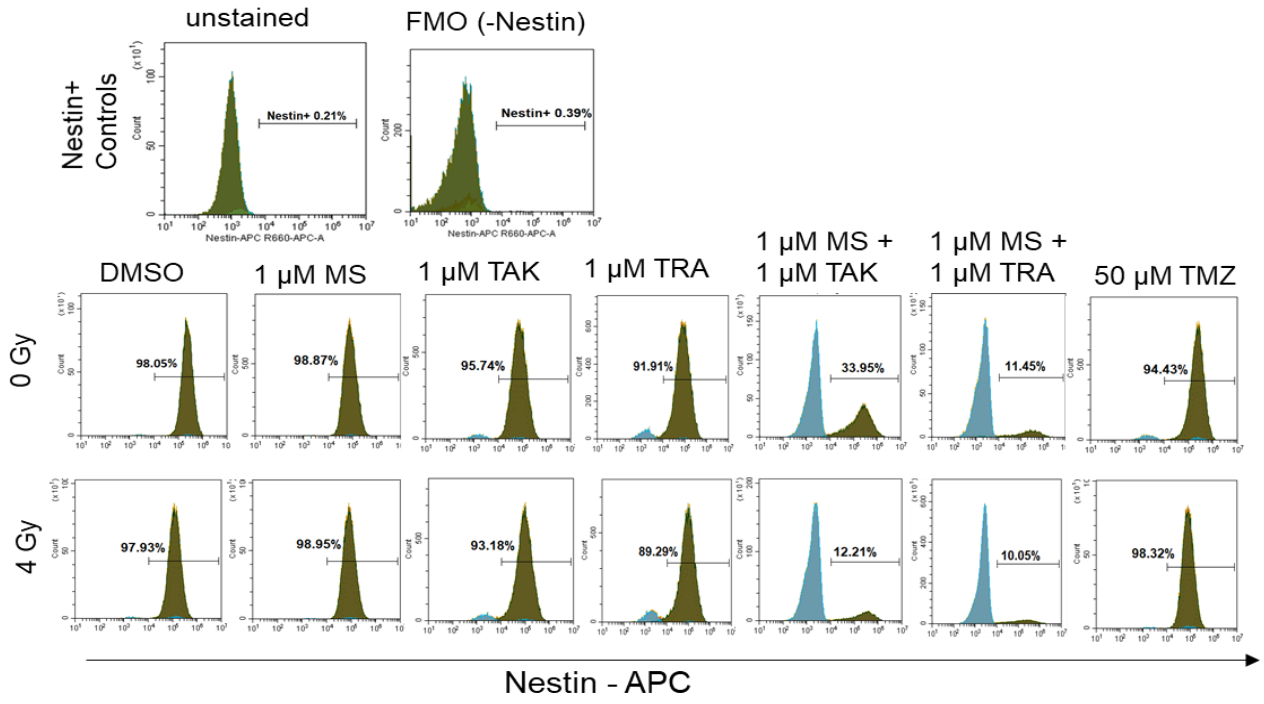

Figure A15: Representative flow cytometric histograms for the single positive populations of Nestin+ in U251-sph after the indicated treatment conditions. Unstained and FMO controls for gating positive populations are shown (upper rows). Percentage values inside each flow cytometric plot represents percentage of single positive cells from a total of approximately 2 x 10^4 cells acquired.

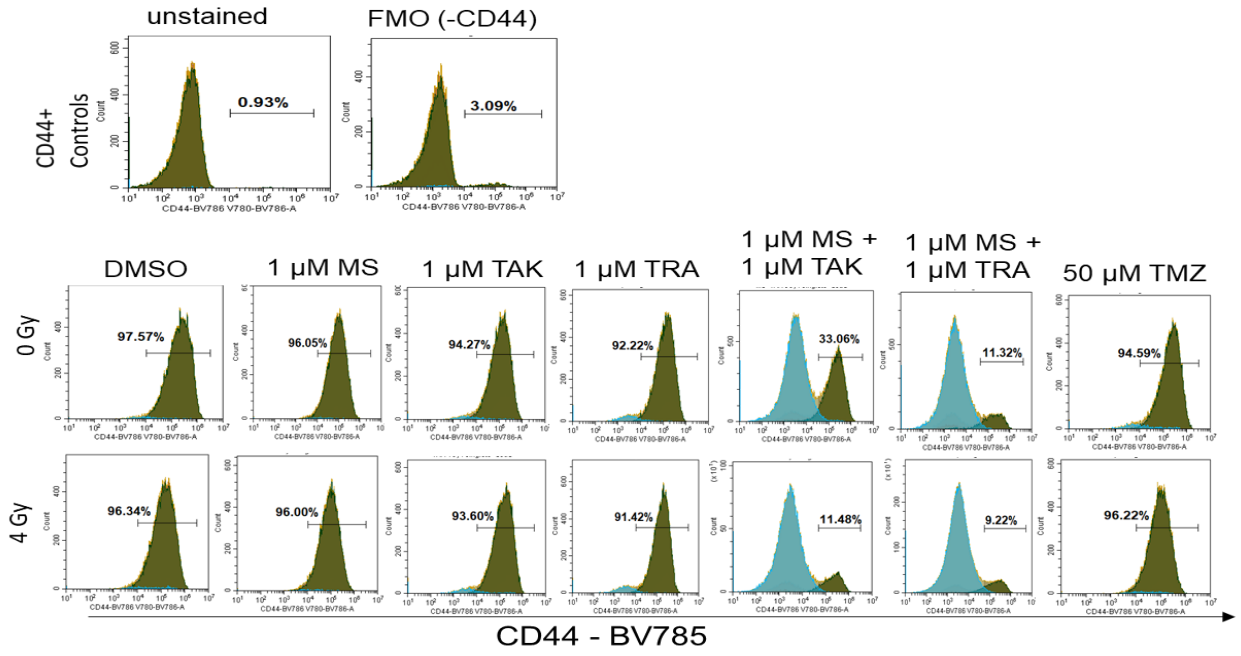

Figure A16: Representative flow cytometric histograms for the single positive populations of CD44+ in U251-sph after the indicated treatment conditions. Unstained

and FMO controls for gating positive populations are shown (upper rows). Percentage values inside each flow cytometric plot represents percentage of single positive cells from a total of approximately 2 x 10^4 cells acquired.

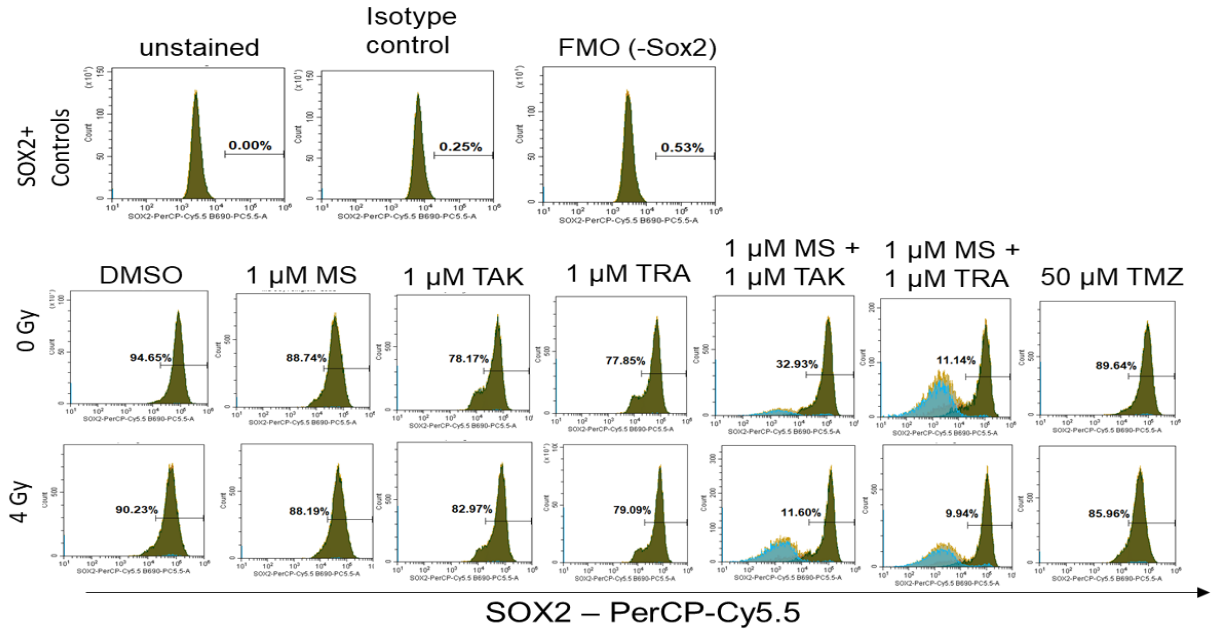

Figure A17: Representative flow cytometric histograms for the single positive populations of SOX2+ in U251-sph after the indicated treatment conditions. Unstained and FMO controls for gating positive populations are shown (upper rows). Percentage values inside each flow cytometric plot represents percentage of single positive cells from a total of approximately 2 x 10^4 cells acquired.

Appendix F: Representative pictures of flow cytometric plots of double GSLC markers after combined HDACi and MEKi with radiation.

The gating strategy and FMO controls for the flow cytometry analysis are shown in Figure A18. First cells were gated based on size and granularity using side scatter area (SSC-A) vs forward scatter area (FSC-A) to remove debris and clumped cells. From this cell gate, single cells (singlets) were sub-gated using forward scatter height (FSC-H) vs FSC-A to remove doublets. From the singlets gates, the control (DMSO) and treated samples were sub-gated into quadrants. Lastly the FMO controls containing all antibody staining except the indicated one was used to adjust the gate against any spillover and obtain the negative and positive double populations of CD44+Nestin+,

Nestin+SOX2+ and CD44+SOX2+. The percentage values for the double positive populations are located on the upper right region of the quadrants.

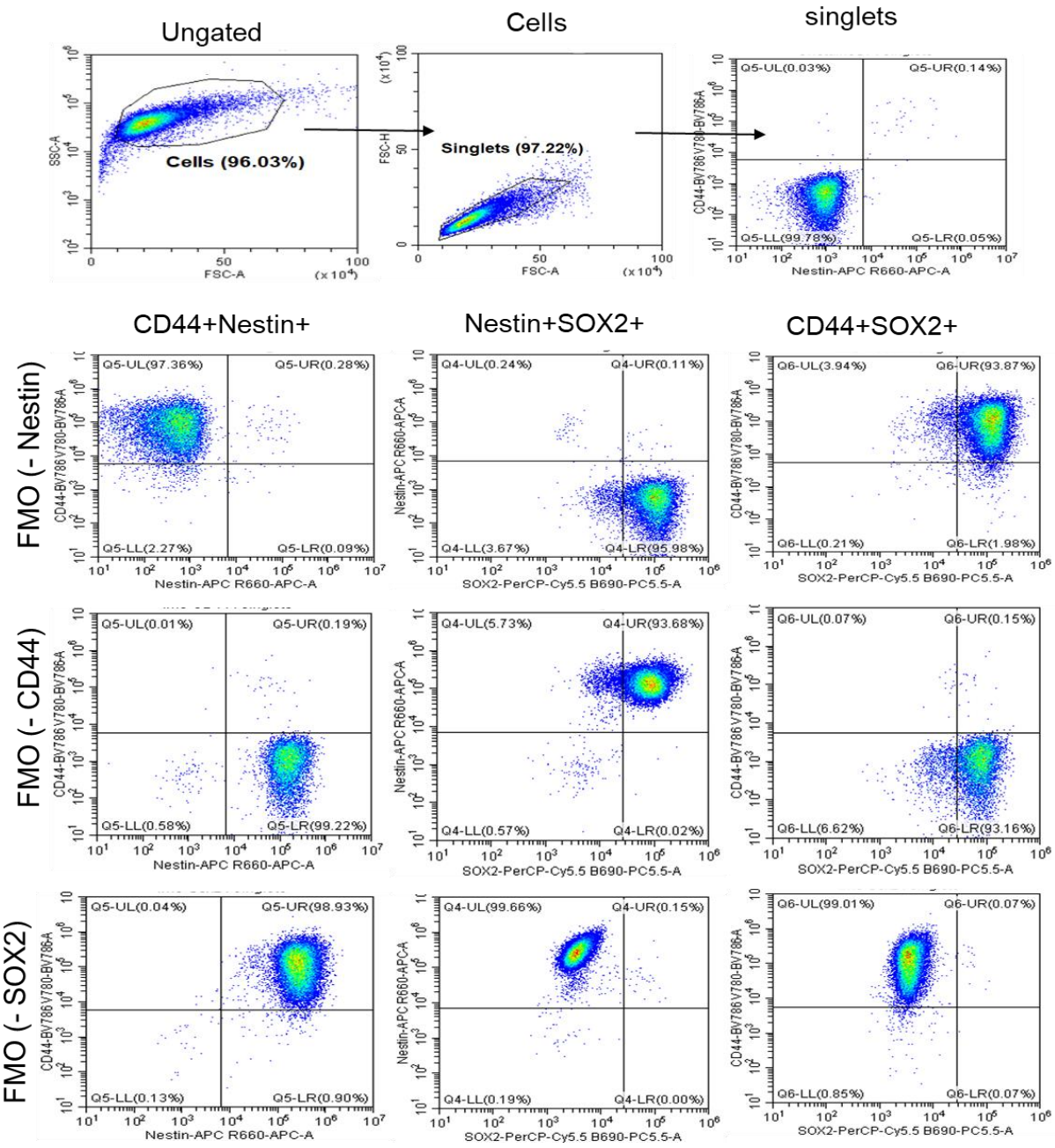

Figure A18: **Gating strategy and controls for flow cytometry analysis of double positive populations (CD44+Nestin+, Nestin+SOX2+ and CD44+SOX2+).** The first row shows the total population from which cells and single cells (singlets) are gated from. The FMO controls minus (-) the indicated antibodies used to gate the double positive populations (upper right region in the quadrants) are shown. The gating region on the FMO controls were set to contain less than 1% of the cells for double positive populations.

LN229-sph: The representative pictures for LN229-sph in Figure 35 showing the percentage values for CD44+Nestin+, Nestin+SOX2+ and CD44+SOX2+ populations after the different treatments are shown in Figure A19, Figure A20, Figure A21 respectively.

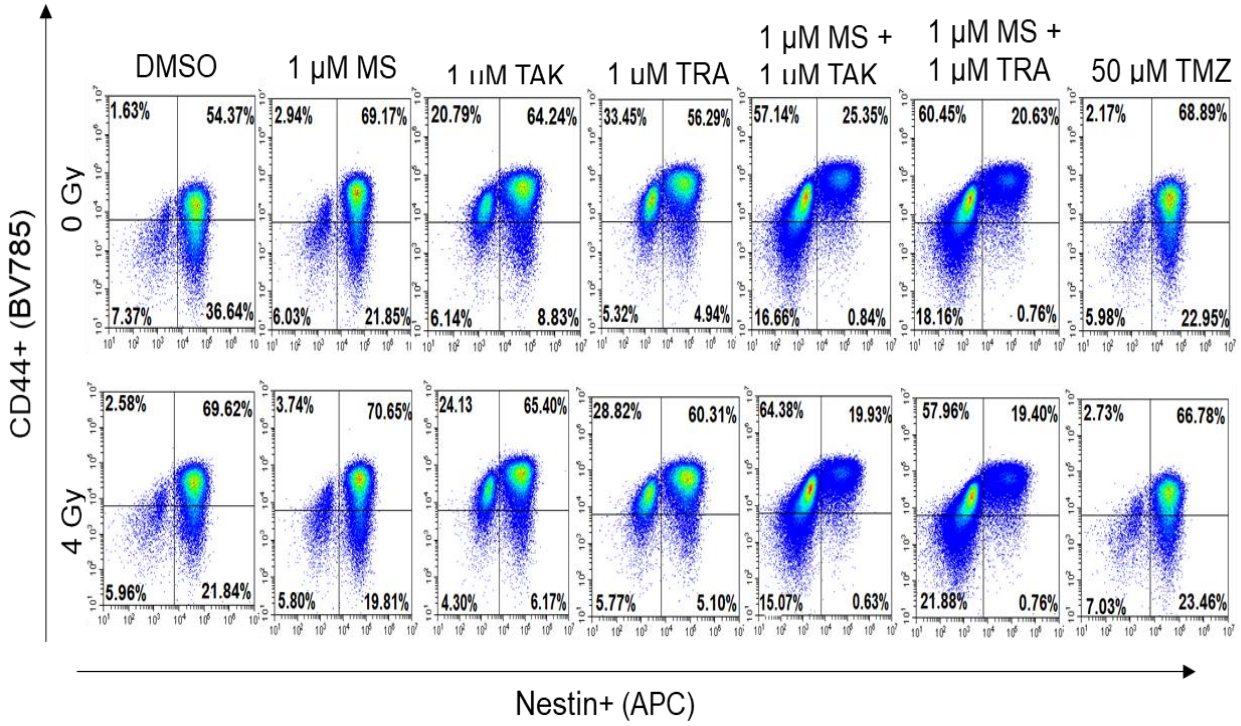

Figure A19: Representative flow cytometric plots for the double positive populations of CD44+Nestin+ in LN229-sph after the indicated treatment conditions. Percentage values of double positive cells for CD44 and Nestin (CD44+Nestin+; Upper right quadrant) after the indicated treatment conditions are shown. Values inside each flow cytometric plot represents percentage of double positive cells from a total of approximately 2 x 10^4 cells acquired.

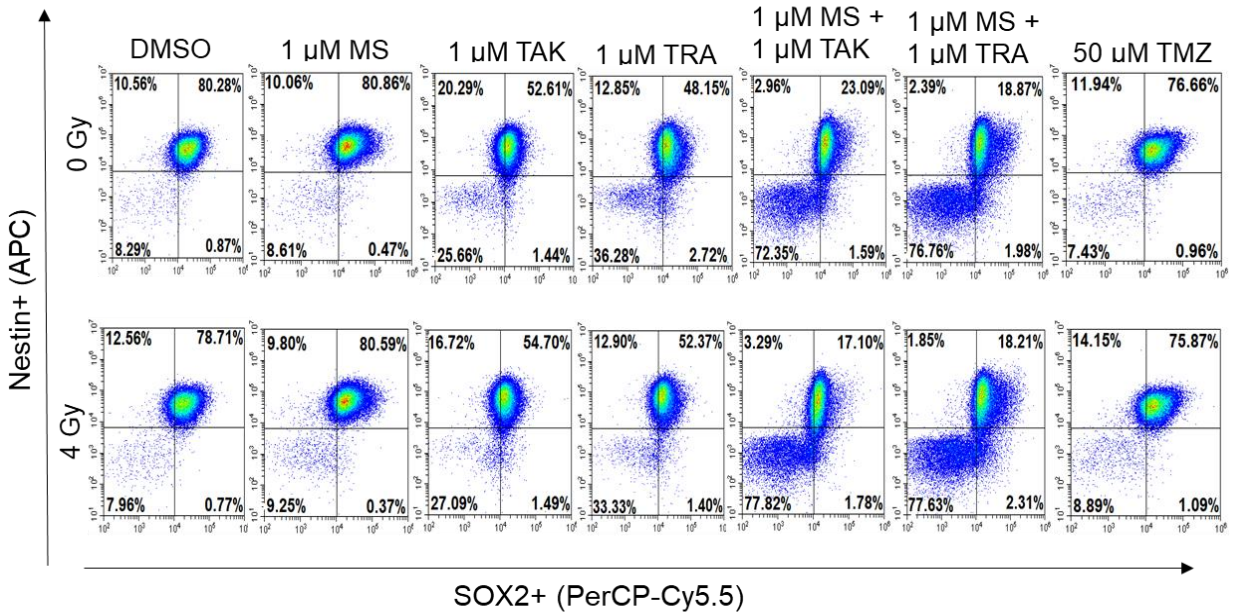

Figure A20: Representative flow cytometric plots for the double positive populations of Nestin+ SOX2+ in LN229-sph after the indicated treatment conditions. Percentage values of double positive cells for Nestin and SOX2 (Nestin+SOX2+; Upper right quadrant) after the indicated treatment conditions are shown. Values inside each flow cytometric plot represents percentage of double positive cells from a total of approximately 2 x 10^4 cells acquired.

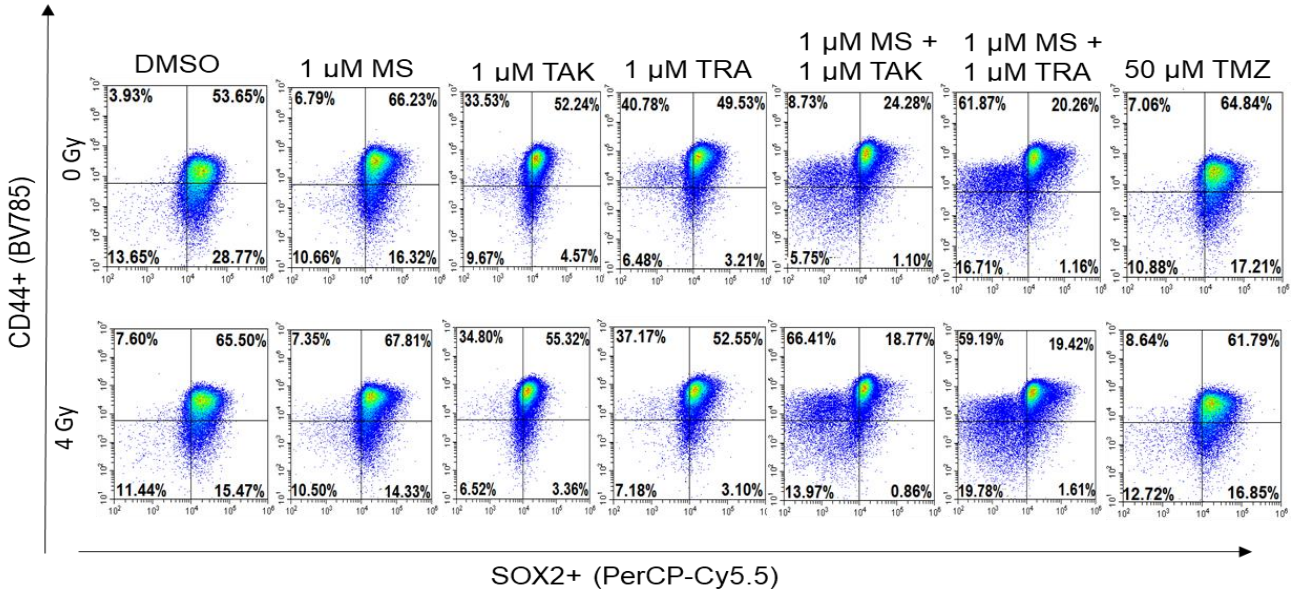

Figure A21:**Representative flow cytometric plots for the double positive populations of CD44+ SOX2+ in LN229-sph after the indicated treatment conditions.** Percentage values of double positive cells for CD44 and SOX2 (CD44+SOX2+; Upper right quadrant) after the indicated treatment conditions are shown. Values inside each flow cytometric plot represents percentage of double positive cells from a total of approximately 2 x 10^4 cells acquired.

U87-sph: The representative pictures for U87-sph in Figure 36 showing the percentage values for CD44+Nestin+, Nestin+SOX2+ and CD44+SOX2+ populations after the different treatments are shown in Figure A22, Figure A23, Figure A24 respectively.

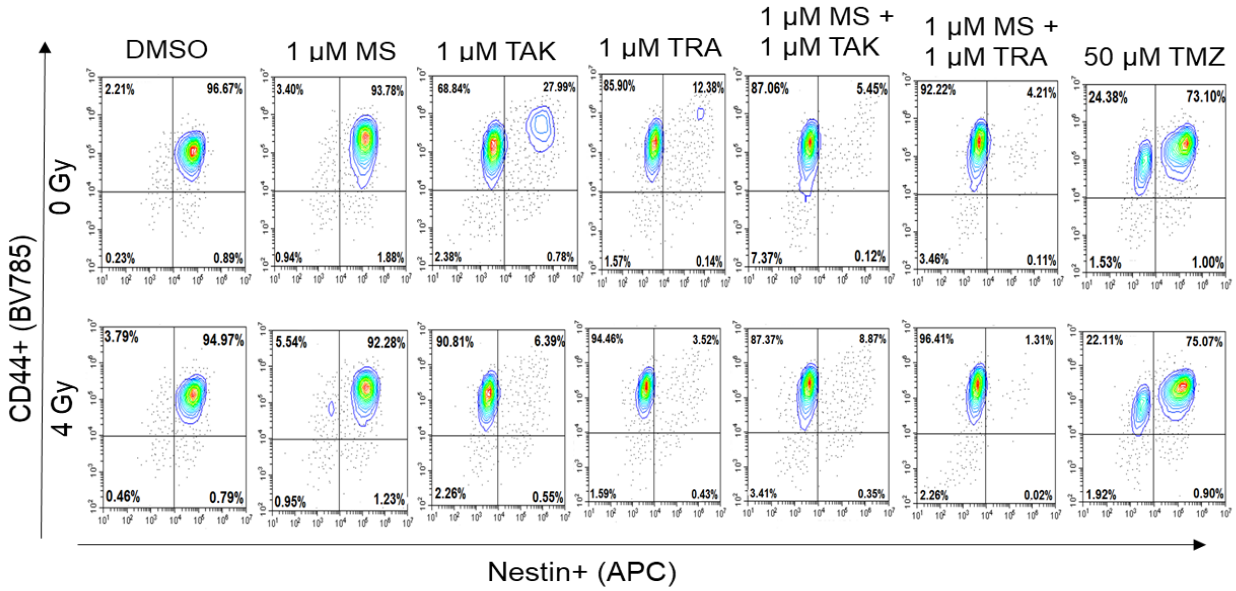

Figure A22: **Representative flow cytometric plots for the double positive populations of CD44+Nestin+ in U87-sph after the indicated treatment conditions.** Percentage values of double positive cells for CD44 and Nestin (CD44+Nestin+; Upper right quadrant) after the indicated treatment conditions are shown. Values inside each flow cytometric plot represents percentage of double positive cells from a total of approximately 2 x 10^4 cells acquired.

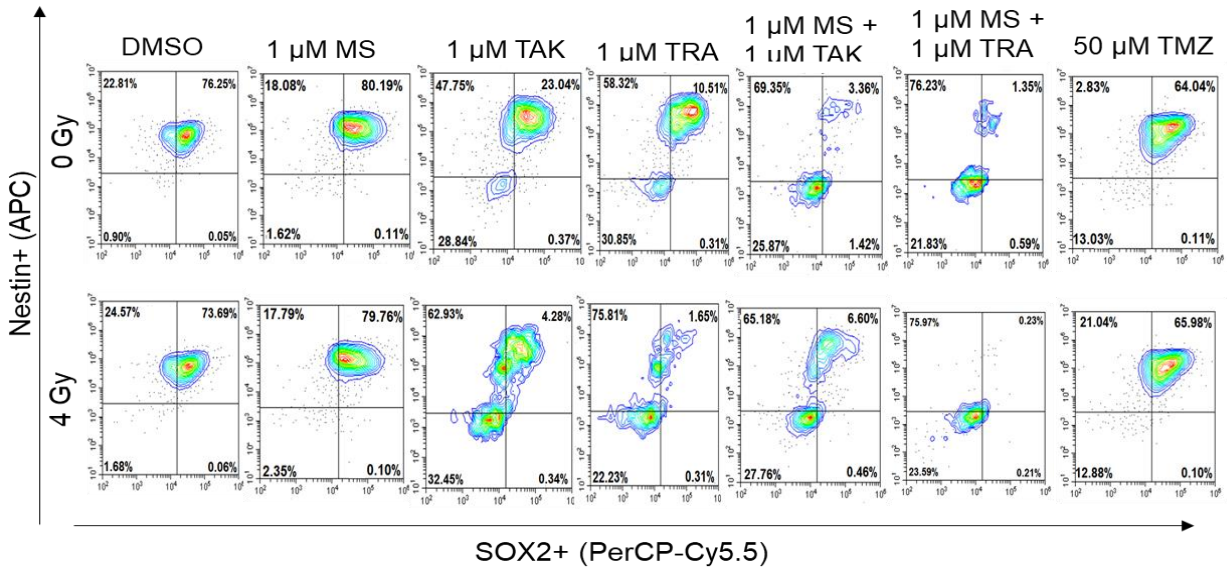

Figure A23: **Representative flow cytometric plots for the double positive populations of Nestin+SOX2+ in U87-sph after the indicated treatment conditions.** Percentage values of double positive cells for Nestin and SOX2 (Nestin+SOX2+; Upper right quadrant) after the indicated treatment conditions are shown. Values inside each flow cytometric plot represents percentage of double positive cells from a total of approximately 2 x 10^4 cells acquired.

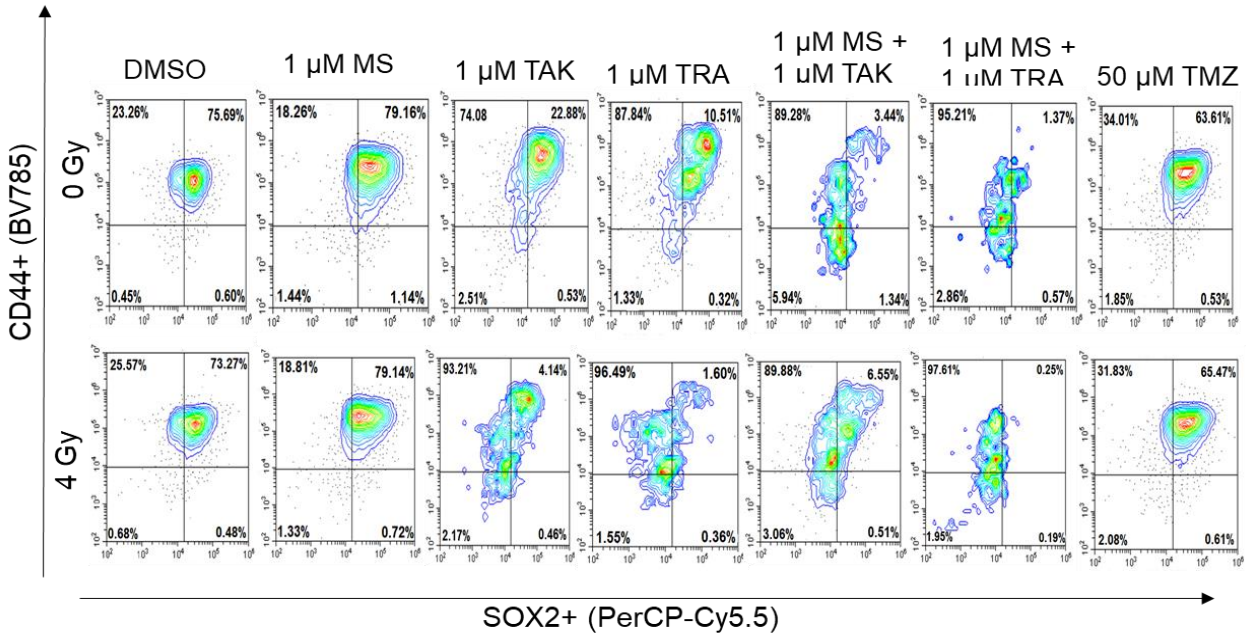

Figure A24: **Representative flow cytometric plots for the double positive populations of CD44+SOX2+ in U87-sph after the indicated treatment conditions.** Percentage values of double positive cells for CD44 and SOX2 (CD44+SOX2+; Upper right quadrant) after the indicated treatment conditions are shown. Values inside each flow cytometric plot represents percentage of double positive cells from a total of approximately 2 x 10^4 cells acquired.

U251-sph: The representative pictures for U251-sph in Figure 37 showing the percentage values for CD44+Nestin+, Nestin+SOX2+ and CD44+SOX2+ populations after the different treatments are shown in Figure A25, Figure A26, Figure A27 respectively.

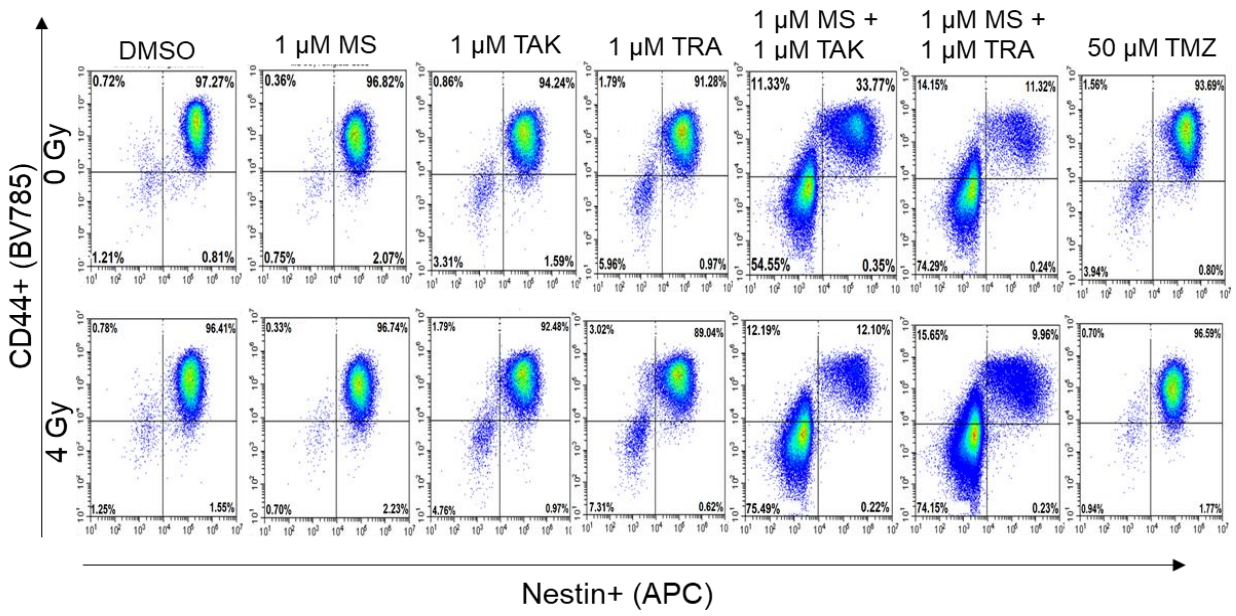

Figure A25: Representative flow cytometric plots for the double positive populations of CD44+Nestin+ in U251-sph after the indicated treatment conditions. Percentage values of double positive cells for CD44 and Nestin (CD44+Nestin+; Upper right quadrant) after the indicated treatment conditions are shown. Values inside each flow cytometric plot represents percentage of double positive cells from a total of approximately 2 x 10^4 cells acquired.

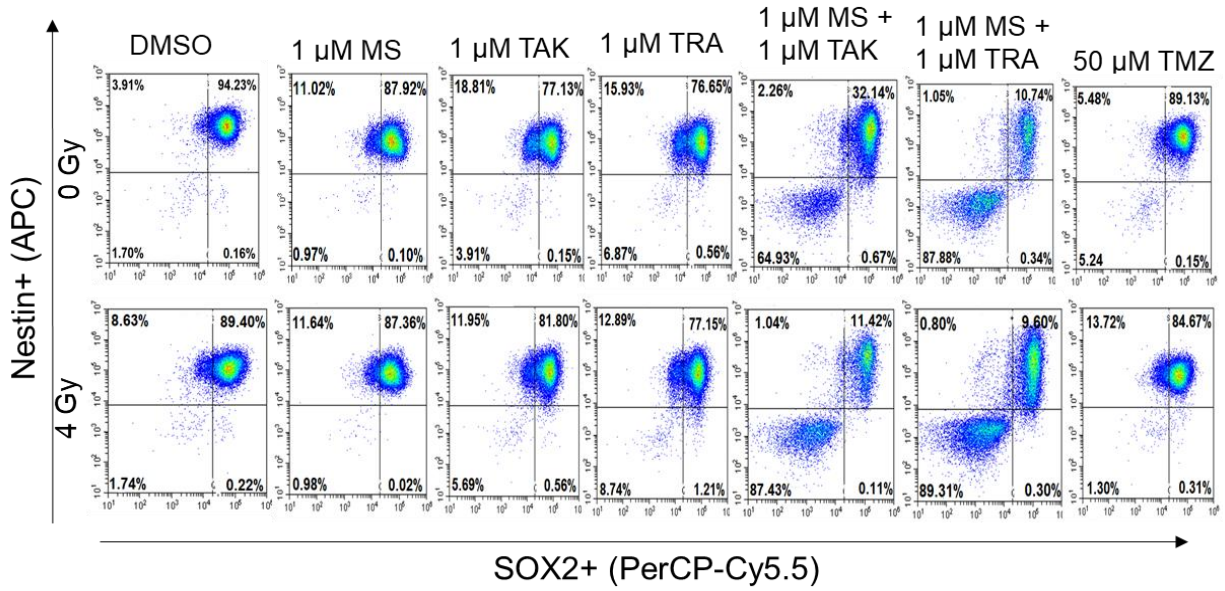

Figure A26: Representative flow cytometric plots for the double positive populations of Nestin+SOX2+ in U251-sph after the indicated treatment conditions. Percentage values of double positive cells for Nestin and SOX2 (Nestin+SOX2+; Upper right quadrant) after the indicated treatment conditions are shown. Values inside each flow cytometric plot represents percentage of double positive cells from a total of approximately 2 x 10^4 cells acquired.

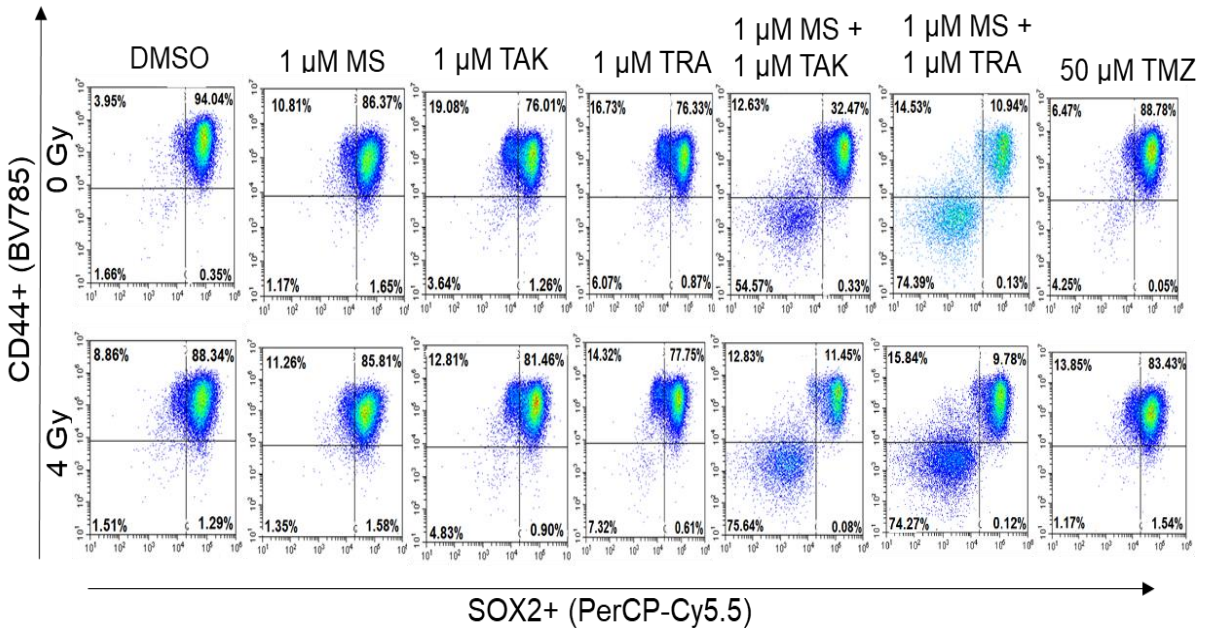

Figure A27: Representative flow cytometric plots for the double positive populations of CD44+SOX2+ in U251-sph after the indicated treatment conditions. Percentage values of double positive cells for CD44 and SOX2 (CD44+SOX2+; Upper right quadrant) after the indicated treatment conditions are shown. Values inside each flow cytometric plot represents percentage of double positive cells from a total of approximately 2 x 10^4 cells acquired.

Appendix G: Repeated Expression analysis of GSLC marker genes after combined treatment of HDACi and MEKi with radiation

The quantitative real time PCR results to analyse the single expression of *NES*, *CD44* and *SOX2* were repeated with an additional analysis of *ALDH1* expression. The experiment was repeated at least three times using *GAPDH* as the endogenous control to validate the upregulation observed after the combined treatment of HDACi and MEKi with radiation (Figure 39 - Figure 41).

It can be seen that compared to the control cells (DMSO), there was an upregulation of *NES*, *CD44*, and *SOX2* in LN229-sph (Figure A28) and U251-sph (Figure A30) by the treatment of HDACi and MEKi with radiation. In U87-sph on the other hand, the combined treatment with radiation only upregulated *NES* but significantly downregulated *CD44* expression while only the combination of MS-275 and TAK-733 with radiation significantly reduced *SOX2* expression (Figure A29). The expression of *ALDH1* was significantly downregulated by the combined treatment with radiation in LN229-sph and U87-sph but not in U251-sph (Figure A28 - Figure A30). No significant effect of the standard TMZ and radiation on the GSLC markers was detected in all glioblastoma-derived spheres.

In general, the results were comparable to the results presented in (Figure 39 - Figure 41) where *TBP* was used as the endogenous control.

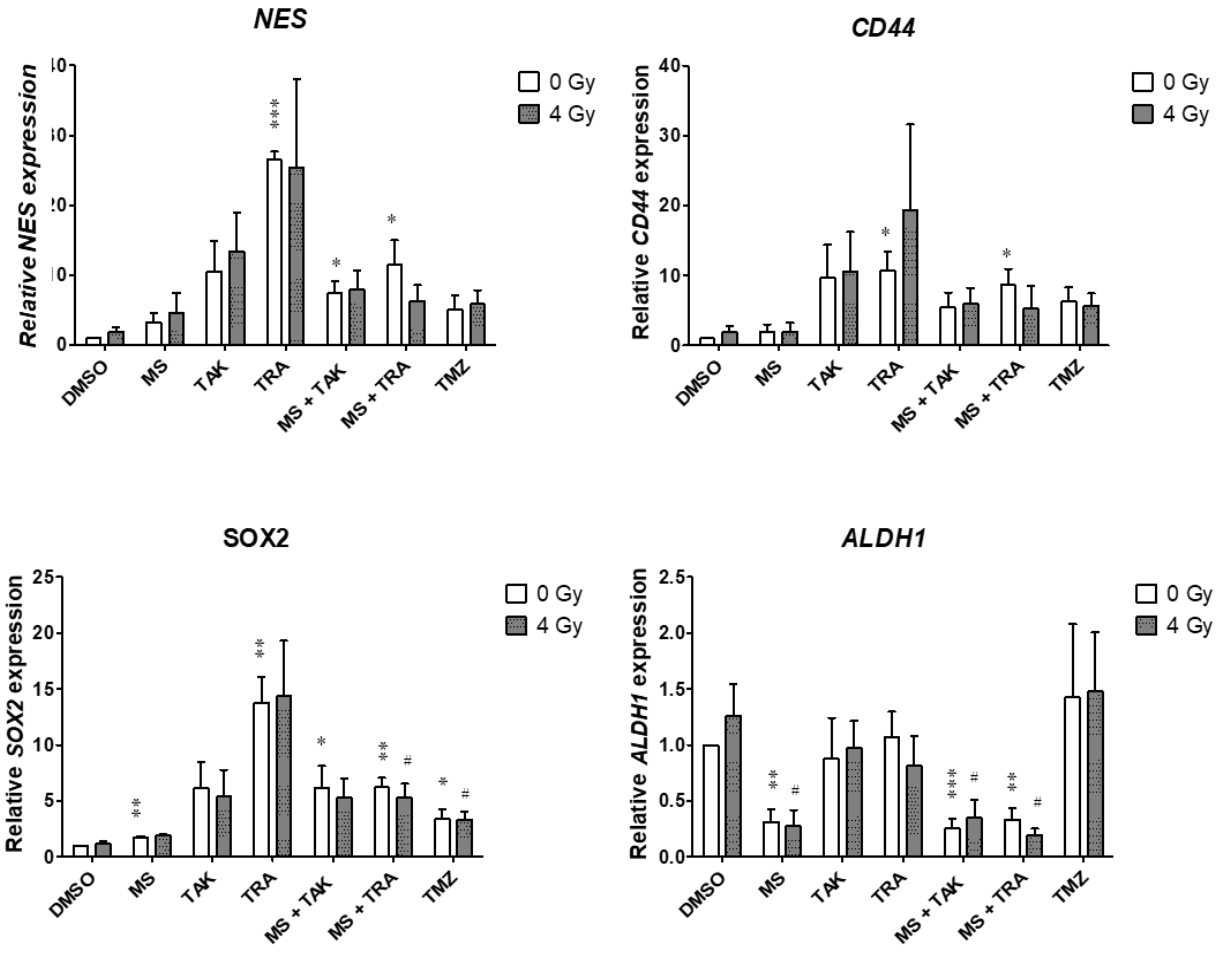

Figure A28: GSLC marker gene expression in LN229-sph after treatment with HDACi or MEKi as single or combined drugs with radiation. Fold changes of *NES*, *CD44* and *SOX2* 72 hours after the combined treatment and 4 Gy radiation are shown. The fold changes were calculated compared to sham irradiated control cells (DMSO) set to one. Data represents mean values ± SEM (n = 3). [*Student's t-test; *p ≤ 0.05, ***p ≤ 0.001 (versus DMSO 0 Gy), #Student's t-test; $^{\#}$p ≤ 0.05, $^{\#\#}$p ≤ 0.01, $^{\#\#\#}$p ≤ 0.001 (versus DMSO 4 Gy). 2-way ANOVA; *p*-value <0.05 (CD44); *p*-value <0.0001 (*NES, SOX2, ALDH1*)].

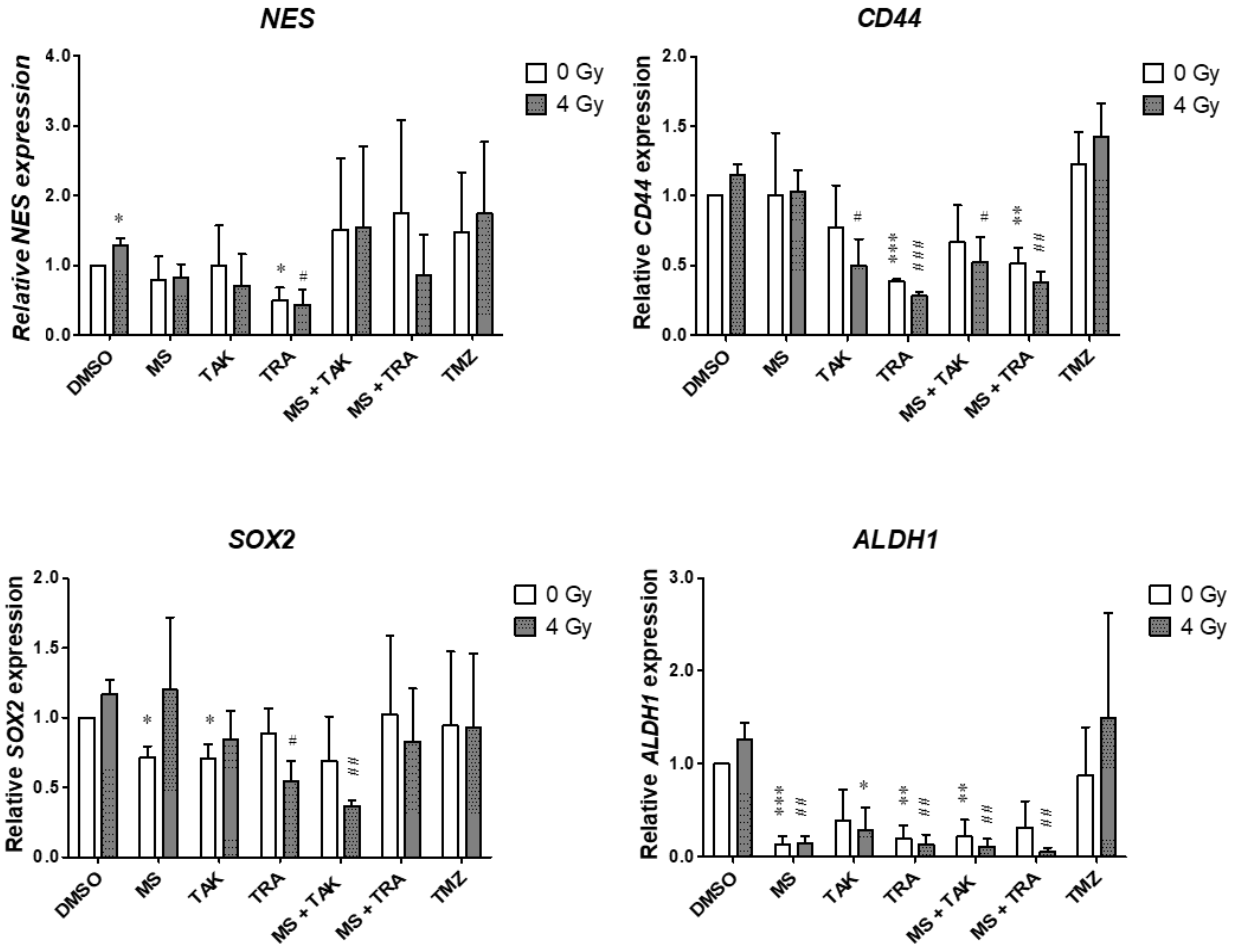

Figure A29: GSLC marker gene expression in U87-sph after treatment with HDACi or MEKi as single or combined drugs with radiation. Fold changes of *NES*, *CD44* and *SOX2* 72 hours after the combined treatment and 4 Gy radiation are shown. The fold changes were calculated compared to sham irradiated control cells (DMSO) set to one. Data represents mean values ± SEM (n = 3). [*Student's t-test; *p ≤ 0.05, ***p ≤ 0.001 (versus DMSO 0 Gy), #Student's t-test; $^{\#}$p ≤ 0.05, $^{\#\#}$p ≤ 0.01, $^{\#\#\#}$p ≤ 0.001 (versus DMSO 4 Gy). 2-way ANOVA; *p*-value <0.0001 (*CD44*); *p*-value <0.05 (*ALDH1*)].

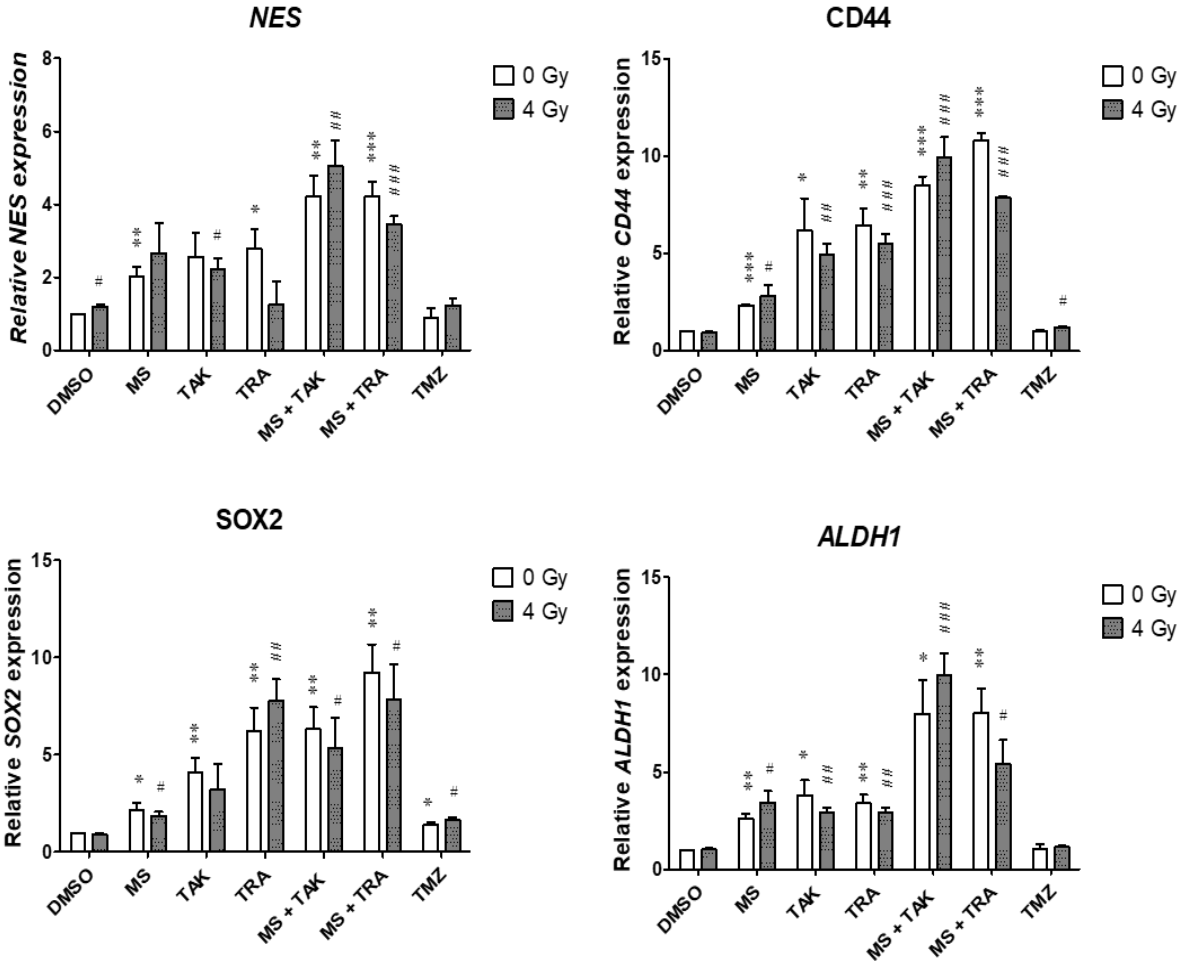

Figure A30: GSLC marker gene expression in U251-sph after treatment with HDACi or MEKi as single or combined drugs with radiation. Fold changes of *NES*, *CD44* and *SOX2* 72 hours after the combined treatment and 4 Gy radiation are shown. The fold changes were calculated compared to sham irradiated control cells (DMSO) set to one. Data represents mean values ± SEM (n = 3). [*Student's t-test; *p ≤ 0.05, ***p ≤ 0.001 (versus DMSO 0 Gy), #Student's t-test; $^{\#}$p ≤ 0.05, $^{\#\#}$p ≤ 0.01, $^{\#\#\#}$p ≤ 0.001 (versus DMSO 4 Gy). 2-way ANOVA; *p*-value <0.0001 (*NES, CD44, SOX2, ALDH1*)].

LIST OF FIGURES

LIST OF FIGURES (APPENDIX)

LIST OF TABLES

LIST OF TABLES (APPENDIX)

ACKNOWLEDGEMENTS

I would like to thank Prof. Dr. Michael J. Atkinson for giving me the opportunity to carry out my doctoral research under his expert supervision in the institute of Radiation Biology (ISB). I am very grateful for his mentorship, support and guidance that has helped me to advance my scientific career.

I want to extend my gratitude towards late PD. Dr. Nataša Anastasov for the opportunity to work in her personalized radiation therapy group. Her supervision and mentoring in her research group has improved my knowledge in cancer research, molecular biology techniques, scientific writing and presentation. I also appreciate the funding Dr. Anastasov procured to allow me finish my PhD thesis.

I am thankful to Prof. Dr. Gabriele Multholf as my thesis committee member and second advisor for her expert contributions, advices and suggestions during my thesis committee meetings.

I thank all members of the former Institute of Radiation Biology for their support, co-operation, wonderful time and memories at ISB. I especially thank Silvia Köhn and Solvejg Schröder and Bahar Sanli-Bonazzi for their administrative support and lovely discussions and laughs. Also not forgetting Klaudia Winkler, Rosi Kell and Stephanie Winkler for their help and support in the laboratory always. I thank my former PhD colleagues and group leaders of ISB who have helped me in many ways, especially Dr. Michael Rosemann for his technical support and help in statistics. Thank you all very much for your care!

I also want to thank HELENA and RS2 members for the exciting scientific trips, opportunities for personal developments and great time at the Helmholtz Munich campus.

I am grateful to the HMGU Immunoanalytics-Core Facility for their support with the flow cytometry experiments. I especially thank Dr. Thomas Höfer for his help and assistance with the flow cytometry design and analysis.

I would also like to thank all IBMI members for their support in the transition from ISB. I am thankful for the scientific discussions and the opportunities to collaborate and participate in the IBMI seminar meetings.

Finally, and importantly, I am grateful to my father in heaven for his unfailing love and strength to finish this work. I thank my family and friends for their prayers and support always and a special thanks to my husband Gboluwaga O. Oguntona for his love, continuous encouragements and understanding all through the duration of my doctoral research. Thank you for always being there!